Intergovernmental Oceanographic Commission
technical series

62

Geological processes in the Mediterranean and Black Seas and North East Atlantic

Preliminary results of investigations during the TTR-11 cruise of RV *Professor Logachev* July-September, 2001

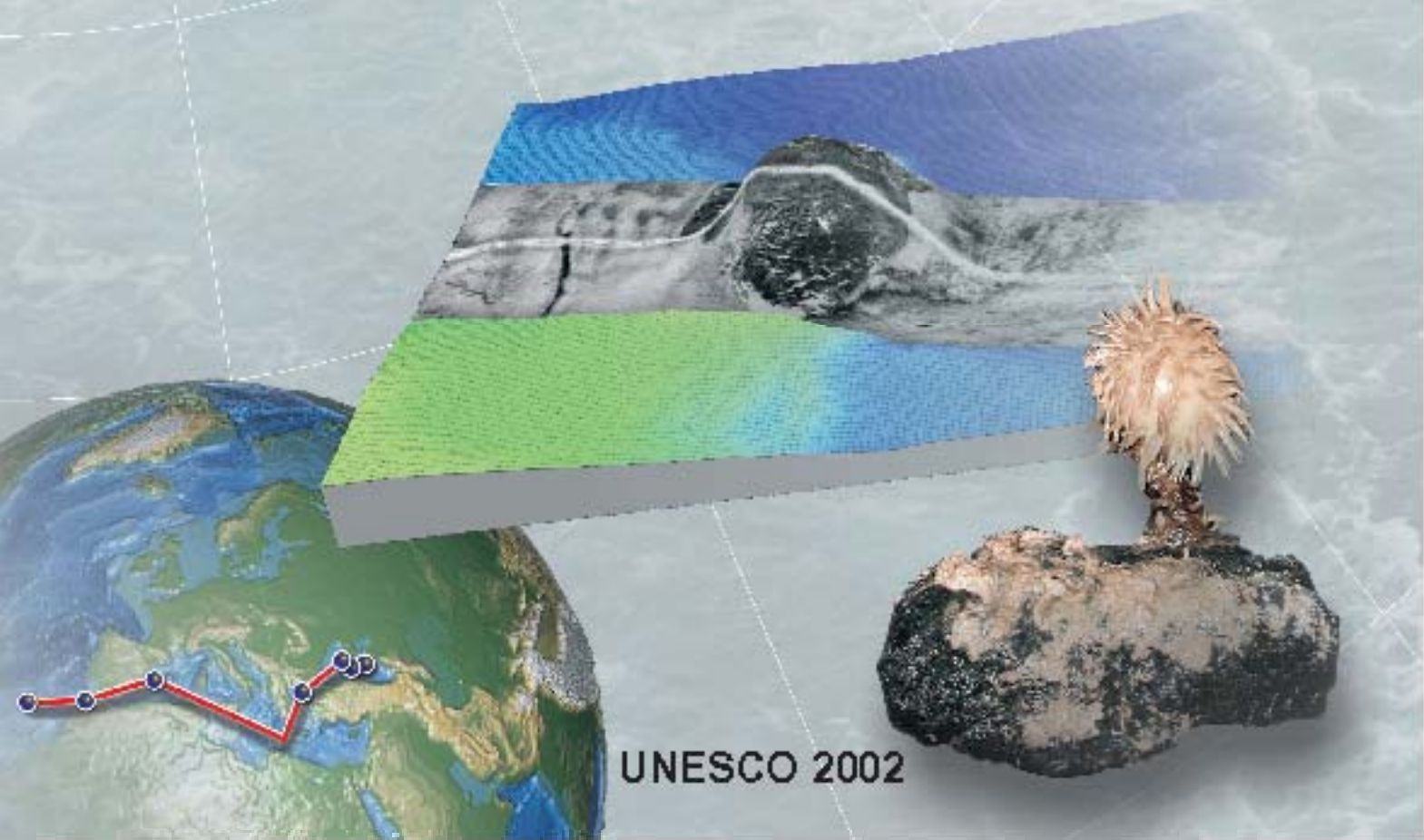

UNESCO 2002

Intergovernmental Oceanographic Commission technical series

62

Geological Processes in the Mediterranean and Black Seas and North East Atlantic

Preliminary results of investigations during the TTR-11 cruise of
RV *Professor Logachev*
July-September, 2001

Editors: N.H. Kenyon
M.K. Ivanov
A.M. Akhmetzhanov
G.G. Akhmanov

SC-2002/WS/62

UNESCO 2002

For bibliographic purposes, this document should be cited as follows:
Geological Processes in the Mediterranean and Black Seas and North East Atlantic
IOC Technical Series No. 62, UNESCO, 2002 (English)

Printed in 2002
by the United Nations Educational, Scientific and Cultural Organisation 7, place de Fontenoy, 75352 Paris 07 SP

Printed in UNESCO's Workshops

Printed in France

TABLE OF CONTENTS

ABSTRACT

The research programme of the 11th Training-through-Research Cruise encompassed a broad range of scientific problems, which were studied at locations in the Black and Mediterranean Seas, the Gulf of Cadiz and in the North- Eastern Atlantic. The major topics were: fluid escape related processes (Black Sea, Gulf of Cadiz), recent tectonic and sedimentary processes related to active faults (Aegean Sea), slope instability (Ebro margin), sand trasport and deposition processes in the deep-sea (Gulf of Cadiz), formation of polimetalic crusts and nodules (Madeira Seamounts).

Gas hydrates were recovered for the first time in the Northwestern part of the Black Sea in the area without mud volcanoes and at a water depth of 900 m. Most of the fluid escape features were observed along faults suggesting that the latter are important conduits for the upwards migration of fluids. Numerous sediment failures and buried debris flows found in the study area indicate that a large portion of the slope was prone to failure in the near past. The sediment failures can be related to fluid escape structures and/or to gas hydrate dissociation events.

New seismic and high resolution sidescan sonar data provided new insights on the morphology and internal structure of hitherto poorly studied mud volcanoes in the Central Black Sea. It was suggested that various morphologies of mud volcano edifices might be characteristic of different stages of their evolution.

New seismic records were obtained across Kazakov and NIOZ mud volcanoes in the Sorokin Trough (Northeastern Black Sea). Kazakov mud volcano has deeper roots which lie below the penetration of the seismic system used and were not observed on the records. NIOZ mud volcano crowns a large diapir seen on the seismic image.

An area of complex interaction between growing clay diapirs and bypassing turbidity currents was observed during high resolution deep-towed sidescan sonar survey. Some of the mud volcanoes showed evidence of recent activity. Gas hydrates and carbonate crusts recovered from many of them suggest that seepage of fluids enriched in hydrocarbons takes place at the present time.

Clear evidence for strike-slip faulting were found within the North Aegean Trough (Mediterranean Sea). Prominent fault scarps were imaged bounding the north and south sides of the North Aegean basin with significant vertical displacement in excess of 700 m.

A large landslide occupying more that 2200 km² was mapped in detail with the deep-towed MAK system on the Ebro margin (Mediterranean Sea). Two surveys provided high resolution visualization of a slide scar and a blocky debris flow, initially recognized on the EM12 multibeam echosounder bathymetry and reflectivity maps. New data suggest that the sliding occurred as a series of events, closely spaced in time, rather than as a single event. Underwater TV surveying showed that the slide is draped by a relatively thick hemipelagic veneer suggesting the lack of recent activity.

Detailed investigation of the Iberico High and surrounding diapiric ridges in the Gulf of Cadiz showed that carbonate chimneys are widespread in the area and form large fields on the tops and slopes of the outcropping diapiric structures. Their presence probably reflects the fact of intensive fluid escape from the sediments involved in the diapiric process. Most of the chimneys were seen to have fallen, suggesting that the chimney's formation took place in the past and that at the present time their growth is negligible or has ceased.

A new, conically-shaped mud volcano, named Aveiro, was mapped in detail with the 30 kHz MAK system and sampled in the Portuguese sector of the Gulf.

The importance of channelised sand transport was recognised after an analysis of sidescan and high resolution seismic data obtained by a 100 kHz deep-towed MAK-1M survey across a sandy depositional lobe formed by gravity flows at the termination of the Gil Eanes contourite channel.

Several fields of ferromanganese crusts were identified on underwater TV footage obtained on the slopes of Unnamed and Unicorn seamounts in the vicinity of the Madeira Island. An extensive collection of ferromanganese crust was retrieved from Unnamed Seamount slopes with the TV guided grab and kept for further laboratory analyses.

ACKNOWLEDGEMENTS

The eleventh Training-through-Research Cruise has received financial support from a variety of sources among which were: the Intergovernmental Oceanographic Commission (IOC) of UNESCO, Royal Netherlands Institute for Sea Research (NIOZ), School of Ocean and Earth Sciences of the Southampton Oceanography Centre (UK), University of Barcelona (Spain) through the frame of the project COSTA funded by the European Union and project GRANDES funded by the "Comisión Interministerial para la Ciencia y la Tecnología", Instituto Geologico e Mineiro (Portugal), University of Aveiro (Portugal), the Russian Ministry of Science and Technological Policy, the Polar Marine Geological Research Expedition (PMGRE) of the Russian Ministry of Natural Resources and the Moscow State University (Russia). Logistic support was provided by NIOZ.

A number of people from different organizations supported the Training-through-Research Programme and were involved in the cruise preparation. The editors would like to express their gratitude for the contributions made by Prof. I. F. Glumov (Ministry of Natural Resources of the Russian Federation), Dr. A. Suzyumov (UNESCO), Dr. P. Bernal (Executive Secretary, IOC), and Mr. V. Zhivago (Ministry of Science and Technological Policy of the Russian Federation).

Credit also should be given to Dr. Maarten van Arkel of the NIOZ and Prof. Dr. B. A. Sokolov (Moscow State University) for their continuous administrative support.

Thanks are due to the administration and staff of the PMGRE (St. Petersburg) for their co-operation and assistance with the cruise organization. Captain A. Arutyunov and the skilful crew of the R/V *Professor Logachev* are thanked for the successful carrying out of the operations at sea.

Staff and students of the UNESCO-MSU Marine Geosciences Centre were very instrumental in processing the acoustic data and in the preparation of illustrations.

INTRODUCTION

The 11th cruise (TTR-11) of the UNESCO-IOC "Training-through- Research" programme was carried out on board the R/V *Professor Logachev* (Russia) from 25 July to 3 September. The cruise got underway from Constantsa (Romania) and terminated in Funchal, Madeira (Portugal). The cruise was subdivided into three legs separated by two port calls, where partial exchange of the Scientific Party was made: in Istanbul (Turkey) on 6-7 August and in Valencia (Spain) on 20-21 August. In addition, partial exchange of the scientific party was performed in the middle of the 2nd Leg at a roadstead stop in Valencia (Spain) on 15 August.

An international team of 67 scientists, post- and undergraduate students (in addition to a group of Russian technicians who had been working with the *Logachev* equipment) from 13 countries (Belgium, Brazil, Georgia, Greece, France, The Netherlands, Portugal, Russia, Spain, Turkey, U.K., Ukraine, U.S.A.) participated in the cruise.

The objectives of the cruise were to study various geological processes, such as manifestations of shallow gas, mud volcanism, neo-tectonics, slope processes, etc. in the Black and Mediterranean Seas and on the North East Atlantic margin, and to train students in marine geoscience research. During the cruise the TTR programme operated in the western and central parts of the Black Sea, in the Sorokin Trough (Black Sea), in the Aegean Sea, in the Gulf of Valencia (Mediterranean Sea), in the Gulf of Cadiz and in the area of Unnamed and Unicorn seamounts (vicinity of Madeira Islands, NE Atlantic).

The main objective of the Black Sea leg was to undertake high-resolution studies of sites with manifestations of hydrocarbon fluid venting.

The scientific aim of the study in the northern Aegean Sea was to investigate the westward extension and propagation of the North Anatolian Fault into the Aegean and its transition from strike-slip/transtensional to extensional deformation towards Greece. By collecting sidescan data along the fault we hoped to be able to investigate strike-slip vs. normal offset complementing earlier subsurface datasets along parts of the fault system.

Principal scientific tasks for the Ebro continental slope and rise, within the Valencia Gulf, off the Columbretes Islets included optical and acoustical imaging of a large debris flow discovered in the area by previous multibeam studies.

The area of the Gulf of Cadiz has been intensively studied during recent TTR expeditions. Several mud volcanoes have been discovered and confirmed by sampling. Gas hydrates, carbonate crusts and nodules, as well as benthic chemosynthetic communities were sampled from some of these structures. Within the TTR-11 Cruise, further detailed investigations of known mud volcanoes, fluid escape features and gas hydrate accumulations were conducted, together with searching for yet unknown structures of similar origin.

The principal purpose of the cruise in the area of the Madeira Islands was to investigate sedimentological, geochemical and oceanographic processes related with ferromanganese deposits and phosphorites, occurring on the Ampère, Lion and other seamounts in the region. As phosphogenesis and Mn-oxide precipitation are mutually exclusive processes, the sequence of phosphatic and Mn-oxide layers represents important signals of changing paleoceanographic and paleoclimatic conditions. We also wanted to find out whether any remaining influence of the Mediterranean Water could be identified there.

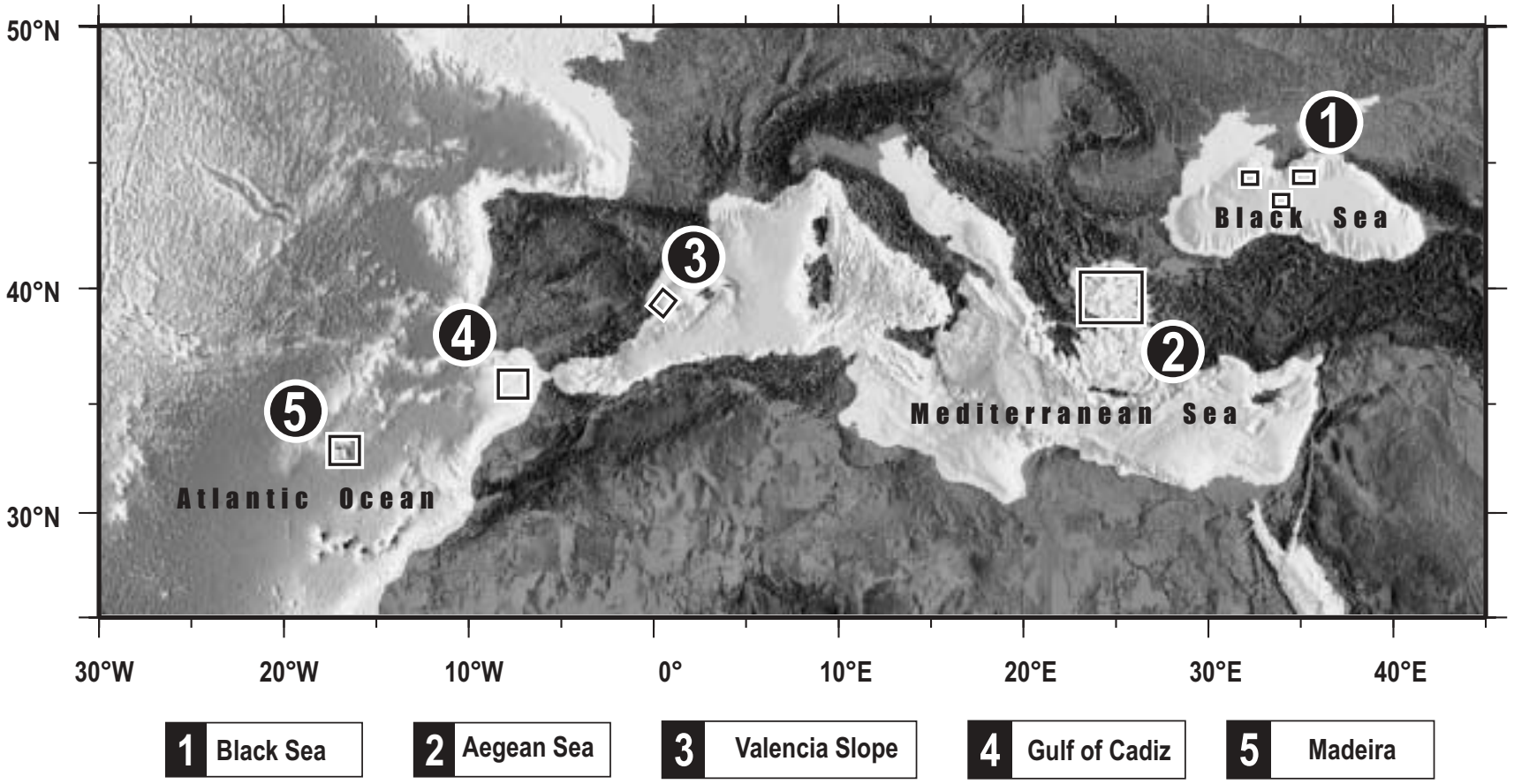

TTR-11 cruise location map

LIST OF PARTICIPANTS

TTR-11 "Floating University" Cruise, 25 July - 3 September, 2001, RV *Professor Logachev*

BELGIUM

Peter Staelens	Ghent University
Peggy Vermeesch	Ghent University
Rien Descamps	University of Leuven
Sofie L.M. Vandendriessche	Ghent University

BRASIL

Simone Schreiner	Petrobras
Viviane Testa	University of Salvador

GEORGIA

Tea Mumladze	Tbilisi State University
Avtandil Maglakelidze	Tbilisi State University

GREECE

Marianthi Lavrentaki	National Centre for Marine Research (NCMR), Athens

THE NETHERLANDS

Alina Stadnitskaya *(co-chief scientist, Leg 1)*	Royal Netherlands Institute for Sea Research (NIOZ)
Marianne Baas	NIOZ
Tiphaine Zitter	NIOZ

PORTUGAL

Luis Pinheiro *(co-chief scientist, Leg 3)*	University of Aveiro
Jose Monteiro *(co-chief scientist, Leg 3)*	Instituto Geologico e Mineiro (IGM)
Joao Rego	University of Lisbon
Tiago Cunha	IGM
Vitor Magalhaes	IGM
Susana Muinos	IGM
Teresa Rodrigues	IGM
Marina Cunha	University of Aveiro
Dulce Subida	University of Aveiro
Ines Lima	University of Porto
Henrique Duarte	University of Aveiro

RUSSIA

Mikhail Ivanov *(co-chief scientist)*	Moscow State University (MSU)
Pavel Shashkin	MSU
Anna Volkonskaya	MSU
Sergey Shkarinov	MSU
Dmitry Modin	MSU
Sergey Bouryak	MSU
Roman Repin	MSU
Sergey Agibalov	MSU
Anna Korneva	MSU
Grigorii Akhmanov	MSU
Elena Kozlova	MSU
Dmitrii Ovsyannikov	MSU
Alexey Sadekov	MSU
Tatiana Bespalova	MSU
Vladislav Torlov	MSU
Valentina Blinova	MSU
Elena Poludetkina	MSU
Natalia Tyrina	MSU
Olga Kovalenko	MSU
Oleg Krylov	MSU

Leonid Mazurenko	VNIIOkeangeologia
Leonid Meisner	NIPIOkeangeophysika
Alexey Krotov	PMGE
Vladimir Markov	PMGE
Alexandr Machulin	PMGE
Evgeny Samsonov	PMGE
Nikolay Volkov	PMGE
Gennady Antipov	PMGE
Irina Antipova	PMGE
Roman Safronov	PMGE
Sergey Zheleznyak	PMGE
Alexander Kurilovich	PMGE
Maksim Kuryschkin	PMGE
Dmitry Gagarin	PMGE
Victor Sheremet	PMGE
Valentin Konfetkin	PMGE
Alexandr Plakhotnik	PMGE
Sergey Lyubimov	PMGE
Konstantin Plakhotnik	PMGE
Alexandr Ivanov	PMGE
Vladislav Malin	PMGE
Alexey Ivanov	PMGE
Alexandr Nescheretov	PMGE
Andrey Rumjancev	PMGE
Vladimir Tarasov	PMGE

SPAIN

Roger Urgeles Esclasans *(co-chief scientist, Leg 2b)*	University of Barcelona
Antonio Calafat	University of Barcelona
Jose Luis Casamor	University of Barcelona
Galderic Lastras	University of Barcelona
Jaime Frigola	University of Barcelona
David Amblas	University of Barcelona
Veronica Willmott	University of Barcelona
Carmen Fernandez-Puga	Geological Survey of Spain, Madrid

TURKEY

Gunay Cifci	Dokuz Eylul University, Izmir
Sebnem Onder	Dokuz Eylul University, Izmir
Derman Dondurur	Dokuz Eylul University, Izmir
Omer Faruk Elbek	Dokuz Eylul University, Izmir

UK

Neil Kenyon *(co-chief scientist)*	Southampton Oceanography Centre (SOC)
Lisa McNeill *(co-chief scientist, Leg 2a)*	SOC
Jeffrey Priest	University of Southampton, Engineering Department
Andrey Akhmetzhanov	SOC
Helen Fergusson	SOC
Arnaud Mille	SOC
Adriano Mazzini	University of Aberdeen
Rebecca Fenwick	University of Birminghem

UKRAINE

Eugenii Larchenkov	Odessa University

USA

Tim Lyons	University of Missouri

METHODS

The RV *Professor Logachev* is a Russian 104.5m marine geology research and survey vessel equipped with seismic and seabed sampling equipment. She is operated by the State Enterprise "Polar Marine Geosurvey Expedition" St. Petersburg. The vessel has: a draught of 6.66 m, width of 16 m, net tonnage of 1351 ton, displacement of 5700 ton and is powered by two 3500 hp diesel engines.

Navigation

Positioning during the TTR-11 cruise was acquired using an Ashtech GG24 GPS + GLONASS receiver. The use of both GPS and GLONASS satellite configurations allows for greater accuracy than is available from conventional GPS alone, with up to 60% greater satellite availability. Positions are calculated in real-time code differential mode with 5 measurements per second and an accuracy of +/- 35 cm (75 cm at 95% confidence limits) with optimal satellite configuration. Realistic positioning accuracy under normal satellite configuration for European waters is assumed as ca. 5 m. Positioning when the vessel is moving also utilizes Doppler velocity determinations from the differential code signal to generate a vessel speed accuracy of 0.04 knots (0.1 at 95% confidence limits) with optimum satellite configuration.

The GPS+GLONASS receiver is located centrally on the vessel with accurate levelling to sampling and equipment deployment positions on the vessel allowing precise back navigation. Seabed sampling positions with the gravity corer is normally 5% of the accuracy of the vessel position due to their rapid deployment. MAK1-M side-scan sonar and deep-towed video system are all fitted with a pinger allowing precise navigation between the vessel and sub-sea surface position. This is necessary as deep-towed equipment is subject to greater spatial differences with respect to the vessel. This underwater navigation is based on the Sigma-1001 hydroacoustic system. Four stationary aerials, spaced 14 m apart, are hull mounted and receive acoustic signals from pingers attached to deployed equipment in short-base mode operating between 7-15 kHz. The signal emitted by the sub-surface pinger is tracked on board and accurate x,y positioning of the device relative to the vessel is computed taking into account vessel roll, trim and ship's speed. Accurate level of the GPS+GLONASS antennae with the hull-mounted transducers allows precise positioning of deployed equipment. Error positioning by the method usually does not exceed 1-2% of water depth.

Additional thrusters linked with the navigation system allow dynamic positioning of the ship. This is particularly useful during high resolution surveys or precise bottom sampling operations.

Seismic profiling

The seismic source consisted of one 3 litre airgun, at a pressure of 120 bar (12 MPa). The airguns were towed at a depth of approximately 2-2.5 m and were fired every 10 seconds (i.e. approximately every 30 m). The streamer consisted of one active section, 30 meters long, with 50 hydrophones, towed at a depth of approximately 2.5-3 m. The offset between the seismic source and the centre of the live hidrophone array was135 meters.

The data was acquired digitally using the MSU developed software and preliminarily processed with the RadExPro software, which was provided to the UNESCO MSU Centre for Marine Geosciences by GSD Productions, Moscow. The signals were low-pass filtered analogically to 250 Hz in the acquisition stage. The sample interval was 1 ms and the record length 3 seconds.

The basic processing sequence con-

sisted of definition of the acquisition geometry, static shift correction, spiking deconvolution, amplitude recovery by spherical divergence correction and Butterworth bandpass filtering (20-60-180-240 Hz).

Hull-mounted acoustic profiler

A hull—mounted 5.1 kHz profiler was routinely used during most of the operations with a continuous paper output and a selective recording of the digital data.

Sidescan sonar systems

OKEAN

The OKEAN is a long-range sidescan sonar operating at a frequency of 9.5 kHz, which with its up to 15 km swath range and 6 knots towing speed, is well suited for reconnaissance surveying of large deep-sea areas. The OKEAN vehicle is towed behind a ship at about 40-80 m below the sea surface. Depending on the waterdepth and resolution required the swath could be set to 7 or 15 km.

MAK-1M sidescan sonar system: preparation for deployment

MAK-1M

The MAK-1M deep-towed hydroacoustic system contains a high-resolution sidescan sonar operated at frequencies of 30 and 100 kHz, with a total swath range of up to 2 km (1 km per side) and a subbottom profiler, operated at frequency of 5 kHz. The sonar has a variable resolution of about 7 to 1 m across track (maximum range to center) and along track (center to maximum range). During TTR-11, the fish was towed at a nearly constant altitude of about 100-150 m above the seafloor at a speed of 1.5-2 knots for 30 kHz surveys and about 50 m above seafloor for 100 kHz surveys. The positioning of the tow-fish was archived with the short-based underwater navigation system.

The data from the tow-fish was transmitted on board through a cable, recorded digitally, and stored in Seg-Y format, with a trace length of 4096 2-byte integer samples per side. Time-variant gain was applied to the data while recording, to compensate the recorded amplitudes for the irregularity of the directional pattern of the transducers as well as for the spherical divergence of the sonic pulse.

Onboard processing of the collected data included slant-range-to-ground-range (SLT) correction of the sonographs, geometrical correction of the profiles for recovery of the real seafloor topography, and smoothing filtering of both types of records. Individual lines were geometrically corrected for the towing speed of the fish, converted into a standard bitmap image format. Some image processing routines, such as histogram equalization and curve adjustment, which are aimed to improve the dynamic range of the imagery were also applied before printing out. Geographic registration of the acquired images was also done onboard.

Underwater photo and television system

The television system operating onboard cruise TTR-11 is a deep towed system designed for underwater video surveys of the seabed at depths of up to 6000 m. The

TV system consists of the onboard and underwater units. The onboard part comprises the control desk with video amplifier. The power for the underwater system is supplied through a special cable. The underwater equipment comprises the frame-bearer with light unit, the high-pressure housing containing a "Canon M1" digital camera and the power supply unit.

The TV system is directly controlled from onboard by the winch operator controlling visually the distance from the camera to the seafloor. There is a rope with a weight attached to the frame which is usually towed on the seafloor and used to control the camera-seafloor distance. The rope is 1.5 m long. On/off switching of lights and video camera is done by the operator in the laboratory. The non-stop underwater record on the digital camera lasts for 2 hours in the "LP" mode. Onboard video-TV keeps a continuous record during the whole survey, which allows for up to 6 hours recording.

Sampling Tools

Gravity corer

Coring was performed using a 6 m long c. 1500 kg gravity corer with an internal diameter of 14.7 cm.

One half of the opened core was described on deck paying particular attention to changes in lithology, colour and sedimentary structures. All colours relate to Munsell Colour Charts. The other half was measured for changes in magnetic susceptibility using a Bartington Instruments Magnetic Susceptibility meter with a MS2E1 probe. Magnetic susceptibility reflects the ease with which a material can be magnetised. This property is most strongly influenced by grain-size, heavy mineral content and is inversely related to carbonate content and diagenetic ferric mineral reduction.

Samples were also taken for coccolith and micropalaeontological assays from smear slides. This was done to generate a preliminary chronostratigraphy for the cores.

Dredge

The dredge comprises a $1m^2$, circular steel gate with chain mesh bag trailing behind and a 0.5 tonne weight leading by 3m in front of the gate. The mesh bag also has a rope bag inside and the mesh size is ~5 cm. The dredge was deployed ~250 m in front of the identified target site and the ship moved at 0.5 kts between 500 and 1500 m ensuring the dredge was pulled up-slope. On some sites, the bottom was monitored with a 3.5 kHz hull-mounted single-beam echosounder. At all times, the ship's velocity and position were monitored using GPS. Tension on the trawl-wire was monitored in the winch cab by both ink-line paper roll and with a tension meter. "Bites" of up to 10 tonnes on the trawl wire were recorded in this way.

TV-guided grab

The DG-1 grab system was used during the TTR-11 cruise. The 1500 kg system is able to sample dense clayey and sandy sediments as well as deep water basalts and sulphide ores. DG-1 can be used at the depths up to 6000 m and closes by the difference in hydrostatic pressure. The maximum sample volume for soft sediment is 0.4 m^3. The triggering mechanism is set off when the seabed is touched. The grab is positioned with the short base SIGMA 1001 underwater navigation system. The grab is equipped with a build-in camcorder which uses 90 minute cassettes and records in Hi-Fi Video8 format. Video signal is also transmitted on board enabling control for the grab operation and back-up recording. The lights are powered by a rechargeable battery enabling 1 hour of continuous operation. A second battery kept on board, was used to perform subsequent dives.

I. THE BLACK SEA (LEG 1)

I.1.Introduction

The main objective of the Black Sea leg was to undertake high-resolution studies of sites with manifestations of hydrocarbon fluid venting. Three principal areas were identified (Fig. 1). Area 1 is located on the continental slope and its rise close to the broad northwestern shelf of the Black Sea. Previous studies, performed mainly by the Ukrainian and Russian scientists, as well as by several international research programmes, revealed numerous hydrocarbon vents exhausting onto the seafloor within the area. Manifestations of gas venting were reported to be present both in the water column (plumes) and in the bottom sediments. Among features known from the area carbonate build-ups and chemosynthetic biological communities associating with gas seepages were of particular interest.

Area 2, located in the deep Central Black Sea, is a well-known mud volcano field. Mud volcanoes were investigated here during the TTR cruises of 1991, 1993 and 1996 and a comprehensive set of multidisciplinary data was obtained. The expedition of 2001 was concentrated on detailed examination of the 3 less studied mud volcanic structures in the area: the TREDMAR, Vassoevich, and Kovalevsky mud volcanoes.

The TTR-6 studies of the Sorokin Trough (Area 3) in 1996, discovered a variety of bottom features, related to fluid escape. Gas seeps were sampled and the presence of gas hydrates, diagenetic carbonates and microbial mats were reported. Fluid-escape structures and mud volcanoes presumed to be most active were the targets of the detailed studies.

I.2. Northwestern Black Sea

I.2.1. Geological Setting

Area 1 is offshore the SW Crimean Peninsula and south Ukraine, within 400-1600 m water depth.

The Crimean platform consists of a Hercynian basement of Mesozoic-Cenozoic age sediments, in contrast with the European platform, which is composed of crystalline Archean-Proterozoic basement (Hain, 1984; Milanovskii, 1991).

This part of the shelf exhibits the combination of the following structures:

1. Kraevaya Step. This is one of the structures of the Scythian Hercynian platform, located west of the Crimean Peninsula.
2. North slope of the Western Black Sea subbasin
3. Offshore continuation of the Crimean Mountains

The Kraevaya Step is an EW elongated monocline formed by Mesozoic and Cenozoic rocks gradually subsiding southwards. The Mesozoic rocks in this region are Jurassic and Lower Cretaceous clastic sedi-

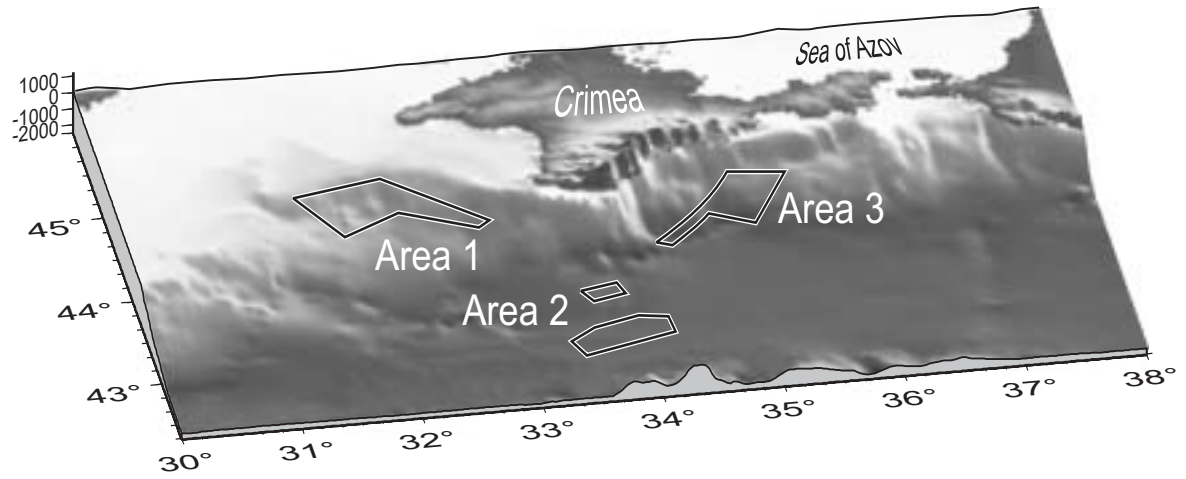

Figure 1. Location of the Leg 1 study areas.

ments, represented predominantly by shales with some sandstone layers. They are overlaid by carbonates of Upper Cretaceous and Lower Palaeocene age.

In the Western Black Sea subbasin the Cenozoic sequence reaches up to 12 km thick and the Palaeocene-Eocene sediments up to 6 km thick. These series decrease upslope, towards the northwest, where the layers eventually pinch out against the Mesozoic surface. Before the Quaternary an erosional continental slope was developed. Cenozoic sediments had been partially or completely eroded from the upper part of the slope.

Oligocene-Early Miocene (Maykop Suite) sediments are represented by shales with some lenses and/or layers of sand and silt In some parts of the Black Sea area the thickness of this sedimentary unit exceeds 5 km. The Maykop Suite is the regional source rock in basins from the Carpathians in the west of the Black Sea region, through the Crimea and the Caucasus Mountains, to the South Caspian Basin in the east. The Maykopian sediments locally include reservoirs containing significant oil and gas accumulations.

Quaternary sediments in Area 1, have a considerable thickness of about 1 km, mainly due to accumulation of Danube Fan sediments The sediment supply from the River Danube induces an increase of thickness of Quaternary sediments towards the northwest. The study area captures the left flank of the fan system.

The continental slope of the southwestern part of Crimean Mountains has an erosional nature, and consists of terrigeneous flysch of the Tavric Series and Jurassic-Cretaceous igneous rocks exposed on the sea floor.

I.2.2. Seismic reflection profiling

L. MEISNER, O. KRYLOV, G. A. VOLKONSKAYA, CIFCI, S. ONDER, D. DONDURUR, O. F. ELBEK, S. BOURYAK, S. SHKARINOV, AND S. OGIBALOV

High resolution seismic reflection profiling was carried out along four lines (PS289BS to PS292BS) roughly parallel to the slope of the NW Crimean margin in water depths of about 800 m to 1400 m (Fig. 2). The penetration reached about 400 ms two-way travel time. The profiling was accompanied by OKEAN sidescan sonar survey and 5.1

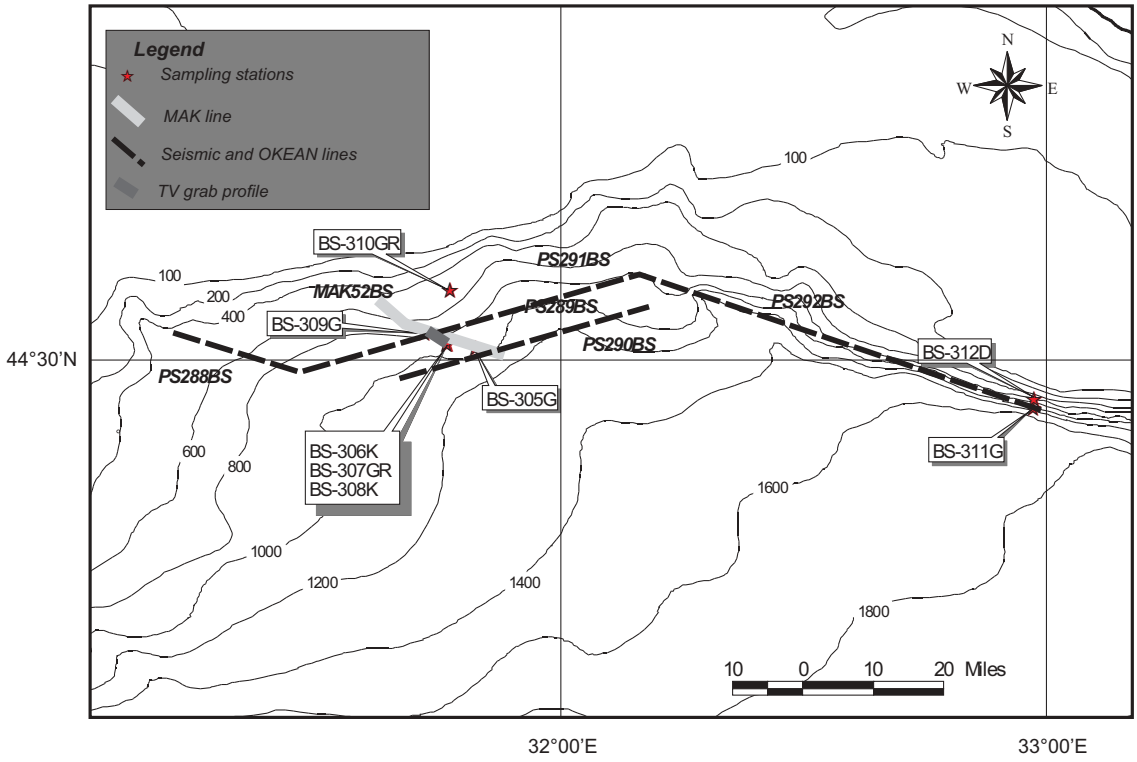

Figure 2. Location map of the Leg 1, Area 1.

kHz subbottom profiling. A MAK deep-towed sidescan sonar line crossed lines PS289BS and PS290BS.

PS289BS to PS291BS

PS289BS and PS290BS were parallel lines of about 40km, spaced 7 km apart and running from SW to NE. A 20 km long line PS291BS was run oriented WSW-ENE.

Seismic units

The seafloor along the profile is quite irregular and shows some rises and valleys. At its eastern end the slope is very steep. This feature is seen as an elongated rise with NNE-SSW.

Three main seismic units were determined along the these lines (Fig. 3). Upper unit (1) is observed in the middle of the line as a well-layered package with high amplitude parallel reflections. The unit shows discontinuity towards the rise at the eastern part of the profile. It is also hardly distinguishable at the western end of the profile due to chaotic facies. The thickness of the unit varies from 50 ms in the middle of the profile to 250 ms in the deepest part of the section. The horizon at the base reaches 1.6 s deep in this area.

The middle unit (2) has parallel bedded layers only in some relatively undisturbed places. On PS291BS there is a transparent to semi-transparent facies. Thickness varies less than in the previous unit, from 50 ms to 150 ms, with the thickest part also corresponding to the basinal part. The upper and lower reflections of this unit converge as far as the top of the rise, reaching the unit's minimal thickness.

The lower unit (3) is a transparent layer of 100 ms on PS289BS. On PS291BS it shows some faint dipping reflectors and pinches out against the rise at around 3:20.

An acoustic basement can be seen about 400 ms below the seafloor indicating the Quaternary age of the overlying sequence. Occasionally below the acoustic basement a reflector can be seen, e.g. at 2.4 s deep on PS291BS. This reflector is inferred to be the base of Cenozoic deposits, which gives a total thickness of Cenozoic sediments of 1500 m.

Gas-related structures

Numerous gas seepage structures were observed on both PS289BS and PS290BS.

A wide transparent vertical area is observed on PS289 at 10:00 (Fig. 4). Reflectors are masked, probably due to gas seepage. This gas seepage area has been confirmed by sampling. Close to this location, the kasten

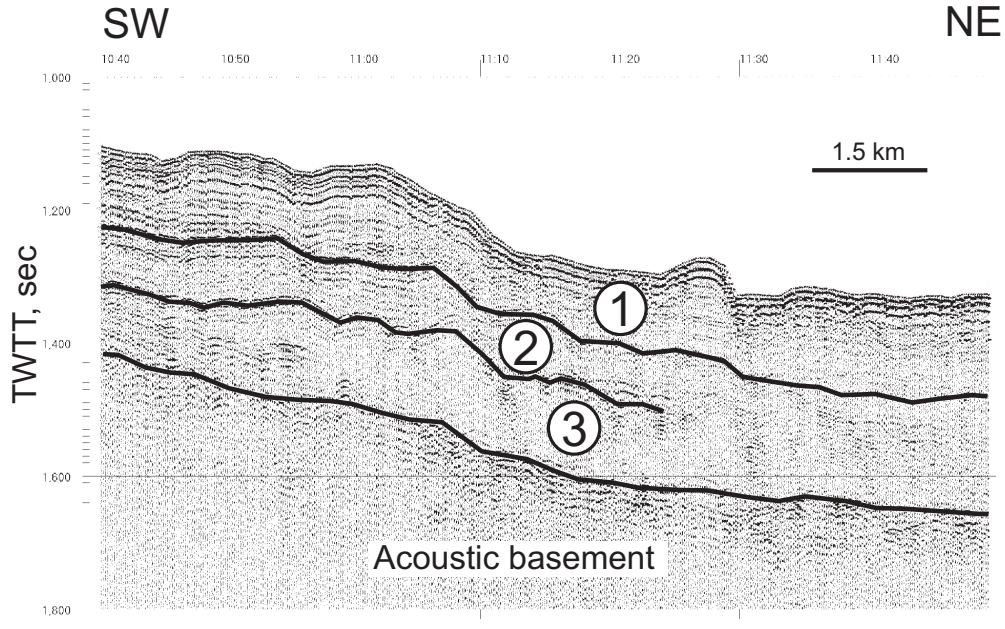

Figure 3. Fragment of seismic line PS-289BS showing main seismic units distinguished in Area 1.

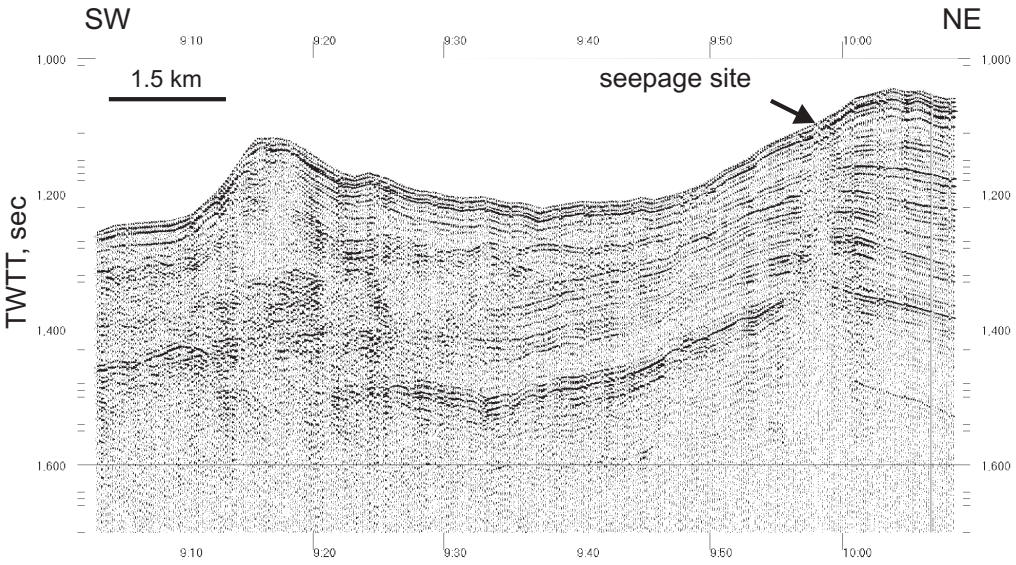

Figure 4. Fragment of seismic line PS-289BS across a fluid seepage site.

cores BS306K and BS308K recovered some layers of thin carbonate crust and even gas hydrates in the case of BS308K. This area can also be correlated with a vertical transparent area seen on line PS289BS at 16:50, which indicates an important extension of this gas seepage environment.

Some feeder channels have also been recognised on PS289BS at 16:50, and shallow gas pocket can be detected.

Faults are observed only on the eastern part of the profiles. On line PS289BS, to the west, two important faults can be seen disturbing the reflectors from the surface to the acoustic basement. A surface fault scarp marks one of more than 50 ms, the other one is seen small, narrow valley. Between these two faults, the loss of continuity of the two units previously described is noticeable.

Generally, seismic profiles show a prograding sediment wedge, as well as the disturbance of the layers by the faults penetrating to the seafloor.

PS292BS

The line is about 70 km long and SE-NW oriented. It exhibits the transition from an accumulative deep-sea fan type slope to an erosional slope at the west of the Crimean Mountains (Fig. 5). The line consisits of two sections with a sharp change from one slope environment to another at 6:45.

From 4:00 to 6:45

In this section, reflecting an accumulative slope, four main horizons can be seen.

The upper unit is a well bedded layered unit up to 100 ms thick in some places. The bedded layers also shows very well on the subbottom profiler down to about 100 m. Between 5:20 and 6:00 the reflectors are disturbed by microfaulting. Recent slumps, about 10-20 m thick, characterise this faulted area.

The upper middle unit is a transparent layer which thickens westward up to 200 ms.

The lower middle unit shows a thick transparent facies (up to 250 ms) but pinches out and disappears at about 6:00. The base is very irregular and deepens from 1.7 s at 8:00 to 2.1 s at 6:00.

The base of the Cenozoic, previously identified in PS291BS, can be followed along this section, shallowing eastward from 2.4 ms deep to 2.1 ms deep (Fig. 5).

The transition with the second section is by a very steep rise of 500 ms high. At the base of this rise a large, 50 ms thick, slump is situated.

<u>From 6:40 to 7:50</u>

This section shows the continuation

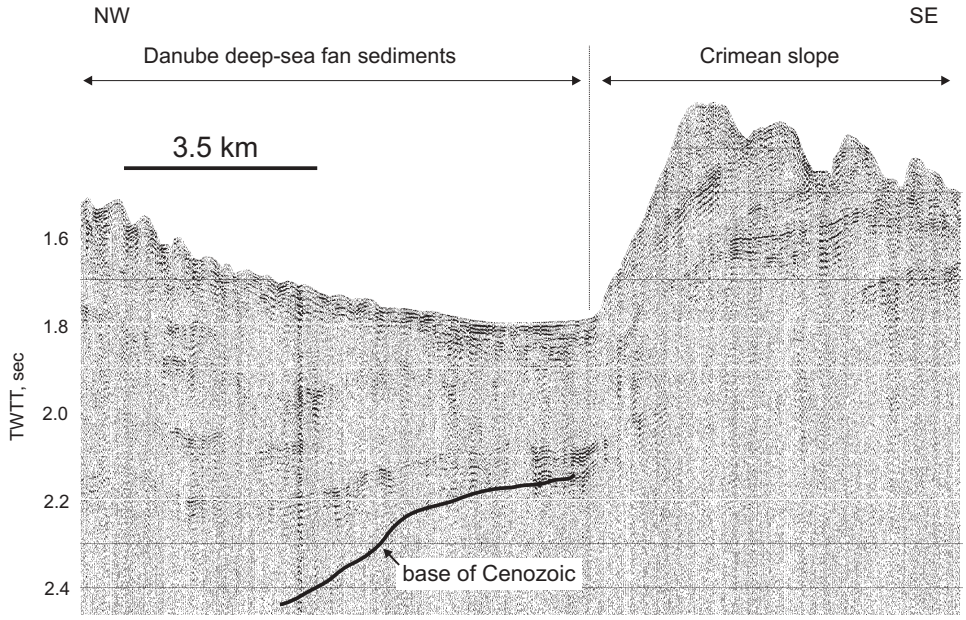

Figure 5. Fragment of seismic line PS-292BS showing a transition between two different types of slope.

towards SW of the Crimean Mountains and the features are typical of an erosional slope.Three main valleys can be seen.

The first valley, 300 ms deep, extends from 6:40 to 7:50. The seafloor is cut by several U-shaped channels about 100 ms deep and a few kilometers wide. Coarse material and erosion in the middle of each channel gives strong reflection packages on the seismic line as well as on the subbottom profiler. A package of very strong reflections can be seen in the upper part of the seismic section and probably correspond to an ancient erosional surface.

The second valley (from 7:50 to 9:20) and third valley (9:20 to 10:40), respectively 500 ms deep and 1 s deep, has deeper and narrower channels, characterized by a V-shape with depth from 200 ms to 600 ms. The strong horizon can be followed between 200 ms and 300 ms below the seafloor.

I.2.3. Sidescan sonar survey

L. MEISNER, O. KRYLOV, A. AKHMETZHANOV, P. SHASHKIN, M. IVANOV, G. CIFCI, S. ONDER, D. DONDURUR, AND O. F. ELBEK

Five OKEAN sidescan sonar and 5.1 kHz subbottom profiling lines (288 to 292) run along the slope of the Crimean margin at water depths of 400 to 1400 m. Four of them (289 to 292) were accompanied by air gun seismic profiling.

PS288BS

Line 288 runs NW-SE for 30 km, except between 5:10 to 5:40 where the ship made a turn. Thus the geometry and direction of the features that occur in this section of sonograph are significantly distorted. An area of slumping can be distinguished on the sonographs around 5:30 (Fig. 6). On the subbottom profiler, from 5:10 to 5:30, several vertical transparent areas can be seen attributed to the presence of shallow gas. From 5:30 to 6:25, the 5.1 kHz profiler shows a surficial transparent layer underneath a very strong reflector possibly reflecting gas hydrate presence. This transparent reflector is inferred to be caused by the accumulation of shallow gas, about 5 to 7 m thick.

From 6:25 to 7:30 the backscattering of the sonograph is higher and irregular. Large circular features, 5 km wide, are seen. This area corresponds to two different environments of gas accumulation. From 6:25 to 7:00 several vertical transparent columns mask layers on the subbottom profiler (Fig. 7). The biggest is observed at 7:10 and is 400 m wide. Another environment is shallow gas layer shown by a transparent layer under-

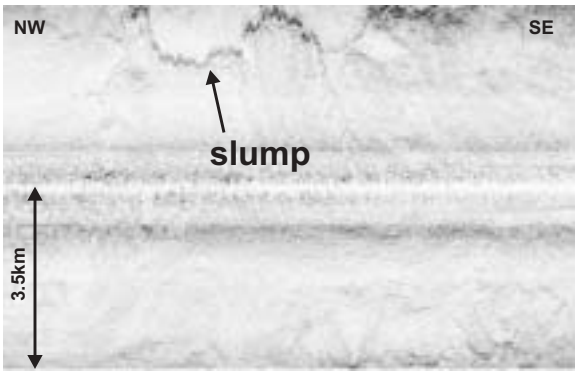

Figure 6. Fragment of 10 kHz OKEAN sidescan sonar line PS-289BS showing the edge of a large slump.

neath the surface. It extends from 7:22 until 7:33. A possible buried debris flow is observed on the profiler record at 6:50 as an acoustically transparent lens. Its initiation could be related to the fluid escape structures found further upslope (Fig. 7).

From 7:30 to 8:50 extensive linear features, NS oriented, with high backscatter, dominate the sonograph. This is interpreted to be initial tensional fractures of recent sediments related to gas accumulation. The reason for high backscattering is not obvious since these fractures do not show significant relief on the subbottom profiler. It could result from sliding triggered by gas expulsion from gas hydrates or is caused by associated elements of gas seepage such as carbonate crust.

PS289BS

On the first part of the sonograph (8:50 to 9:10) irregular shaped areas of medium backscatter can be identified. These correspond to a thick transparent layer on the subbottom profiler. It reflects a 25 m thick gas pocket 10 m below the seafloor. Another smaller gas pocket of 5 to 10 m in thickness occurs just beneath the surface extending from 8:50 to 8:57.

Between 9:45 and 10:30, round high backscattering patches, 500 m across, are inferred to be pockmarks. They align along a predominantly EW trend (Fig. 8).

Occasional vertical transparent areas, very typical of energy absorption by gassified sediments are observed from 9:40 to 10:30 on the subbottom profiler.

From 10:30 to 11:00, EW lineations are seen as medium backscattering linear areas on the sonograph, corresponding to the faulted area seen on seismic profile.

From 11:00 to 12:50 the line crosses a 20 km wide valley which is characterised by variable backscatter pattern on the sonograph and chaotic reflection in several places of the subbottom profiler. Both edges show a linear medium backscatter on the sonograph, the eastern edge running EW and the western NS. A channel runs through the middle

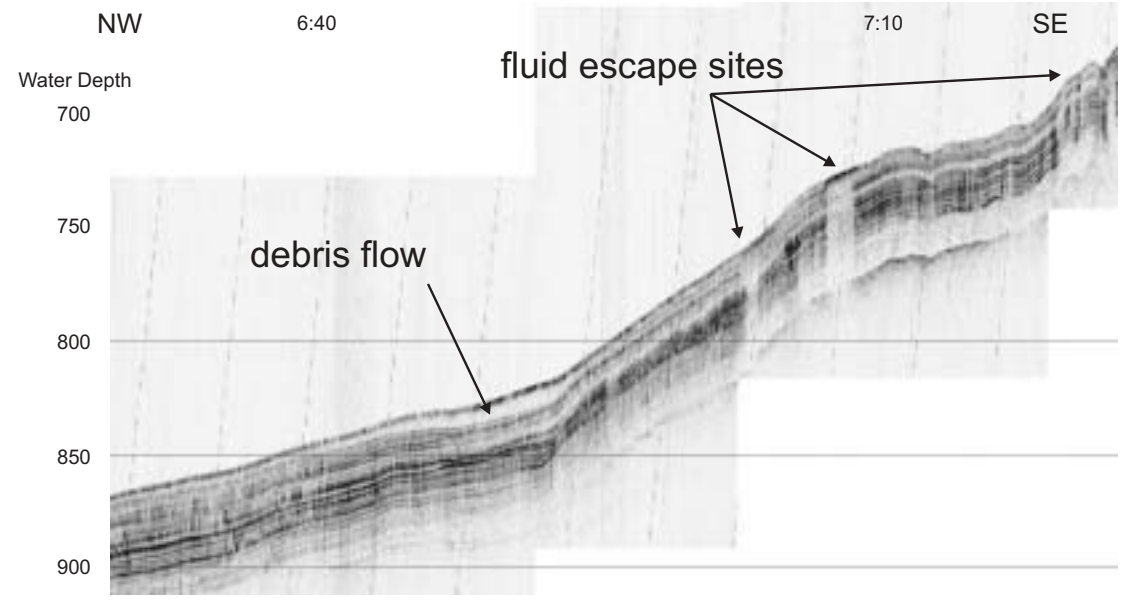

Figure 7. Fragment of 5 kHz profiler record showing acoustically transparent zones due to fluid escape and possibly related debris flow.

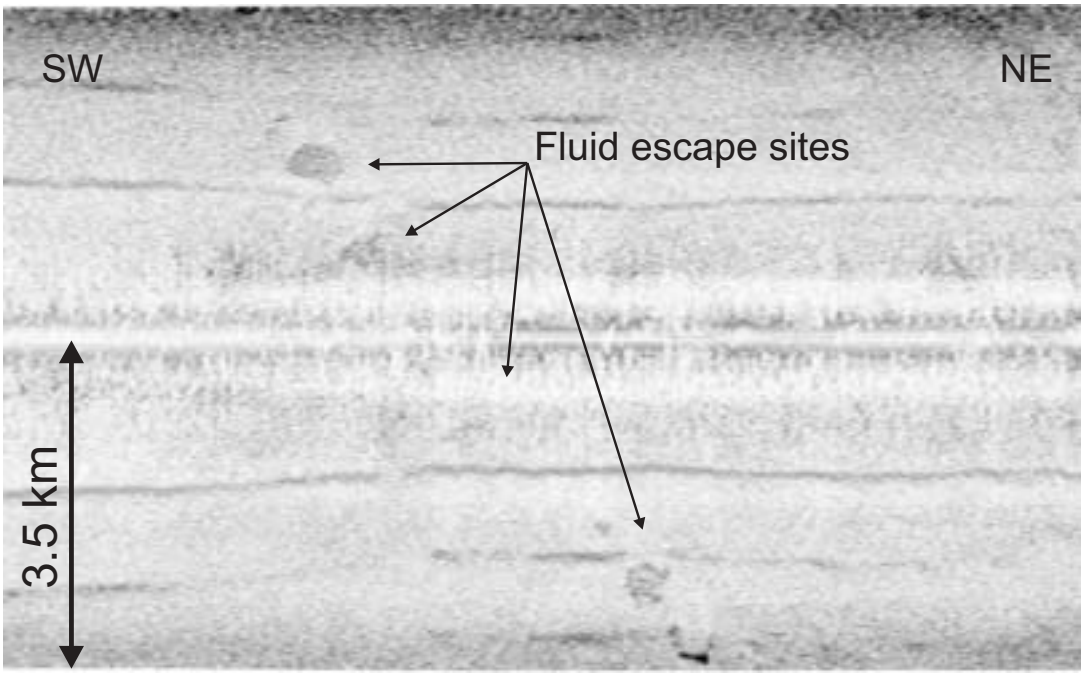

Figure 8. Possible pockmarks on the 10 kHz OKEAN sidescan sonar line PS-289BS.

of this valley. It is delimited by two layered levees at 11:30 and 12:10. Sediment infill of this channel shows a chaotic transparent facies on the subbottom profiler record. It is crossed by another, more recent, leveed channel at 11:55. A small channel is also recognised at 13:00.

PS290BS

At 14:15 an irregular shaped channel is observed with slightly enhanced backscatter on the sonograph. Its width varies from 800 m to 2700 m and it is slightly sinuous. It can be observed on the subbottom profiler and is 30 m deep with well bedded levees. From 14:30 to 14:50 a series of almost parallel semi-linear features, oriented NNE-SSE, with medium to high backscattering characterise the slope of the rise. The latter is very steep and shows a chaotic transparent facies on the subbottom profiler. It could be related to slumping or creeping down the slope. A zone of irregular low backscattering extends from 15:10 to 16:00. In this area the subbottom profiling shows one laterally inconsistent layer. The absence of any layering reflects either recent sedimentation due to turbidity flows, supported by the presence of a channel at 15:21, or an erosional surface from a large slump.

On the second part of this sonograph, a gas seepage area is observed between 16:50 and 17:20 as high backscattering patches on the seafloor. Gas seepages are indicated in several places on the profiler and on the seismic section by transparent areas. Between 17:00 and 17:20, irregular shaped high backscattering corresponds to a small NS channel.

At about 18:00 the sonograph exhibits a high backscattering radial pattern produced by a slump and suggesting mass transport to S-SE (Fig. 9). Subbottom profiler data show several acoustically transparent lenses 10 m below seafloor which are interpreted as buried debris flows resulting from the slumping.

PS291BS

The line PS291BS runs WSW-ENE through a portion of the slope dissected by several small canyons converging downslope (Fig. 10). At the beginning of the sonograph (1:00) there is a curvilinear feature characterised by high backscatter. This feature continues into a linear medium back scattering NNW-SSE trend until 1:30 perhaps indicating sediment sliding or slumping.

From 1:30 to 2:35 the sonograph is characterised by 5 medium backscattering

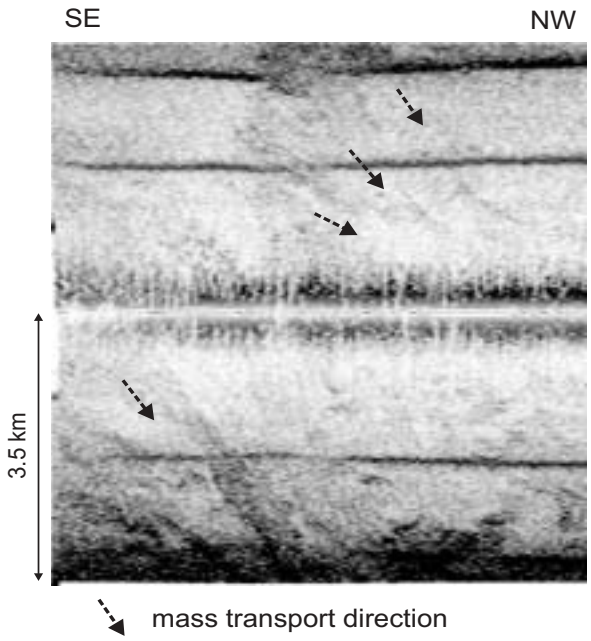

Figure 9. Fragment of 10 kHz OKEAN sidescan sonar line PS-290BS showing sediment flows.

canyons also running NNW-SSE, between 2000 and 4000 m wide, with a maximum depth of 55 m. The subbottom profile of these canyons indicates recent sediment transport as the canyon floor has a hummocky surface and no penetration underneath.

PS292BS

Line PS292BS is a continuation of line PS291BS, with a change in direction of profiling to the NW-SE. The sonograph can be divided into 2 main sections; 4:00-6:50 is a valley, and 6:50-10:50 is the continuation of the Crimean Mountains.

There is a high backscatter linear feature running N-S on the sonograph crossing the central part at 4:30, which corresponds to a channel on the subbottom profile 55 m deep. From 4:50 to 6:50 the sonograph shows continuous irregular low to medium backscatter with no obvious features. On the subbottom profiler this area is the gently sloping north-western margin of the valley with small step like topography showing laterally inconsistent reflectors with some acoustically transparent regions (4:55, 5:02, 5:07), chaotic transparencies underlie an area of higher relief (5:15-5:48) and the final section of the valley (5:48-6:30) shows recent sediment deposits overlying stronger reflections. The sediment thickness is at most 20m, at the base of the steep SE valley wall (6:38-6:50)

The sonograph between 6:50-10:50 shows high backscattering in characteristic channels running NNE-SSW with linear features within the channels indicating the direction of sediment transportation, as well as erosion and slumping along the walls of the channels. The subbottom profile details these channels with a maximum depth of 400 m.

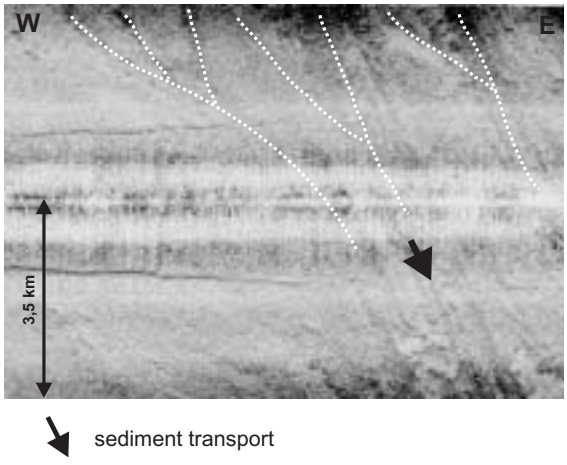

Figure 10. Fragment of OKEAN sidescan sonar line PS-291BS showing a system of converging canyons.

MAK52BS

The survey was done in the 30 kHz mode running from NW to SE and crossing seismic lines PS289BS and PS 290BS. The line was planned to cross several high backscatter patches previously described on the OKEAN sonographs. Several of them are seen on the MAK records between time marks 23:30 and 02:05 (Fig. 11). A subbotom profiler record across a well-marked, 500 m wide, patch shows a 0.5 m high elevation with a vertical acoustically transparent zone underneath. Fragments of authigenic carbonates were recovered from one of the patches which explains their nature as fields of carbonate crust formed above fluid escape sites. Faults seen on the subbottom profiler records underneath these fields are believed to be the conduits of the upwards migrating fluids.

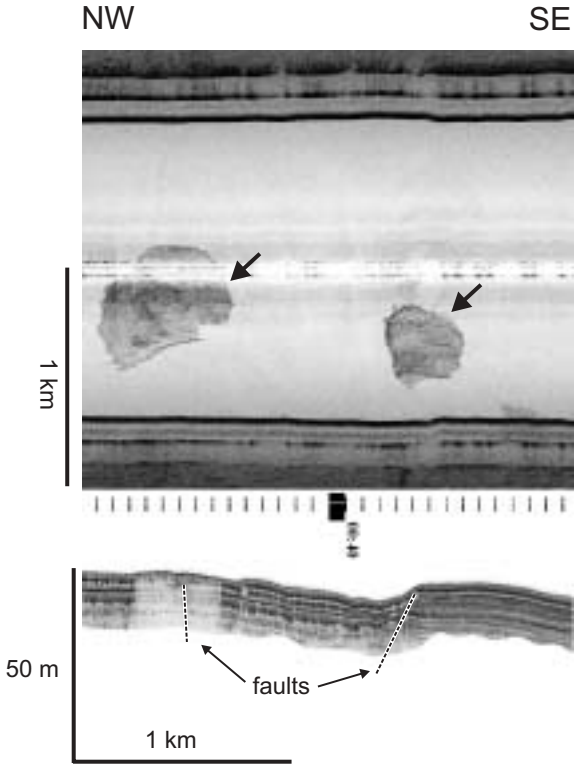

Figure 11. Fragment of 30 kHz MAK-52BS sidescan sonar sonograph and subbottom profiler record showing fault-related high backscattering fields of carbonate crusts on the seabed at a depth of 790 m.

This is in agreement with OKEAN data which also shows the fields to be preferably aligned along major faults.

Between time marks 02:40 and 03:20 the line crosses a high bacscattering, cauliflower-shaped headwall of a 3 km wide sediment collapse structure (Fig. 12). On the subbottom profiler record it corresponds to a 40 m deep, gentle depression which is partially draped with a veneer of stratified hemipelagic sediments.

I.2.4. Bottom sampling

G. AKHMANOV, A. MAZZINI, A. STADNITSKAIA, M. IVANOV, D. OVSIANNIKOV, A. SADEKOV., E. KOZLOVA, V. BLINOVA, V. TORLOV, E. POLUDETKINA, N. TYRINA, T. BESPALOVA, O. KOVALENKO AND P. STAELENS

Bottom sampling locations were chosen on the basis of the deep-towed sidescan sonar data and were mainly features interpreted as fluid escape structures. Table 1 summarises core location details and core logs can be found in Annexe I.

Kalamitian continental slope

Core BS-305G

The core was collected from the cauliflower-shaped sediment collapse structure described in the previous chapter (Fig. 12). A 603 cm thick sediment section was recovered within which units 1, 2 and 3 of the recent Black Sea sediment were recognised. The sapropel layer of unit 2 was diluted with clay laminae suggesting high input of terrigenous material during its deposition. Banded appearance of the unit 3, due to the presence of laminae of turbiditic origin, also indicated a high level of terrigenous input.

Core BS-309G

Two attempts were tried at recovering sediment at this station (Fig. 11). On the first attempt, the core catcher was empty. On the second attempt, a small amount of centimetre-sized pieces of carbonate crust were recovered.

Cores BS-306K & BS-308K

Two previous attempts with a gravity corer to retrieve any sediment from a high

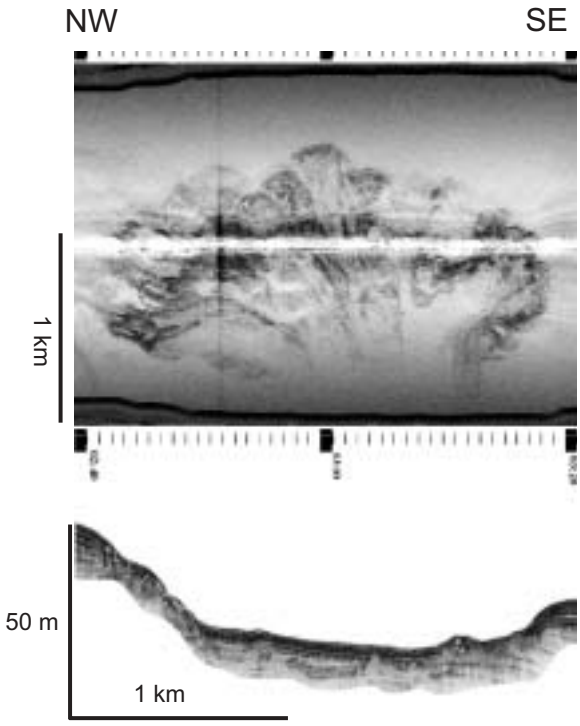

Figure 12. Fragment of 30 kHz MAK-52BS sidescan sonograph and subbottom profiler record across a large sediment collapse structure with a cauliflower-shaped headwall.

Table 1. Sampling sites of the Black Sea Leg 1

Core No	Date	Area	Latitude	Longitude	Depth (m)	Recovery (cm)	Setting
BS-305G	27.07.01	1	44°32.445	31°49.479	1031	603	Area of gas seeps on the Kalamitian continental slope
BS-306K	27.07.01		44°33.032	31°46.061	880		
BS-307GR	27.07.01		44°33.090 44°33.001	31°46.112 31°46.046	877 902		
BS-308K	27.07.01		44°32.997	31°46.046	909		
BS-309G	27.07.01		44°34.336	31°43.185	791		
BS-310GR	27.07.01		44°39.738 44°39.727	31°46.474 31°46.333	590 594		
BS-311G	28.07.01		44°25.067	32°58.490	1730	608	Crimean continental slope west of Sevastopol
BS-312D	28.07.01		44°25.871 44°26.149	32°58.747 32°58.560	1220 889		
BS-313G	29.07.01	2	43°43.620	33°28.962	1992	123	Crater of the Kornev mud volcano
BS-314G	29.07.01		43°20.341	33°26.751	2179	377	Crater of the Vassoevich mud volcano
BS-315G	29.07.01		43°20.324	33°26.752	2160	165	
BS-316G	30.07.01		43°13.835	33°43.155	2202	519	abyssal plain near Kovalevsky mud volcano
BS-317G	30.07.01		43°13.841	33°42.138	2176	94	Crater of the Kovalevsky mud volcano
BS-318GR	30.07.01		43°13.805 43°13.860	33°41.957 33°42.214	2188 2188		
BS-319G	31.07.01		43°14.013	33°42.310	2169	229	
BS-320G	31.07.01		43°14.887	33°06.199	2172	406	Crater of the TREDMAR mud volcano
BS-321G	31.07.01		43°15.018	33°06.268	2190		
BS-322G	31.07.01		43°15.016	33°06.260	2170	286	
BS-323B	31.07.01		43°14.894	33°06.200	2170		
BS-324G	01.08.01		44°23.055	35°08.610	1782	159	Mud flow from the system of parallel faults
BS-325G	02.08.01	3	44°18.787	35°04.391	2015	88	Crater of the NIOZ mud volcano
BS-326G	02.08.01		44°18.786	35°04.384	2018	191	
BS-327G	02.08.01		44°18.716	35°04.303	2028	104	
BS-328G	02.08.01		44°18.951	35°04.435	2020		
BS-329K	02.08.01		44°18.951	35°04.430	2020		
BS-330B	02.08.01		44°18.789	35°04.379	2021		
BS-331G	03.08.01		44°17.690	35°10.607	1918	166	Crater of the Kazakov mud volcano
BS-332G	03.08.01		44°17.716	35°10.618	1920	144	
BS-333G	03.08.01		44°17.671	35°10.557	1919		
BS-334GR	03.08.01		44°17.642 44°17.695	35°10.540 35°10.660	1920		
BS-335D	03.08.01		44°17.712 44°17.747	35°10.684 35°10.422	1928 1929		
BS-336G	04.08.01		44°23.011	35°09.269	1816	167	Crater of the Odessa mud volcano
BS-337G	04.08.01		44°22.843	35°09.033	1836	384	
BS-338G	04.08.01		44°22.581	35°10.459	1900	474	Mud flow from the system of parallel faults
BS-339G	04.08.01		44°22.768	35°11.031	1890	393	

backscattering patch seen on the MAK52BS sonograph (Fig. 13) were unsuccessful. During a retrieval of the second gravity core onto the ship's deck a large plume of gas bubbles was observed breaking onto the sea surface. Small slabs of debris were observed floating on the surface suggesting that the core could contain gas hydrates which dissociated during transit from the sea floor to the surface. The sediment retrieved in 306K and 308K were heavily disturbed but it was still possible to observe units 1 & 2. Small fragments (3-4 cm in diameter) and 1 large fragment (25 cm in diameter) of carbonate crust

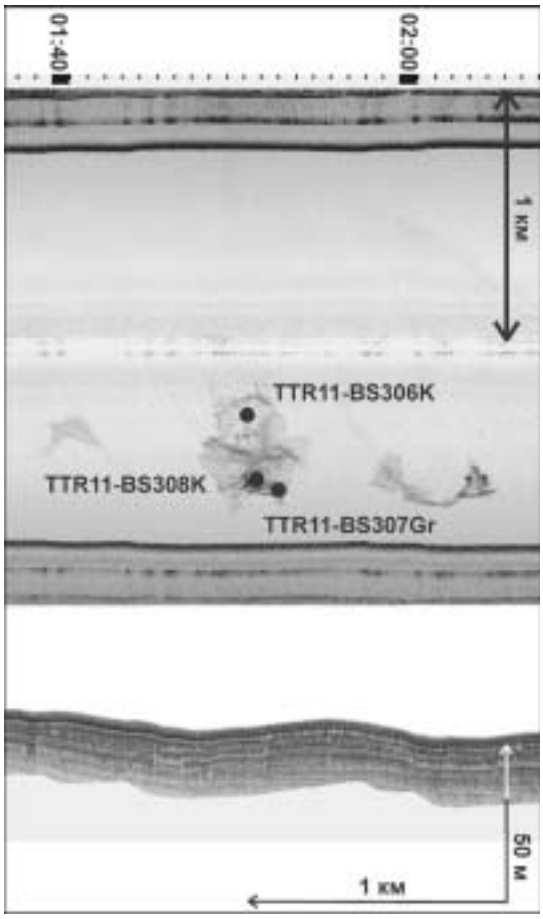

Figure 13. 30 kHz MAK52BS sidescan sonograph and subbottom profiler record with sampling sites BS306G, BS307Gr and BS308K shown.

were found in 306K. Small tabular fragments of gas hydrate (1-2 cm long and 2-3 mm thick) were observed within the sapropel layer in 308K (Fig. 14). In spite of the core disturbances, a hemipelagic character of the recovered sequences could be recognised.

BS-307GR & 310GR

An attempt to recover carbonate crust with a TV-guided grab was undertaken at station 307GR. On the first attempt, the TV grab arrived empty with small fragments of slightly lithified carbonate crust found on the external mechanism. This suggest that the thickness and competence of the carbonate crust were beyond the grab's capacity to obtain a decent sample. The second attempt (310GR) at the same place failed due to a power problem.

Section westward of Sevastopol

Core BS-311G

The sequence retrieved from the site contained sediments of units 1 and 2 which were separated by an interval of slumped material.

Dredge BS312D

The dredge was deployed in an attempt to recover carbonate crusts from the seafloor. The dredge brought up a large number of differing types of metamorphic and volcanic rock fragments, ranging in size from a few to more than 25 cm in diameter. Such a composition indicates that an outcropping basement has been dredged.

I.2.5. Conclusions

M. IVANOV, G. AKHMANOV, L. MEISNER, G. CIFCI AND O. KRILOV

Two morphologically different provinces of the north-western Black Sea continental slope can be recognised within the study Area 1: the accumulative slope formed by the Danube Fan, and the outcropping offshore continuation of the Crimean Mountains.

Relief on accumulative slopes is smooth and is characterised by the presence of gentle rises and valleys. Two valleys were detected on seismic records. They are filled

Figure 14. Gas hydrates in the Core BS308K.

with large amounts of fresh sediments and have no observable internal structure. The offshore continuation of the Crimean Mountains, which consists of rocks ranging from Triassic to Cretaceous in age, has much more abrupt relief.

On the seismic sections the eastern boundary of the thick Quaternary sedimentary pile is bounded by a narrow valley, the origin of which may be associated with a fault. In this region faults are important for fluid migration to the surface sediments. Fluid flow pathways can be identified as narrow vertical acoustically transparent columns.

These columns were recognized on the sidescan sonographs as patches of high backscatter with a diameter up to 500 m. Ñarbonate crusts and gas hydrates were recovered from these locations. Ñemented Holocene sediments appear to serve as a base of the carbonate crusts. Up to 20 cm thick crusts outcropping onto the seabed were observed on the underwater TV records. It should be noted that in this part of the Black Sea gas hydrates were recovered for the first time, from the water depth of 900 m in the absence of mud volcanoes.

Most of the studied structures were observed along faults suggesting that the latter are important conduits for the upwards migration of fluids.

Numerous sediment failures and buried debris flows indicate that a large portion of the slope was unstable and prone to hazards in the near past. The collected dataset is insufficient to evaluate to what extent it applies to the present day. The sediment failures may be related to fluid escape structures and/or caused by gas hydrate dissociation events, as is suggested for the other continental margins e.g. off Norway (Bugge et al., 1987; Mienert et al., 1998).

I.3. Central Black Sea

I.3.1. Geological setting

Area 2 is located in the deepest part (>2000 m) of the Western Black Sea subbasin adjacent to the Andrusov Ridge, separating the Eastern and Western Black Sea subbasins. This part of the basin is 190 km long and 140 km wide. It shows generally flat seafloor topography with water depths of 2100-2200 m. Mud volcanism occur in the north-eastern part of the area within a region which differs structurally from the main part of the Western Black Sea subbasin by the presence of small folds, flexures and faults.

Nine mud volcanoes were documented in this area, and seven of them were intensively studied during TTR cruises in 1991 (TTR-1) and 1993 (TTR-3) (Limonov et al., 1992; Limonov at el., 1994). Mud volcanoes located in the southern part of the area (Vassoevitch, Kovalevsky and TREDMAR) were the main target of the present survey. Post-Cenozoic sediments are mainly represented by clays and have a considerable thickness. The thickness of Cenozoic sediment is about 12 km, and the Palaeocene-Eocene is about 4 km. The Maykopian Suite (Oligocene-Early Miocene) also does not exceed 4 km, and upper Miocene-Pliocene sediments are 1.8 km. They are overlain by Quaternary sediments of about 1.8 km in thickness.

Based on the seismic records, the upper part of the sedimentary sequence is characterised by numerous fractures and small faults related to low amplitude anticlines. This is an unusual structure for both the Western and the Eastern Black Sea subbasins. Mud volcanoes were not observed in the places where fractures were absent. Mud volcanoes are well-expressed in the seafloor topography being from 20 to 150 meters high. Various acoustic anomalies (bright spots, acoustic voids, acoustic turbidity, etc.), indicating accumulations of hydrocarbons, were recognised on seismic records up to 7 km below the seafloor. Buried mud volcanoes were also identified on seismic sections. The acoustic reflectors around feeder channels are often bent down due to the velocity anomaly of gas/fluids-saturated sediments. Roots of the mud volcanism cannot be seen on the seismic records. They could be associated with the thick Maykopian clay sequence. However, there is no direct evidence for this.

I.3.2. Seismic reflection profiling

L. MEISNER, O. KRYLOV, G. A. VOLKONSKAYA, CIFCI, S. ONDER, D. DONDURUR, O. F. ELBEK, S. BOURYAK, S. SHKARINOV, AND S. OGIBALOV

Two seismic lines were shot in the area in order to cross Kovalevsky and TREDMAR mud volcanoes (Fig. 15)

PS-293BS

Line PS-293BS runs SE-NW for about 25 km, and the section shows predominantly flat lying reflectors, which are laterally consistent and uniform. Kovalevsky mud volcano is identified on the record between time marks 4:34 and 4:45 (Fig. 16).

The mud volcano is 1.2 km wide at the base and 800 m at the crest, and is 50 m high. On the subbottom profiler record the layers around the mud volcano bend downward towards it, most noticeably on the NW side where they are steeply dipping. Beneath the mud volcano there is a vertical acoustic transparent area (4:37), corresponding to the feeder channel. The feeder channel is narrow near the surface, 600 m, and widens with the visible part reaching 2.4 km width at 700 ms depth. Bright spots have been observed in the vicinity of the feeder channel indicating the presence of gas at 3.4 s, 3.3 s and 3.17 s depth.

PS-294BS

PS-294BS line runs EW for about 40 km, and can be divided into three sections, a deep fractured zone (6:30 – 7:15), a region of flat lying reflectors (7:15 – 9:03), and TREDMAR mud volcano. The seismic section shows two different units, the upper member (UM) and the lower member (LM) as detailed in TTR3 (Limonov et al., 1994). The division between the two can be observed at 3.3 s, as a strong horizon. Two other horizons can be identified in the UM at around 3.2 s and 3.0 s.

The fracture zone (6:30 – 7:15) has strong reflectors indicating possible free gas trapped beneath (Fig. 17). Several possible

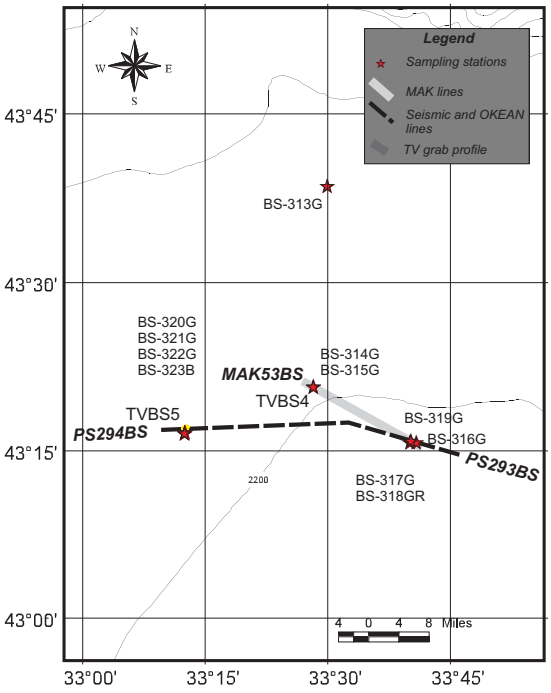

Figure 15. Location map of the Leg1, Area 2.

explanations have been put forward: a new mud volcano developing, the rising diapir below the visible section disturbing the layers above; the seismic section cuts through the edge of a buried mud volcano as they have been described 20 km from the present location (Limonov et al., 1994); a gas trap that has developed in the area because of locally high concentrations of free gas. Disturbances from this feature only affect the lower part of the section below 3.2 s depth, however other near surface faults directly above this area are observed on the subbottom profile (6:45), as small near vertical faults.

Horizontal layers continue across the seismic section (7:15–9:03) with a strong intermittent reflector at the sea floor (8:00–8:50). Subbottom profiler records show that recent sediments pinch out on the flanks of the mud volcano (7:20–7:50). A shallow fault is also observed (8:22) forming a 4 m high escarpment on the seabed.

TREDMAR mud volcano was crossed by the seismic profile at 9:10 (Fig. 18). It is a mound 60 m high, and 1.5 km wide at the base. A small depression is visible at the surface of the eastern side of the mud volcano corresponding to the rim already observed on the previous TTR3 MAK line. Around the feeder channel depletion of reflectors can

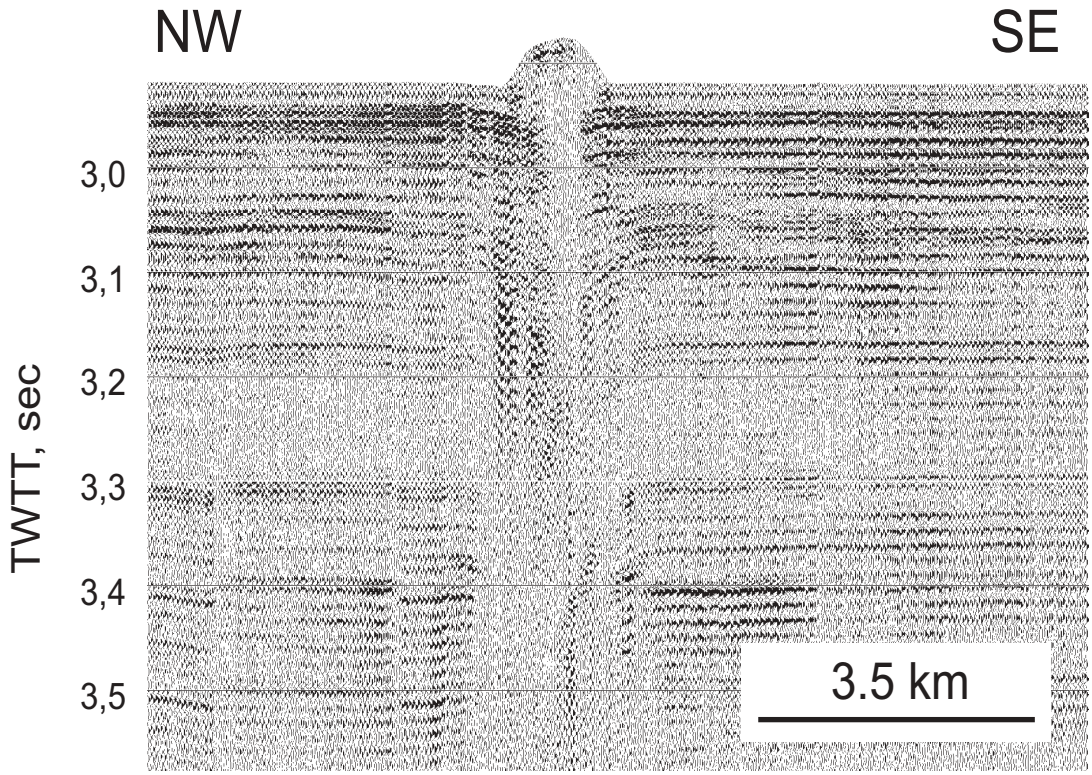

Figure 16. Fragment of seismic line PS-293BS across the Kovalevsky mud volcano.

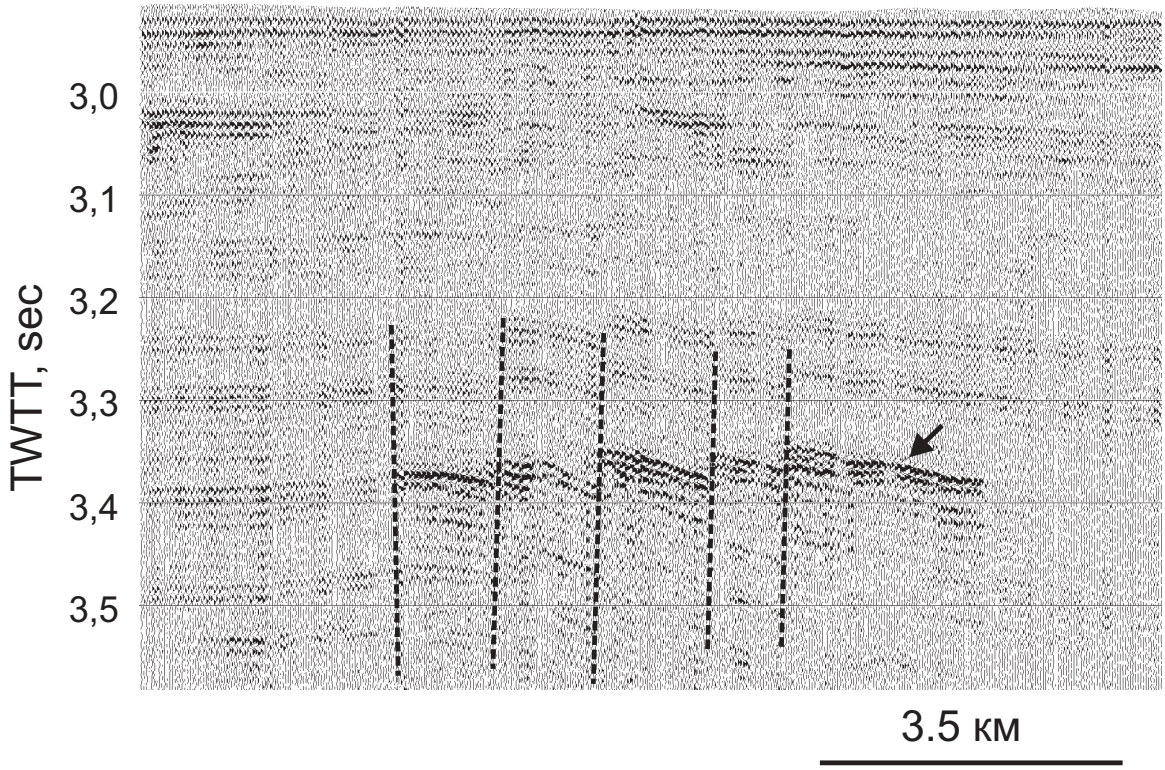

Figure 17. Fragment of seismic line PS-294BS showing a deep fault system with an associated bright spot (arrow).

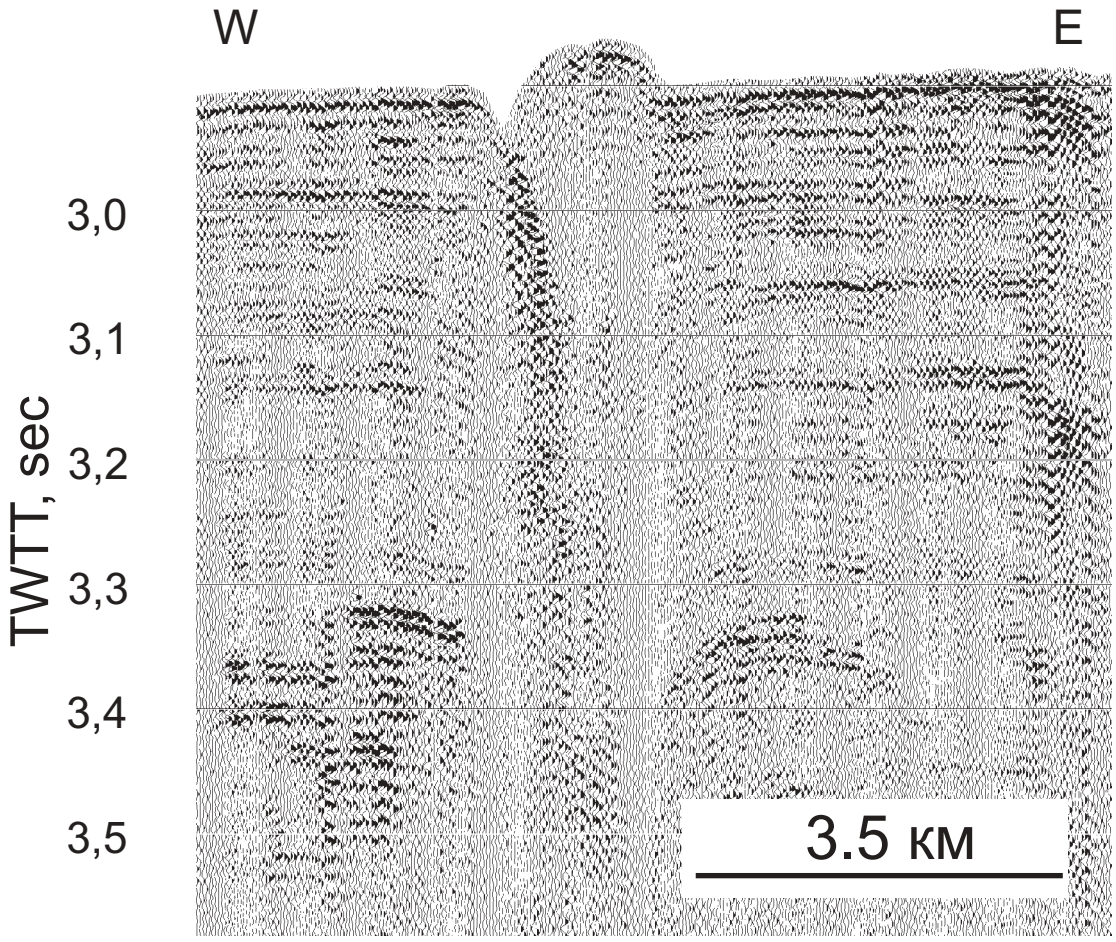

Figure 18. Fragment of seismic line PS-294BS across the TREDMAR mud volcano.

also be observed in the same way as around the Kovalevsky mud volcano The feeder channel is about 2 km wide and shows small variations in width with depth, a slight widening down section is also observed. This seems to be a common feature for all mud volcanoes studied in this area. A bright spot related to a fault system was observed at the depth of 3.3 s on the eastern side (Fig. 18). This is the first observation of a bright spot in the vicinity of the TREDMAR.

I.3.3. Sidescan sonar survey

L. MEISNER, O. KRYLOV, A. AKHMETZHANOV, P. SHASHKIN, M. IVANOV, G. CIFCI, S. ONDER, D. DONDURUR, AND O. F. ELBEK

MAK line 53BS

Line MAK 53BS was run from NW to SE for about 30 km. It crossed the Vassoevitch mud volcano at 5:20 and the Kovalevsky mud volcano at 12:00.

The Kovalevsky mud volcano

The sonograph across the Kovalevsky mud volcano (Fig. 19) shows a radial pattern of very high backscattering mudflows, which probably are formed during recent events and still not draped by a hemipelagic veneer. The mud flows extend the diameter of the structure up to 1200 m. Older, less backscattering, mudflows, can be observed in some places in the central part and on the western side of the feature. Some of them are overlaid by more recent mudflows. A NW-SE oriented ridge on the top of the mud volcano produces an extended shadow on the sonograph and multiple hyperbolic reflections on the subbottom profiler record. The mud volcano is a 40 m high, 900 m wide mound and is represented by transparent acoustic facies sug-

gesting the lack of the internal structure. On the subbottom profiler record it has an asymmetrical shape with slopes of about 4.7° on the southeastern side and 8.5° on the northwestern side. On the outer parts of the mud volcano, the profiler record shows mud flows interbedded into the surrounding hemipelagic sequence. Almost 45 m of the hemipelagic sequence is seen and the beds are slightly bent downward towards the feeder channel. The sequence is disturbed on the western side of the mud volcano by normal faults with an offset of 2 to 4 meters. These faults are shown on the sonograph as semicircular enhanced backscatter rims around the mud volcano and are inferred to be due to subsidence.

The Vassoevitch mud volcano

The Vassoevitch mud volcano is seen on the sonograph as an area of variable

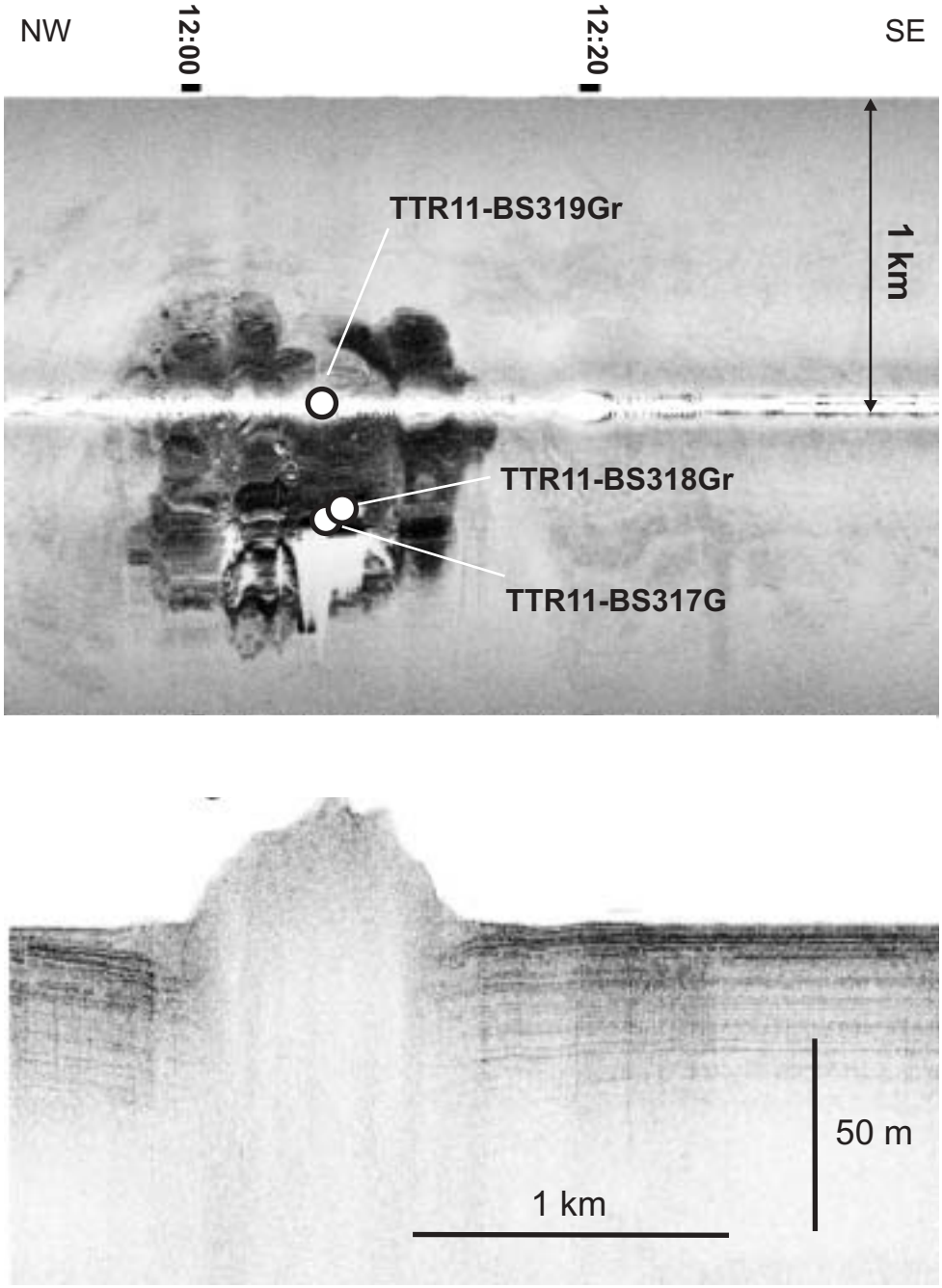

Figure 19. Fragment of 30 kHz MAK-53BS sidescan sonar sonograph and subbottom profiler record across the Kavalevsky mud volcano. Sampling stations are shown.

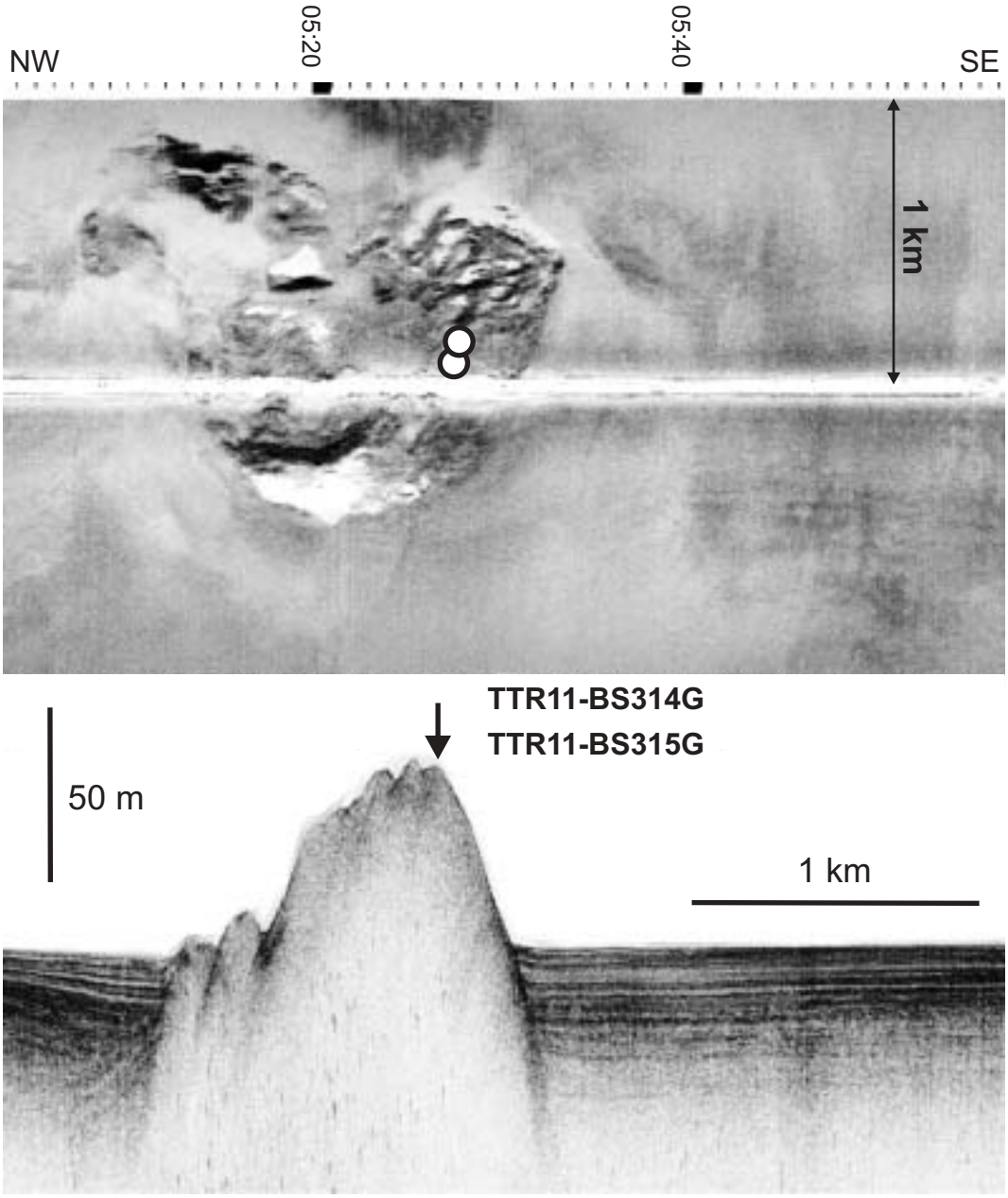

Figure 20. Fragment of 30 kHz MAK-53BS sidescan sonograph and subbottom profiler record across the Vassoevich mud volcano. Sampling stations are shown.

backscatter with irregular outline (Fig. 20). The average backscatter level is not as high as for Kovalevsky mud volcano. On the southwestern side of the volcano an escarpment is seen as a high backscattering semicircular feature; 415 m wide with a talus of collapsed sediments expanding for about 1 km to the north.

On the subbottom profiler the mud volcano is represented by typical acoustically transparent facies, is 2 km wide and 60 m high. The contact with surrounding hemipelagic sequence is sharp and on the eastern side layers are bent upwards at the contact, suggesting that extrusive processes took place during the mud volcano's formation. On the western side the hemipelagic sequence dips toward the mud volcano as a result of subsidence.

The morphology of the edifice is effected by the collapse of it western flank with the remaining eastern flank being 20 m higher. The undisturbed slope of the eastern flank is 9.5° and the collapsed slope is 4.1°.

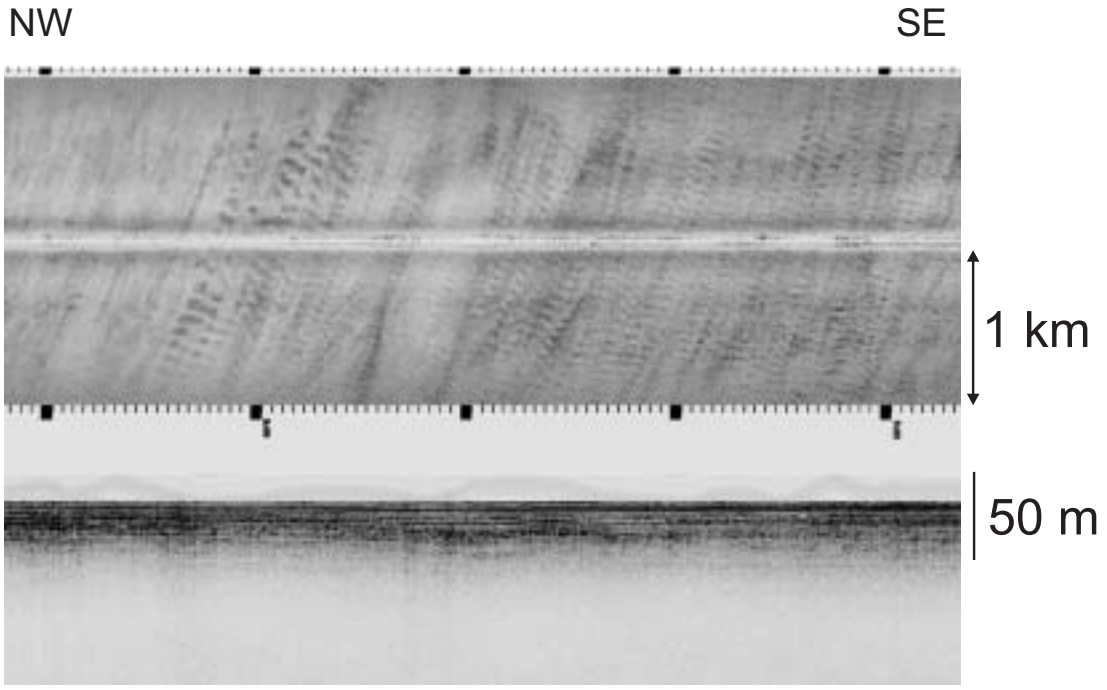

Figure 21. Fragment of 30 kHz MAK-53BS sidescan sonograph and subbottom profiler record showing turbidity current pathways on the Black Sea abyssal plain.

The abyssal plain

Between both mud volcanoes (6:20-11:40) the sonograph shows a seabed lineation of low to medium backscatter broad bands with a rippled pattern. These features are interpreted as turbidity flow pathways, with a sediment transport direction from N to S (Fig. 21).

The subbottom profiler shows a completely flat seafloor in this area. A parallel well-bedded sequence is in some places disturbed by wipe-out of the acoustic signal, probably due to gas presence in the sediments.

I.3.4. Bottom sampling

G. AKHMANOV, A. MAZZINI, A. STADNITSKAIA, M. IVANOV, D. OVSIANNIKOV, A. SADEKOV., E. KOZLOVA, V. BLINOVA, V. TORLOV, E. POLUDETKINA, N. TYRINA, T. BESPALOVA, O. KOVALENKO AND P. STAELENS

A total of eight cores were taken from Kornev, Vassoevich, Kovalevsky and TREDMAR mud volcanoes and one reference core was taken from the abyssal plain (Table 1, Annexe I).

Core BS-316G

This core contained a typical hemipelagic sequence with units1, 2 and 3. The sequence also contained a large number of turbidites of different thickness which were observed in all three units.

Core BS-313G (Kornev mud volcano)

This core recovered a silty clayey, matrix supported mud breccia (clasts < 2 cm) covered by a 50 cm thick hemipelagic sequence with units 1 and 2.

Cores BS-314G & BS-315G (Vassoevich mud volcano)

The cores recovered mud breccia overlaid by hemipelagic sediments of units 1 and 2. The presence of unit 3 was also noticed in the Core BS-314G. Fragments of lithified carbonate crust were found at the base of the hemipelagic sequence.

Cores BS-317G, BS-319G & BS-318GR (Kovalevsky mud volcano)

These two cores and a grab recovered hemipelagic sediments of units 1 and 2 and mud breccia. Accumulations of gas hydrates was found in the mud breccia interval at the base of the cores. Clasts from the mud brec-

cia were well rounded and friable. Their average size did not exceed 0.5 cm and they seemed to increase in amount downcore.

Cores BS-320G, BS-321G, BS-322G, BS-323B (TREDMAR mud volcano)

The samples recovered from the crater of TREDMAR were remarkably different from the other mud volcanoes. Most of the cores contained stiff mud breccia with no, or very little, hemipelagic draping. Cores BS-320G and BS-321G recovered a 80-cm thick homogeneous water-saturated clay layer, which probably is a muddy turbidite, on the top of the mud breccia interval.

I.3.5. Conclusions

M. IVANOV, G. AKHMANOV, L. MEISNER, G. CIFCI AND O. KRILOV

Results of the TTR-11 cruise provided more details on the mud volcanoes of the Central Black Sea, and expanded the data set collected during TTR-1 and TTR-3 cruises. New seismic and high resolution sidescan sonar data provided new insights on the morphology and internal structure of hitherto poorly studied mud volcanoes.

Different morphologies of mud volcano edifices were observed. Each morphology may represent a particular stage of the evolution of an individual mud volcano. Kovalevsky mud volcano, for instance, probably has been formed relatively recently and its cone-shaped edifice is still well preserved. The TREDMAR mud volcano could be an older structure and most of the cone has already collapsed. The character of such collapse is not very clear. Catastrophic explosions resulting in destruction of mud volcanoes are known from on-land (Shniukov et al., 1971). Another scenario could consider a less dramatic event when a presumably dormant mud volcano gradually collapses under its own weight. Fractures often observed on the submarine mud volcanoes, and serving as conduits for migrating upward fluids, can facilitate such a collapse.

I.4. Southeastern Crimea margin (Sorokin Trough)

I.4.1. Geological Setting

Area 3 is located on the continental slope of the southern Crimean Peninsula within the Sorokin Trough. The Trough lies at the depth range of 600-2100 m. It is filled with Oligocene-Miocene sediments and was formed during Oligocene-Early Miocene time. Structurally the Sorokin Trough is a foredeep stretching along the folded and thrusted Crimean Mountain Belt. To the south it is bounded by the Tetyaev Ridge, an uplift of Mesozoic-Lower Palaeogene rocks. The Maykopian clays form numerous diapiric folds in the trough, and exceed 5 km in thickness. Thrusting often occurs in the southern flanks of many diapirs. The Upper Pliocene-Quaternary sediments of the paleo Don/Kuban fan overlie the eastern section of the area (Tugolesov et al., 1985).

During the last two decades, both CDP and single channel seismic surveys were carried out in the Sorokin Trough by researchers from the MSU, Yuzhmorgeologia, and Sevmorgeologia. In 1996 the ANAXIPROBE/TTR-6 cruise also investigated the Sorokin Trough. As a result of these studies (Woodside et al., 1997), it was established that the inner structure of the Sorokin Trough was produced by lateral compression in the SE-NW direction due to the movement of the Shatsky Ridge and the Tetyaev Uplift. Overpressured fluids are responsible for the formation of mud volcanoes in the area. Gas hydrates were recovered from some of them during the ANAXIPROBE/TTR-6 cruise.

I.4.2. Seismic reflection profiling

L. MEISNER, O. KRYLOV, G. A. VOLKONSKAYA, CIFCI, S. ONDER, D. DONDURUR, O. F. ELBEK, S. BOURYAK, S. SHKARINOV, AND S. OGIBALOV

High resolution seismic reflection profiling was carried out along 4 lines (PS-295BS to PS-298BS) (Fig. 22). Line PS-295BS was shot parallel to the southeastern

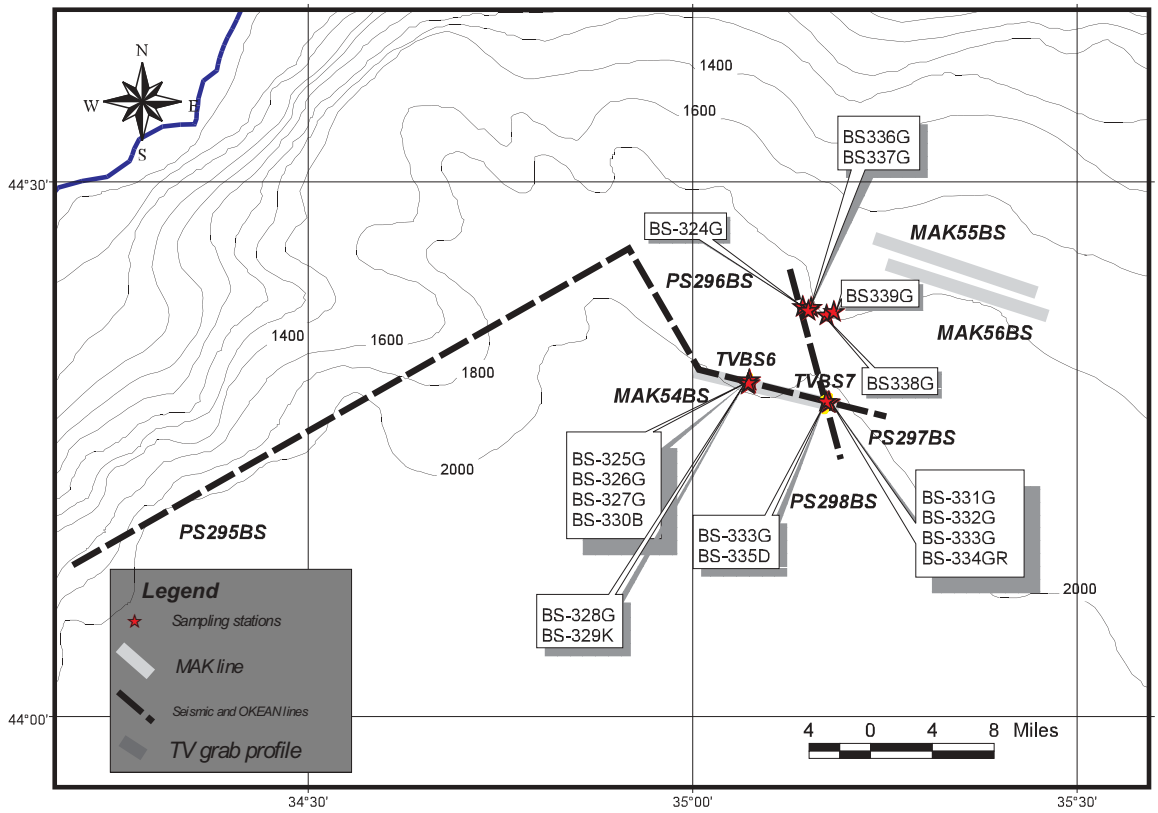

Figure 22. Location map of the Leg 1, Area 3.

Crimean coast in the direction SW-NE. Line PS-296BS runs perpendicular to PS-295BS. Lines PS-297BS and PS-298BS in order to cross Kazakov mud volcano in E-W and N-S directions.

PS-295BS

The profile is about 60 km long and runs in the SW-NE direction. The seafloor along the profile is irregular and varies in depth from 2000 m in the SW to 1660 in the NE.

A section of the line between 12:10 and 13:30 mainly shows a layered and folded sediment sequence, 1 km thick. There is a cyclic interbedding of well-layered and more acoustically transparent intervals. Several structures can be recognised on the seafloor. A 60 m high escarpment produced by an outcropping fault is seen at 13:40. Several small hyperbolic reflections observed at 13:50 are caused by small scale roughness of the seabed above the shallow top of a diapir.

Within a section from 13:30 to 16:00 transparent facies become more common and mud diapirs are abundant. Between 14:20 and 15:20 a large diapir formed by Maykopian Clays (Lower Miocene) can be observed (Fig. 23). A smaller diapir is also visible near timemark 15:30 at a depth of 3.2 s. Above this diapir there is a vertical zone of acoustic wipe-out reaching the seafloor. The formation of such a zone is usually attributed to fluid migration pathways and may correspond to seepage on the seafloor.

PS-296BS - PS-297BS

These two profiles run NW-SE and E-W respectively, crossing two mud volcanoes. PS-296BS was run perpendicular to PS-295BS and the same alternating layered and transparent acoustic facies previously described can be recognized.

Mud volcanoes

Two mud volcanoes studied during the TTR-6 cruise (Woodside et al., 1997) are seen. The larger one is Kazakov mud volcano, and the smaller one is NIOZ (Fig. 24).

Kazakov mud volcano (18:25) is 140 m high and 1.8 km wide, has a conical shape with steep flanks. It is interesting to note that of both mud volcano their bases lie deeper on

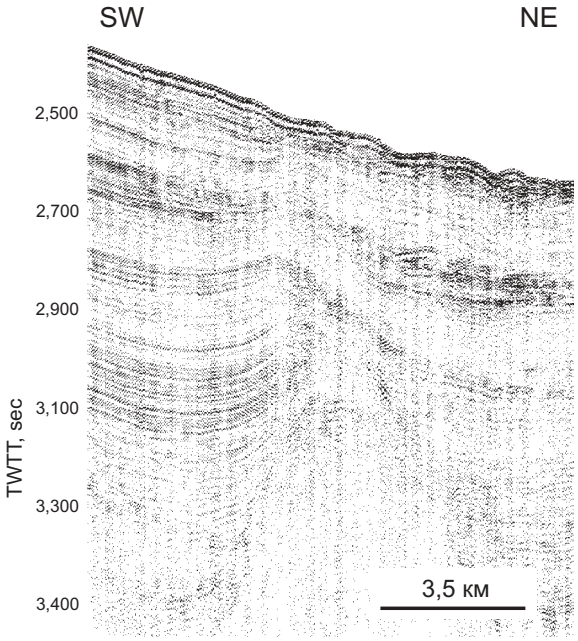

Figure 23. Fragment of seismic line PS-295BS across a diapiric structure in the Sorokin Trough.

the west side than on the east side, and in the case of Kazakov the difference is 45 m. The feeder channel is seen as a weak vertical transparent acoustic facies, has a width of 2 km and does not show any variation of width with depth. Roots of the mud volcano are not visible in the section but the feeder channel can be identified to a depth of 3.4 s TWTT. Reflectors adjacent to the feeder channel do not bend down, unlike those surrounding mud volcano feeder channels in Area 2.

NIOZ mud volcano (17:40) is imaged by the seismics as a conical feature, 70 m high and 1.2 km wide. A 1.2 km wide feeder channel develops from the top of a rising diapir at a depth of about 3.5 s TWTT.

PS-298BS

This profile is run perpendicular to PS-297BS (N-S) and crosses the Kazakov mud volcano in the N-S direction. The mud volcano is seen in the southern section of the line as a 140 m high and 2.5 km wide mound. The line also shows that its base is found deeper on the northern side.

To the north the seafloor gently rises due to the presence of a large diapiric ridge topped by a mud volcano (Odessa) seen on the record at (21:03) (Fig. 25).

I.4.3. Sidescan sonar survey

L. MEISNER, O. KRYLOV, A. AKHMETZHANOV, P. SHASHKIN, M. IVANOV, G. CIFCI, S. ONDER, D. DONDURUR, AND O. F. ELBEK

Line MAK54BS

Line MAK54BS was run almost in a W-E direction for about 15 km, roughly par-

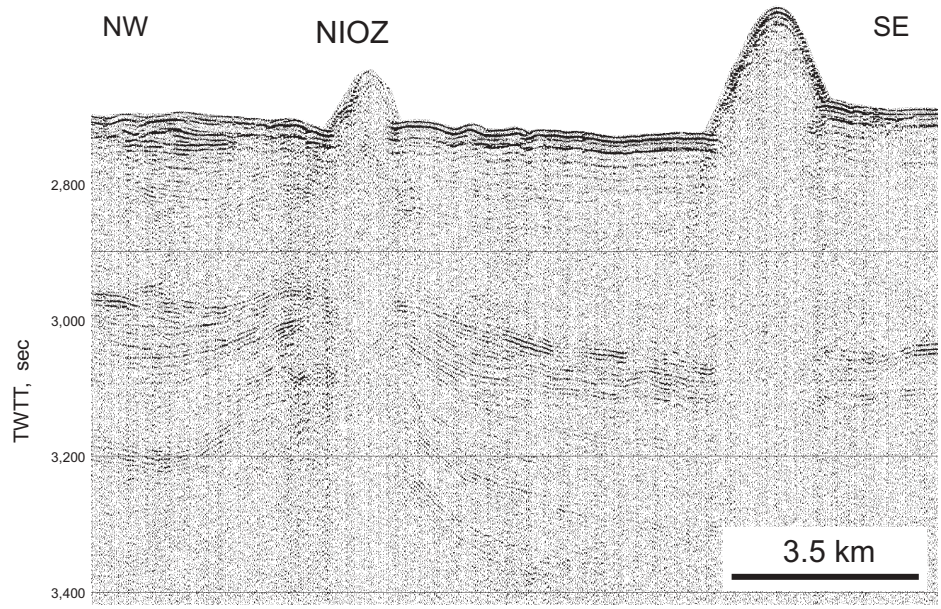

Figure 24. Fragment of seismic line PS-297BS across NIOZ and Kazakov mud volcanoes.

allel to seismic line PS-297BS. It crossed Kazakov mud volcano at 23:20 GMT and NIOZ mud volcano at 21:50 GMT.

NIOZ mud volcano

The mud volcano is seen on the sonograph as a highly backscattering ridge 1 km long and 600 m wide with N-S orientation. It is about 75 m high and its slopes are about 11°. There is no penetration on the subbottom profiler record across the mud volcano (Fig. 26).

On either side of the volcano, the subbottom profiler shows a layered sequence of high amplitude reflectors up to 40 m thick with several internal unconformities, truncations of the stratified sediments and undulation of the layers. Numerous evidence for active sediment transport by turbidity flows are seen on the sonograph including sediment waves and "chevron"-shaped bedforms. The profiler record indicates that the latter appear to be positive features up to 1 m high and probably belong to a class of barchan dunes. Bedforms indicate that the flows run from the NE to the SE. The well-layered sequence with undulating surface corresponds to a field of large mud waves which can be observed on the multibeam echosounder data. Similar mud waves were reported from many other turbidite systems in the world (e.g. McHugh and Ryan, 2000; Nakajima et al., 1998; Migeon et al., 2001). The well-layered sequence is underlain by an acoustically transparent unit up to 25 m thick which pinches out to the west. Its origin is not very clear and could be related to an older episode of NIOZ eruptive activity with numerous mud flows spreading from the mud volcano.

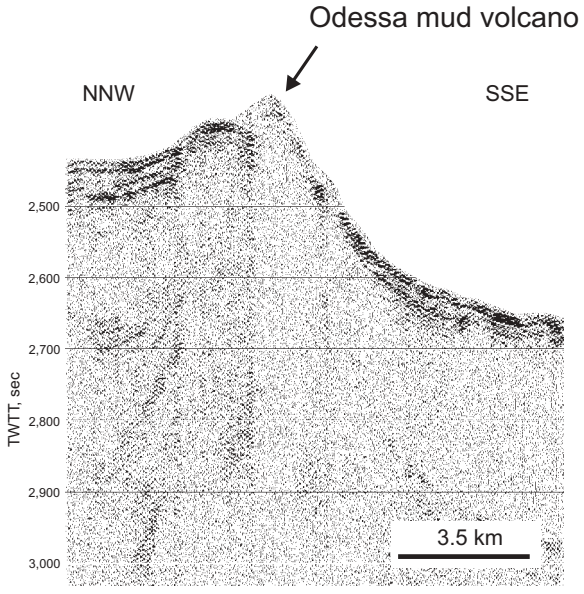

Figure 25. Fragment of seismic line PS-298BS showing Odessa mud volcano developing on the top of a diapiric ridge.

Kazakov mud volcano

Kazakov mud volcano is seen on the sonograph as a 1.5 km wide elongate patch of high backscatter (Fig. 27). It has a common appearance for a mud volcano, with a well-developed circular crater on the top and fields of mud breccia on the peripheral parts. Several concentric features seen within the crater probably represent ridges formed by extruding mud breccia or subsidence cracks. The mud volcano is seen on the subbottom profiler record as a 140 m high mound with 8.1° slopes. As for the NIOZ mud volcano, the record does not show any penetration across the structure. Large fields of mud breccia are seen on the northwestern (Fig. 28) and southeastern flanks of the mud volcano, which explains its ellipsoidal shape on the EM12S reflectivity map.

Sidescan sonar data show that Kazakov is located on the pathway of bypassing turbidity currents, evidence of which are seen immediately to the west of the mud volcano. Sediment waves and "chevron" dunes indicate that the flows are sourced from the northeast. The flows must have been sweeping the area for a while, thus preventing deposition of hemipelagic sediments. Monotonous, low backscattering seafloor seen on the sonograph to the east of the mud volcano apparently is not affected by the flows and as a result the sedimentary cover here is 40 m thicker than on the western side. The subbottom profiler record, however, does not show as much penetration here as would be expected. This may indicate that the deposited sequence lacks any internal structure or that the sediments are gas-

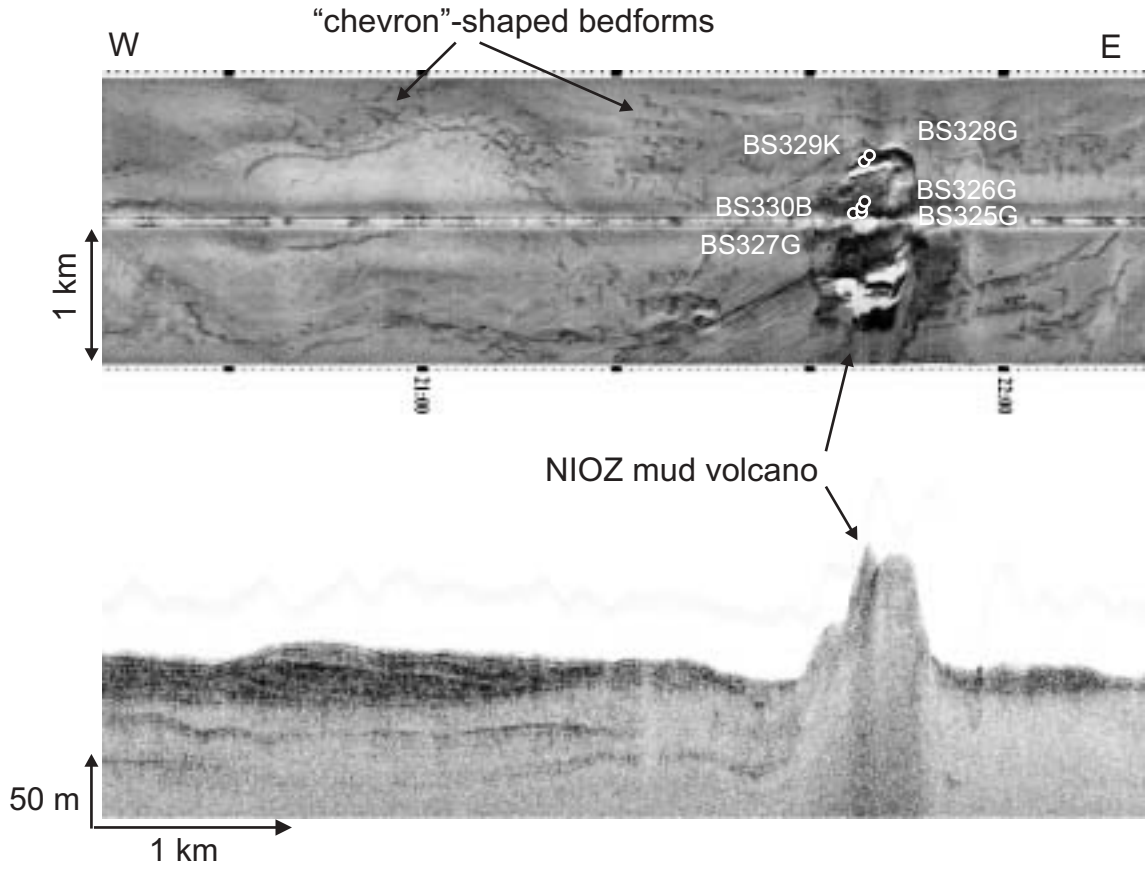

Figure 26. Fragment of 30 kHz MAK-54BS sidescan sonograph and subbottom profiler record across NIOZ mud volcano. Sampling stations are shown.

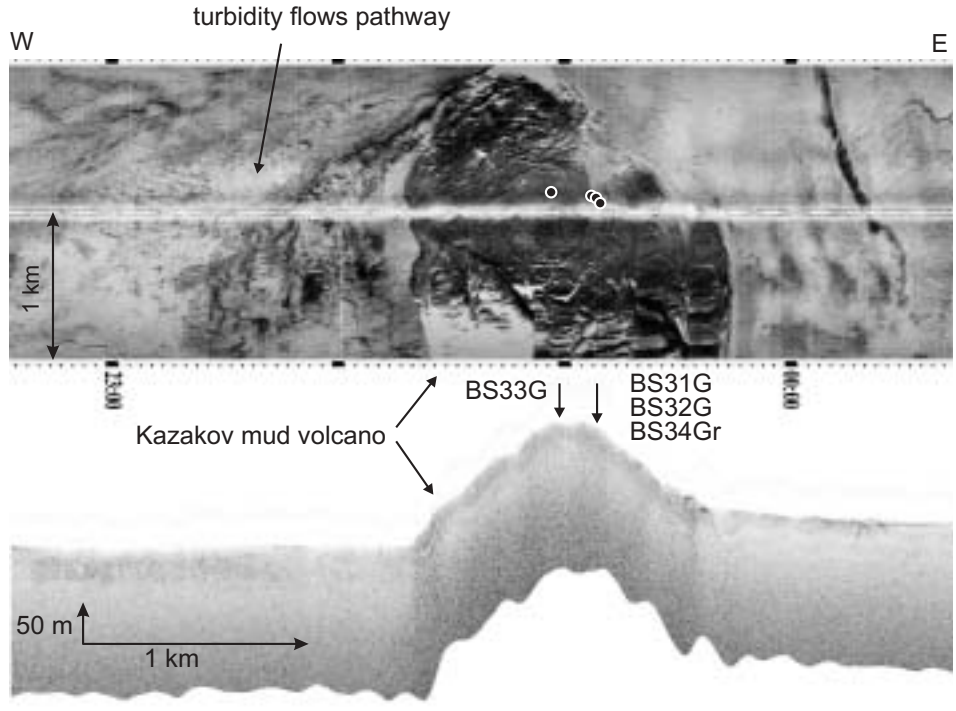

Figure 27. Fragment of 30 kHz MAK-54BS sidescan sonograph and subbottom profiler record across Kazakov mud volcano. Sampling stations are shown.

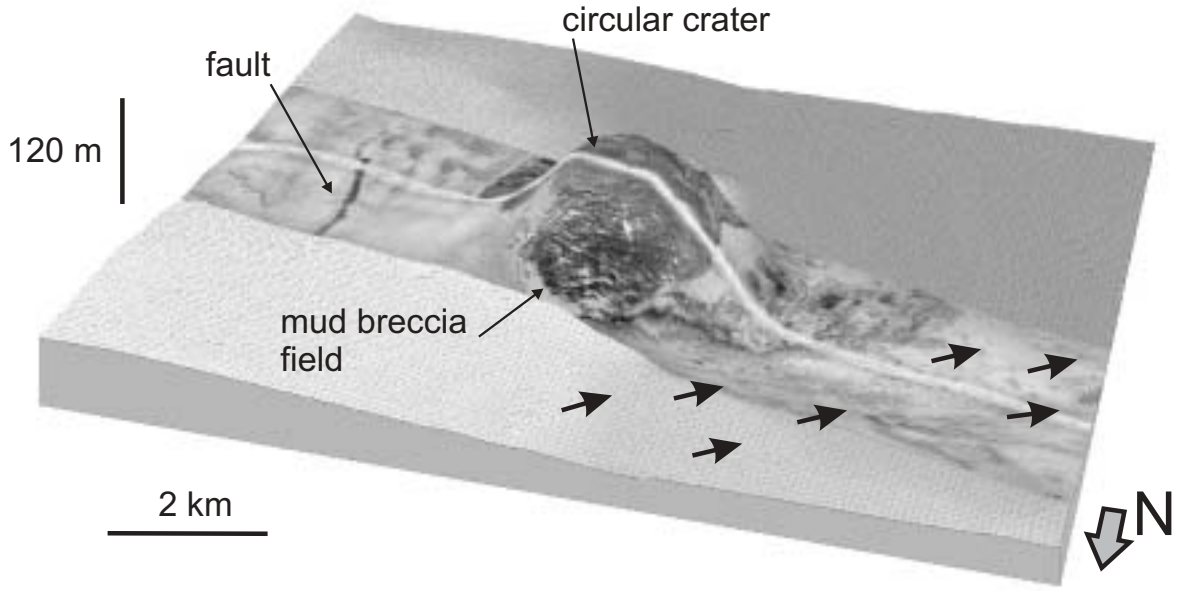

Figure 28. 30 kHz sidescan data draped over EM12S bathymetry of Kazakov mud volcano. A large field of mud breccia is seen on the northwestern slope. Arrows indicate turbidy flow pathways.

saturated which causes a significant attenuation of the acoustic signal.

In the area between both volcanoes, a fault, NE-SW trending, runs from 22:10 on one side of the sonograph until 23:00 on the other side, and can also be observed on the subbottom profiler as a small depression in the seafloor (22:40).

Lines MAK 55BS and MAK56BS

Two MAK-1 lines were run in a N-SE direction roughly parallel to the slope in water depth of 1700-1800 m. 2 km spacing ensured partial overlapping of the lines and an acoustic map of the seafloor has been produced by mosaiking of the two sonographs.

On the NW of the map the seafloor is characterised by generally low backscatter. There is a banded pattern at the very western end of the line MAK55BS which corresponds to a field of mud waves, also identified on the EM12S bathymetry.

A mud volcano, named Tbilisi, is observed near the western end of the line MAK 56BS. It is 50 m high, 500 m wide and has a conical shape with steep flanks (Fig. 29). No reflectors can be observed under the mud volcano on the subbottom profiler record. Chaotic hyperbolae on the top of the mud volcano suggest rugged topography. Adjacent to the volcano there is an acoustically bedded sequence of strong, parallel reflections up to 20 m thick A high backscattering mud flow spreading for about 600 m in to the basin is observed on the southwestern flank of the volcano.

In the middle part of the map (between 35°18′E and 35°24′E) the seafloor is characterised by a complex pattern of medium to high backscatter. The subbottom profiler shows that this area is a rise formed by a diapiric ridge. The ridge is clearly seen on the multibeam bathymetry data to have a W-E trend. The situation is complicated by the presence of a large submarine canyon approaching the rise from the northeast. The canyon is displayed on the EM12S reflectivity map as a well-marked, high backscattering feature which suggests that it certainly has been active in the near past and may still be active today. The last assumption is confirmed by the newly acquired subbottom profiler data showing active seabed erosion along the top of the ridge (Fig. 30). The record does not show much penetration here which could be due to the acoustical properties of the outcropping stiff clay. The sonograph also shows lineation and erosional grooves, all indicating that the seabed is affected by bypassing gravity flows. East from the ridge the backscatter level becomes

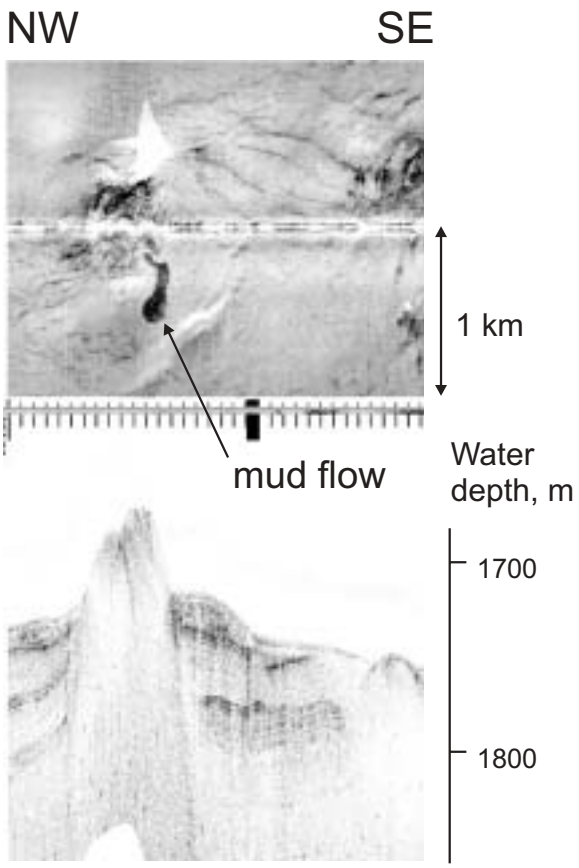

Figure 29. Fragment of MAK-56BS line across Tbilisi mud volcano.

low again and the profiler registers a well-stratified sedimentary sequence up to 25 m thick (Fig. 30). A field of "chevron" dunes is seen here on the sonograph. The dunes have dimensions of about 100 m between wing tips and indicate sediment transport to the southwest. Another mud volcano (Istanbul) is observed on the eastern end of the MAK56BS line. It has a similar morphology to Tbilisi being 50 m high and 700 m wide. Istanbul is crowned by a circular crater, which gives a flat-topped appearance to the structure on the subbottom profiler record. The volcano is surrounded by a 10-20 m deep rim which could have been formed as a result of subsidence of the edifice or is a kind of erosional moat formed by the bypassing turbidity currents. The fact that the similarly located, apart from being outside of a sediment pathway, mud volcano Tbilisi does not have such a rim may favour the latter explanation.

I.4.4. Bottom sampling

G. Akhmanov, A. Mazzini, A. Stadnitskaia, M. Ivanov, D. Ovsiannikov, A. Sadekov., E. Kozlova, V. Blinova, V. Torlov, E. Poludetkina, N. Tyrina, T. Bespalova, O. Kovalenko and P. Staelens

A total of 16 sampling stations were identified on the basis of the MAK-1 high-resolution deep-towed sidescan sonar data (Table 1, Annexe I). The sampling confirmed the presence of two mud volcanoes, assumed from previous expeditions, which were named NIOZ and Odessa.

Core BS-324G

The recovered sequence from a suspected mudflow consisted of laminated layers of clay with hydrotroilite. The top 4 cm of the sample contained mud breccia. However, during the retrieval of this core the pulley cable became entangled in the gravity corer weights and as a result the corer was raised out of the water upside down. It is possible that the soft, water-saturated uppermost section of the core was lost.

Core BS-325G (NIOZ mud volcano)

An 88 cm long sedimentary section was recovered. The core was topped by a 12 cm interval of soft mud breccia. Below an interval of stiff, hydrotroilite-bearing clay overlain by a thin layer of carbonate crust was seen. The latter interval probably represents older mud breccia.

Core BS-326G& BS-327G (NIOZ mud volcano)

Both these cores contained 5-7 cm thick intervals of unit 1 sediments overlaying dense silty clay of unit 3. Microfaults and mud chips were observed within the lower interval suggesting some slumping activity. A carbonate crust was found on the boundaries between units in Core BS-327G.

Cores BS-329K & BS-330B (NIOZ mud volcano)

These cores were similar to the above cores. However, the depth of unit 1 was slightly greater and the underlying clay had no structure and no evidence of slumping.

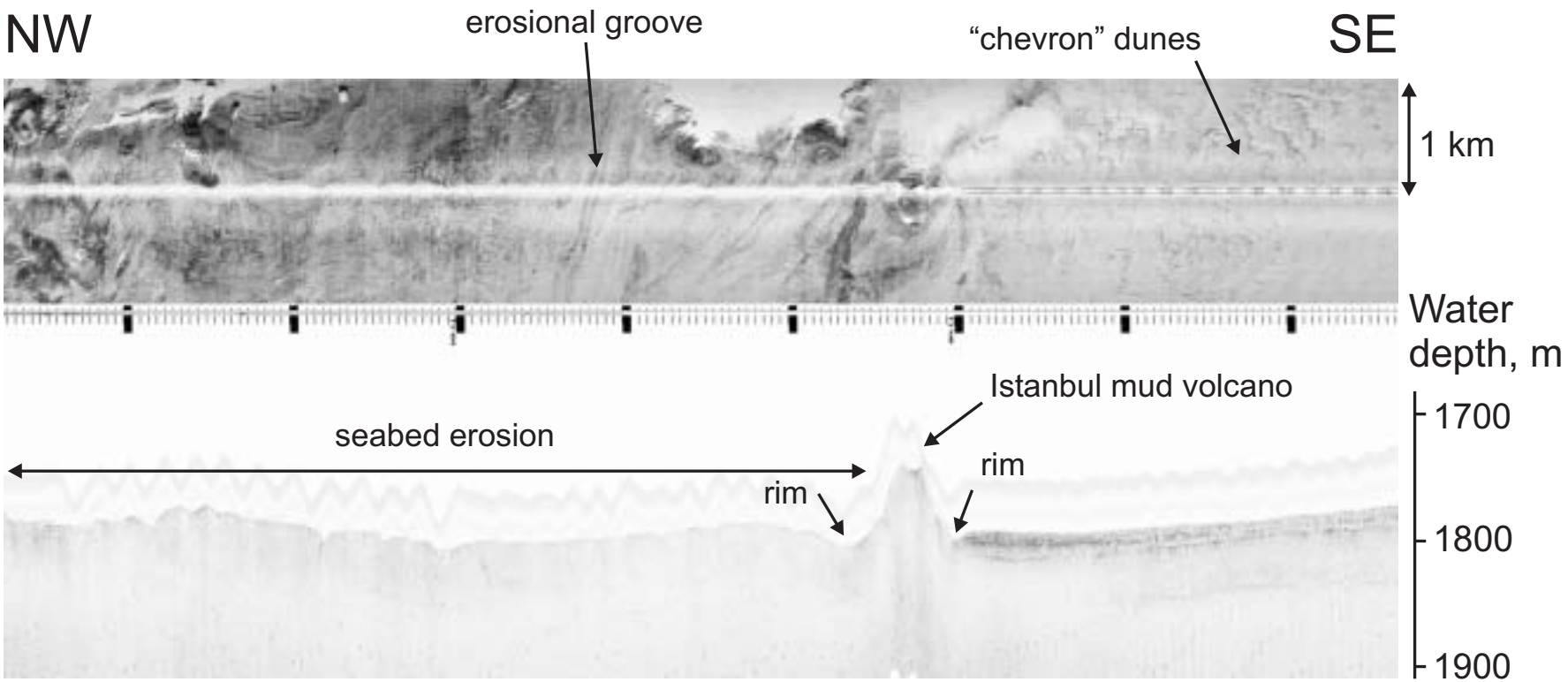

Figure 30. Fragment of MAK-56BS line across the outcropping diapiric rise, Istanbul mud volcano and adjacent seafloor with field of "chevron" dunes.

Core BS-328G

No sediment was recovered due to a large fragment of carbonate crust blocking the core catcher. Bacterial mats were found on this crust

Cores BS-331G, BS-332G and BS-334GR (Kazakov mud volcano)

All these cores recovered mud breccia with very little hemipelagic draping. Small leaf-shaped gas hydrates were found on the base of BS–332G. All samples contained a variety of clasts of differing lithology and roundness with BS-334GR containing clasts with sizes ranging from 1 to 5 cm in diameter. Fragments of carbonate crust were also found in BS-334GR.

Core BS-333G and BS-335D

Almost no sediment was recovered an these stations except small fragments of carbonate crust found in the dredge net.

Cores BS-336G, BS-337G (Odessa mud volcano)

All cores contained units 1, 2 and 3. Leaf and vein-shaped aggregates of gas hydrates were found in the lower section of the cores. In core BS-337G there was evidence of slumping within different intervals. Thin turbidites were observed in the cores BS-336G and BS-337G. Carbonate crusts were found in all cores usually at the boundary of unit 1 and 2.

Cores BS-338G, BS-339G

Units 1, 2 and 3 were recovered. Microfaulting and irregular boundaries observed within Core BS-338G suggest slumping activity.

I.4.5. Conclusions

M. IVANOV, G. AKHMANOV, L. MEISNER, G. CIFCI AND O. KRILOV

New seismic records were obtained across Kazakov and NIOZ mud volcanoes. Kazakov mud volcano has deeper roots which lie below the penetration of the seismic system used and were not observed on the records. NIOZ mud volcano crowns a large diapir seen on the seismic image.

An area of complex interaction between growing clay diapirs and bypassing turbidity currents was observed during high resolution deep-towed sidescan sonar survey. Some of the mud volcanoes showed evidence of recent activity. Gas hydrates and carbonate crusts recovered from many of them suggest active seepage of fluids enriched in hydrocarbons take place at the present time.

I.5. Geochemical sampling

I.5.1. Introduction

The aims of the geochemical programme and the methods used during the first leg of the cruise were focused on the two different topics. The first was directed towards petroleum geochemical perspectives. It included subsampling for identifying the source/nature and intensity of up-going fluid via investigation of hydrocarbon gas and organic matter from gas saturated sediments and mud volcanic deposits (mud breccia matrix and rock clasts).

The second part of the geochemical subsampling aimed to collect material for studying diagenetic alterations associated with migrating hydrocarbon gas, especially methane. Special interest was directed towards pathways of anaerobic methane oxidation. It involved a set of organic/inorganic geochemical subsamples of sediments and mud breccia matrix, pore waters, authigenic carbonate crusts, and chemosynthetic communities in the form of microbial mats. Consequently, emphasis has been placed on high-resolution sampling (at 2 cm intervals) spanning approximately the upper 60 to 80 cm. Reactions of specific interest involve anaerobic bacterial reduction of sulphate with concomitant oxidation of methane. In association with mud volcanoes, communities of anaerobic methanotrophs thrive at the interface between appreciable dissolved sulphate concentrations derived from overlying seawater and high methane fluxes originat-

ing from below, giving rise to subsurface maxima in rates of sulphate reduction and corresponding methane oxidation. The sampling protocol includes both solid- and dissolved-phase constituents spanning a range of organic and inorganic species. This protocol is designed to directly constrain activities of anaerobic methane oxidation (e.g., 16s rRNA in tandem with cell counts), as well as the isotopic, elemental and molecular (biomarker) products of bacterial metabolism. These procedures and initial results are outlined below.

I.5.2. Sampling strategy

Hydrocarbon gas sampling

A. STADNITSKAIA, V. BLINOVA AND E. POLUDETKINA

A total of 571 gas samples were taken from 18 sampling locations, which were selected for further determination molecular and carbon isotopic composition of hydrocarbon gas. The cores sampled were taken either from areas of gas seeps or from gas escape structures, such as mud volcanoes (BS-306K, BS-308K, BS-311G, BS-313G, BS-314G, BS-315G, BS-316G, BS-317G, BS-319G, BS-320G, BS-322G, BS-325G, BS-326G, BS-327G, BS-331G, BS-332G, BS-336G, and BS-337G). The description of subsampling procedure is not included since it was already described in previous reports of the Training Through Research expeditions (Ivanov et al., 1996; Woodside et al., 1997; Kenyon et al., 1998).

Depending on the lithology, subsampling intervals varied from 2 cm to 5 cm in the uppermost 60 to 100 cm. Below this the core was sampled every 10 to 20 cm.

Gas phase from sediments and gas hydrates was transferred into glass jars filled with saturated NaCl solution.

Total organic carbon

For total organic carbon and fluorescent analyses, approximately 100 g of wet sediments were taken from the same intervals as for the gas analysis. Sediments were covered by aluminium foil, and afterwards stored in a freezer at – 10°C to -12°C.

Pore water

T. LYONS, N. TYRINA AND L. MAZURENKO

The following cores were sampled as part of the study: BS-305G, BS-311G (sections 1-9), BS-313G, BS-314G, BS-315G, BS-316G (sections 1-5, 8,9), BS-319G, BS-320G, BS-322G, BS-323B, BS-325G, BS-327G, BS-330B, BS-331G, BS-332G, BS-336G.

With the exception of core 305G (collected for inorganic analysis only) and 320G (collected for organic/microbial analysis only), all cores will be characterized using all or some combinations of the organic/microbial and inorganic procedures outlined below. The "inorganic" analyses were selected based on the intimate relationship between methane oxidation and sulphate reduction (and the corresponding dissolved and mineral products).

Inorganic analyses

From the above list of sampled cores, the following were processed onboard for dissolved pore-water species: 305G, 314G, 319G, 330B and 332G. The pore waters were isolated using high-speed centrifugation (7000-8000 rpm) for 10 minutes with 2 ml centrifuge tubes. Pore-water yields varied significantly as a function of sediment type and depth within the section; however, 16 to 20 ml of centrifuged sediment generally provided <1 ml to >10 ml of pore water (mean: 1 ml to 4 ml). Sediment samples were loaded and centrifuged aerobically. Pore-water isolates from a given interval were then filtered (0.45 micrometers) and subdivided and prepared for later analysis via a fourfold fixation scheme: (1) acidification [trace metal-grade HCl], (2) zinc acetate fixation of dissolved sulphide [for concentrations], (3) cadmium acetate fixation of dissolved sulphide [for isotopic determinations] and (4) an untreated aliquot. Filtration and pore-water fixation were performed under an inert He atmosphere within a glove bag to minimize oxidation effects. In brief, pore-water analyses at the University of Missouri will include each of the following:

(1) Concentrations of total dissolved

sulphide (colorimetry/spectrophotometry) and S isotope compositions (on-line combustion/mass spectrometry of silver sulfide; pore-water yields were generally insufficient for analysis of dissolved sulphide isotope compositions),

(2) Concentrations of dissolved sulphate (ion chromatography) and S and O isotope compositions (on-line combustion / mass spectrometry of barium sulfate for S and high-temperature pyrolysis of barium sulphate for O),

(3) Chloride concentrations (ion chromatography),

(4) Trace metals, major and minor cations (inductively coupled plasma-emission spectrometry [ICP]).

(5) Depth-integrated sulphate reduction rates by modeling pore-water profiles.

Analysis of solids

Samples for solid-phase procedures were immediately frozen for later analysis at the University of Missouri. Other than core 320G, samples are available from each of the cores listed above. The planned analyses include:

(1) Sulfur as iron monosulfide ("FeS", acid-volatile sulfide [AVS], hydrotroilite) using cold 6 N HCl/15% stannous chloride (zinc sulfide reprecipitation followed by titration for concentrations and silver sulfide reprecipitation followed by on-line combustion/mass spectrometry for isotopic compositions),

(2) Sulfur as pyrite via chromium reduction of the AVS residue (concentration and isotopic determinations as for AVS),

(3) Speciation of reactive Fe phases using 12 N HCl and a buffered Na dithionite solution,

(4) Bulk analysis for a broad range trace, minor and major elements (total sample, multi-acid, microwave digestion followed by ICP quantification),

(5) Total organic carbon (TOC) via carbon dioxide coulometry.

Organic/microbiological sampling

M. BAAS, T. MUMLADZE AND A. STADNITSKAIA

Samples were prepared onboard for the following organic/microbiological procedures:

Acetate analysis: A 1:1 mixture of sediment and methanol was prepared for layers from cores 311G, 314G and 330B. The samples were stored at –22°C.

Cell count: A 4% solution (3 ml) of formaldehyde fixative was added to 1 ml sediment. After an incubation time of 1-4 h at 4°C the samples were centrifuged (5000 rpm, 5 min.), and the pellet was rinsed and stored at –22°C in 1:1 phosphate buffer/ethanol mixture.

PCR-analysis: All samples were stored at –22°C. PCR analysis will be preformed on selected intervals from five selected cores

Lipid analysis: All samples were stored at –22°C. The samples will be extracted and analyzed via gas chromatography (GC) and gas chromatography mass spectrometry (GC/MS). After screening the extracts for biomarkers the extracts will be divided into different compound classes and analyzed using a variety of techniques (e.g., column chromatography, Ag+ thin layer chromatography, liquid chromatography mass spectrometry, isotope ratio monitoring GCMS).

I.5.3. Observations

Gas hydrates

A.STADNITSKAIA, V. BLINOVA AND E. POLUDETKINA

Gas hydrate inclusions were documented for pelagic sediments and mud breccia deposits from sampling locations BS-308K, BS-317G, BS-319G, BS-331G, BS-332G, BS-334Gr, BS-336G, and BS-337G. Different morphological types of gas hydrates were found. Some fragments were characterized by a tabular shape of irregular thickness (up to 1-2 mm), forming layers within the sediment. Another gas hydrate morphology is isometric sub-rounded aggregates, from millimetric to 1 cm in diameter.

Microbial mats

The majority of chemosynthetic communities associated with fluid venting spots often occur in the form of microbial mats. Microbial mats were observed in three sedimentary cores, BS-325G, BS-328G, and BS-336G. All of them were associated with methane-derived carbonates of different size and morphology. Based on the colour two types of microbial mats were distinguished. The first type is represented by gel-like drops of brownish material, which is plainly visible in the porous spaces of the carbonates. This type was observed at two locations, BS-325G and BS-328G.

The second type of microbial mat is characterised by pinkish-brown gel-like matter attached to holes at the lower part of the crust, forming "colonies spots". It is worth noting, that the microbial mass of this type is higher than that of the other one. This microbial mat was found in carbonate crust within the sapropel layer of the site BS-326G.

Authigenic carbonates

A. MAZZINI AND O. KOVALENKO

Various investigations have reported that a significant portion of methane produced in marine sediments is converted to CO2 by anaerobic oxidation. It is directly related to carbonate genesis and diagenesis. Carbonate precipitation at gas venting locations is a consequence of microbial activity.

Authigenic carbonates were found at seventeen locations. The full set of recovered carbonate fragments was described and analysed with a binocular microscope. Based on macro and micro observations an initial classification of the crusts was attempted. Four main types of crusts were recognized, and a further subdivision was performed based on peculiar differences. Further and more detailed analyses are needed to confirm this preliminary interpretation.

Type 1a is composed of friable and poorly cemented Unit 1 sediments, light grey in colour (Fig. 31). The slabs (BS-306K, BS-307GR, BS-308K, BS-309G, BS-317G, BS-333G, BS-334GR, BS-335D) preserved the millimetric sedimentary layers and their sub-parallel orientation. The layer thickness varies from 1 mm or less (the majority). The laminations that make up the crust consist of alternations of clay and carbonate rich layers. The external flat surfaces show micro vesicles probably due to gas seepage. Well preserved and fragmented Ostracods shells were also identified in the cement. The possible presence of a microbial mat (darker in colour) was also observed.

Type 1b also involves cementation of Unit 1 (Fig. 31). Type 1b has similar characteristics to type 1a but looks to be better cemented (BS-314G, BS-324G, BS-334GR) and therefore less friable. The internal clay rich and cement rich interlaminations are less visible due to the better cementation, the majority of the pores are filled with micritic carbonate cement.

Type 2a- friable and poorly cemented Unit 2 (Fig. 31). The sample was recovered (BS-314-G) in the central part of Unit 2. It was poorly cemented and dark in colour due to the high organic content. The crust easily peels off along less cemented layers. Ostracods and possible microbial mats were observed between the layers. Small vesicles were also observed

Type2b- well cemented top of Unit 2 (Fig. 31). Cemented fragments and slabs were retrieved from the upper (BS-315-G) part but mainly from the base (BS-315G, BS-336G, BS-337G) of the sapropel. They appeared very well lithified and the usual layered structure was less visible. The darker grey colour indicates higher organic content present in the sapropel. Some lighter layers might indicate the thin coccolith ooze layers present in the sapropel. On the outside were seen some fossils (mainly crustaceans) to be cemented within layers. The samples retrieved from the bottom of Unit 2 have a darker colour and bigger (up 1 cm in size) vesicles, possibly indicating a greater seep-

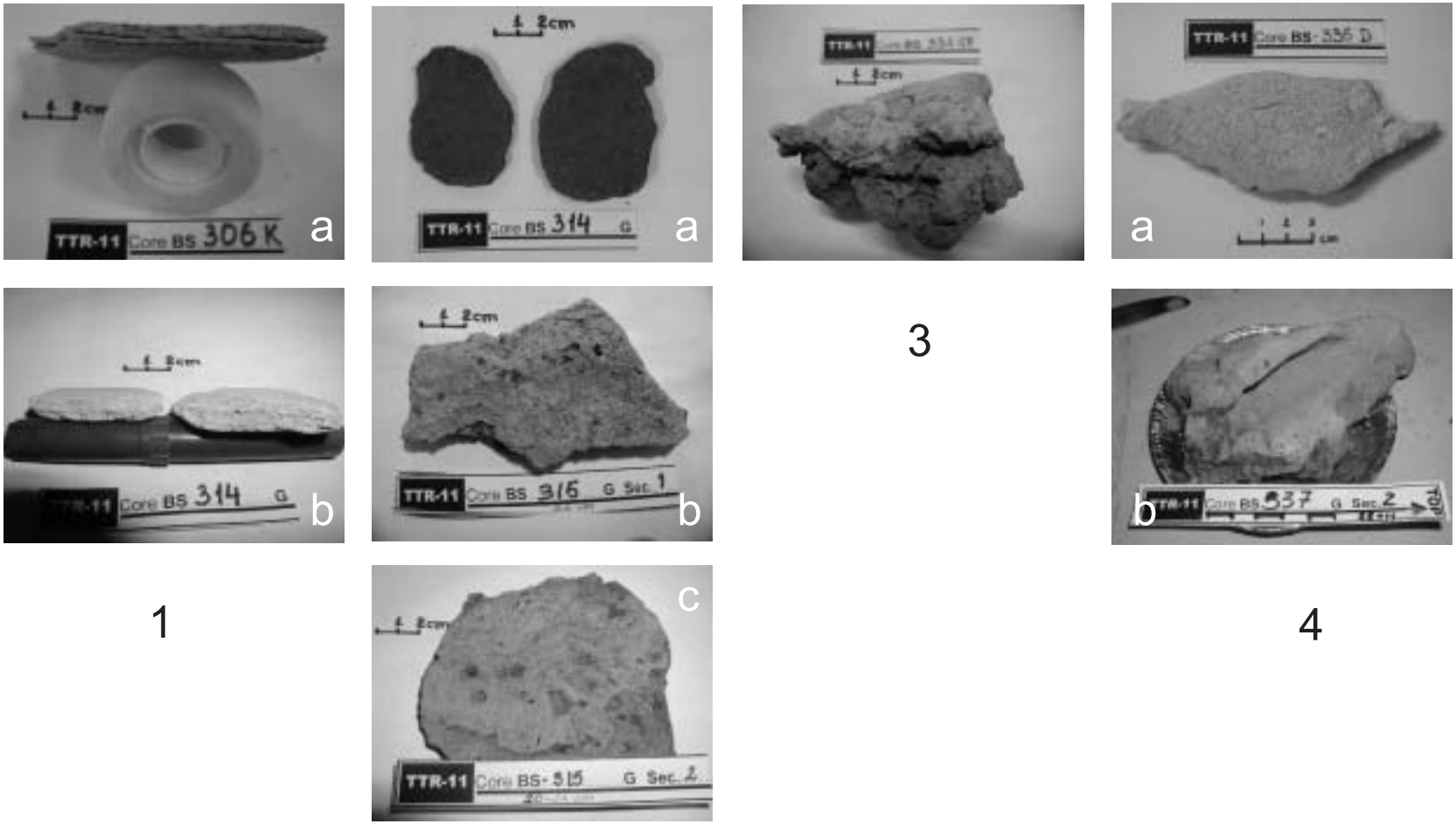

Figure 31. Types of carbonate crust.

age. Inside the vesicles evidence of a bacterial mat was observed (darker colour or pinkish and brownish).

Type MB– Cemented mud breccia (Fig. 31). The cemented mud breccia fragments (BS-333G, BS-334GR, BS-335D) appear irregularly shaped and very angular. They are brownish grey in colour, poorly cemented and very friable. Micritic cement binds together the fine fraction of the matrix and centimetre clasts of different roundness and lithology.

Type MSa - Cemented structure-less porous fine fraction (Fig. 31). It appears as light grey smoothed slabs (BS-334GR, BS-335D) of fine fraction cemented together by micritic calcite. One of the external surfaces (presumably the top one) appears very porous and covered by micro vesicles. The internal structure also shows the presence of cavities giving the sample a high porosity and a light weight. Some of the samples reveal a lower porosity. Generally no evidence of microfossils was observed.

Type MSb - Cemented structure-less fine fraction (Fig. 31). It is similar to type MSa, having light grey smoothed slabs (BS-306K, BS-326G, BS-327G, BS-336G, BS-337G) of fine fraction, cemented together by micritic calcite. No micro vesicles are observed on the surface or in the low porosity internal structure. This type of crust might represent an earlier stage of type MSa that has been exposed and possibly bioturbated by bacterial activity.

I.5.4. Conclusions

Several preliminary conclusions can be made after analysis of the newly obtained geochemical data:

1. The high gas saturation is associated with a fault system and mud volcanoes
2. The occurrence of gas hydrates is an indicator that the seeps are active.
3. Fluids in the seeps contain a large amount of petroleum-associated products. This may result in a high diversity microbial community involved in biodegradation processes of these products and inducing authigenic precipitation of carbonates and sulphides.
4. The two types of microbial mats observed suggest diversity of microbes formed in gas-seeping environments. The activity, metabolic pathways and growing rate of microbial groups and/or consortia are also different depending on the source of soluble and metabolised matter, chemical environments in the sediments and water column, saturation of Ca2+, Mg2+ and metal ions in pore waters, intensity of hydrocarbons (methane) supply, etc.
5. The majority of the studied carbonate crusts comprise poorly to medium cemented sediments of Unit 1 (type 1a). Optic microscope observations of crusts show interbedding of micritic calcite and unlithified clayey layers. This indicates that methane-derived carbonate precipitation tends to occur mainly along coccolith-rich lamina. Clay lamina would serve as seals. Methane can diffuse vertically through the clay lamina along microfractures and this process would result in the formation of vesicles.
6. Carbonate crust of type 2a, 2b, also show similar characteristics but they are much better cemented. Tabular aggregates of gas hydrates found within Unit 2 (sapropel) suggest lateral migration of gas in the sediment. Physical properties of the sapropel layer can facilitate better migration of gas, which, in turn, would enhance carbonate precipitation.
7. Formation of a carbonate crust would be expected underneath a layer with improved sealing characteristics. This model may apply to Core BS-315G, where carbonate slabs were found underneath a 2 cm layer of structureless clay.
8. The origin of carbonate crust type MSa remains unclear although an underwater video survey and dredging data suggest that this type of crust forms directly on the seabed.

II. THE MEDITERRANEAN SEA (LEG 2)

II.1. Aegean Sea

Extension of the North Anatolian Fault into the North Aegean: Transition from strike-slip faulting to extension within the North Aegean and Central Greece.

L.C. McNeill, A. Mille, N.H. Kenyon, M. Ivanov and TTR11, Leg 2 Scientific Party

II.1.1. Introduction

Tectonic Setting

The North Anatolian Fault of northern Turkey represents the tectonic boundary between the Anatolian microplate and the Eurasian plate. Recent geodetic data (GPS) show motion of the Anatolian plate westward as a result of the collision between Africa and Eurasia. This motion is largely taken up by the right-lateral North Anatolian Fault (NAF), at a geodetically measured rate of 30 mm/yr (Reilinger et al., 1997). Motion changes toward the southwest, west of Turkey in the Aegean Sea, and towards the Hellenic trench south of Crete. Motion of the Anatolian plate along the North Anatolian Fault may also be responsible for rapid extension in central Greece, the Aegean Sea, and western Turkey. Various hypotheses have been proposed to explain the extension in this region, including back-arc extension, roll-back of the subducting African plate, and gravitational forces resulting from over-thickened Anatolian crust driving Turkey westward and ultimately southwest towards the Hellenic trench (e.g. Taymaz et al., 1991).

This region of the eastern Mediterranean is consequently highly seismically active, with destructive strike-slip and normal faulting earthquakes throughout Turkey and Greece. Deformation and seismicity in northern Turkey is focused on the North Anatolian Fault. Towards the Sea of Marmara and northwestern Turkey, deformation is more distributed and the NAF splits into several fault splays, the two northernmost strands forming the Sea of Marmara itself. The Sea of Marmara can be most simply described as a pull-apart basin with several sub-basins, but models of its formation and relative components of strike-slip and extensional deformation are currently being debated. Interest in this region has been renewed following two destructive earthquakes on the NAF in 1999, with the prospect of future earthquakes within the Sea of Marmara in close proximity to the populous city of Istanbul (Hubert-Ferrari et al., 2000; Parsons et al., 2000). To the southwest, extensional deformation within central Greece is clearly defined by normal faulting focal mechanisms in the Gulf of Corinth, Gulf of

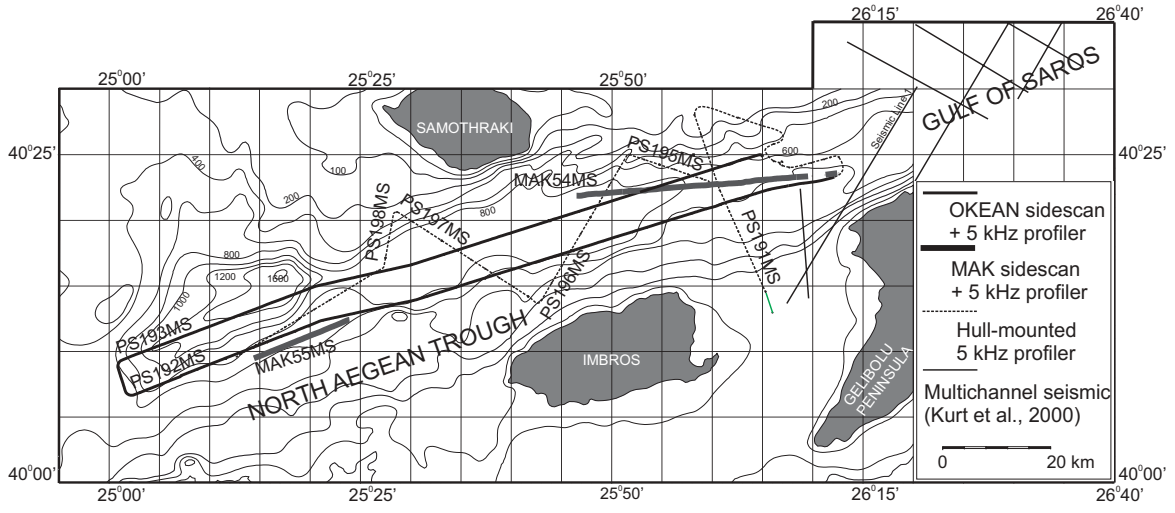

Figure 32. Trackline map of all data collected during Leg 2A and seismic reflection data of Kurt et al. (2000) in the Gulf of Saros. Contour intervals in meters.

Evvia and elsewhere, supported by geomorphic, palaeoseismologic and other geological evidence. However, it is unclear exactly how the transition between these two regions occurs, from pure strike-slip faulting along the eastern-central NAF to pure extension in central Greece and western Turkey, with transtensional deformation within the Sea of Marmara and North Aegean in the transition zone. Motion of the Anatolian plate rotates counterclockwise from westward within central Turkey to southwest within the Aegean (Reilinger et al., 1997). Deviations of actual GPS (Global Positioning System) -measured crustal velocities from the small circle of rotation in the Marmara Sea and northern Aegean Sea explain the increased extensional component in these two regions (Reilinger et al., 1997). Earthquakes within the northern Aegean Sea, in this transitional zone, consist of normal faulting, strike-slip and oblique faulting mechanisms.

Between the Sea of Marmara and the North Aegean Trough (Fig. 32), the North Anatolian Fault ruptured in 1912 with pure strike-slip motion and possible extension of fault rupture offshore into the Gulf of Saros, where the fault is known as the Ganos Fault (Fig. 33; Kurt et al., 2000).

Objectives

The purpose of Leg 2A, was to investigate the recent tectonic and sedimentary processes occurring within the North Aegean Trough, formed by the westward propagation of the North Anatolian Fault (NAF) into the northern Aegean Sea. Leg 2A was designed to determine how the extensional and lateral components of deformation are distributed and to investigate the transition between strike-slip and extensional deformation in the easternmost North Aegean Trough.

Existing geophysical data in the region largely consists of boomer, 3.5 kHz profiles, and seismic reflection data particularly in the Gulf of Saros east of the TTR study area, supported by a few cores. However, little or no seafloor imaging data has been collected which would allow detection of lateral fault motion and determination of fault trends. The objective of this study was to obtain images of the seafloor in tandem with subsurface data in order to improve our understanding of recent tectonic and sedimentary processes within part of the North Aegean basin. Two days of survey time were available, therefore the study was restricted to the easternmost North Aegean Trough, west of the Gulf of Saros where the North Anatolian Fault enters the North Aegean (Fig. 32). The

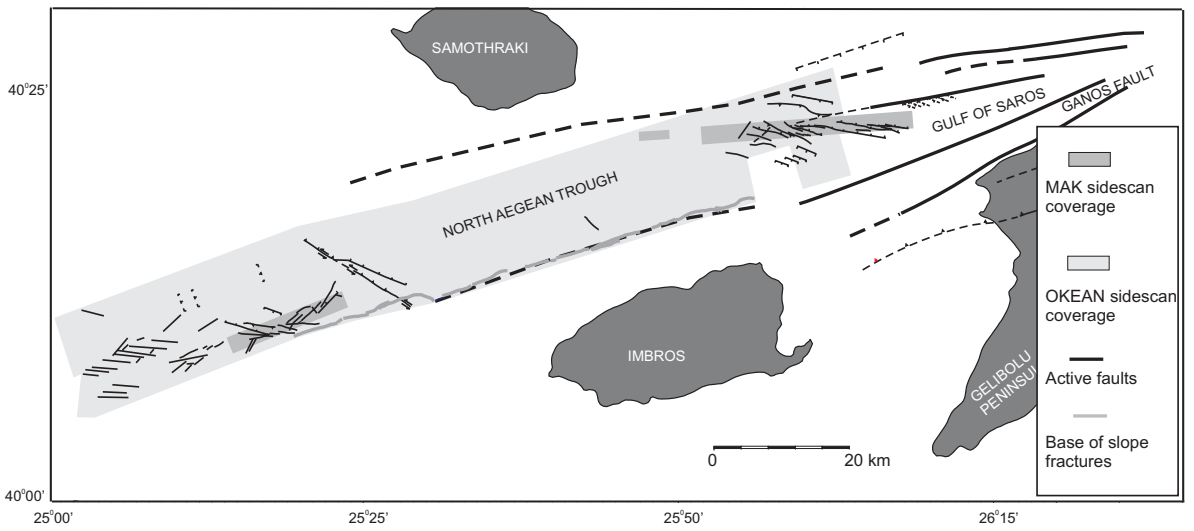

Figure 33. Active faults identified from TTR11 sidescan and 5 kHz data and reinterpreted from published seismic reflection data in the Gulf of Saros (Kurt et al., 2000).

Gulf of Saros has been studied previously (e.g. Kurt et al., 2000) and structural interpretations can be compared with those determined here.

II.1.2. Data collected

Acoustic and sub-bottom profile data

Two lines of OKEAN 10 kHz long-range sidescan sonar were run in an WSW-ENE direction parallel to the basin (PS192ms and PS193ms. Fig. 32), with a total length of ~170 km. Operating in water depths of 500-1500 m, the OKEAN produced a swath width of 2 x 3.5 km. This reconnaissance survey was able to image the central and southern part of the basin including faults bounding the basin and deforming the centre of the basin. Following this reconnaissance survey, two lines (MAK54MS and MAK55MS) of deep-towed MAK sidescan sonar, operating at a frequency of 30 kHz and totalling ~45 km length (also approximately parallel to the basin) were collected for higher resolution imagery of particular tectonic features. The 30 kHz MAK sidescan data produced a swath of 2 x 1 km and was collected concurrently with sub-bottom profile data from the towfish. Shipboard 5 kHz sub-bottom profile data was collected and recorded digitally throughout the sidescan surveys.

In addition to the sidescan data, a series of 5 kHz profiles were run across the basin to provide cross sections of the tectonic and sedimentary features within the graben (Fig. 32). The shipboard 5 kHz sub-bottom profiler data was recorded along the following lines - PS191MS, PS195 MS, PS196 MS, PS197 MS, and PS198 MS, with a total additional length of ~140 km.

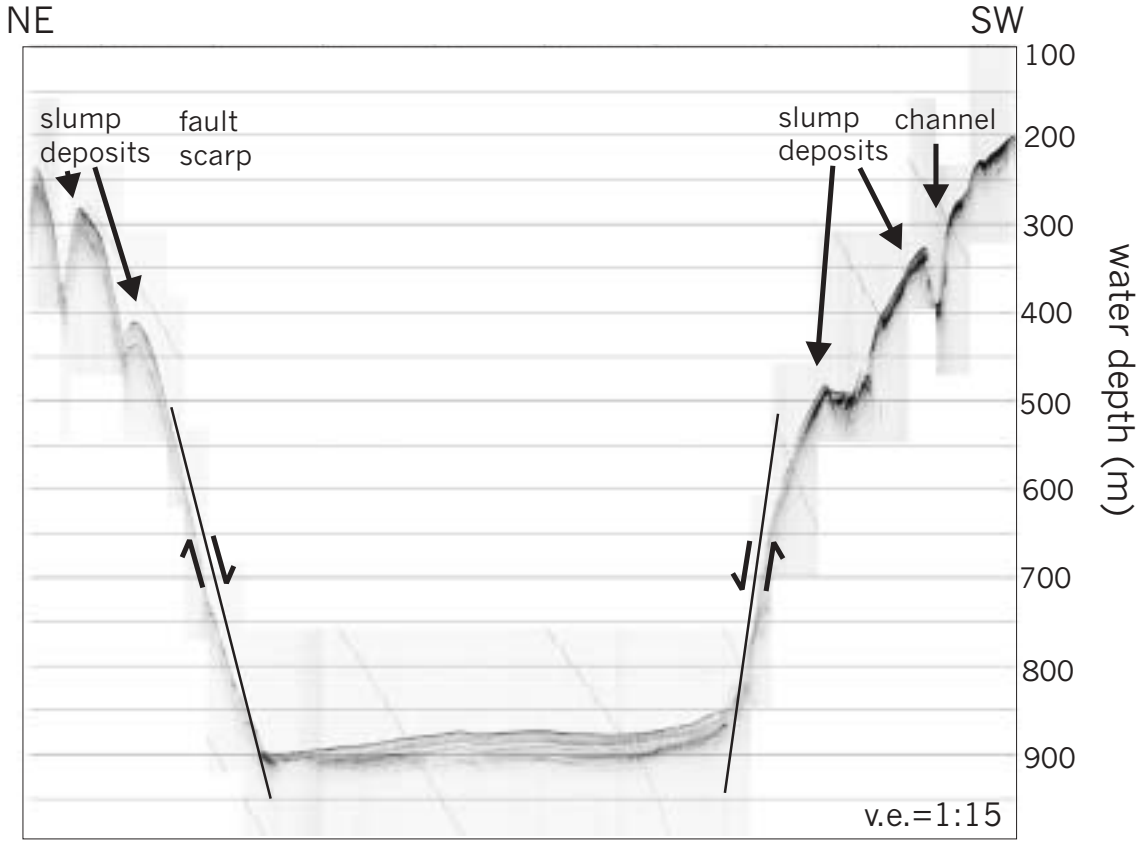

Figure 34. Cross section of the North Aegean Trough from shipboard 5 kHz sub-bottom profiler. Profile is vertically exaggerated but shows the steep-sided basin margins, evidence of mass wasting and channeling on the margin slopes and extensional fault scarps.

Deep-towed video imagery

A camera profile was run along part of the line MAK54MS within the basin floor in order to image a) high backscatter material hypothesised to be carbonate crusts associated with faulting and methanogenic gas accumulation, and b) scarps and evidence of recent faulting on a series of WNW trending en echelon faults (probable strike-slip deformation, see below). The results of the camera tow were inconclusive with regards to these objectives. Throughout the profile, the seafloor was dominated by pelagic sediments with evidence of prolific bioturbation (e.g., burrows and other trace fossils). In the region marked by scattered irregular patches of high backscatter, fine grained sediment covers the seafloor. We hypothesise that the 30 kHz sidescan is penetrating the uppermost 10's cm of sediment to image a higher backscatter substrate lying beneath a thin veneer of hemipelagic silts and clays. Very limited evidence of cementation within the pelagic sediments was observed during the 3 hours of video imaging.

II.1.3. Preliminary Results and Interpretation

Tectonic Interpretation – Evidence for Strike-Slip Faulting within the North Aegean Trough

Prominent fault scarps were imaged bounding the north and south sides of the North Aegean basin (Figs. 33 and 34) and with significant vertical displacement (in excess of 700 m). The basin does not appear to have the asymmetrical form of a half-graben (although this is difficult to determine with the limited penetration of the 5.1 kHz data and consequent inability to image tilted sediments), therefore we expect significant displacement on both major bounding faults. The fault scarps themselves are somewhat masked by mass wasting of the steep basin margins (Fig. 34). Smaller faults within the basin also show some vertical displacement, with the majority showing normal offset.

On the basin floor and margins a number of fault traces were identified from the sidescan data with trends oblique to the WSW basin axis (Figs. 33, 35 and 36). Orientations were WNW-ESE (dominant), NE-SW and NW-SE (rare). These faults were near vertical in profile with minimal vertical displacement and near-linear traces. Many of the faults have en echelon or stepping fault traces, often a characteristic of strike-slip faulting. An example of WNW-trending en echelon faults is shown in Figure 35 from the northeast of the study area and in the centre of the basin. A few examples of lateral offset were identified in sidescan images although geomorphic features suitable for determining lateral displacement, e.g. channels, are rare. The trends of these faults and their offset is compatible with a model of Riedel shear in an ENE-WSW dextral shear zone (Fig. 36). Evidence of strike-slip offset includes offset folded bedding planes and an offset margin of slump debris.

Steeply-dipping faults were also identified in the centre of the Gulf of Saros basin in seismic reflection data to the east of the study area (Kurt et al., 2000). These faults correlate with en echelon probable strike-slip fractures mapped from MAK and OKEAN sidescan sonar data in the area of overlap between the two study areas (Figs. 33 and 35). We were unable to confirm lateral disaplacement on these faults. Despite small vertical displacement, these basin floor faults all break the surface and are therefore recently active (assuming average sedimentation rates within the basin). In parts of the basin, fault traces are associated with high backscatter material (Fig. 35). Possible explanations for the irregular shaped bodies of high backscatter material include carbonate crusts associated with methane fluid venting along fault planes or exposure and erosion of coarser siliciclastic sediment (e.g. sands) on the fault footwall. These features were targeted during the deep-towed camera run but it seems that the features are draped by a thin veneer of hemipelagics (see above).

The region of the North Aegean Trough surveyed in this study can be divided into two sub-basins based on bathymetry and geometry (Fig. 32) with a deeper basin to the

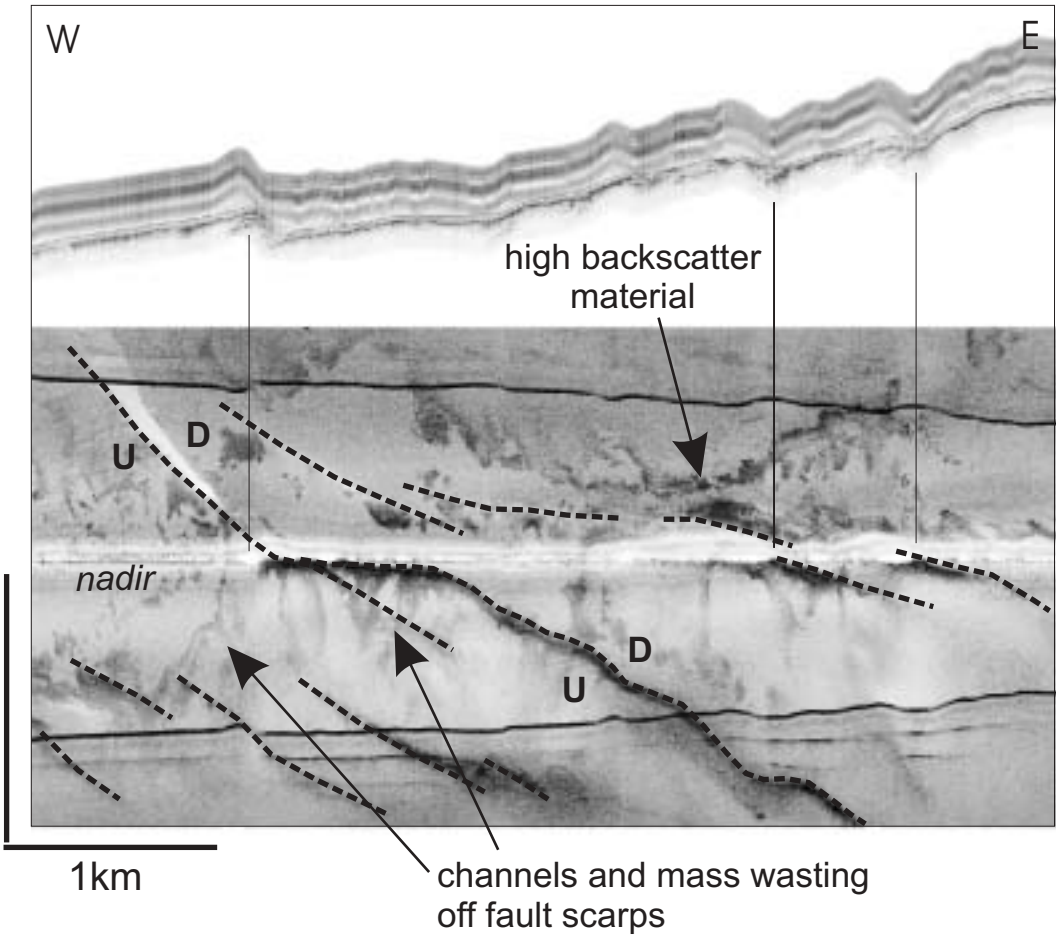

Figure 35. Oblique-trending faults imaged in MAK-54MS sidescan image (bottom) with MAK sub-bottom profile (top). Faults have small vertical displacement (indicated by shadow and high return of fault scarps in sidescan and by profile) but are thought to also have lateral displacement. Patchy high backscatter (dark) material may represent carbonate crusts north of the nadir, and downslope southward transport of high backscatter material off the fault scarps to the south of the nadir (channelised in places). U=up; D=down for fault scarps.

west. The sub-basins are separated by a NW-trending fault with left-lateral displacement (Fig. 33). The trend and displacement of this fault fits a model of block rotation under dextral shear conditions and indicates a significant tectonic boundary separating two basins. Similar individual pull-apart basins have been identified within the Sea of Marmara to the east (e.g. Aksu et al., 2000).

Sedimentary Processes

The steep sides of the basin margins are clearly characterised by mass-wasting with evidence of slump deposits at the base of slope on both sub-bottom profiles and sidescan images. Away from the edges of the basin, the basin is characterised by well-stratified sediments (Fig. 34). Evidence of canyons and channelling across the basin margins was obtained from both sub-bottom profiles and sidescan data. In profiles, evidence of truncation on the channel walls and stratified channel fill can clearly be seen. The precise orientation of these channels cannot be determined due to the spacing of profiles. However, sidescan data suggest channels dominantly traversing the steepest gradients across the basin margins. No evidence of along-axis channel activity was observed on the basin floor in either OKEAN sidescan or the 5 kHz sub-bottom profiles. At the base of slope, high backscatter (coarser sand and gravel?) debris accumulates at the termina-

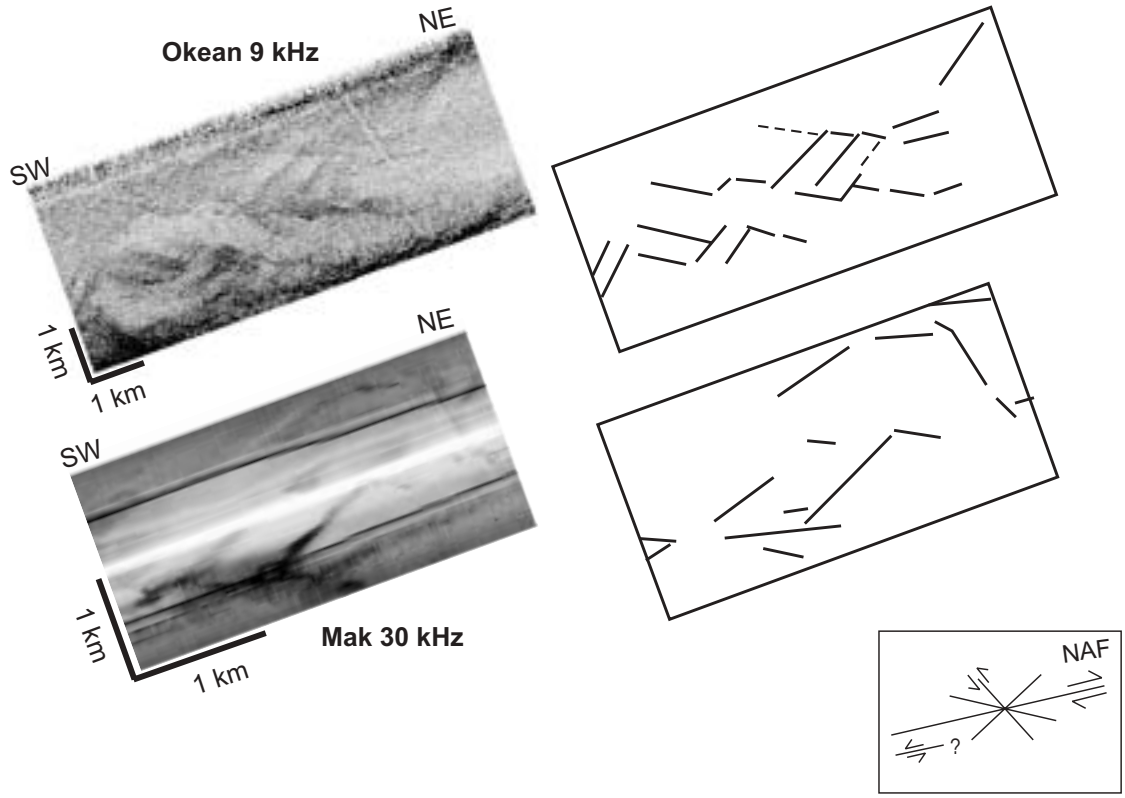

Figure 36. Oblique-trending faults imaged in OKEAN and MAK (line 55) sidescan images in the western study area. Several fault orientations can be picked out which fit a Riedel shear model for a dominant WSW dextral fault (box, NAF=North Anatolian Fault), with the exception of one anomalous WSW-trending left-lateral fault. Faults exhibit en echelon (stepping) traces in the OKEAN image.

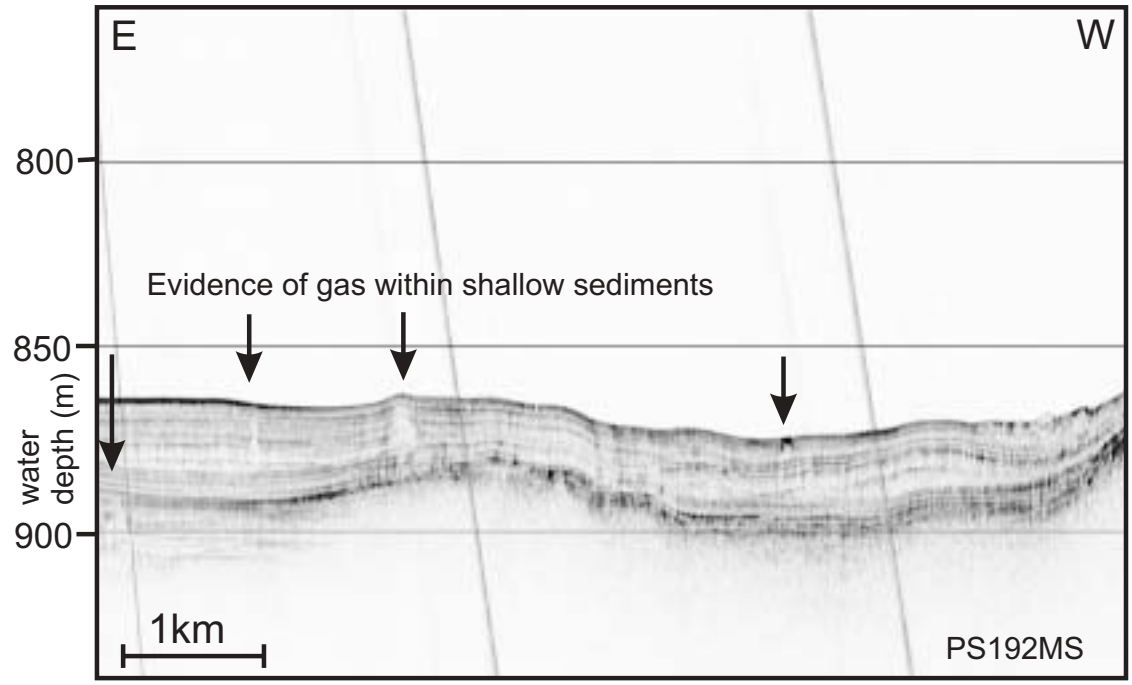

Figure 37. 5 kHz profile across the basin floor of the North Aegean Trough showing evidence for gas in the form of opaque gas columns, some associated with seafloor deformation (pock marks or small mud volcanoes?) and predominantly sourced from a common horizon.

tions of smaller gullies and channels (imaged in MAK sidescan sonar). On a smaller scale, there is evidence for unconfined mass wasting and channelised deposits of high backscatter (coarser?) material off the uplifted footwall block of the oblique-trending fault scarps (Fig. 35). Movement of this material is downslope along the surface of the uplifted and presumably backtilted fault block.

A strong reflector, ~ 10-20 m below the seafloor, occurs throughout much of the well-stratified basin. The overlying sediments are commonly less well-stratified and often acoustically transparent. A similar horizon has been observed elsewhere within the North Aegean (Piper and Perissoratis, 1991) and in the Sea of Marmara and has been hypothesised, based on accompanying cores, to represent the last glacial-interglacial transgression ~ 18 ka. Unfortunately, limited survey time prevented collection of further core material during this leg, but correlation to other datasets or collection of core material in the future may allow us to use this horizon as a strain marker for fault displacement.

Gas Features

Evidence of gas within the sediments of the North Aegean Basin was observed in several sub-bottom profile records (e.g. Fig. 37). Evidence includes high amplitude reflectors coincident with common horizons and vertical transparent gas columns in the shallow sediments. The latter are sourced in a common horizon (often associated with the high amplitude reflectors) and are often associated with deformation at the seafloor presumably related to fluid escape. We would expect to find pockmarks on the seafloor above these "columns". Methane venting may also be related to high backscatter material (carbonate?) associated with active fault planes see above, Fig. 35).

II.2. Ebro margin, Valencia Trough

R. U. ESCLASANS, A. CALAFAT, M. IVANOV , J. L. CASAMOR, G. LASTRAS, J. FRIGOLA, D. AMBLAS, V. WILLMOTT AND TTR11, LEG 2 SCIENTIFIC PARTY

II.2.1. Introduction

Geological framework

The Ebro margin is located on the western side of the Valencia Trough, an early Miocene-Pleistocene extensional basin (Díaz del Río et al., 1986; Clavell and Berastegui, 1991) that lies between the Balearic Islands and the Iberian Peninsula. In the Ebro margin, Neogene sediments are characterized by a thick progradational sequence of mostly Pliocene to Pleistocene sediments, the Ebro Group. It includes the lower Ebro Clay, a prograding Pliocene shale unit, and the upper Ebro Sand, a Pleistocene clastic shelf complex (Soler et al., 1983). This sequence overlies the Messinian unconformity (Clavell and Berastegui, 1991; Maillard et al., 1992).

The North-western Mediterranean region is, compared to other Mediterranean sub-basins, relatively quiet seismically and there is no active volcanism (Grünthal et al., 1999). Nevertheless, many catastrophic slope failures have also been identified in this area. Some of them have occurred in modern times and have affected coastal and offshore infrastructures such as telephone cables, e.g. the failure event off Nice airport in 1979 (Gennesseaux et al., 1980; Malinverno et al., 1988). Other geologically recent although imprecisely dated major landslide deposits, tens to hundreds cubic kilometres in volume have been identified in the Valencia Trough (Canals, 1985; Field and Gardner, 1990; Alonso et al., 1990), the Western Gulf of Lions (Canals, 1985; Canals and Got, 1986; Berné et al., 1999) and on the flanks of the Rhone Deep-sea Fan. However, the largest mass wasting deposit in the Western Mediterranean Sea is the 500-km^3 Balearic mega-turbidite, which covers 60,000 km^2 of the Balearic Abyssal Plain (Rothwell et al., 1998, 2000).

The BIG'95, the landslide occupying

the area of study during the present cruise, is a 200 km^2, 26 km^3 recent debris flow. It affects the Ebro slope and base-of-slope at depths ranging from 600 to 2000 m. Swath bathymetry data has shown an area of uneven topography in the Ebro slope with several main and secondary scars identified at depths between 600 and 1200 m (Lastras et al., 2000; Canals et al., 2000). Profiles showed a large sediment body with transparent seismic facies covering the entire sea-floor, thus indicating the event's youth.

Previous work

In 1995 during a reconnaissance survey aboard the ship Hespérides a large mass with transparent acoustic facies was identified. During this cruise Simrad EM-12S swath bathymetry, Simrad TOPAS very high-resolution parametric 3.5 kHz profiles and deep-towed 30 kHz TOBI (Towed Ocean Bottom Instrument) sidescan sonar system were used. Further processing of the swath bathymetric data allowed identification of a characteristic pattern of high and low backscatter facies related to the debris flow, which indicates that the debris flow extends over an area of 2200 km^2. The landslide was named BIG'95 in relation to the name of the cruise during which it was discovered.

A further cruise was carried out in 1997 on board the ship L'Atalante with the priority of coring the landslide material and neighboring sediments. The coring was accomplished using a piston core recovering variable core lengths of up to 6 m. During this cruise 3.5 kHz profiles were also acquired as well as Simrad EM12 dual swath bathymetry.

In 1999 again the GRC Marine Geosciences of the University of Barcelona went back to this area in the ship Hespérides in order to complete the multibeam coverage of the more proximal areas of the upper slope and shelf surrounding the Columbretes islands and to obtain seismic reflection profiles. This task was accomplished using air gun seismic reflection profiling as well as the Simrad EM1002. In addition to this data Simrad TOPAS very high-resolution parametric 3.5 kHz profiles were acquired.

Backscatter data from the BIG'95 debris flow area have been processed using state-of-the-art software. The images obtained provide significant information on the dynamics of the debris flow and sediment dispersal paths (Lastras et al., 2000). The debris flow area consists of a pattern of low-backscatter patches, representing large blocks of sediment, which moved down-slope without loosing their internal coherence, separated by topographically depressed lineations of high backscatter representative of coarse sediment pathways that buried at their terminus the uppermost course of the Valencia Channel. The large sediment blocks appear only between 1200 and 1550 m water deep, while coarse sediment paths are present all along the debris flow.

These features, together with the presence of multiple secondary scars, show up the complexity of the BIG'95 mass movement. The most probable sequence of events was (1) a major general destabilisation of the area, led to the formation of the main scar at the base-of-slope (1000-1200 m) from which the large blocks of fine material were detached and moved down-slope without loosing their internal coherence; and (2) the formation of the main scar induced the destabilisation of the shallower slope areas and thus to the formation of multiple secondary scars, where coarser material began to flow down-slope following the depressed areas between the large blocks till reaching the Valencia Channel (Lastras et al., 2000).

Seven piston cores up to 8.6 m long have shown that the BIG'95 deposit, which is overlain only by a thin (up to 20 cm) hemipelagic drape, is mostly made of fine grained contorted beds and clay chunks where backscatter is low, and unsorted chaotic sands along the elongated, high-backscatter pathways.

Objectives

By the summer of 2001 a large pool of geophysical and geological data was available, however high resolution visualization

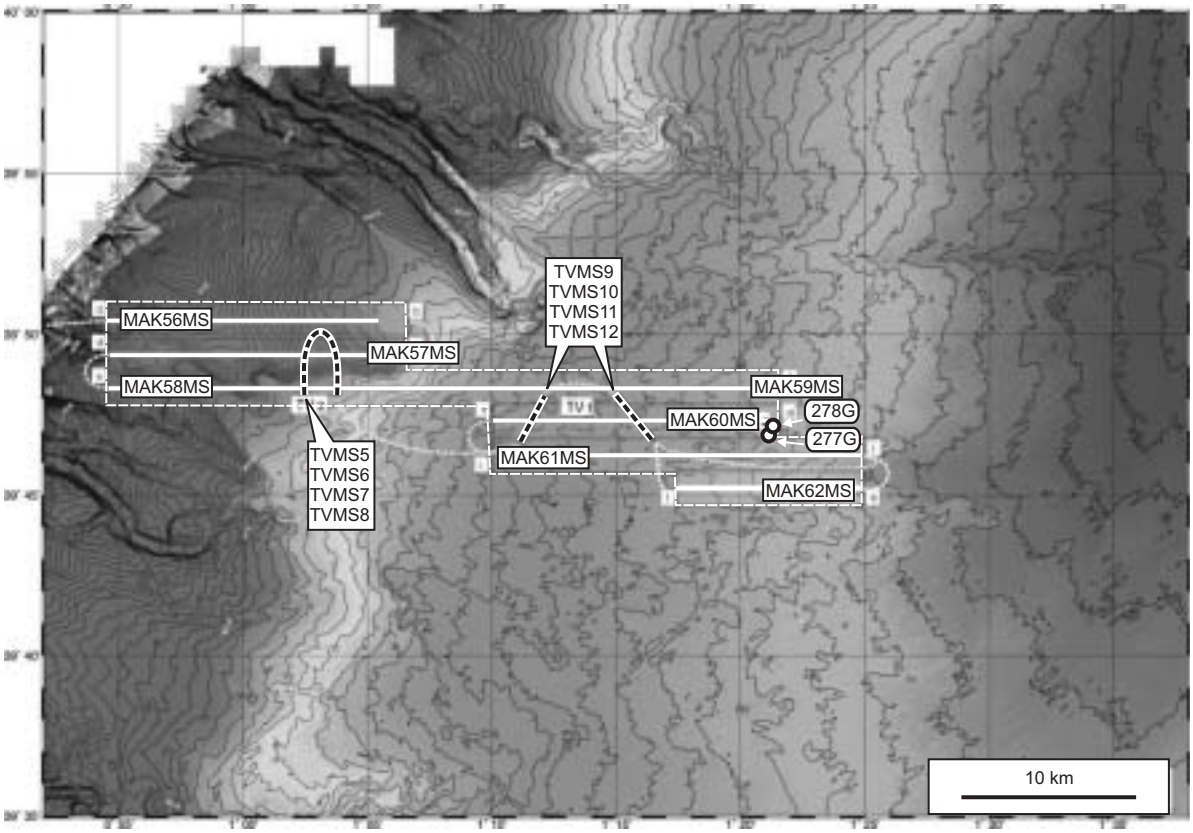

Figure 38. Location map of the study area on the Ebro margin. Core sites shown as circles.

of the landslide was lacking. The main goal of the BIGIMAGE Leg of TTR in the area was to run a high-resolution sidescan survey over the landslide scar and area of the blocky terrain with the distinctive high-low backscatter patches and then to groundtruth the existing geophysical interpretations with underwater TV survey and bottom sampling.

II.2.2. Preliminary Results and Interpretation

Sidescan sonar survey

Geometry of the BIG'95 debris flow headwall scar

Three MAK-1M sidescan sonar lines covering an area of approximately 100 km^2 have been run in the area of BIG'95 debris flow headwall scar, between 39°47′ and 39°51′ N and between 0°54′ and 1°08′ E (Fig. 38). Good quality sonographs showed new details of the landslide scar. The headwall develops between 600 m water depth at its westernmost end and 1230 m water depth at its easternmost end and has a sinuous shape. Its total length is about 17 km and its mean height is 75 m, although in its middle part it is up to 200 m high.

From the deepest end of the scar to the shallowest end, three different morphologies have been distinguished namely: (1) stair-like, (2) stair-like evolving into slope and (3) buried geometry.

The stair-like geometry is only developed where the scar is less than 60 m high. It occurs in the easternmost part, between 1°02 and 1°08 E. Here the scar is built up of several steps (Fig. 39). Around ten major steps and many minor ones are identified in this area. Usually, the most prominent step is located in the uppermost part while the size, height and lateral continuity of other steps decreases down the scar.

The stair-like evolving into slope geometry develops between 0°59 and 1°02 E and displays less steps than the stair-like geometry. It is concentrated in the uppermost part of the scar, while at the foot of the

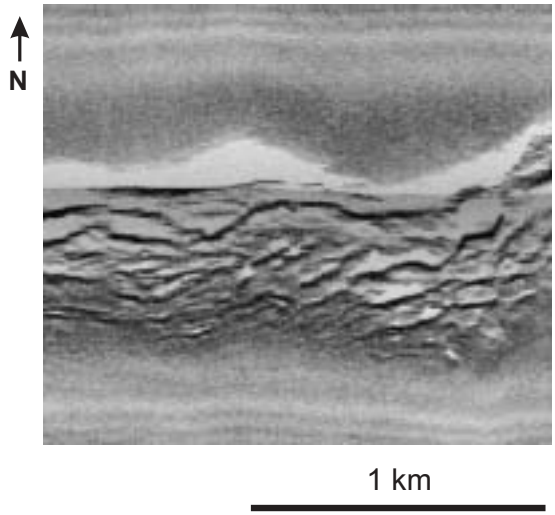

Figure 39. 30 kHz MAK-1M sidescan sonar image of the easternmost part of the BIG'95 debris flow headwall scar showing stair geometry. Note that this image is built up of two sidescan lines. Insonification at the top of the figure is from the north and at the bottom insonification comes from the south.

scar a regular dipping slope is present. In the area with this geometry the scar reaches up to 200 m. The upper steps are not always present in some sections, and thus the scar becomes just a regular dipping slope (Fig. 40).

Finally, in the easternmost part (between 0°54 and 0°59 E) the scar appears to be buried by material released by several secondary scars, which can be identified further upslope. This material shows a blocky morphology in some areas, while compression ridges can be observed in other locations (Fig. 41). The scar in this area is almost completely buried and its geometry cannot be described. The presence of the upslope secondary scars is indicative of the complexity of the BIG'95 debris flow event, whose deposit is not the result of a single failure but of the superposition of two or more events, which probably occurred very close in time.

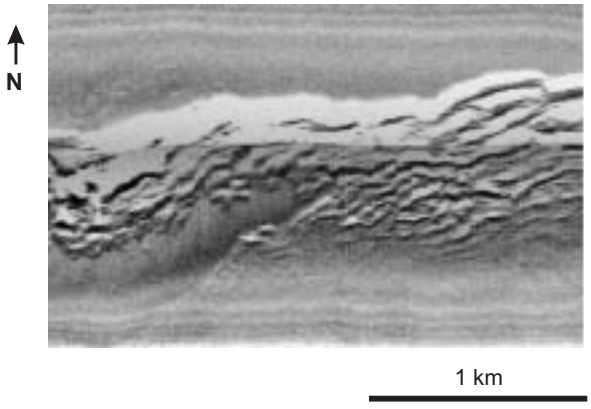

Figure 40. 30 kHz MAK-1M sidescan sonar image of the middle part of the BIG'95 debris flow headwall scar showing the transition between stair-like geometry to stair-like evolving into slope geometry.

<u>The blocky area (BIG'95 debris flow middle depositional area)</u>

Four MAK-1M sidescan sonar lines with a total surveyed area of approximately 128 km^2 have been aquired in the middle depositional area of the BIG'95 debris flow. The total length of the lines is 70 km. The sidescan sonar mosaic displays a pattern of linear depressed areas surrounding topographically elevated blocks (Fig. 42).

The individual blocks are up to 1 km long and are limited by narrow depressions. They are grouped in elongated block clusters of up to 12 km long. These clusters are surrounded by channel-like depressions of up to 600 m wide.

MAK-1M 5 kHz profiler

<u>Debris flow headwall scar zone</u>.

Three parallel MAK-1M (profiles MAK 56MS, 57MS and 58MS) 5 kHz profiles totalling in length 54 km (16.6, 17.6 and 19,6 respectively) were run across the BIG'95 debris flow headwall scar. This area is between 39°47' and 39°51' N and between 0°54' and 1°08' E.

The profiles show a seismic sequence with two distinct units: Unit 1 is a surficial transparent unit with a variable thickness from 6 to 20 m and irregular surface relief onlapping Unit 2. Unit 2 is made of a series of parallel continuous reflectors with high amplitude and frequency with continuity along the profile and a variable thickness of between 21 and 36 m. The reflectors show decreasing amplitude with increasing depth into the seafloor due to the sound energy attenuation.

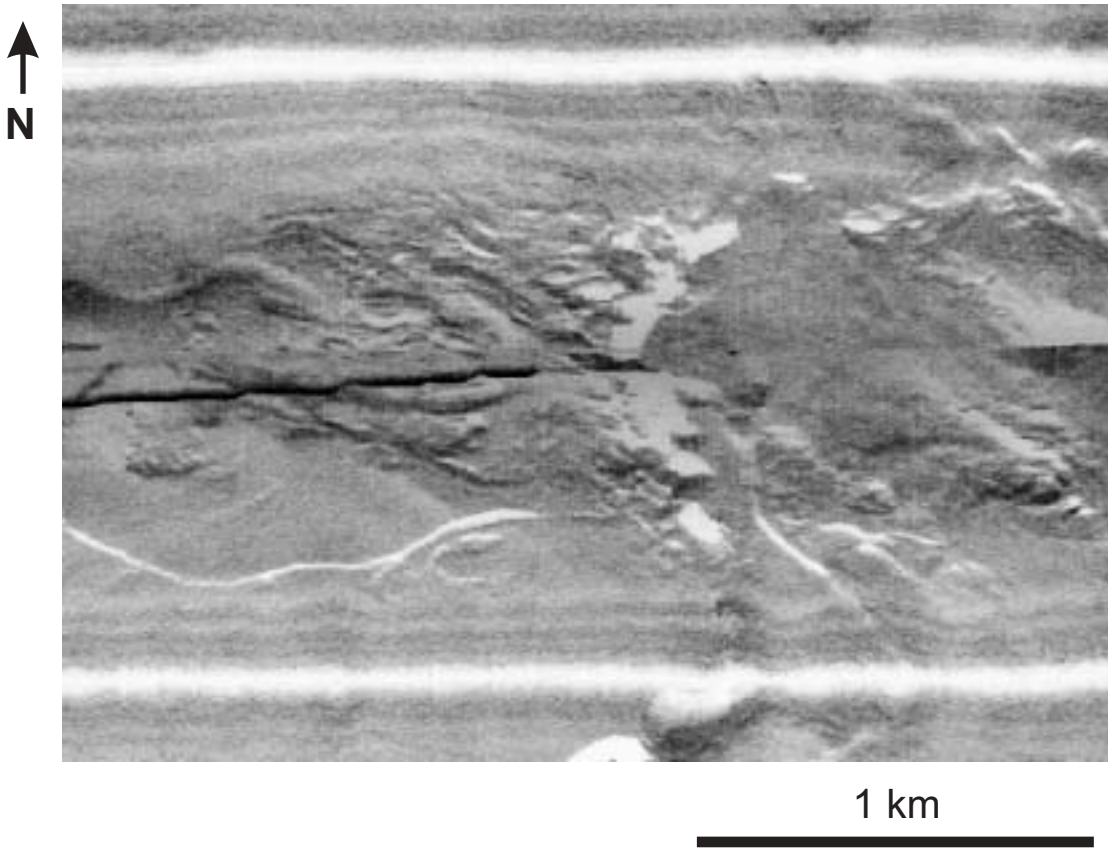

Figure 41. 30 kHz MAK-1M sidescan sonar image of the westernmost part of the BIG'95 debris flow headwall scar showing the main scar buried by sediment released from upslope secondary scars. Blocky morphology and ridges can be identified in the sediment burying the main scar.

Line MAK 56 runs west-east from 600 m to 1300 m depth, crossing the Ebro slope and rise. This line is located above the main scar of the debris flow. Between 11:00 and 12:00, a secondary scar (also present in lines 57 and 58) with respect to the main scar affects Units 1 and 2. The transparent Unit 1 buries the depression originated by the scar. Between 13:20 and 14:30, with a change of the slope, Unit 1 thickness increases progressively from 12 to 20 m. At about 14:30 there is an additional new transparent seismic unit which probably represents a secondary debris flow affecting the main scar area.

Line MAK 57 runs from east to west. The deeper parts of the profile, between 16:50 to 18:40, show a well-stratified sedimentary sequence, with only local zones displaying appreciable thickness of Unit 1. From 18:40 Unit 1 becomes thicker (13 m) and shows an irregular surface. A large depression caused by the main scar is present between 20:00 to 21:00. The eastern side of the depression shows an erosional surface. The materials from Unit 1 bury this depression, with thickness up to 40 m. Sunk into Unit 1 there seems to be a rafted block of well-stratified material.

Line MAK58 runs from west to east between depths of 800 m and 1350 m. From 22:50 to 23:50 a gentle slope of well-stratified sequence is observed. This slope is interrupted by a depression (between 23:50 and 00:30) observed in the other lines, with the west side showing an erosional base, which is buried by the transparent Unit 1.

Between 00:30 and 01:00 a high, forming the upslope part of the scar is also covered by transparent material coming from the secondary scarps. In the eastern part of this high, between 01:00 and 02:50, Unit 2 seems to show several compressive structures. These structures are overlain by a variable thickness of Unit 1 material. From 02:50 onwards the profile shows a well-stratified sequence.

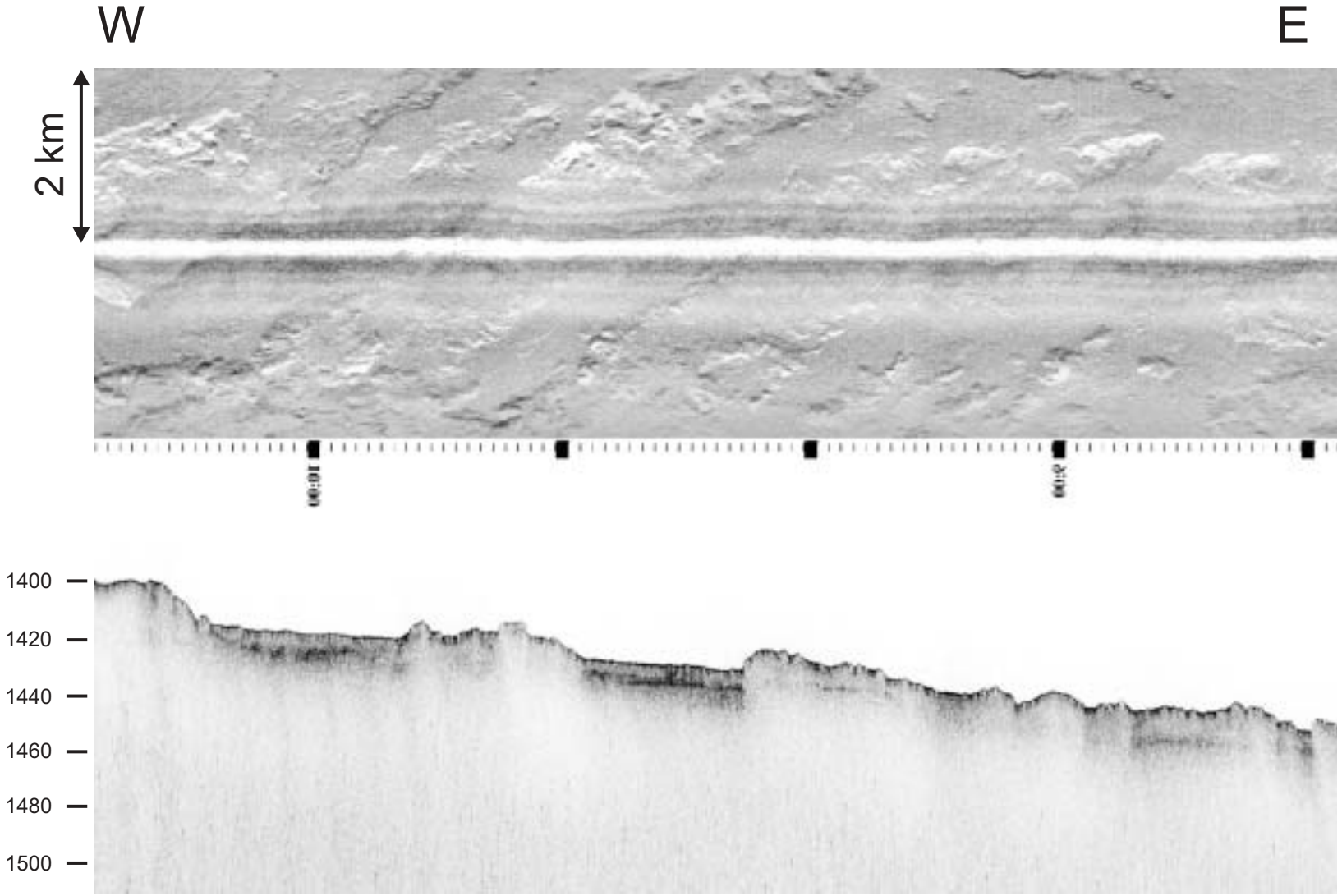

Figure 42. Fragment of MAK-60MS line showing depositional zone with rough topography.

Depositional zone.

Four MAK-1M (profiles MK 59MS, 60MS, 61MS and 62MS) 5 kHz profiles with a total length of 70 km have been carried out in the middle part of the BIG'95 debris flow area, where the "rafted" blocks are present. This area is between 39°45′ - 39°49′ N and 1°09′ - 1°29′ E.

The complete seismic sequence described in the previous zone can only be described from Line 59MS, between 02:20 and 02:40. The rest of the profiles show only the most superficial transparent unit (Unit 1), overlaying an erosive (?) surface.

All profiles have a uniform gentle slope with an irregular topography which is mostly due to the presence of the "rafted" blocks. Unit 1 has a thickness of 5 to 13 m and covers most of the mapped area.

Underwater TV system survey

In order to visualize the sea-floor affected by the BIG '95 landslide, 9 TV profiles were carried out. Profiles TVMS5 to TVMS8 were obtained in the zone of the main landslide scar. Profiles TVMS9 to TVMS12 were obtained in the area of debris and "rafted" blocks.

Headwall scar

Unfortunately the camera, which is towed quite close to the bottom is unable to show large structures such as those that are expected on the BIG'95 landslide. Also a large amount of hemipelagic draping is present making it difficult to directly observe any structures associated with the landslide.

This area appears to have very fine grained sediment, which does not seem to be very cohesive in the light of the clouds created by the camera when it hits the bottom. There are widespread bioturbation marks, especially holes formed by prawns and fish.

In profiles TVMS5 and TVMS8 some fractures and small steps at about 1200 m depth, perhaps related to the main landslide scar were observed. As the camera range does not allow visualisation of structures larger than 1 m size, it is very difficult to determine the true origin of these structures.

Depositional zone

All issues concerning camera limitations apply as above. The sediment here seems to be more cohesive and finer than in the former area. There are less marks of bioturbation and, at a first glance, it is hard to relate any structures or sediment composition to the rafted blocks.

Gravity cores

Two cores were taken in order to investigate the differences in backscatter observed in the Simrad EM12 data. See Annexe I for the core logs. Core 277G was taken on top of one of the supposed "rafted blocks" and recovered 1.1 m, while core 278G was taken on the depression immediately north of the block, where high backscatter facies are observed on the EM12 data and almost 2 m were recovered. Both cores show a similar upper part made of hemipelagics with an upper oxidized horizon, but the deeper core 278G shows a homogeneous sand interval with mud clasts.

III. NORTH-EAST ATLANTIC (LEG 3)

III.1. Iberia margin and Gulf of Cadiz

III.1.1. Introduction and Objectives

During the TTR-9 (1999) a large mud volcano field was discovered in the Spanish and Moroccan sectors of the Gulf of Cadiz (Kenyon et al., 2000, Gardner, 2001), under the coordination of Dr. Joan Gardner, from the Naval Research Laboratory (NRL), Washington DC, based on a sidescan mosaic and multibeam bathymetry (SeaMap) collected in the area in 1992 by the Marine Physics Branch of the Naval Research Laboratory (NRL), Washington D.C., in cooperation with the Hawaii Mapping Group and the Naval Oceanographic Office. Mud volcanoes discovered were: TTR, Kidd and Adamastor, in the *Eastern Moroccan Field*, and Yuma and Ginsburg, in the *Middle Moroccan Field*.

During the TTR-10 cruise (2000), this area was again investigated, based on the NRL mosaic and the data acquired during the previous TTR-9 cruise. In the Moroccan Sector, besides revisiting the Ginsburg mud volcano and recovering gas hydrates, several new mud volcanoes were discovered: Jesus Baraza, Student and Rabat. In the Spanish sector, a new mud volcano, Tasyo, was also discovered. Finally a new deep-water mud volcano field was discovered in the S. Portuguese Margin (Bonjardim, Olenin and Carlos Ribeiro mud volcanoes), at depths between 2300 and 3150 m.

The main objectives of the first part of TTR-11, Leg 3 were: (1) to investigate a large, circular structure located approximately at 36°08'N/8°56'W; (2) to investigate the Iberico high, from which carbonate chimneys had been recovered during the ANASTASYA 00/09 cruise (Diaz del Rio et al., 2001), to run digital video camera profiles over the chimney field and to collect some chimneys by dredging; (3) to investigate the extent of the area with carbonate chimneys; (4) to investigate several new structures identified on the NRL sidescan mosaic, which are suspected to represent mud volcanoes; (5) to investigate the sandy lobes at the distal part of one small channel observed on the NRL mosaic and the TOBI sidescan mosaic; (6) to revisit the Olenin and Carlos Ribeiro mud volcanoes in the deep South Portuguese Mud Volcano Field, to try to retrieve gas hydrates, whose presence is suggested by studies of the composition of the pore-water samples retrieved from the TTR-10 cores; (7) to investigate the fauna associated with the mud volcanism and other fluid escape structures in the study area. For this purpose, single channel seismics, long range sidescan sonar (OKEAN), high resolution deep-towed sidescan sonar (MAK-1), hull mounted 5 kHz profiler, deep-tow analog/digital TV camera, dredging and gravity coring were used.

III.1.2. Geological Setting

The Gulf of Cadiz is an area of active tectonics and seismicity related to the NW directed convergence between the Africa and the Eurasia plates since the Cenozoic (Eocene). This area has had a very complex geological history and undergone several episodes of rifting, compression and strike-slip motion, since the Triassic (Wilson et al., 1989; Maldonado et al., 1999). It is located at the front of the Betic-Rifian Arc, which is the westernmost tectonic belt of the Alpine-Mediterranean compressional zone, where south to north thrusting has over-ridden the thinned passive margins of Morocco and Iberia.

During the Mesozoic and the Early Cenozoic this area was undergoing rifting, with the formation of half-graben structures and carbonate platforms (Maldonado et al., 1999). The westward migration of the Gibraltar arc during the Late Tortonian caused the Gulf of Cadiz to form as a forearc basin and induced gravity sliding with the emplacement of an olistostrome (Bonnin et al., 1975, Auzende et al., 1981) in an accretionary wedge type depositional environment with strong deformation of the sediments derived from the S. Iberian and N. African margins of the Tethys (Maldonado et

al., 1999).

The olistostrome body consists of a chaotic mixture of Triassic, Cretaceous, Paleogene and Neogene sedimentary units, overlying a Palaeozoic basement, and it is characterized on seismic reflection profiles by chaotic, high-amplitude reflectors with diffractions and hyperbolic reflections (Riaza and Martínez del Olmo, 1996). The lower boundary fault, serving as a basal decollement, is usually characterized by a strong, discontinuous, high amplitude reflector dipping south-eastward and becoming obscure beneath the olistostrome front. These chaotic units involve a huge volume of mud and salt diapirism of Triassic salt units and undercompacted Early-Middle Miocene plastic marls (Maldonado et al., 1999). The olistostrome units extend for over 100 km from the shelf of the Spanish and Moroccan margins towards the Horseshoe and Seine abyssal plains, west to the Gibraltar Arc, where their thickness exceeds 4 km (González et al., 1996; Torrelli et al., 1997; Somoza et al., 1999). The maximum thickness of the olistostromic body in the Gulf of Cadiz has been calculated, based on refraction profiles to reach 7 km, with a low interval velocity of 2.2 km s^{-1} and a density of 2 g/cm^3.(González et al., 1997). Frontal imbricate thrusting is interpreted as taking place through low-angle planes observed as high-amplitude reflectors within the chaotic olistostrome body. The deformation front appears to consist of several thrusting wedges whose advances may deform overlying prograding and basement conformable sedimentary deposits of Late Miocene age.

The geometry of the "Olistostrome" in the Gulf of Cadiz resembles that of accretionary wedges formed along a thrust front with a rigid buttress at the rear. In some places, it appears that Triassic evaporites, lower Miocene marls and Palaeozoic shales have acted as detachment layers for the overthrusting. After the emplacement of the thrusting units, gravitational sliding of the mobile shale and salt stocks formed a giant mass-wasting deposit that migrated west towards the Horseshoe and Seine abyssal plains. This resulted in a complex structural pattern in an active compressional setting, where faulting and diapirism have provided conduits for fluid expulsion, including brines, oil, gases and fine sediment, to the continental slope surface. The observed flow patterns of the fluid escape structures are similar to those reported on accretionary wedge settings by contractional structures.

The end of the emplacement of the olistostrome took place in the Late Miocene (Late Tortonian, according to seismic and well data; Martínez del Olmo et al. 1984) and coincided with an accelerated tectonic subsidence and the development of thick progradational and aggradational depositional sequences.

Throughout this area, pockmarks, extensive mud volcanism, carbonate mounds and chimney structures related to hydrocarbon rich fluid venting and mud diapirism are observed (Baraza and Ercilla, 1996; Kenyon et al., 2000). This indicates the existence of gas-rich overpressured sediments at depth, sometimes in compartments generated beneath salt wedges, and the upward migration of the fluids (brine waters), hydrocarbon gases and fluidized sediments along faults and contractional toe-thrust structures to the seafloor (Lowrie et al., 1999). Some of the observed mud volcanoes are located along major NW-SE and NE-SW trending faults identifiable on the NRL sidescan imagery, but this is not always the case. It has also been suggested that some of the widespread shallow fluid venting on the seafloor, particularly in the northern part of the study area can be explained by the destabilization of gas hydrate rich sediments in contact with the Mediterranean Outflow (MOW) (Somoza et al., 2000).

In the northeastern sector of the Gulf of Cadiz, authigenic carbonate chimneys and crusts have been collected from the Iberico high, discovered in 2000 (Diaz del Rio et al., 2001). To the east of this structure a large NE-SW diapiric ridge, the Guadalquivir Diapiric Ridge (GDR) is observed, from the shelf break to 1200 m. This ridge controls the orientation of the main channel of the MOW undercurrent and is composed of a series of wide sub-circular conic mounds surrounded

by ring-shaped seafloor depressions. Most of these depressions are filled by contourite deposits of the MOW undercurrent. Some of them, mainly on the right side of the main MOW channel, are developed as sedimentary "shadow" structures, formed on the down-current side of the mounds and around, which are asymmetrical depressions showing a step-like profile with benches along the slopes.

III.I.3. Seismic and Acoustic Data

III.I.3.1. Seismic data interpretation

L. M. PINHEIRO, M. C. FERNANDÉZ-PUGA, H. DUARTE, T. CUNHA, S. BOURYAK AND A. VOLKONSKAYA

Line PSAT 206

Line PSAT 206 is an ESE-WNW single channel seismic line with a short NE-SW segment in its eastern end. It is located over the accretionary prism units of the SE domain of the Gulf of Cadiz, between the S. Iberian and N. Moroccan margins (Fig. 43). The sea bottom shows a gentle WSW slope (790 ms to 1020 ms TWT). This line crosses 3 targets identified on the NRL sidescan mosaic: two small approximately circular high backscatter structures that could represent mud volcanoes and the distal sandy lobe of a small submarine channel.

On the eastern portion of the profile a small, slightly asymmetrical sedimentary basin is observed downslope from a plateau (19:20 to 20:10, at approximately 1080 ms TWT) between two shallow intrusions that could represent NE-SW trending diapiric ridges (based on the interpretation of the OKEAN record). The development of this basin appears to have been controlled by the uplift of these diapiric structures, which probably consist of Triassic salt. The asymmetry of this basin, with a long eastern flank suggests a westward directed compression.

Between 20:10 and 21:54 on the profile (Fig. 44), the seafloor morphology along the slope is irregular, with lobular bedforms that can be interpreted as contourite mud waves above a highly deformed sedimentary section located between two weakly deformed sedimentary basins.

A sand lobe deposited at the distal part of a small channel, visible on the sidescan mosaics, is observed on the western portion of the seismic line as a thin lens at the base of the slope, above a thick sedimentary

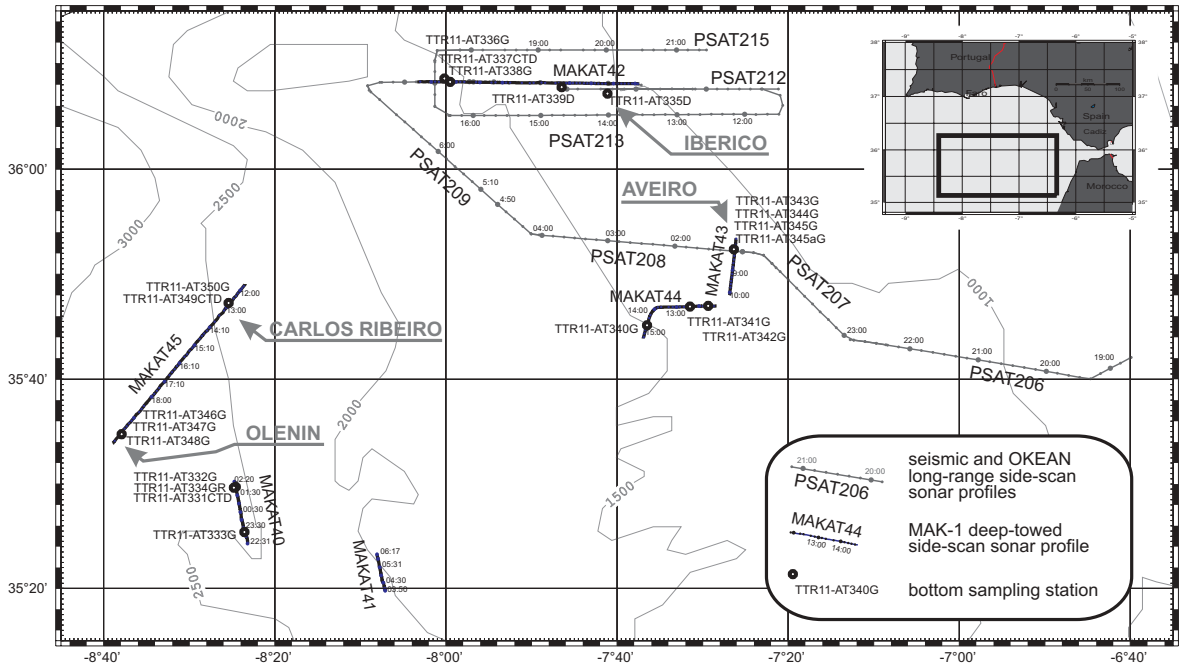

Figure 43. Location map of Leg 3 studies in the Gulf of Cadiz.

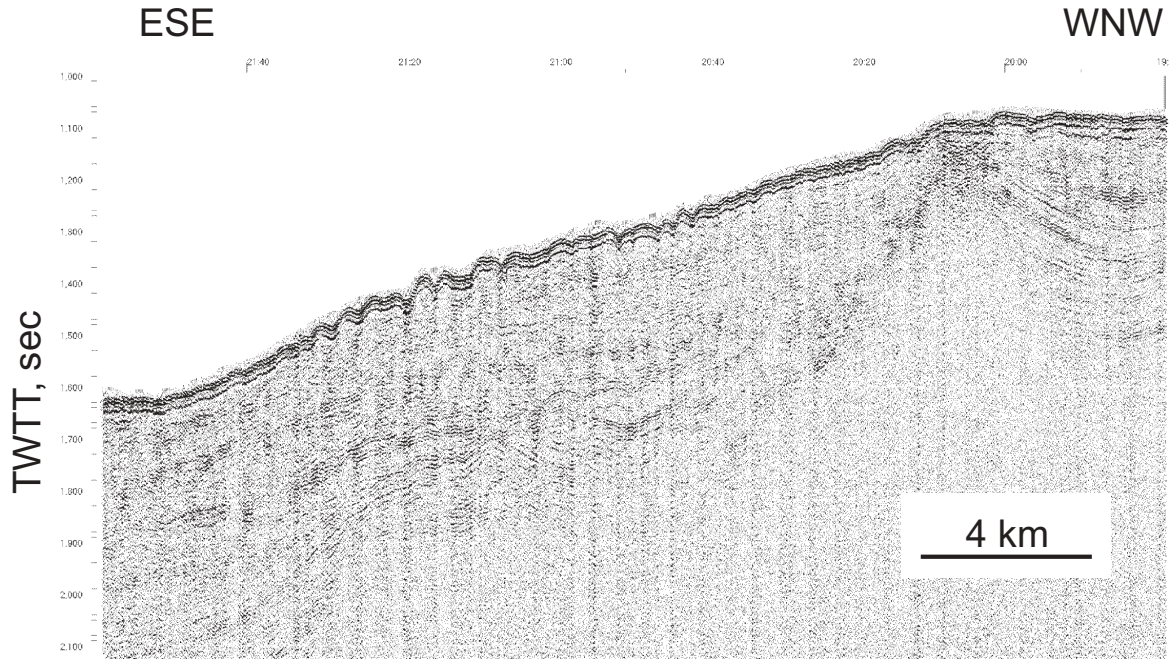

Figure 44. Fragment of seismic line PSAT-206 showing a sequence of contourite with mud waves.

basin (over 1.000 ms TWT). It should be noted that one high backscatter target structure identified on the NRL mosaic has no expression either on the seismic profile (at 22:31), or on the corresponding OKEAN record.

PSAT 207

This SE-NW line crosses the Gil Eanes channel (Kenyon et al., 2000). It is located over the transition between the accretionary complex units in the east and the Olistostrome units in the west. The seismic profile (00:02 to 00:11 on Fig. 45) shows that the Gil Eanes channel has a strongly incisive V shape (over 175 ms TWT from bottom to top). This channel runs in the midst deposits with wavy bedforms. The ridge on top of which the channel lies could be as wide as 17 km.

Bedform morphology and the depth

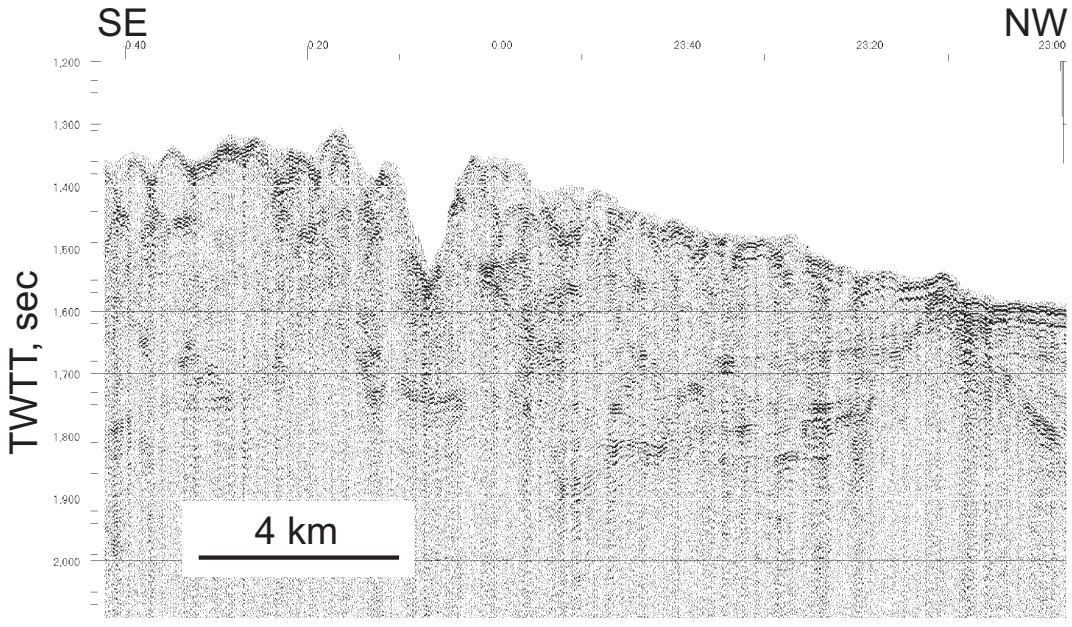

Figure 45. Fragment of seismic line PSAT207 across the Gil Eanes contourite channel, showing that its location is not controlled by a diapiric ridge..

of deposition, which is within the range of MOW currents, suggest a contourite origin for these deposits.

A fairly large diapiric structure is observed on the SE portion of the line, which appears to be delimited by a NW dipping fault. This fault approximately coincides with the inferred NE-SW contact between the accretionary complex units, to the east and the Olistostrome units, to the west (Maldonado et al., 1999; Somoza et al., 1999).

PSAT-208

This ESE-WNW line crosses two interesting structures observed on the NRL sidescan mosaic. This seismic line is located over the olistostrome units.

The overbank deposits described on PSAT-207 continue in the eastern part of this line, where they are interrupted by a structure, which is 100 ms (TWT) high, has a strong backscatter signature and looks like a mud volcano (this was confirmed by coring during this Leg; see relevant section further in the text).

West of the mud volcano, all the sedimentary section has been deformed, forming several asymmetric folds with a westward vergence, interrupted in the western part of the line by the intrusion of two diapiric structures (salt or shale diapirs) (Fig. 46). Within the easternmost asymmetric fold (between 01:10 to 02:16), a small graben structure is observed from 01:30 to 01:40. Its western limit coincides with a major NW-SE trending normal fault (or possibly a transtensional segment of a strike-slip fault) observed on the NRL mosaic and also, although not so clearly, on the OKEAN record.

The observed deformation and faulting in the sedimentary section is consistent with a series of basement thrusts to the west, along eastward-dippping faults that can be interpreted on from the seismic section.

PSAT-209

This is a SE-NW line that runs toward the Portimão Canyon. The profile starts near the longitudinal axis of the olistostrome units and ends a few miles after the contact with the accretionary prism units.

Most of this profile, from 04:12 to 06:50, crosses a deformed sedimentary sequence, 500 ms thick, where folds have vertical or SE dipping axial planes. This deformation seems to be partially due to neotectonics, for the folds are closely mirrored by seabed topography and mini-basins commonly occur along the syncline axes.

Most of the core zones of the anti-

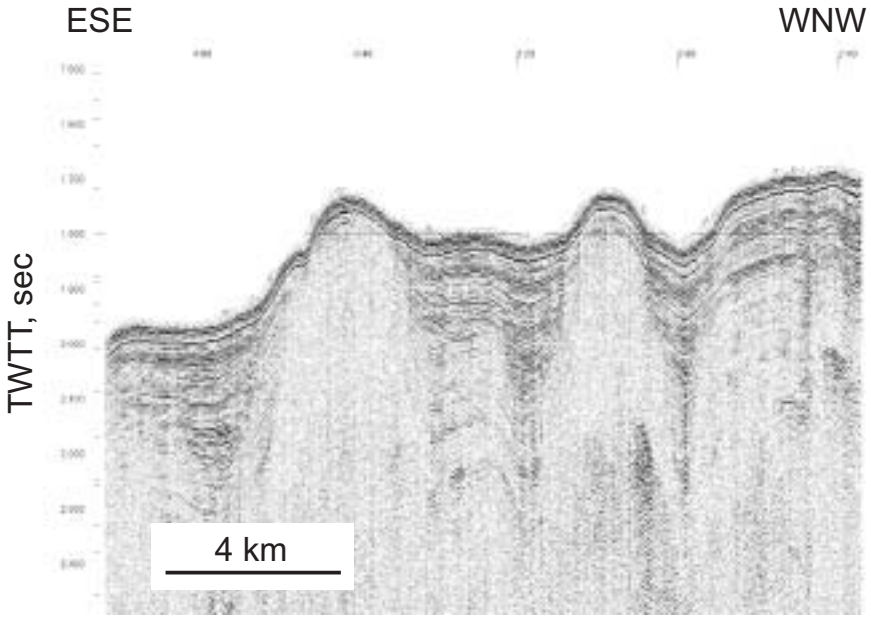

Figure 46. Fragment of seismic line PSAT-208 across several diapiric structures.

clines present low reflectivity and low frequency reflectors, a fact that, associated with some cone like sea-bottom morphologies, suggests the ubiquitous presence of diapiric structures. Two salt/shale diapiric structures, clearly identified at 04:48 and 05:22, reach near sea-bottom depths and probably outcrop along steep northwest facing slopes. A third salt/shale diapir at 05:35 can also be identified through the sediment uplift around a dome structure at a depth of 2.4 s.

PSAT-210

PSAT-210 crosses two important structures. The first one is seen on the sidescan mosaic as a circular body surrounded by an E-W channel branching around it. The seismic record shows a sediment covered dome, from 8:10 to 8:50, with chaotic and low amplitude internal reflections. The eastern branch of the channel shows an asymmetrical minibasin, with steeper western flank, possibly as a consequence of diapiric uplift.

An irregular topography occurs between 09:35 to 10:12. One of its slopes shows outcropping chaotic, low amplitude reflectors which, considering the nature of the "olistostromic" sequence in depth, suggests the presence of a shale diapir.

From 10:12 to 10:57 the seabed is covered by a contouritic, irregular deposit with possible internal tectonic deformation.

The Iberico high structure appears at 10:58, roughly on the axis of a minibasin (Fig. 47). The seismic signal at depth is masked by a hard surface reflector, composed of carbonate chimneys and crust, through which seismic waves do not penetrate.

PSAT-211

PSAT 211 is a N-S profile that crosses the Iberico high from 12:40 to 13:00. This structure shows low or no seismic wave penetration caused by a hard surface at the sea floor.

PSAT-212

A west dipping fault with an apparent reverse movement can be seen at 8:24 near the outcrop of the Iberico high (from 8:30 to 8:38). This diapiric structure has no internal reflections and is surrounded by uplifted sediments.

A second diapir, outcropping between 19:16 to 9:22, exhibits a seismic response very similar to Iberico and also uplifts neighbouring sediments.

The Cadiz Channel, crossed between

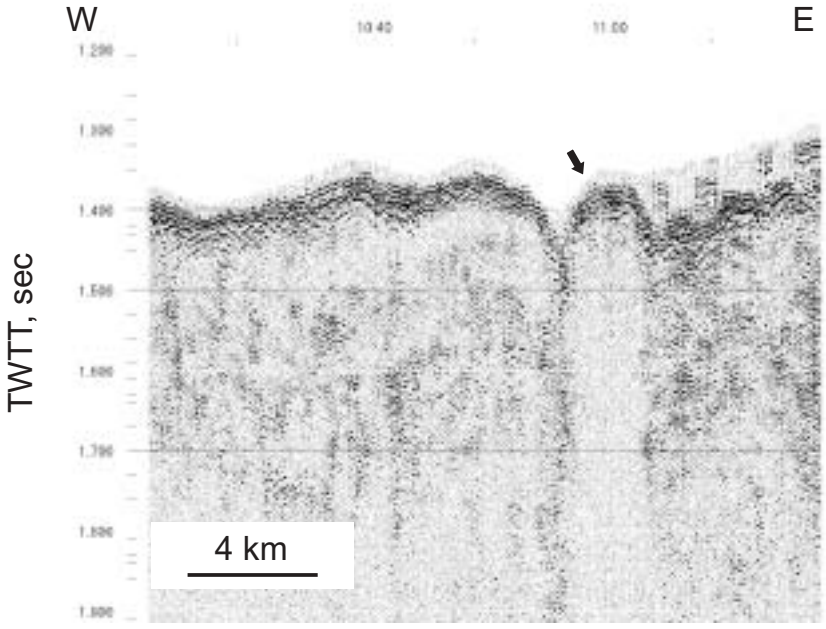

Figure 47. Fragment of seismic line PSAT-210 across Iberico High (arrow).

09:22 and 10:00, runs on a gentle west facing slope with outcropping layers of uplifted and eroded sediments.

A flat sea bottom over an undisturbed sedimentary sequence is crossed at the end of the Cadiz Channel, from 10:00, to 10:33.

From 10:33 to 10:57 the seabed is irregular and the sedimentary sequence is acoustically transparent within the upper 100 ms. This may be due to the presence of mud waves on the seabed but also may indicate that sediments are gas-charged.

PSAT-213

From the beginning of the line to 11:43 a well-stratified sequence up to 700 msec thick and probably of contourite origin is seen. From 11:43 to 12:03 an acoustically transparent diapiric structure outcrops on the seafloor. Incision observed at 12:10 on the seismic record corresponds to an arcuate feature on the NRL sidescan sonar mosaic and is produced by the fast flowing Mediterranean Undercurrent.

From 12:10 to 12:24 another fragment of well-stratified contourite sequence is visible. The line then runs across an acoustically chaotic uplifted structure (Lolita Dome) between 12:24 and 12:50. Cadiz Channel is crossed between 12:50 to 14:50, and the seabed has an irregular topography. Truncated reflections or hummocky surfaces with limited penetration underneath are common. Several diapiric structures can be recognised within the underlying sequence.

From 14:50 to the end of the line the seabed gently dips and fragments of contourite sequence, possibly displaced by faults, are observed.

PSAT-214

This seismic line is a short section whose principal objective was to determinate if the Lolita Dome represents a mud volcano feature. The profile is oriented in a S-N direction. The structure appears at 16:42 and is seen to the end of the line (Fig. 48). No internal structure is observed.

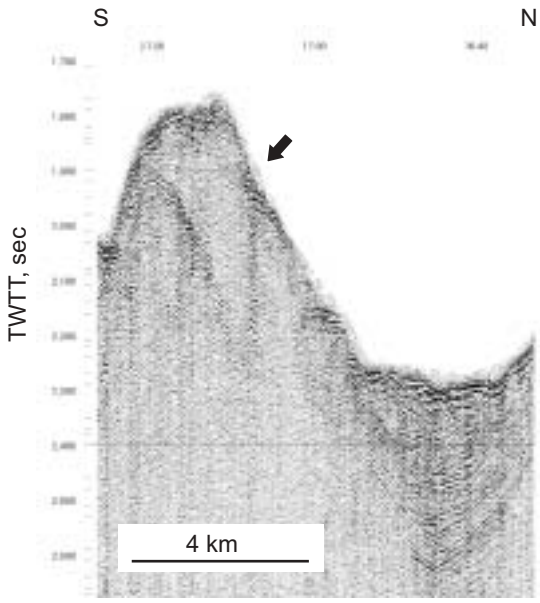

Figure 48. Fragment of seismic line PSAT-214 across Lolita Dome (arrow).

PSAT-215

This line runs in a W-E direction and crosses an incised contourite channel between 18:30 and 18:50. To the west of the channel till almost 21:00 a well-layered contourite sequence up to 500 msec is seen. The continuity of the sequence along the line is interrupted by a diapiric structure outcropping on the seafloor between 20:00 and 20:20. Another 150 m high diapir is seen at the end of the line at 21:10.

III.1.3.2. Sidescan sonar interpretation

V. TESTA, N. H. KENYON, A. AKHMETZHANOV AND M. IVANOV

OKEAN and 5 kHz hull-mounted profiler data

Approximately 320 km of profiles of OKEAN long-range sidescan sonar (9 kHz) and hull-mounted sub-bottom profiler (5 kHz) data were acquired in the Gulf of Cadiz.

Lines 206 to 209 run across part of the proximal contourite system of the Mediterranean Outflow Water (MOW) to as far as a shallow branch of the Portimao Canyon.

Figure 49. 5 kHz sediment profile along Line PSAT-206 showing contourite mud waves and basin floor.

Line 206

The line crosses the contourite sediment waves overbank of the main terrace formed by the MOW. Part of the line crosses a narrow plateau (19:30-19:45) with uniform backscatter and a gentle slope. The beginning of the slope (20:00-20:30) has subtle NW-SE oriented bedforms, about 10 m in height. These bedforms are interpreted as contourite mud waves and develop between 900 and 1200 m water depth (Fig. 49). Bedforms increase in magnitude down slope up to about 50 m high in the middle part of the slope (21:00 to 21:30). Between 21:45 and 22:25 the low backscattering identified on the OKEAN record corresponds to a sand lobe (Fig. 50).

Line 207

This line crosses the distal portion of the Gil Eanes Channel, which is oriented NE-SW and extends for about 40 km. The channel floor shows higher backscatter than the neighboring seabed sediments. This portion of the channel is about 1000 m, 150 m deep and with its eastern margin lower then its western margin (Fig. 51a-b). The channel is flanked by mud waves that are located on levees and are up to 30 m in height.

Line 208

This line runs E-W from a depth of 1010 to 1500 m, and shows the gradient of the

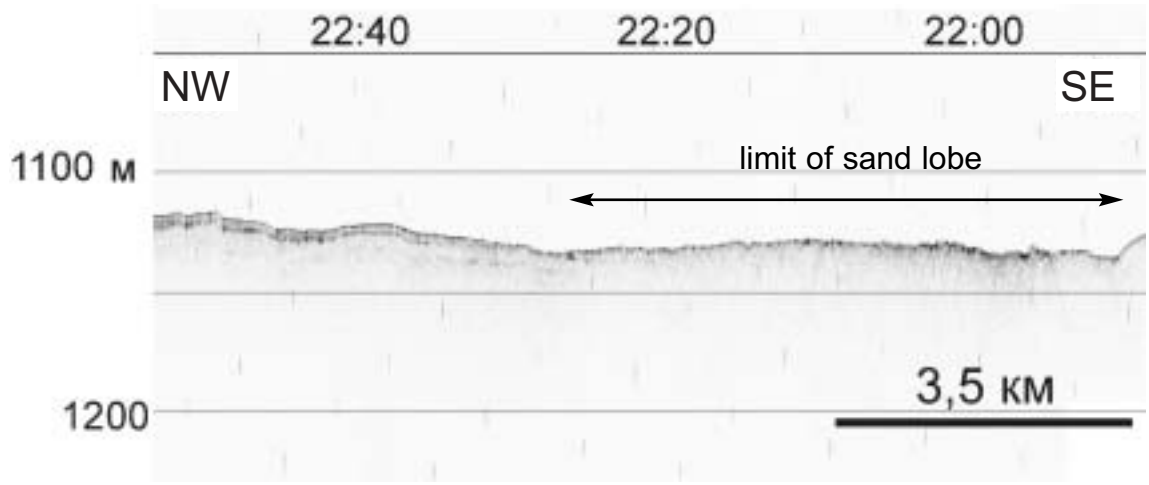

Figure 50. 5 kHz sediment profiler section along Line PSAT-206 across a sand lobe on the basin floor.

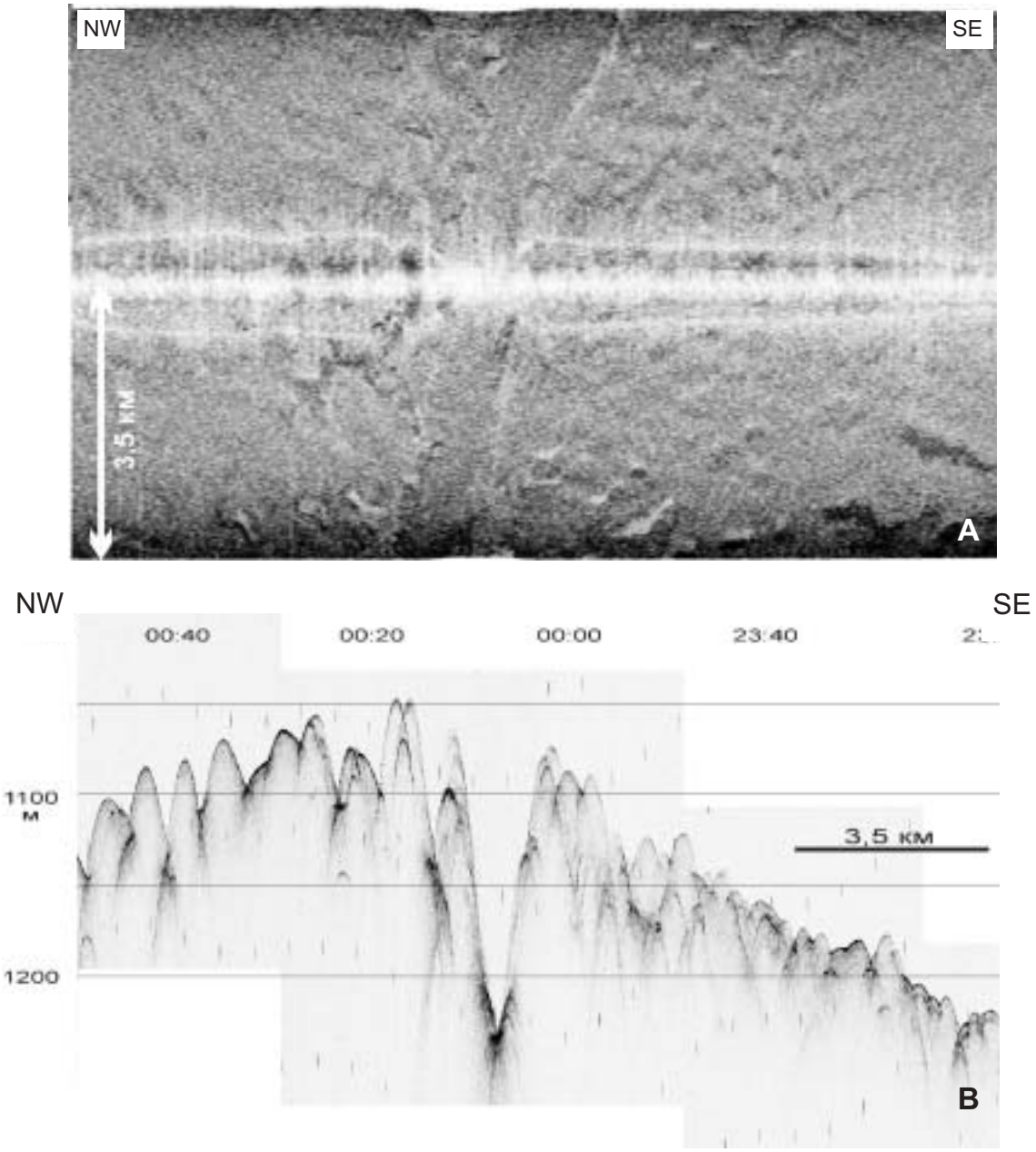

Figure 51. Crossing through Gil Eanes Channel, section of Line PSAT-207. a) Detail from OKEAN sidescan record; b) 5 kHz sediment profiler, vertical exaggeration 25 to 1.

continental slope in this area The line crosses a strongly backscattering steep sided feature, 80 m high (1:08), which appears on the SeaMap sidescan mosaic as part of a larger sub-rounded structure of about 1900 m in width. OKEAN showed high backscatter features associated with sharp changes in depth at 2:00. This structure is oriented SW-NE and was confirmed as a new mud volcano and named Aveiro (Fig. 52). Additional highs were identified on the sidescan sonar mosaic and on the 5 kHz profiles at 3:05 and 3:36, with heights of about 60-80 m.

Line 209

The line starts with a section through a branch of the Portimao Canyon. Positive structures can be seen at about 5:00, 5:13, 5:48, and are associated with subsurface diapiric structures. These highs are SW-NE oriented and vary from 120 to 190 m in height. The highs show high backscatter whilst the inter-high areas show low backscatter. High backscatter on the OKEAN record is also associated with steep slopes, seen at 5:20 where a slope with a relief of 120

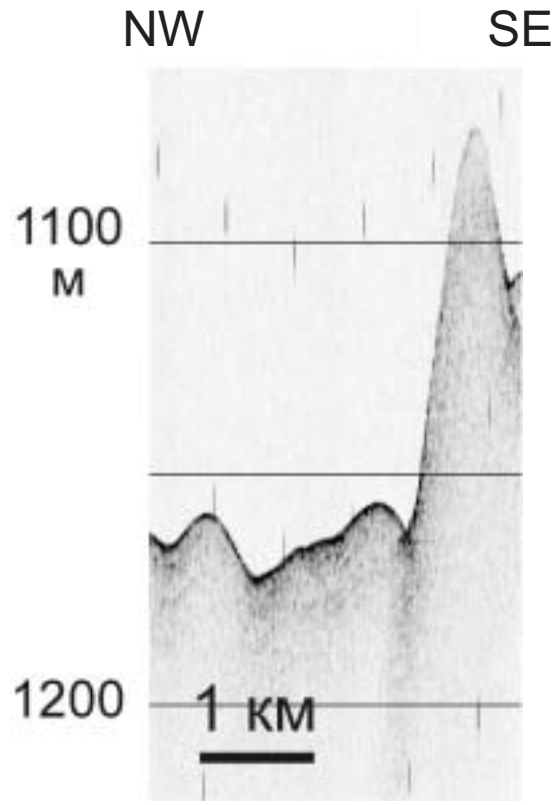

Figure 52. Fragment of 5 kHz sediment profiler line PSAT 208 across Aveiro mud volcano.

m is related to local tectonics. Another slope, crossed at 6:50, has a ENE-WSW orientation. The end of the profile shows low backscatter and has SE-NW oriented features, which are probably associated with sand waves as the result of reworking by strong sea-bottom currents.

Lines 210 to 215

Two hundred kilometers of lines were run to produce a complete overlapping OKEAN mosaic. Lines 210, 212, 213, 215 run E-W and lines 211 and 214 run S-N. The lines were run in order to map the distribution of mud volcanoes in the area of four regional features, from west to east, **1)** a possible mud volcano on the top of a circular high (line 210, 8:10-8:50); **2)** various structures on the Guadalquivir Diapir Ridge (GDR, lines 210 and 215), such as the Ibérico High (line 210, 10:04); **3)** various topographic highs located in the Cadiz Channel (Lines 210, 211, 212, 213 and 215); **4)** to map possible mud volcanoes on the mud wave field (east of line 215).

The topographic highs investigated as possible mud volcanoes generally showed as small patches of high backscatter on the sidescan sonar, a common pattern for mud volcanoes. Although many features showed this pattern, none of the surveyed structures in this area had been confirmed as mud volcanoes. However, a number of other important features had been identified.

The GDR and the Cadiz Channel, which are very well defined on the sidescan mosaics as very large-scale features, were crossed on various lines. The GDR controls the pathway of the MOW in the area of the Cadiz Channel. A number of mud wave fields are identified to the south of the channel, as seen in the OKEAN record (Line 213,

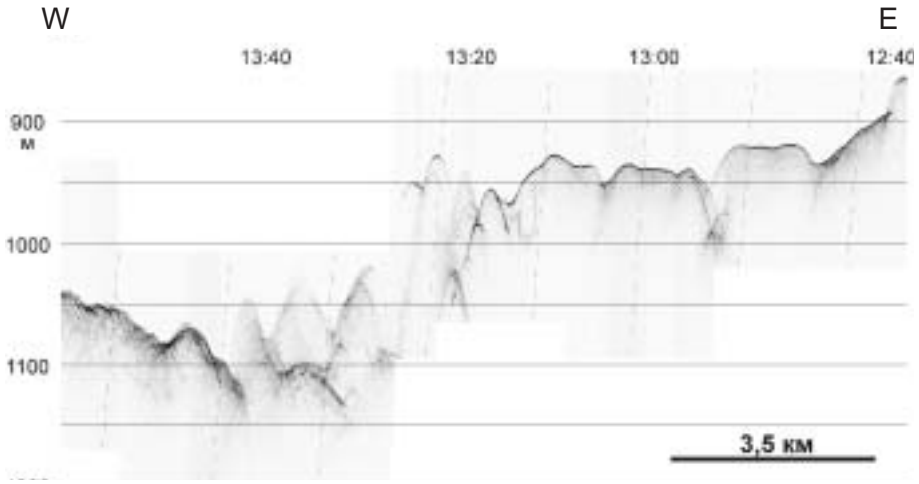

Figure 53. Detail of 5 kHz profiler along PSAT-213 showing mud wave field southeast of the Cadiz Channel.

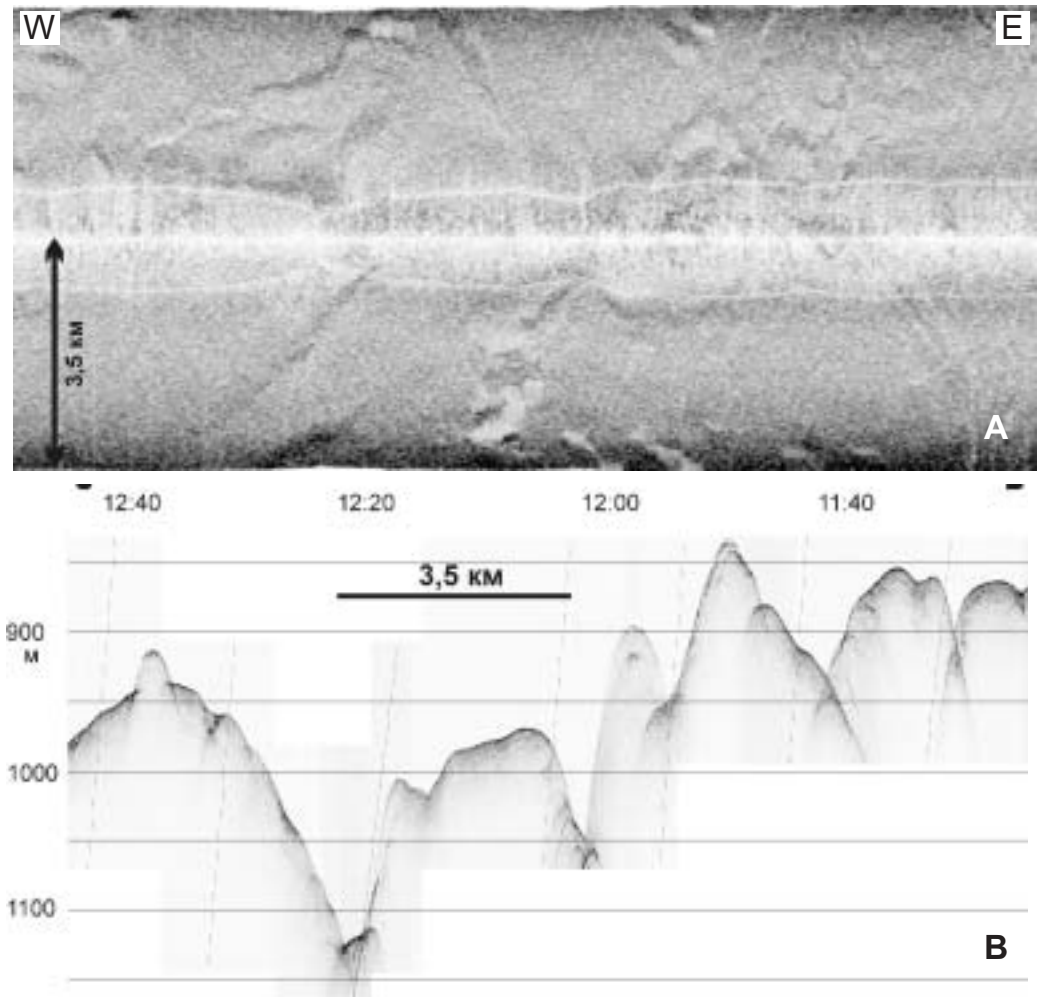

Figure 54. Detail of secondary channels, NE-SW oriented identified along Line PSAT-213 at 12:23 and 12:04 and NW-SE oriented ridge at 12:40. a) OKEAN record; b) 5 kHz profile.

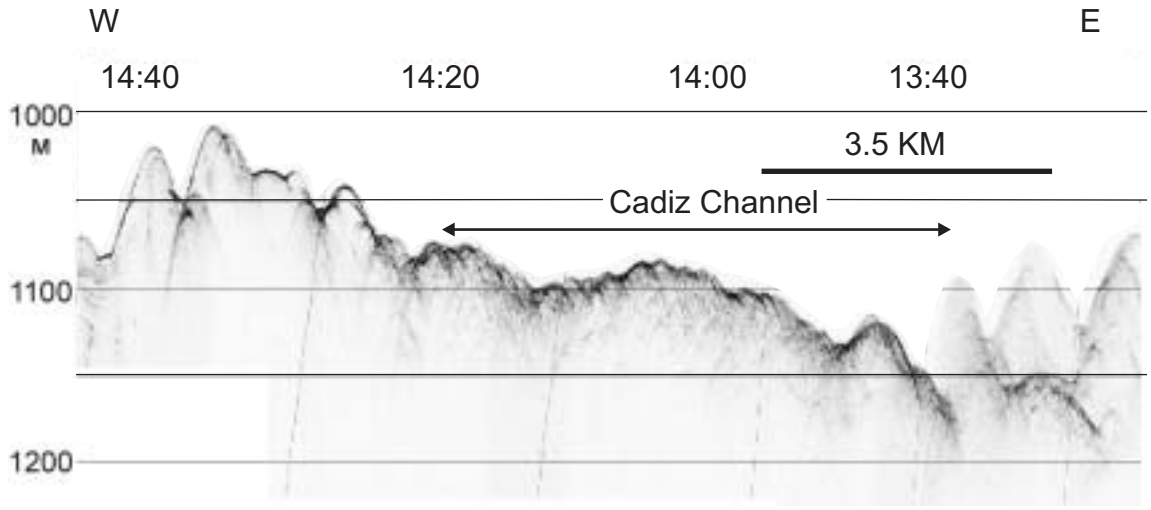

Figure 55. Detail of 5 kHz profile showing a sand wave field identified in the southern part of the Cadiz Channel (Line PSAT-213).

13:00) (Fig. 53). The OKEAN also recorded abandoned channels as deep as about 100 m and with a NE-SW orientation (Lines 213 at 12:23 and 12:04). Other NW-SE oriented features can also be seen, but seem to be related to another process (Lines 213 at 12:40) (Fig. 54 a-b). Other more subtle patterns are seen over the southern part of the Cadiz Channel (14:00) (Fig. 55). The NE-SW trend of features is in agreement with the orientation of the recognized channels in the region, such as Gil Eanes and Cadiz Channels. Sand waves were identified on the OKEAN, and appear also on the 5 kHz profiler as high backscatter with no sub-bottom penetration (line 213 at 12:04). Similar bedforms were also seen north of the Iberico High (Line 211, 13:10, Figure 56) and inside the Cadiz Channel, as confirmed from Line 211 (Figure 56).

Particular targets were surveyed in detail using MAK 30 kHz sidescan sonar and are described below.

MAK deep-towed sidescan sonar data

Line MAK-42AT

A 30 kHz deep towed sidescan sonar and profiler line was run from east to west, passing through the Iberico High and the southern flanks of the circular high in the headward reaches of a branch of the Portimao Canyon, named Lolita Dome. A field of sand waves (up to 7 m high) and longitudinal sand ribbons (Fig. 57) marks the bend in the sand transport path that extends northwestwards from the bottom end of the Cadiz Channel. The Iberico High (Fig. 57) has strong backscatter and a pattern of sharp, near parallel shadows indicative of bedding and faulting in a rock outcrop. To the northwest of the High there is an asymmetrical 60 m deep, presumed to be an erosional scour hole, downstream of the obstacle. It is comparable with, for instance, the deeps in the strong bottom currents of the Faeroe-Shetland Channel (Kenyon et al., 2000). A drift that is low backscattering, parallel bedded and without any ornamentation by bedforms, extends as far as another strongly backscattering area. It has the same pattern

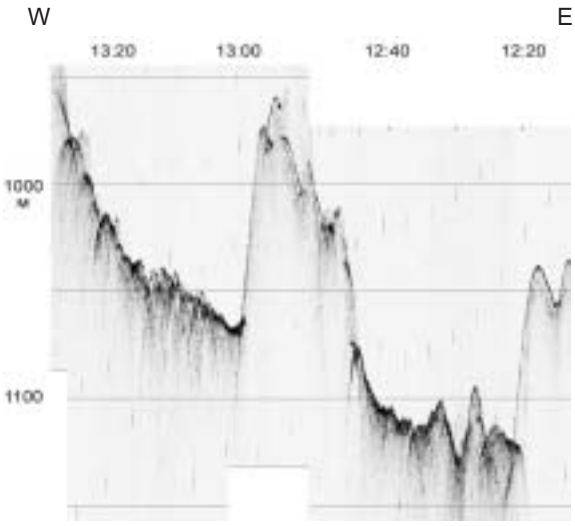

Figure 56. Sand waves field identified north of the Iberico High and in the south Cadiz channel, Line PSAT-211.

of sharp shadows (Fig. 58) as seen on the Iberico High and presumably has a similar origin and history. This pattern is seen both on the high and on the east side of a canyon. To the west of this high are the rocky walled and floored canyons (Fig. 58) at the head of a branch of the very extensive Portimao Canyon system. The exposed rocks are bedded and faulted. To the south of the canyon the seafloor shows good penetration on the profiles and low backscatter on the sidescan record. Ridges in this area trend mainly NE-SW. The floor of the canyon (Fig. 58) shows little penetration on the profiles but has low backscatter on the sidescan sonar. On the SeaMap sidescan sonar the backscatter was medium, implying that there are coarser sediments at a shallow depth below a possible hemipelagic surface layer. A steep sided, narrow channel (about 60 m wide) crosses the broad floor of the canyon. It has a moderate sinuosity and is about 15 m deep, where crossed, and is without obvious levees. The channel seems to originate to the north of the MAK line. The circular high has a pattern resembling bedding and faulting in rock outcrops (Fig. 59). This is similar to the pattern on the other exposed rocks along this MAK line but here there is relatively low backscatter. This is in keeping with it having a thin cover of hemipelagic sediment, deposited from the overlying MOW. The

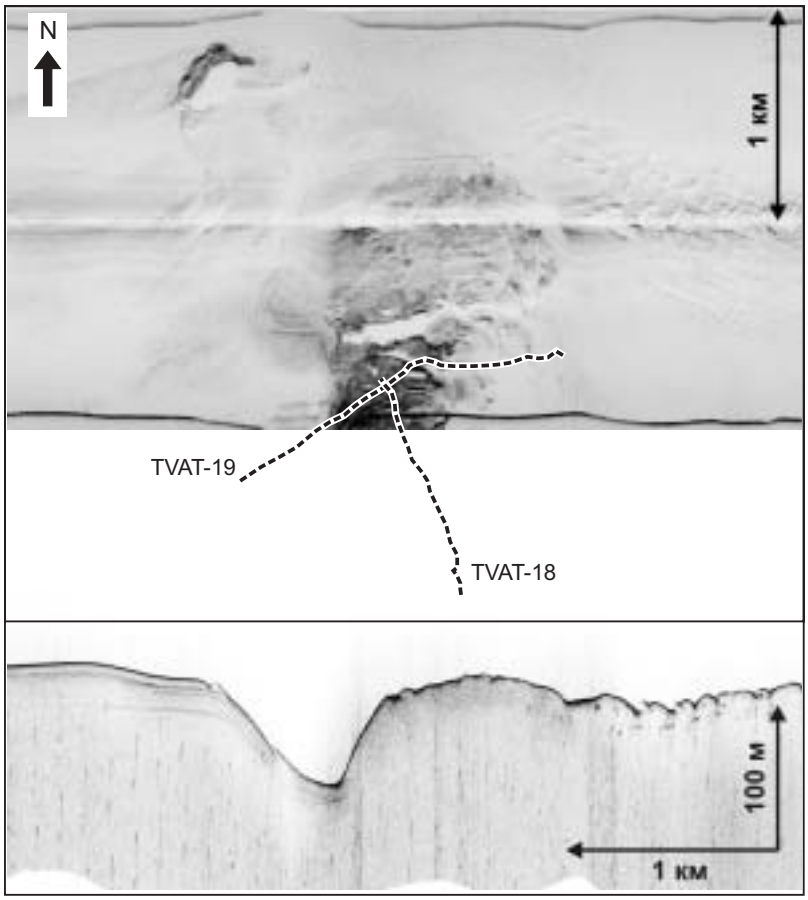

Figure 57. Part of the Iberica High with sand waves and sand ribbons on its eastern side and an asymmetrical scour hole on its downstream side. The strong backscatter on the high is interrupted by scarps, seen as shadows. The track of camera runs TVAT 18 and TVAT 19 are marked.

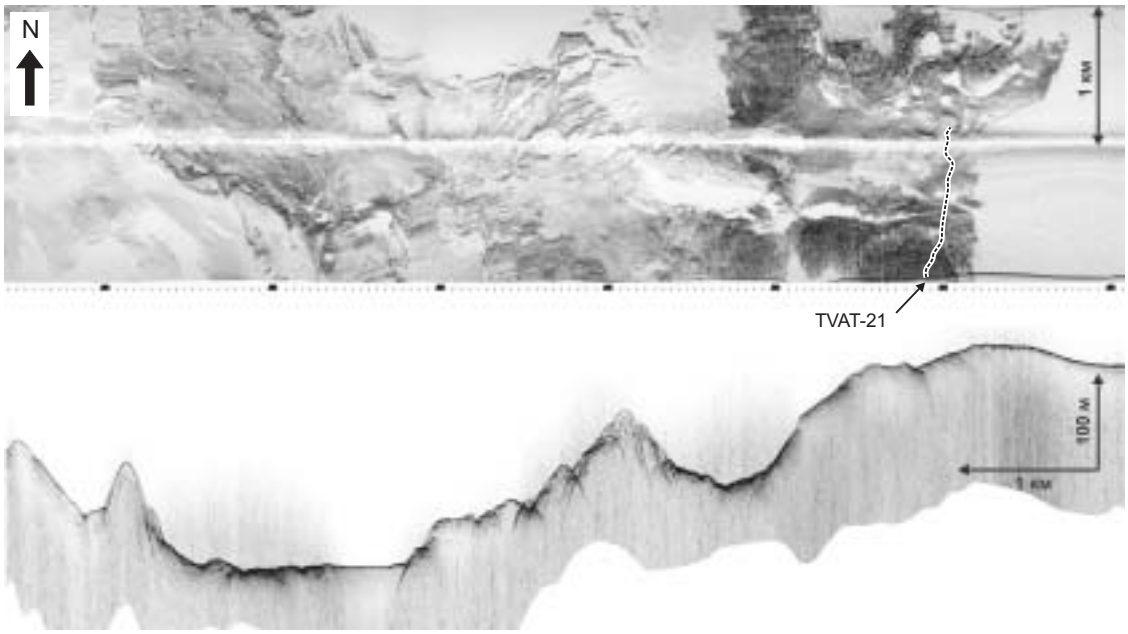

Figure 58. Part of a strongly backscattering diapiric high and the rocky headward reaches of the Portimao Canyon. The track of TVAT-21 is marked.

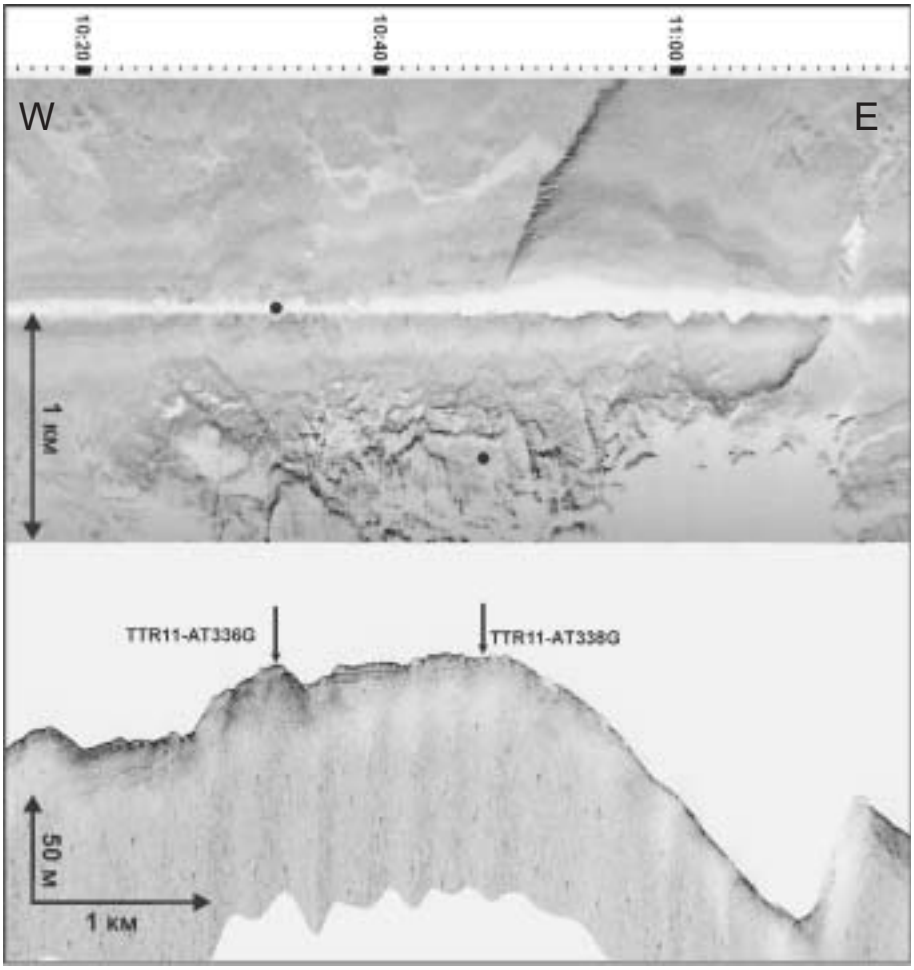

Figure 59. The southern part of a circular high (Lolita Dome) that is surrounded by the Portimao Canyon. The dominant structural trends are NE-SW. Slabs of bedded sediment have slid off the SW slopes of the high.

west side of the high has been subject to sliding as slabs of layered sediment are missing. The overall low backscattering appearance of the area of instability implies that the sliding is not recent.

Line MAK-43AT

A line was run in order to get an image of a possible mud volcano, that had been seen on the seismic profile of PSAT 207 to pierce through the surrounding sediments. The line was run from north to south with the 30 kHz sidescan and 7 kHz profiler. The feature is 100 m high, measured from its base to the north, and 120 m high, measured from its southern base (Fig. 60). It appears to have been crossed a little to the east of its summit. The profile shows very limited penetration compared with the 30-40 m or so of the surrounding mud wave field. High backscatter, attributed to mud flows, occurs mainly on the west side. The lower flanks of the hill appear to have a cover of the surrounding contourite mud. A hole, possibly a pockmark, is seen about 700 m east of the summit. The shape and configuration of the flows is in keeping with it being a mud volcano and has been named Aveiro.

The mud waves are oriented NW-SE and have relatively rounded crests and troughs, typical of mud waves at this depth in this region. There is a slump scar on the crest of one mud wave (Fig. 61).

Line MAK-44AT: channel and lobe system beyond Gil Eanes Channel

A 100 kHz MAK line was run to investigate a small channel and lobe system

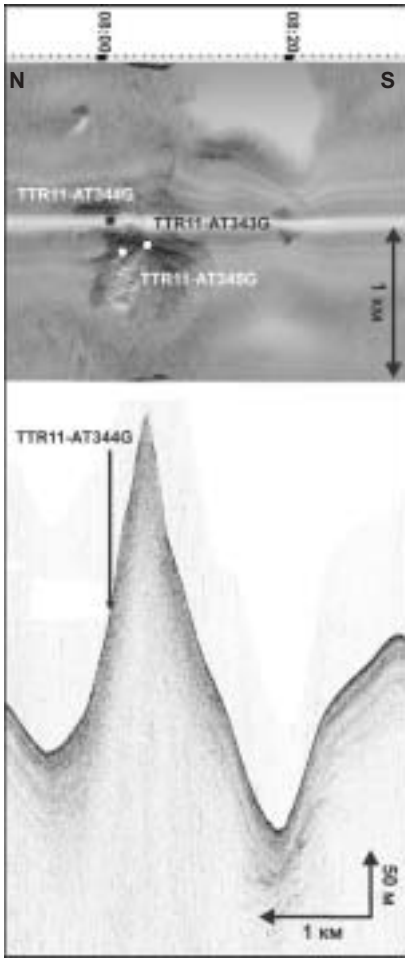

Figure 60. Aveiro mud volcano seen on MAK 30 kHz sidescan sonar and 5 kHz profiler records. (Line MAK-43AT)

that had been detected on the SeaMap and TOBI sidescan sonar mosaics as an area of low backscatter. A piston core (D13682), taken on RRS Discovery cruise 244 had confirmed that there were ungraded fine sands in the northern part of the lobe. The height of the MAK fish above the seafloor was 100 m on average, which was expected to give a better resolution of deep towed profile and sidescan sonar record than had previously been obtained over such features in the deep ocean. Unfortunately the starboard channel was not working and time constraints prevented repair or the replacement of the MAK fish with the second vehicle. The line started from the end of the contourite channel, where sands are believed to be accumulating at the point where the MOW leaves the seafloor at a depth of about 1200 m. The gradient descends steeply at first, through an area of contourite mud waves which extend down to a depth of 1300 m. A channel crosses at right angles to the track, i.e. close to an along slope direction, and may be running along a trough between mud waves. The channel is fairly sinuous (sinuosity about 1.2) and crosses the track in five places in the part of the slope where the profile shows good penetration and many near parallel beds that thin downslope. The channel depth at the uppermost two crossings is about 5 m whereas on the next three crossings the channel is about 1 to 2 m deep and is braided (Fig. 62). The cross sectional area of the channel seems to remain constant.

The lower part of the line turned to the south in order to cross the proximal part of the lobes. The lobe surface is fairly bumpy and the upper layer is almost transparent, with a thickness of 15 m in the north and about 8 m at the southern end of the line. There are parallel beds below the near transparent layer. Several channels, up to 2 m deep, cross the proximal lobe and appear to be on top of low elevations (levees?) lying above the transparent deposit (Fig. 63). The edge of the southernmost channel-levee complex marks the edge of the lobe as determined by the SeaMap mosaic. One channel

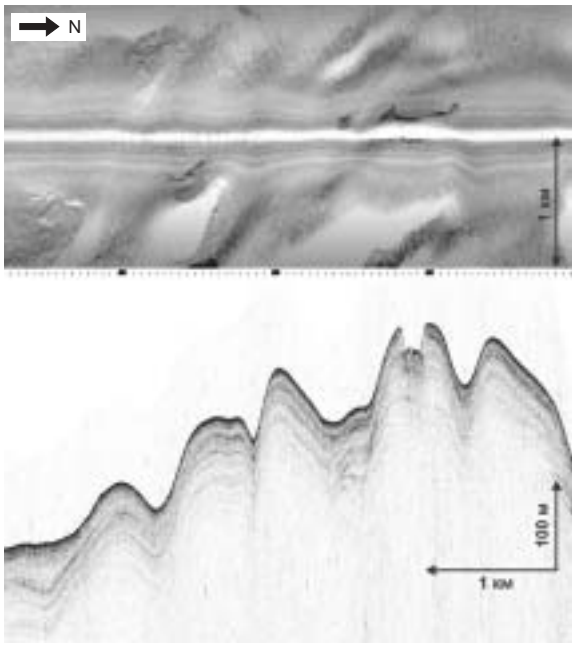

Figure 61. Fragment of Line MAK-43AT across several mud waves. A possible slide scar is seen on the crest of one of them.

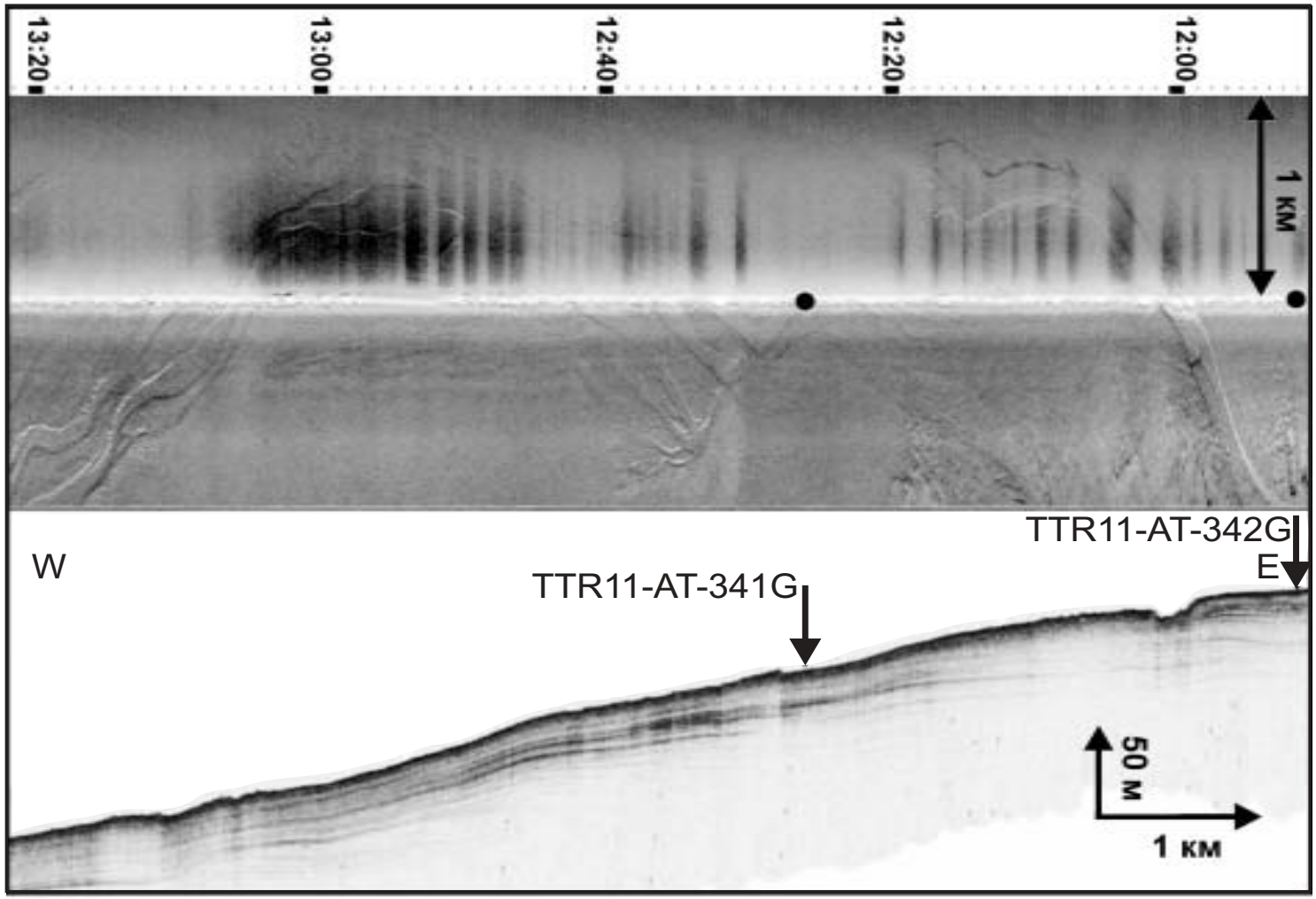

Figure 62. Fragment of 100 kHz sidescan and profile (MAK-44AT) showing several crossings of sinuous and braided channels. The part of the channel is about 5m deep. Braided channels are about 2 m deep (12:57-13:28).

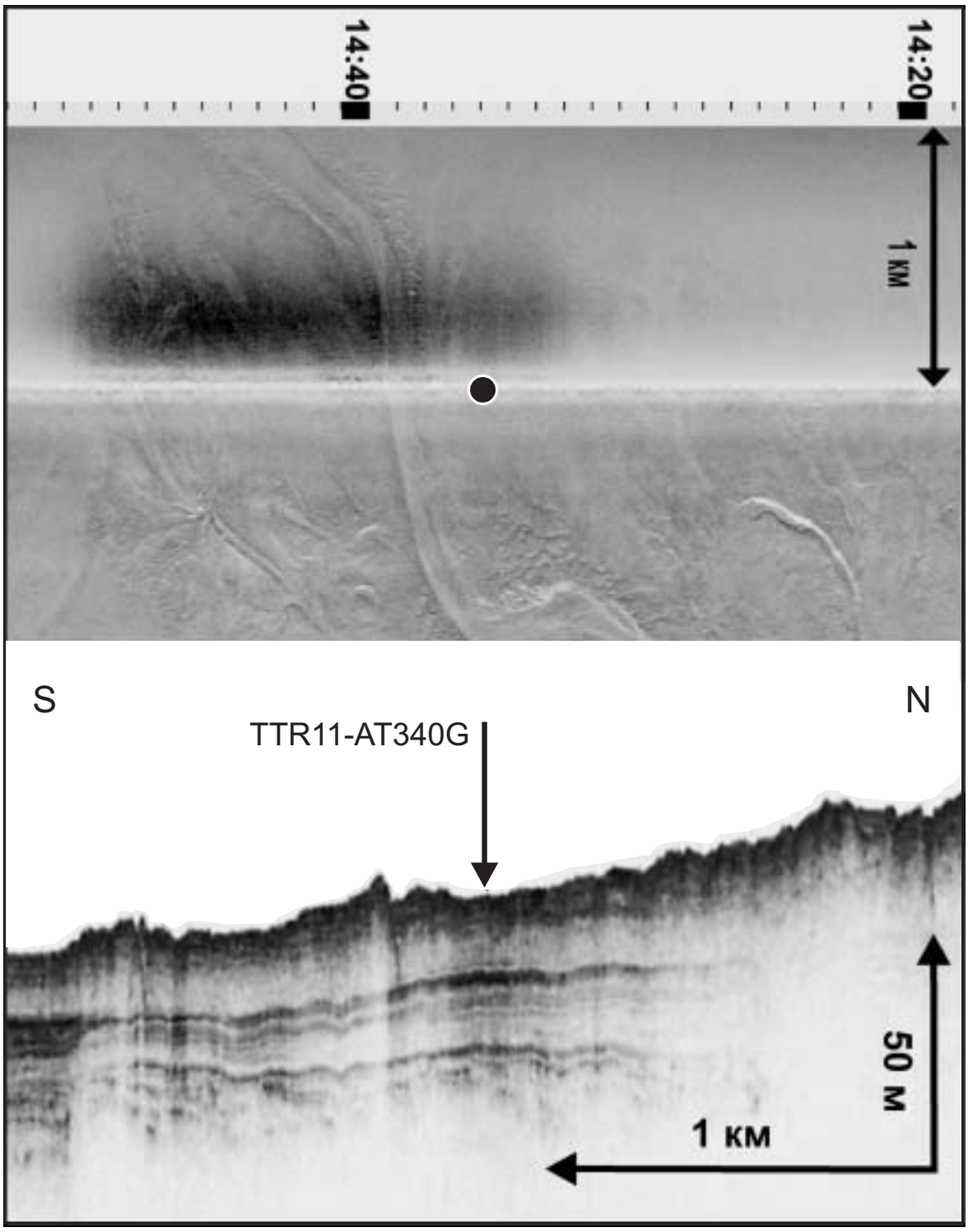

Figure 63. 100 kHz sidescan and profile of channels on top of presumed sand lobe(s). The channels are associated with slightly higher, and thicker, parts of the lobe.

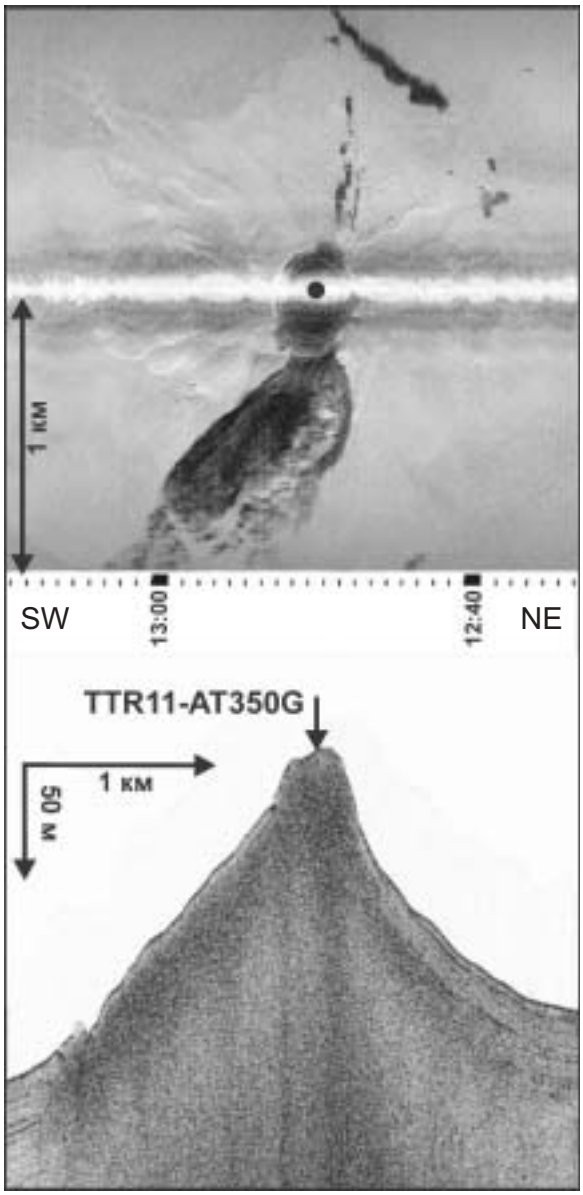

Figure 64. Carlos Ribeiro mud volcano seen on MAK 30 kHz sidescan sonar and 5 kHz profiler records. Sampling station AT-350G is shown (Line MAK-45AT, 12:25-13:20).

has, what seems to be, a pattern of regular, transverse bedforms along its flanks. These may be sand waves or scours.

Line MAK 45AT

This 30 kHz sidescan and 5 kHz profiler line was run in order to obtain details of the Carlos Ribeiro and Olinin mud volcanoes, first recognized during the TTR-10 cruise. The Carlos Ribeiro mud volcano was crossed through the centre of its circular summit crater and was found to be about 100 m high (Fig. 64). Only one high backscattering mudflow was seen, extending to the southeast. The area of the mud volcano could clearly be mapped, from the prolonged reflection on the 5 kHz profile and from faint patterning in the sidescan record, as having a diameter of about 2.2 km. The middle and lower northeastern flanks of the mud volcano are covered in thick, parallel bedded sediments. The most recent flows are determined from their high backscatter as being to the south of the summit. An east-west trending strongly backscattering lineament is mapped at the northern foot of the mud volcano and may be a fault trace.

The Olinin mud volcano is 70 m high, where crossed, and its summit appears to be just to the south of the line (Fig. 65). No crater is detected. The most recent mud flow, i.e. the most strongly backscattering, appears to be to the south of the summit, with another, more faintly seen one, to the north. The northern flow is in a place on the profile where there is a thick series of parallel beds. Thus it may be very thin.

The intervening low backscattering area has an irregular topography rather than the type of profile found where there are regular contourite mud waves. It is thought to be in an area where a tectonically formed topography is covered by a drape of at least 50 m of parallel bedded sediment. No obvious thickening is seen in the deeps and there are some possible examples of small scale vertical faults.

III.1.4. Bottom Sampling Results

G. Akhmanov, A. Stadnitskaia, A. Akhmetzhanov, M. Ivanov, D. Ovsiannikov, A. Sadekov, H. Duarte, V. Magalhaes and Sedimentogical Team of TTR-11, Leg 3

The bottom sampling programme in the Gulf of Cadiz was aimed mainly at obtaining material for sedimentological, geochemical, biological and micropaleotological studies of fluid escape features, either known from previous studies or presumed on the basis of the large geophysical data set available. Three cores were taken from a sandy

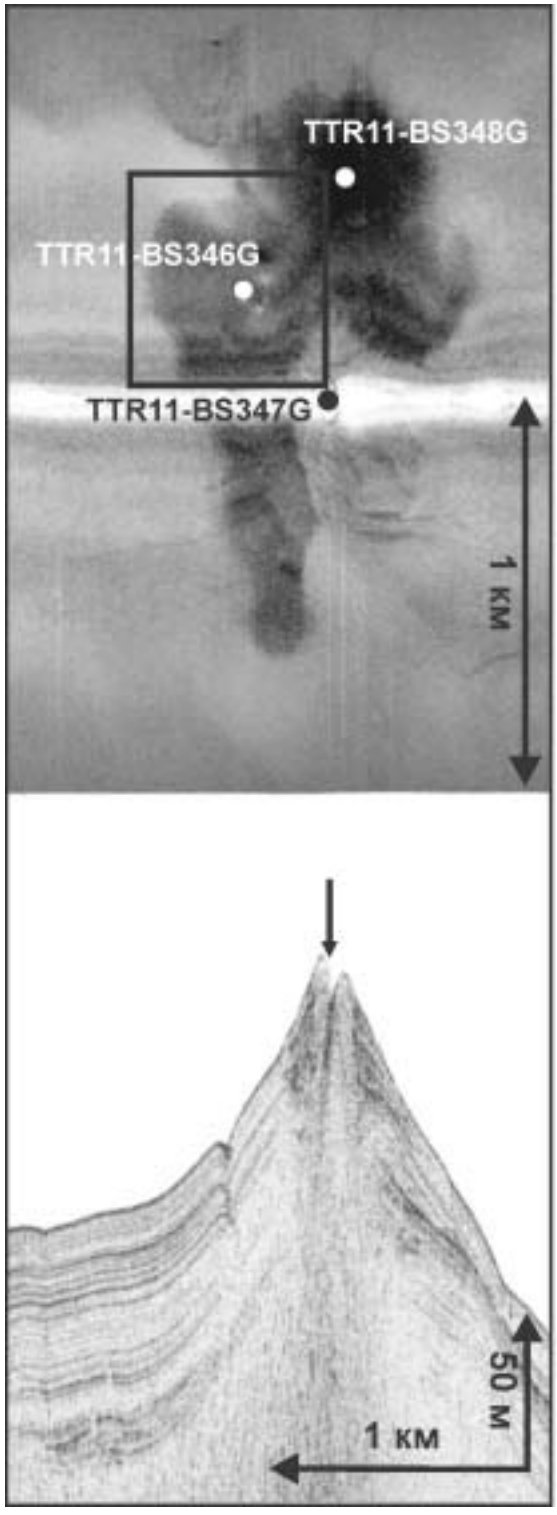

channel-lobe system found immediately beyond the mouth of the Gil Eanes contourite channel.

A total of 18 sites (Fig. 43) in the South Portuguese field and the Eastern Portuguese field were chosen to be sampled

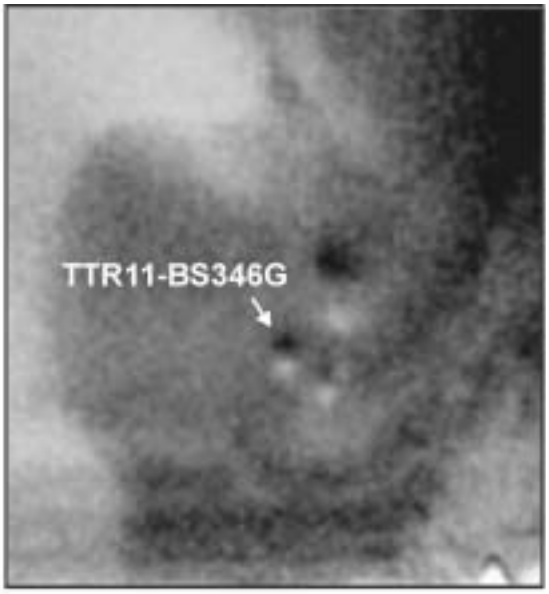

Figure 65. Olenin mud volcano seen on MAK 30 kHz sidescan sonar and 5 kHz profiler records. Sampling sites are shown. (Line MAK-45AT, 19:20-20:23)

based on the interpretation of the SeaMap mosaic of NRL, and seismic and acoustic data obtained during the cruise: 15 by gravity coring (total recovery 31.92 m), 2 by dredging, and one by TV-controlled grab system. Three CTD lines were performed also and seawater samples were taken along the profiles.

Main results of bottom sampling are summarized in core logs (see Annexe I) and Tables 2 and 3.

The South Portuguese Field

Two main targets were investigated on the South Portuguese Field during the Leg 3 of the principal TTR11 cruise – the Olenin and Carlos Ribeiro mud volcanoes, discovered and sampled for the first time during TTR10 cruise (Kenyon et al., 2001), when mud breccia with numerous rock fragments were collected from both structures.

Olenin mud volcano

Three sites within the Olenin mud volcanic structure were chosen for sampling by gravity corer on the base of interpretation of the MAK-1 line carried out during the

Table 2. General information on the cores sampled in the Gulf of Cadiz, Leg 3

Core No	Date	GMT	Latitude	Longitude	Cable Length (m)	Depth (m)	Recovery (cm)
AT335D	25/08/01	02:15 02:50	36°07.159 36°07.405	-7°41.129 -7°41.198		1037 905	
AT336G	25/08/01	20:09	36°08.284	-7°59.498	1467	1485	147
AT337CTD	25/08/01	21:01 21:23 21:45	36°08.590 36°08.586 36°08.589	-8°00.191 -8°00.187 -8°00.182		1340	
AT338G	25/08/01	22:14	36°08.585	-8°00.175	1347	1340	184
AT339D	26/08/01	05:22 06:08	36°07.765 36°07.591	-7°46.461 -7°46.587		1086 1021	
AT340G	27/08/01	19:23	35°45.146	-7°36.495	1475	1475	
AT341G	27/08/01	21:24	35°46.914	-7°31.487	1360	1365	
AT342G	27/08/01	22:53	35°46.983	-7°29.355	1290	1291	224
AT343G	28/08/01	00:38	35°52.311	-7°26.318	1094	1090	191
AT344G	28/08/01	01:33	35°52.400	-7°26.223	1115	1099	175
AT345G	28/08/01	02:30	35°52.391	-7°26.353	1120	1107	144
AT345aG	28/08/01	03:11	35°52.389	-7°26.351	1115	1108	
AT346G	29/08/01	01:47	35°34.909	-8°37.709	2644	2649	515
AT347G	29/08/01	03:20	35°34.878	-8°37.968	2634	2636	334
AT348G	29/08/01	04:55	35°34.748	-8°37.915	2643	2651	446
AT349CTD	29/08/01	15:27 16:08 16:59	35°47.246 35°47.246 35°47.275	-8°25.425 -8°25.423 -8°25.418		2219 2212 2237	
AT350G	29/08/01	17:33	34°47.272	-8°25.408	2208	2227	192

cruise: AT346G from a pockmark area on the slope on the structure; AT347G from the old crater; and AT348G from a mud flow on the slope (Fig. 65). Although all three cores were represented by marly pelagic sequences and no mud volcanic deposits were collected, every core contained strong indicators of recent intensive fluid venting in the area. Among these are authigenic carbonate infills of burrows (analogues of carbonate crusts) in AT346G, a well-developed reduction front in AT347G, and a *Pogonophora* enriched layer in AT348G. Besides, all cores were characterized by a very strong smell of H_2S and bioturbation typical for seepage areas.

Taking into account that mud volcanic breccia was previously collected from this structure during the TTR-10 cruise in 2000, the bottom sampling data implies a recent activity of the Olenin mud volcano, at least in terms of gas seeping. No evidence of recent eruptive activity was found in the two of sampling campaigns.

Carlos Ribeiro mud volcano

The only core (AT350G) was from the Carlos Ribeiro mud volcano, sampled the crater of the structure (Fig. 64). It consisted of 191 cm of mud breccia, oxidized in the upper 10 cm and topped with a thin recent pelagic marl, suggesting recent eruptive activity. The whole sequence was characterized by a strong smell of H_2S.

The Eastern Portuguese Field

The Iberico fluid seepage structure, discovered and sampled for the first time during the TASYO cruise 2000 of the Spanish Geological Survey, was one of the targets for bottom sampling in the Eastern Portuguese

Table 3. Acoustical and geographical characteristics of sampling stations in the Gulf of Cadiz, Leg 3

Core No	Geographical Setting	Sedimentary Summary	Instrumentation	Acoustic characteristic
AT-335D	Iberico mud volcano	Carbonate chimneys	OKEAN sidescan sonar, single channel seismic system, MAK-1 sidescan sonar, TV record, previous investigation, 5 kHz profiler	High backscatter on the sonar image
AT-336G	Top of the Lolita dome structure	Pelagic sediment	OKEAN sidescan sonar, single channel seismic system, MAK-1 sidescan sonar, previous investigation, 5 kHz profiler	Medium backscatter on the sonar image; dome-like structure
AT-337CTD	Slump near the Lolita dome structure	-//-	-//-	-//-
AT-338G	Slump near the Lolita dome structure	Pelagic sediment	-//-	-//-
AT-339D	Ridge near the Iberico mud volcano	Carbonate chimneys	OKEAN sidescan sonar, single channel seismic system, MAK-1 sidescan sonar, TV record, previous investigation, 5 kHz profiler	High backscatter on the sonar image
AT-340G	Sandy lobe of a small submarine channel beyond the Gil Eanes contourite channel mouth	Contourite sequence	MAK-1 sidescan sonar, previous investigation, 5 kHz profiler	Low backscatter on the sonar image
AT-341G	Band of a small submarine channel beyond the Gil Eanes contourite channel mouth	-//-	-//-	-//-
AT-342G	-//-	Contourite sequence with coarsening upwards units	-//-	-//-
AT-343G	Top of the Aveiro mud volcano	Mud breccia covered by pelagic material	OKEAN sidescan sonar, single channel seismic system, previous investigation, 5 kHz profiler	High backscatter on the sonar image, dome-like structure
AT-344G	Slope of the Aveiro mud volcano	-//-	-//-	-//-
AT-345G	-//-	Mud breccia	-//-	-//-
AT-345aG	-//-	-//-	-//-	-//-
AT-346G	Olenin mud volcano, pockmark area	Pelagic sediment	MAK-1 sidescan sonar, 5 kHz profiler, previous investigation	-//-
AT-347G	Old crater of the Olenin mud volcano	-//-	-//-	-//-
AT-348G	Olenin mud volcano, mud flow	-//-	-//-	-//-
AT-349CTD	Crater of Carlos Ribeiro mud volcano	-//-	-//-	-//-
AT-350G	-//-	Mud breccia covered by pelagic material	-//-	-//-

Field. A large set of data from previous investigations and seismic, acoustic and bottom TV data obtained during TTR11 enabled a suitable slope to be choosen for dredging. The material found in the dredge AT335D was subdivided into 6 main groups:

Group A - Slabs or crusts
Group B - Chimneys with oxide cover
Group C - Chimneys without oxide cover
Group D - Sediment
Group E - Small fragments of slabs or chimneys
Group F - Coral branches and carbonate crusts

Dredging line AT339D was carried out on the slope of a ridge showing very high reflectivity on the NRL SeaMap mosaic, which is located near the Iberico structure. The material of this dredge was subdivided into 4 main groups:

Group A - Chimneys with oxide (Fe, Mg) cover
Group B - Chimneys without oxide cover
Group C – Clasts or fragments
Group D – Sediments

According to bottom sampling data, both structures are of similar origin, related to very active recent fluid venting. No evidence of mud volcanism was found.

Two cores, AT336G and AT338G, were taken from a very large dome-like structure (the Lolita Dome) well expressed on the NRL SeaMap mosaic and seismic and acoustic data collected during the cruise (Fig. 59). Both recovered a succession of pelagic marl with foraminifera and some silty admixture, occasionally bioturbated, and with hydrotroilite spots in the lower parts. No clear sedimentological evidence for the origin of the structure was found.

An area within the lobe of a small submarine channel beyond the Gil Eanes contourite channel mouth was sampled at the station AT340G (Fig. 63). The core hit a channel-levee complex on the lobe and recovered a small portion of fine to medium grained siliciclastic sand, moderately sorted and with some foraminifera admixture, implying a recent activity of the gravity flows supplying sandy material to the lobe.

Two cores, AT341G and AT342G were collected from the upper reaches of a system of small submarine channels beyond the Gil Eanes contourite channel mouth (Fig. 62). Core AT341G recovered only 8 cm of brownish grey silty clay with a soupy top and with silt content increasing downward and traces of fine siliciclastic sand in the core catcher. Core AT342G, recovered a 224 cm thick sequence of silty clay, interlaminated with thin silty layers and laminae of very fine grained sand and with mottles and lenses of fine grained sand typical for contourite deposits.

The cone-shaped Aveiro mud volcano presence was inferred from NRL SeaMap mosaic and geophysical data collected during the cruise, was sampled at four gravity core stations (Fig. 60). Core AT343G, taken from the top of the structure, and the cores taken from its slope consisted of mud volcanic breccia with numerous rock fragments blanketed with a very thin marly pelagic veneer. The cores AT343G and AT344G were characterized by a strong smell of H_2S and the presence of *Pogonophora* rich layer in the uppermost part of the sequence. Sampling confirmed a mud volcanic origin of the structure and its recent activity.

Core AT345aG was taken at the same location as the core AT345G and stored in a plastic liner in order to be studied onshore.

III.1.5. CTD measurements

J. REGO

CTD measurements were performed at two stations in the Gulf of Cadiz. One station (AT-337CTD) was in the vicinity of the Lolita Dome structure within a Mediterranean Undercurrent pathway and another (AT-339CTD) in the deeper part of the Gulf, above the Olenin mud volcano. At the both stations, the Temperature (Potential Temperature), Conductivity (Salinity), Pressure (Depth), and Light Backscattering (Turbidity) sensors worked very well – Sound Velocity and Water Density were then calculated from these data. At the second station (AT-349CTD), values for the water pH and REDOX were also recorded. Unfortunately, the latter parameter recordings showed an anomalously high hysteresis between the down- and the up-cast. We have therefore decided to only use the pH profile. The H_2S and Dissolved Oxygen sensors were out of order.

TTR11-AT-337CTD

This station was performed over the Lolita dome structure which was covered in pelagic sediments; the last depth reading

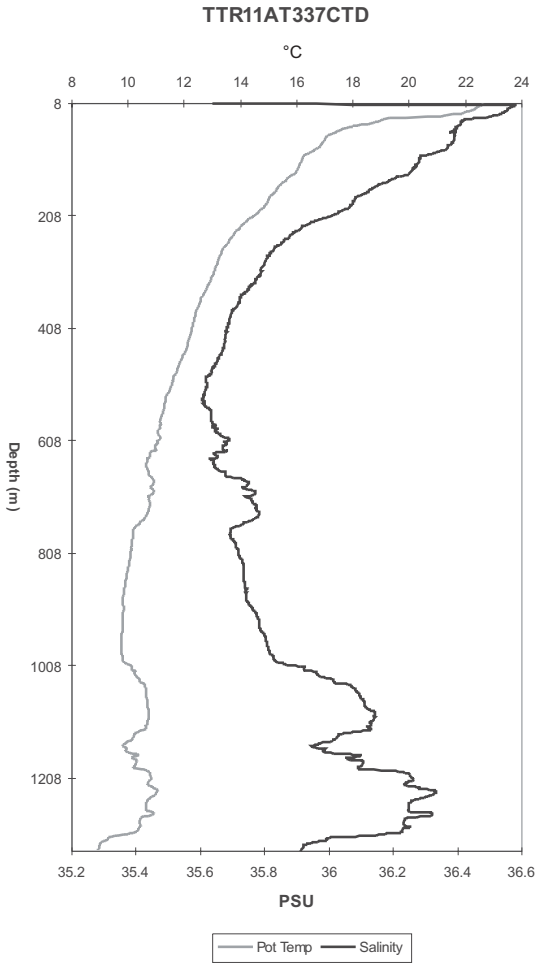

Figure 66. Vertical profiles for Potential Temperature and Salinity at station AT-337CTD

was 1336 m – the CTD stopped 7 m above the bottom. The vertical profiles for Potential Temperature and Salinity (Fig. 66) presented, to a first approximation, the character of a typical water column for this area and time of year. The shallow mid-summer thermocline (~75 m) and the Temperature (~600 m) and Salinity (~1200 m) maxima (an indication of the presence of Mediterranean Outflow Water – MOW) stand out even at a first glance.

As the q-S Diagram (Potential Temperature vs Salinity) shows (Fig. 67), below the separation between the surface layer and the underlying water, the q-S profile "moves" parallel to the ENACW (Eastern North Atlantic Central Water) and to the ESACW (Eastern South Atlantic Central Water) lines just until the ~550 m depth level, where it noticeably shifts towards the upper (core) MOW water-type point (peaking at 736 m). It then decreases in both Temperature and Salinity, only to reach back to the lower (core) MOW point, peaking at 1093 and 1231 m. This "double lower core" of MOW is not commonly seen. It is about 300 m "thick", but there is a clear and sharp division at around 1150 m depth, where the Salinity and the water Temperature both have a significant "drop" (0.2 PSU and 1.0 ºC, respectively). As for the North Atlantic Deep Water (NADW), this station wasn't deep enough (1336 m) for it to be detected.

This strong vertical water separation is even more intriguing when we realize the connection between these parameters (q or S) and the measured Seapoint Turbidity (Fig. 68). Apart from the surface layer (probably due to the euphotic zone biologic activity) highs, it is at the "double lower core" that the Turbidity values stand out; its line "follows" the Salinity's (or Temperature's) lines, having "troughs" and "highs" at the (exact) same depth levels. Trying to understand these peaks in particle concentration (and the mysterious gap in between those peaks) must incorporate a look at the influence that bottom topography has on currents.

The high velocity bottom current that is formed by the dense MOW interacts with the continental slope sediments; in fact, there is a channel which terminates at depths of about 1200 m (where the Mediterranean Undercurrent presumably "detaches" from the seafloor) just ~22 nautical miles due East from this station. Though this structure should help explain the high readings of turbidity in the "Mediterranean levels" of the water column, understanding how the separation of the "double lower core" was formed shouldn't be so straightforward.

A more complete quantitative analysis of the Turbidity profiles will only be performed at a later time, to include comparison with other data from the Gulf of Cadiz. This doesn't prevent a qualitative analysis though, in which we focus on the tendencies, maxima, relation to other parameters, and so forth.

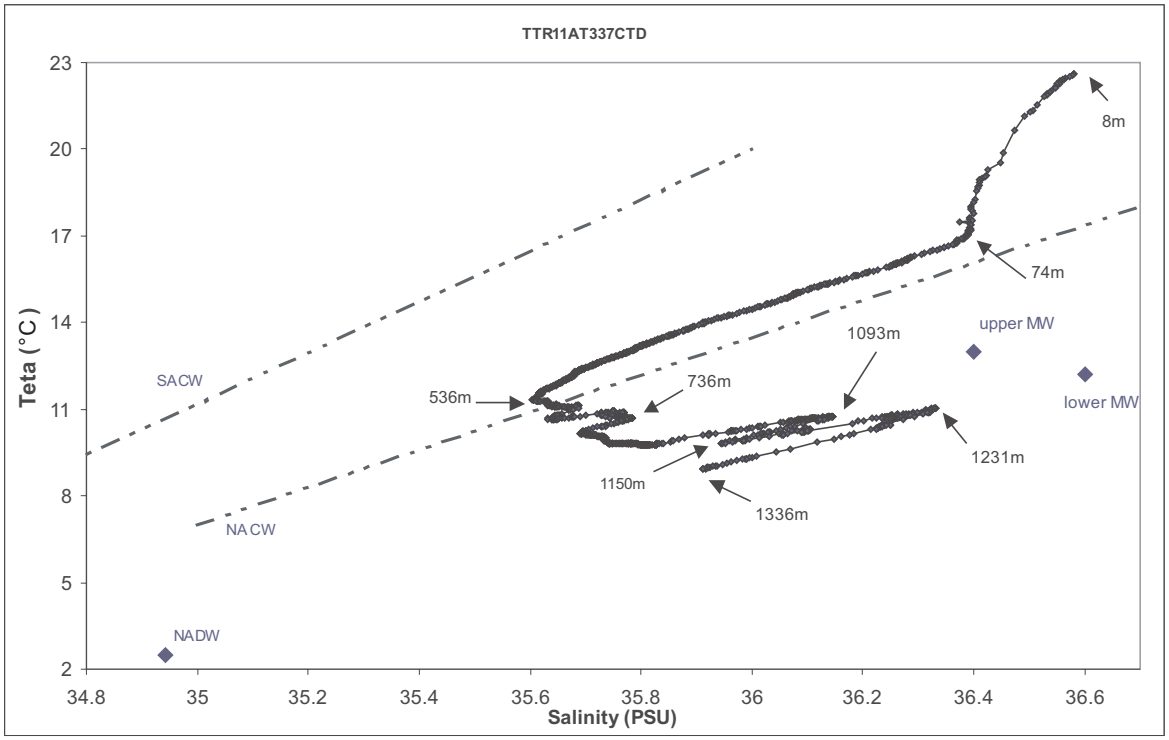

Figure 67. Potential Temperature vs. Salinity at station AT-337CTD showing unusual "double lower core" of MOW (see text).

TTR11-AT-349CTD

The station is over the *Carlos Ribeiro* mud volcano. The last depth reading was 2189 m and once again, the CTD stopped 7 m above the sea floor. The vertical profiles for Potential Temperature and Salinity (Fig. 69) at this station display the more conventional signature of the MOW – a broad and *single* "bulge" from about 600 m to about 1300 m depth. Typically, the maximum Potential Temperature (11.50ºC) is centered at 654 m, while the Salinity maximum (36.17 PSU) is located at 1040 m depth.

As expected, there are no noteworthy Turbidity features (Fig. 70) in this profile (aside from the high values of the first 100 m); in fact, if we compare stations AT-337 and AT-349 (Fig. 71), it is reasonable to say that the latter has much less "personality", that it is more featureless – probably because it is further away from the Strait of Gibraltar (albeit only ~62 km) and because the seafloor is 853 m deeper.

In the q-S Diagram (Fig. 72), below the mixed layer (~70 m), the q-S profile progresses once more between the ENACW and

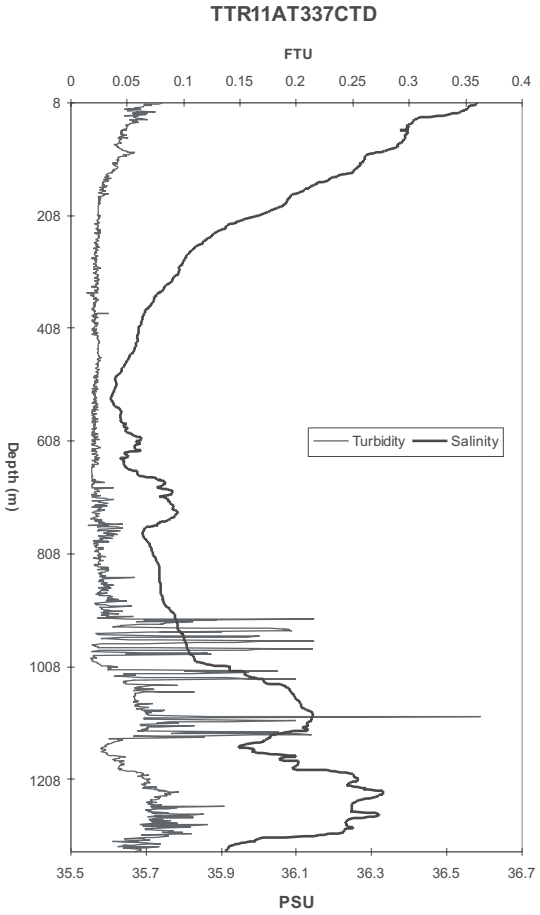

Figure 68. Turbidity and Salinity profiles at station AT-337CTD

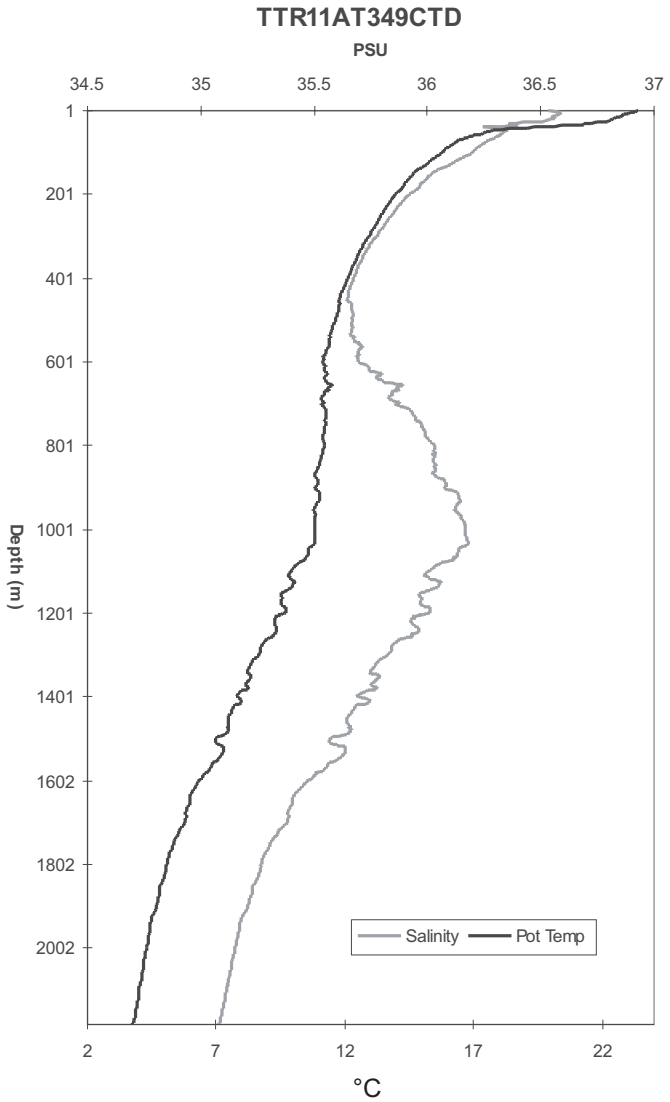

Figure 69. Vertical profiles for Potential Temperature and Salinity at station AT-349CTD

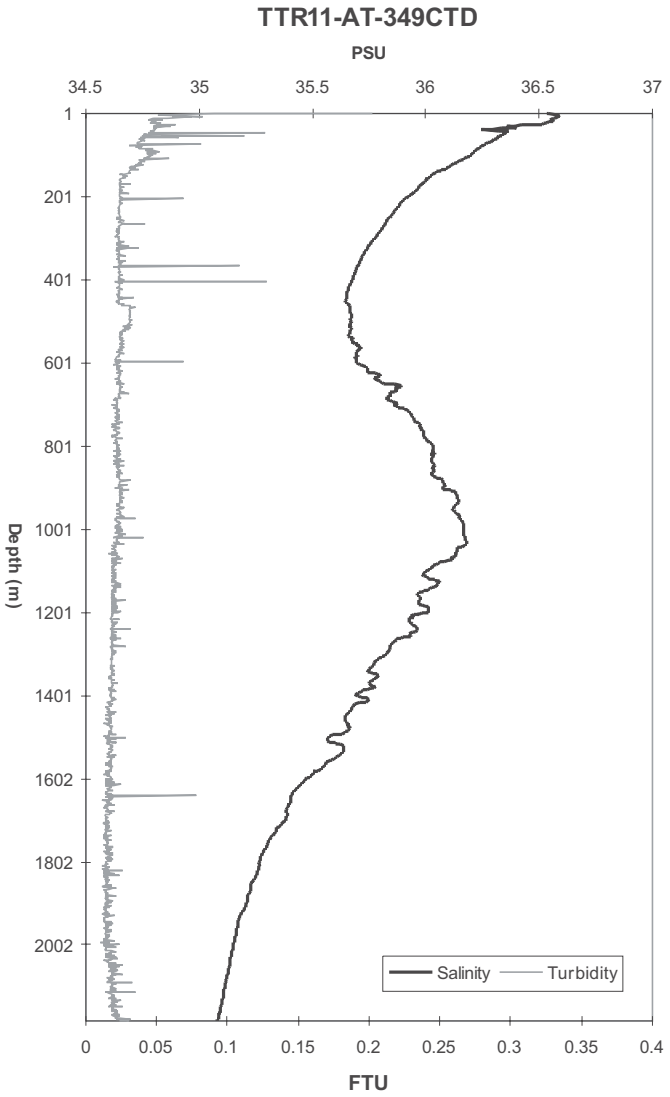

Figure 70. Turbidity and Salinity profile at station AT-349CTD

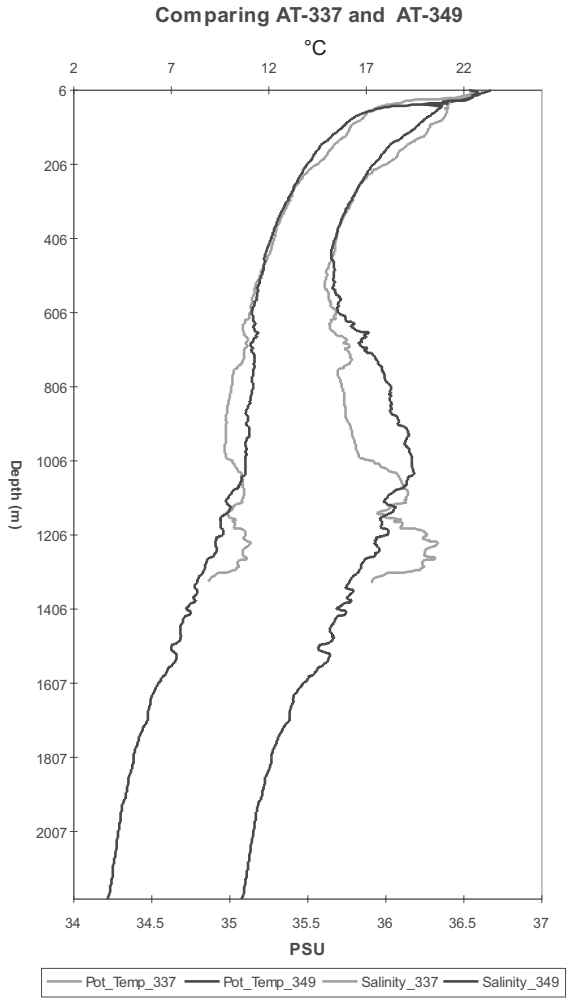

Figure 71. Comparison of Salinity and Potential Temperature profiles on stations AT-337CTD and AT-349CTD

the ESACW lines just until the ~550 m depth level, where it clearly changes direction towards the MOW (small peak at 670 m and bigger one at 1043 m). The presence of this Water Mass is only important to about 1500 m depth; below this level, the profile "heads" for the NADW, nearly reaching it by the 2189 m depth level.

The pH vertical profile (Fig. 73), has a rapid increase (from 8.166 to 8.210) from the surface down to the 61 m depth level (probably the euphotic zone lower limit), followed by a rapid decrease in the pH values (down to 8.080) which stops at the ~610 m depth level, forming a "plateau" of more or less constant pH values down to 1046 m depth (notice that the pH peak at 670 m coincides with the Potential Temperature maximum). From this depth (1046 m) downward, the pH values decrease, at first rapidly (to 8.062) and then slowly, reaching 8.050 at the sea bottom (2189 m). From these observations, it is reasonable to conclude that the presence of MOW produces an anomaly between the 600 to the 1200 m depth levels, increasing the pH readings by about 0.020.

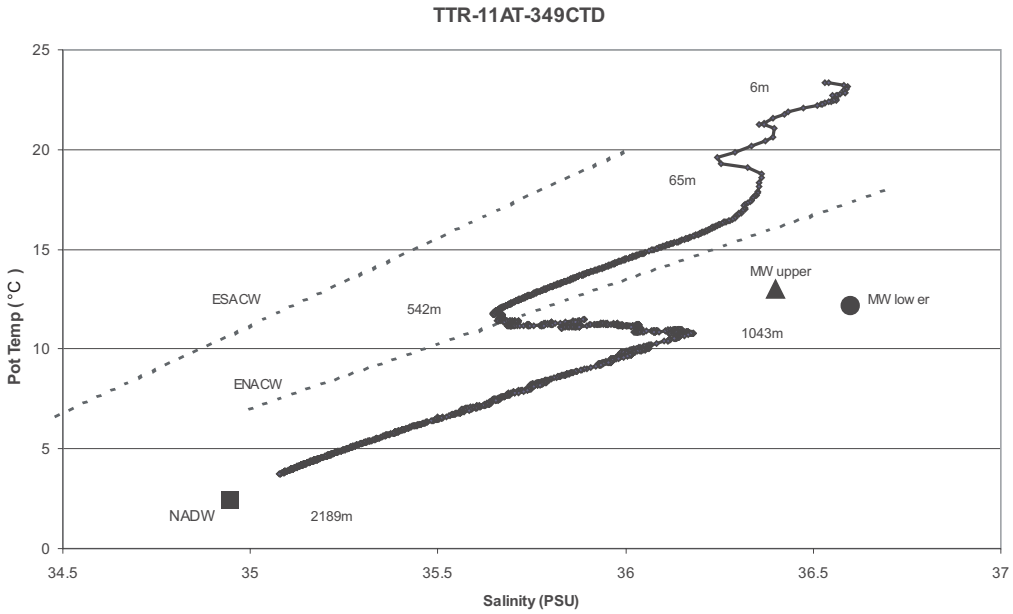

Figure 72. Potential Temperature vs. Salinity at the station AT-349CTD

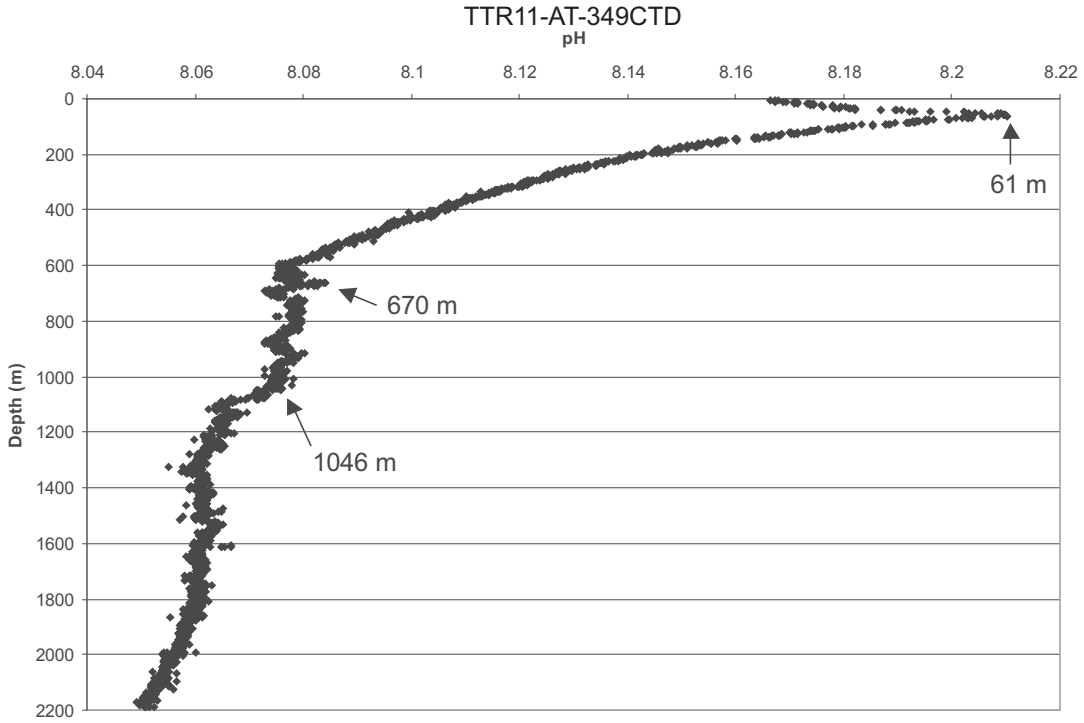

Figure 73. pH vertical profile at the station AT-349CTD

III.1.6. Biology

M. CUNHA, D. SUBIDA, T. RODRIGUES AND I. LIMA

Methods

Dredge samples

The fauna was picked from the surface of the rocks and/or recovered from rock washings and sieved sediments (the finer sieve used was 0.5 mm). The specimens were preserved in 70% ethanol. The finer fraction (0,5 to 1 mm) of the sieved sediments was preserved in 10% neutralised formaline stained with Rose Bengal and it will later be sorted under a stereoscopic microscope.

Core samples

Conspicuous animals were picked from the sediment. Whenever possible at least one quarter of each core sample was used for biological subsampling. The 25-30 cm of the uppermost part were sieved through a sieve column (2, 1 and 0,5 mm). The fauna in the two coarser fractions was sorted and kept in 70% ethanol. The finer fraction (0,5 to 1 mm) of the sieved sediments was preserved in 10% neutralised formaline stained with Rose Bengal and it will later be sorted under a stereoscopic microscope.

Deep towed TV

A preliminary list of the fauna was made from real time observations of video footages.

Results

The listing of biological specimens collected from bottom samples is given in Table 4 and the specimens identified from video footages in Table 5.

AT 335 D

The carbonate chimneys and crusts retrieved in this sample had abundant sessile fauna. A large specimen and some fragments of cf. *Callogorgia verticillata* (Cnidaria) were retrieved. Tubes of different species of Serpulidae (Polychaeta) covered a significant area of most rock samples. Incrusting sponges (Porifera), Bryozoa, Hydrozoa and dead coral branches (*Madreporaria*) were also observed and collected whenever possible.

The most abundant organisms col-

lected from this sample were Brachiopoda (cf. *Gryphus vitreus*). Some bivalves (cf. Fam. Arcidae and other species) but also some Nuculanidae-like specimens, gastropods, chitons, sipunculids and isopods (*Janira* sp.) were collected. Some time after sampling, different species of polychaete worms were observed crawling out of tiny conduits (app. 2-5 mm) of porous rocks and they were picked by hand.

The biological debris in this sample included dead coral fragments, empty shells of bivalves, pteropods and other gastropods, echinoderm spicules and plates and foraminifers (mostly *Globigerina*).

AT 336 G

A few empty polychaete tubes were retrieved from this sample. Biological debris were composed of pteropoda shells and foraminifera.

AT 338 G

A few empty polychaete tubes were retrieved from this sample. Biological debris were composed of pteropod shells and foraminifers.

AT 339 D

The retrieved carbonate crusts and chimneys, one of them reaching approximately 50 cm long, were covered with abundant sessile fauna, dominated by tube-dwelling polychaetes (Serpulidae) and hydrozoan colonies. (*Aglaophenia* sp.). Barnacles (*Veruca stroenia*) on rough surfaces, live coral (*Lophelia pertusa*) in the mouth of chimney holes, some incrusting bryozoans (cf. Fam. Idmoneidae), sponges (Porifera), anemones (Anthozoa) and brachiopods were also observed and collected whenever possible.

The non-sessile fauna included, bivalves (cf. Fam. Arcidae and other species), often found inside chimney conduits and cavities, gastropods, polychaete worms, amphipods, isopods (e.g. Arcturidae and Janiridae), one crab (cf. *Bathynectes*), a sea-spider (Pycnogonida), ophiuroids (Ophiuroidea) and one small sea-urchin (Echinoidea). Different species of polychaete worms were observed crawling out of tiny conduits (app. 2-5 mm) of porous rocks and were picked by hand.

Different species of foraminifers were

Table 4. Listing of the biological material collected during dredge and gravity core sampling in the Gulf of Cadiz during the 3rd Leg

Phylum	Class	Order	AT 335 D	AT 336 G	AT 338 G	AT 339 D	AT 342 G	AT 343 G	AT 344 G	AT 345 G	AT 346 G	AT 347 G	AT 348 G	AT 350 G
Porifera			+			+								
Cnidaria	Hydrozoa		+			+								
	Scyphozoa						T	T	T	T	T			
	Anthozoa		+			+								
Sipuncula			+											
Mollusca	Polyplacophora		+							+				
	Gastropoda		+			+								
	Bivalvia		+			+								
Annelida	Polychaeta		+	T	T	+	T		T				+	
Pogonophora											+	T	T	+
Arthropoda	Pycnogonida					+								
	Cirripedia					+								
	Malacostraca	Decapoda				+								
		Amphipoda				+								
		Isopoda	+			+								
Brachiopoda			+			+								
Echinodermata	Asteroidea					+								
	Ophiuroidea					+								
	Echinoidea					+								
Bryozoa			+			+								

Biological debris	AT 335 D	AT 336 G	AT 338 G	AT 339 D	AT 342 G	AT 343 G	AT 344 G	AT 345 G	AT 346 G	AT 347 G	AT 348 G	AT 350 G
Foraminifera	+	+	+	+	+		+	+	+	+		
Coral	+											
Pteropod shells	+	+	+		+			+		+		
Other gastropod shells	+							+				
Bivalve shells	+							+				+
Echinoderm spicules and plates	+					+						

T: probably empty tubes

Table 5. Listing of the biological specimens identified during real time observation of video footages in the Gulf of Cadiz during the 3rd Leg

Phylum	Class	Order	TV AT 18	TV AT 19	TV AT 20	TV AT 21	TV AT 22	TV AT 23
Porifera			+	+		+	+	+
Cnidaria	Hydrozoa					+	+	+
	Anthozoa		+	+		+		+
Nemertea			+					
Mollusca	Gastropoda		+	+			+	
	Bivalvia		B	B				B
Annelida	Polychaeta		+	+		+		
Arthropoda	Malacostraca	Decapoda	+	+	+	+	+	+
Brachiopoda			+	+		+	+	
Echinodermata	Crinoidea							+
	Asteroidea		+	+		+	+	+
	Ophiuroidea							+
	Echinoidea		+	+		+	+	+
	Holothuroidea			+				
Chordata			+	+	+	+	+	+

B: Burrows

observed in the sieved sediment.

AT 340 G

No biological subsampling from this core (only a very small amount of sediment was collected).

AT 341 G

No biological subsampling from this core (only a very small amount of sediment was collected).

AT 342 G

This sample was characterized by the presence of abundant empty pteropod shells. Some foraminifera and empty bivalve shells were also present. A hydrozoan colony (Fam. Campanulariidae), a few empty tubes of schyphozoan polyp stage (Fam. Nausithoidae) and polychaete and/or pogonophoran worms were collected.

AT 343 G

In this sample some tubes were found from the polyp stage of a scyphozoan (Fam. Nausithoidae). A few spicules from echinoderms were also retrieved.

AT 344 G

Some empty tubes of polychaetes and/or pogonophorans were found after sieving the sediment, together with some foraminiferans and tubes of the polyp stage of a scyphozoan (Fam. Nausithoidae).

AT 345 G

One living polychaete, polychaete tubes and tubes from the polyp stage of a scyphozoan (Fam. Nausithoidae) were found in this sample. The biological debris consisted of pteropod, gastropod and bivalve shells and foraminifera.

AT 346 G

Two species of Pogonophora were found in the sediment of this core: *Oligobrachia* sp. and *Polybrachia* sp. A few Pogonophora juveniles were also observed. After sieving the sediment, Foraminifera and tubes from the polyp stage of a scyphozoan (Fam. Nausithoidae) were retrieved.

AT 347 G

In this sample tubes from Pogonophora, and Foraminifera were found

AT 348 G

Several Pogonophora tubes (juveniles and *Polybrachia* sp.) were picked from the upper part of the core. After sieving several polychaetes and polychaete tubes were found.

AT 350 G

Pogonophora tubes (*Oligobrachia* sp.) and empty bivalve shells (Fam. Thyasiridae) were collected from this sample.

TV AT 18 and TV AT 19 (Iberico structure)

Two video runs were made at the top of the Iberico structure in an area with carbonate chimneys and patches of coral debris. During the first TV run part of the sandy slope in the flank was also recorded.

The most striking feature of the fauna was the presence of large cnidarian colonies of at least two different species. The largest, which could reach 80 cm to 1 m height, could be readily identified as *Callogorgia verticillata* from dredge samples performed in this location. These colonies formed patches of higher density in the chimney areas while in the coral debris areas they appeared rather scattered. Different fish species and specimens of the shrimp *Acanthephyra purpurea* were associated with these three-dimensional cnidarian patches.

Many specimens of a conspicuous Cidaridae sea urchin were observed throughout the record but with a higher density in the cnidarian patches. Sea stars (mainly Fam. Asterinidae), however appeared to occur mainly in more open areas. Brachiopod clusters, identified as cf. *Gryphus vitreus* from specimens collected during the dredge operation, and small sponges were very frequently attached to the surface of carbonated chimneys. Unidentified decapods in the chimneys area and a few gastropods in coral debris patches were also observed.

Sandy surfaces between fallen chimneys were densely inhabited by endofauna. Different types of burrows occurring, isolated or in clusters. From three to more than 12 holes were observed throughout the record but with noticeable fluctuation in density.

Contrasting with the dense and diversified assemblage(s) of the top of the structure the record made at the flank showed a poor assemblage characterised by the presence of large unidentified worms and a few shrimps, fishes and sea stars. Some crab burrows were also observed.

TV AT 20 – Channel near Iberico

This video footage was made in a high-energy site with strong currents. Only a few fishes and crabs could be readily observed. Swarms of small crustaceans, probably amphipods and mysids, were often observed.

TV AT 21 – Area close to Iberico

This video footage was made in two close locations and covered areas with diverse bottom structures (hard clay, chimneys, sand patches/shell debris areas and carbonated crusts). The epifauna was dominated by echinoderms, mainly Cidaridae sea urchins and unidentified sea stars. Several fishes, a few shrimps and some cnidarian colonies were also observed.

TV AT 22 – Guadalquivir diapiric ridge

This footage was made in an area with fallen chimneys, rocky areas with well sorted sand patches and highly variable topography. The epifauna of rocky surfaces was mainly dominated by Cidaridae sea urchins and sea stars (mainly Fam. Asterinidae) but many small sponges and probably also brachiopod clusters were observed. A few decapod specimens were observed hidden in rock crevices.

Well-defined patches of small-sized (5-8 cm) cnidarian colonies occurred in sandy areas with fallen chimneys. A few fishes and shrimps, swimming very close to sandy sediment, were associated with three-dimensional cnidarian patches. Crabs and their burrows as well as a few gastropods were observed in the same areas.

Generally, higher densities of epifauna occurred in rocky areas whereas lower densities occurred in the sandy areas. Burrows (except for the crab burrows mentioned above) and other signs of bioturbation by endofauna were not evident on this location.

TV AT 23 – Carlos Ribeiro mud volcano

This footage was made in an area with mainly soft muddy sediments where very rare crusts were observed. Sessile fauna was abundant and strongly dominated by echinoderms. Sea lilies (stalked Crinoidea) in low-density patches and numerous brittle stars, sea stars and sea urchins were observed throughout the video record. A few fishes and shrimps were associated with three-dimensional sea lily patches.

Some isolated large sponges, Venus' flower basket (Cl. Hexactinellida), anemones and a few squat lobsters were observed but did not show a clear distribution pattern.

Crab burrows, clusters of about 8-10 large burrows (probably decapod burrows) and several types of smaller burrows (bivalves and/or worms) were observed. The distribution of these burrows showed successive high and low-density areas, with the highest density occurring at the top of the mud volcano. Some of these burrows are probably from Thysiarid bivalves. Some empty shells of these bivalves were recovered from core sampling in this area and a live specimen was collected from Bonjardim mud volcano during TTR 10.

Generally, a higher density of epifauna occurred at the top of the mud volcano and decreased downwards on the flank side.

III.1.7. Conclusions

Detailed investigation of the Iberico High and surrounding diapiric ridges showed that the carbonate chimneys are widespread in the area and form large fields on the tops and slopes of the outcropping diapiric structures. Their presence probably reflects the fact of intensive fluid escape from the sediments involved in the diapiric process. Most of the chimneys were observed to have fallen on the video footages, suggesting that the chimney's formation had taken place in the past and that at the present time the growth is negligible or even ceased. The depth of the chimneys falls into the depth range where Mediterranean Outflow water has been encountered during CTD measurements. The NRL SeaMap image and previous publications (Kenyon and Belderson, 1973; Nelson et al., 1999) also indicate that the diapiric ridges are swept by the fast flowing Mediterranean Undercurrent which also can facilitate the collapse of individual chimneys.

No evidence of fluid escape was found on the large circular structure named Lolita Dome. However its diapiric nature still cannot be excluded.

A new conically-shaped mud volcano in the Portuguese sector of the Gulf, named Aveiro, was mapped in detail with 30 kHz MAK system and sampled.

A high resolution 100 kHz line run across a sandy lobe revealed the complexity of its morphology which was not expected from the previously available datasets. The data clearly indicate the importance of channelised sand transport for lobe formation. The channel details were observed with a meter scale resolution.

III.2. Polimetalic crusts and phosphorites of the Madeira Seamounts

J. MONTEIRO, L. PINHEIRO, M. IVANOV AND TTR11, LEG 2A SCIENTIFIC PARTY

III.2.1. Introduction and objectives

The principal purpose of the second part of the 3rd Leg was to study sedimentological, geochemical and oceanographic processes related with ferromanganese deposits and phosphorites, occurring on the several seamounts belonging to Madeira archipelago. As phosphogenesis and Mn-oxide precipitation are mutually exclusive processes, the sequence of phosphatic and Mn-oxide layers represents important signals of changing paleoceanographic and paleoclimatic conditions. The other task was to find out whether any remaining influence of the Mediterranean Water could be identified here.

First studies of the manganese crusts and nodules on the Madeira Seamounts were conducted in December 1992 by the German R/V Sonne. A field of cobalt-rich crusts has been discovered at the depth of 1500 m on the northeastern flank of Lion Seamount situated between the Portuguese coast and the Madeira Islands. Samples of manganese crusts and nodules were collected. Some nodules had fragments of crusts in their core, the others had cores composed of phosphorised limestone. Concentration of cobalt in the samples reached up to 0.8% and nickel up to 1.1%.

The main objectives of Leg 3, part 2 were to investigate the occurrence of polimetalic crusts and phosphorites and

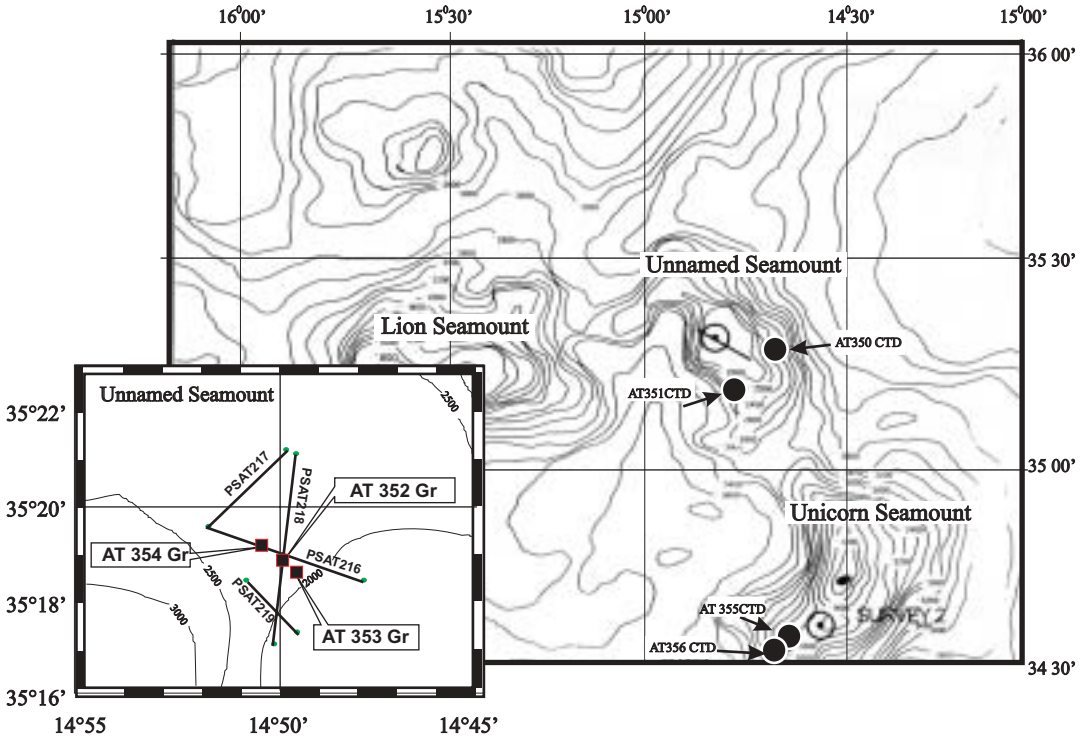

Figure 74. Location map of Leg 3 studies of the Madeira Seamounts with detail from northeast of the Unnamed Seamount.

associated fauna on the Unnamed and Unicorn Seamounts, north of Madeira, using hull mounted 5 kHz profiler, deep-tow analog/digital TV camera, TV-grab and CTD (Fig. 74)

III.2.2. Main results

Unnamed Seamount.

Four echosounder lines were run in order to select a site for a underwater video transect. As a result a flatter portion of the seamount was located, the TV system was deployed and about 5 hours of seafloor record was obtained. Numerous crusts and nodules were observed. Their distribution was patchy and three sites were chosen for bottom sampling.

TV-Grab AT352Gr.

The sample consisted of ferromanganese crusts, fragments of poorly-lithified limestone and a large amount of foraminifera ooze (Fig. 75). The recovered crusts fell into three size categories:

Small (up to 3 cm), spherical and ellipsoidal with smooth surface.
Medium, (3-6 cm), ellipsoidal and tabular with a grainy surface
Large (> 6 cm), tabular with grainy surface. Weight can reach up to 7 kg.

TV-Grab AT353Gr

The sample consisted of foraminiferal ooze, ferromanganese crusts and fragments of poorly lithified sediments (Fig. 76). The crusts were similar to those recovered at the previous station. Sediments were represented by marlstones with foraminifera often covered with a film of Fe, Mg and Mn oxides. Some samples revealed a fine parallel lamination.

TV-Grab AT354Gr

The grab retrieved ferromanganese crusts within foraminiferal ooze (Fig. 77). The crusts were mainly of two sizes:

Small, 3-6 cm, spherical, ellipsoidal and tabular with a smooth or grainy surface.

Figure 75. Polimetalic crusts sampled at station AT-352GR.

Medium, 6-16 cm, ellipsoidal or tabular with a grainy surface.

Unicorn Seamount

An underwater TV run revealed the presence of local accumulations of ferromanganese crusts. The accumulations were significantly smaller in dimensions but otherwise similar to those on the Grifo Seamount. It was decided not to sample these accumulations.

Figure 76. Polimetalic crusts sampled at station AT-353R.

Figure 77. Polimetalic crusts sampled at station AT-354GR.

CTD measurements

Four CTD measurements were performed on the Unnamed (AT-350CTD, AT-351CTD) and Unicorn (AT-355CTD, AT-356CTD) Seamounts. At all of the stations the presence of the Mediterranean Outflow Water was detected from its characteristic maxima on the Temperature and Salinity profiles within the depth range 500-1600 m (Fig. 78). This is very similar to the pattern observed on the CTD stations made earlier during the 3rd Leg in the Gulf of Cadiz. However the profiles obtained in the Madeira area show a more uniform pattern within the MOW compared to the Gulf of Cadiz where the Upper and Lower cores of the Outflow can be clearly identified on the CTD records.

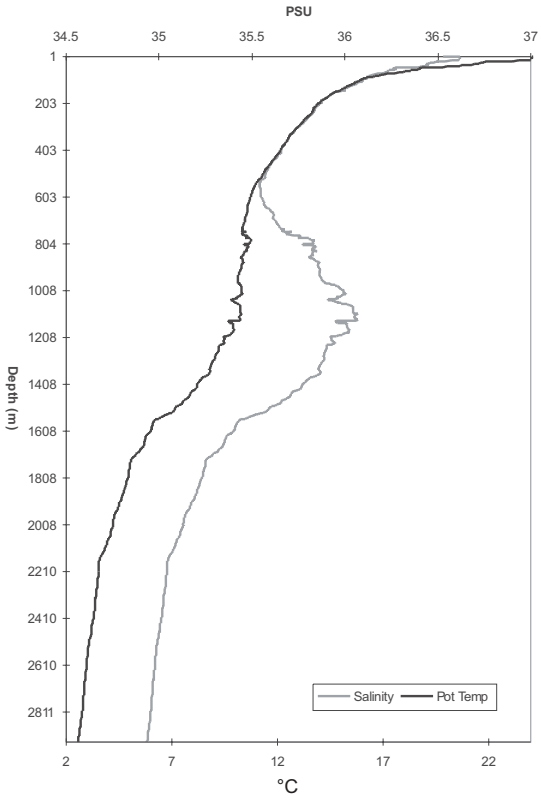

Figure 78. Vertical profiles for Potential Temperature and Salinity at station AT-351CTD.

REFERENCES

Aksu, A.E., Calon, T.J., and Hiscott, R.N., 2000. Anatomy of the North Anatolian Fault Zone in the Marmara Sea, Western Turkey: Extensional basins above a continental transform: GSA Today, 10, 3-7.

Alonso, B., and Maldonado, A., 1990. Late Quaternary sedimentation patterns of the Ebro turbidite systems (northwestern Mediterranean): Two styles of deep-sea deposition. Marine Geology, 95, 353-377.

Auzende, J.M, Olivet, J.L., and Pastouret, L. 1981. Implication structurales et palйogeographiques de la presence de Messinien a lґouest de Gibraltar, Marine Geology, 43, M9-M18.

Baraza, J., and Ercilla, G., 1996. Gas-charged sediments and large pockmark like features on the Gulf of Cadiz slope (SW Spain). Marine and Petroleum Geology, 13, 253-261.

Bernй, S. Loubrieu, B., and l'йquipe Calmar embarquйe, 1999. Canyons et processus sйdimentaires rйcents sur la marge occidentale du golfe du Lion. Premiers rйsultats de la campagne Calmar. C.R. Acad. Sci. Paris, Sciences de la terre et des planиtes, 328, 471-477.

Bonnin, J., Olivet, J.L., and Auzende, J.M., 1975. Structure en nappe a lґouest de Gibraltar: C.R. Acad. Sc., Paris, 280, 5, 559-562.

Bugge, T., Befring, S., Belderson, R.H., Eidvin, T., Jansen, E., Kenyon, N.H., Holtedahl, H., Sejrup, H.P., 1987. A giant three-stage submarine slide off Norway. Geo-Marine Letters, 7, 191-198.

Canals, M., and Got, H., 1986. La morphologie de la pente continentale du golfe du Lion: une rйsultante structuro-sйdimentaire. Vie Milieu, 36, 153-163.

Canals, M., 1985. Estructura sedimentaria y evoluciyn morfolygica del talud y el glacis continentales del Golfo de Leyn: fenymenos de desestabilizaciyn de la cobertura sedimentaria pliocuaternaria. PhD Thesis, Universitat de Barcelona (Spain), 618 pp.

Canals, M., Casamor, J.L., Urgeles, R., Lastras, G., Calafat, A.M., De Batist, M., Masson, D.G., Bernй, S., Alonso, B., and Hughes Clarke, J.E., 2000. The Ebro Continental margin, Western Mediterranean Sea: Interplay between canyon-channel systems and mast wasting processes. GCSSEPM Foundation, 20th Annual Research Conference, Houston, Texas, 152-174.

Clavell, E., and Berastegui, X., 1991, Petroleum geology of the Gulf of Valиncia. In: A.M. Spencer (ed.), Generation, accumulation, and production of Europe's hydrocarbons. Sp. Publ. European Association of Petroleum Geoscientists, Oxford University Press, 1, 355-368.

Dнaz del Rнo, V., Rey, J., and Vegas, R., 1986. The Gulf of Valencia continental shelf: Extensional tectonics in Neogene and Quaternary sediments. Marine Geology, 73, 169-179.

Dнaz del Rнo, V., Somoza, L., Martнnez-Frнas, J., Hernбndez-Molina, F.J., Lunar, R., Fernбndez-Puga, M.C., Maestro, A., Terrina, P., Llave, E., Garcнa, A., Garcнa, A.C., and Vбzquez, J.T., 2001. Carbonate chimneys in the Gulf of Cadiz: Initial report of their petrography and geochemistry. Geological processes on deep-sea European margins. International Conference and Ninth Post-Cruise Meeting of the Training-through-research Programme. Moscow/Mozhenka, Russia, 28 January - 3 February 2001. IOC Workshop Reports, 175, 53.

Field, M.E., and Gardner, J.V., 1990. Pliocene-Pleistocene growth of the Rio Ebro margin, northeast Spain: A prograding-slope model. Geological Society of America Bulletin, 102, 721-733.

Gardner. J. M., 2001. Mud volcanoes revealed and sampled on the Western Moroccan continental margin. Geophysical Research Letter, 28, 339-342.

Gennesseaux, M.A., Mauffret, A., and Pautot, G., 1980. Les glissements sous-marins de la pente continentale nizoise et la rupture de cвbles en mer Ligure (Mйditerranйe occidentale). C. R. Acad. Sc. Paris, 290, 959-962.

Gonzбlez, A., Cyrdoba, D., Matнas, L:M., And Tornй, M., 1997. Estructura de la corteza desde la zona surportuguesa hasta la llanura abisal de la Herradura, a partir de datos de sнsmica de gran бngulo, reflexiyn vertical y gravimetrнa: Abstract Volume II Simposium on Atlantic Iberian Margin, Cбdiz, Spain, 67-68.

Gonzalez, A., Torne, M., Cordoba, D., Vidal, N., Matias, L.M., and Diaz, J., 1996. Crustal thinning in the southwestern Iberia Margin. Geophysical Research Letters, 23, 2477-2480.

Grьnthal, G., Bosse, C., Sellami, S., Mayer-Rosa, D., and Giardini, D., 1999. Compilation of the GSHAP regional seismic hazard for Europe, Africa and Middle East, Annali di Geofisica, 42, 1225-1230.

Hain, V.E., 1984. Regional geotectonics, Volume 4. The Alpine belt. Moscow, Nedra, (In Russian)

Hubert-Ferrari, A., Barka, A., Jacques, E., Nalbant, S.S., Meyer, B., Armijo, R., Tapponier, P., and King, G.C.P., 2000. Seismic hazard in the Marmara Sea region following the 17 August 1999 Izmit earthquake. Nature, 404, 269-273.

Ivanov, M.K., Limonov, A.F., and Cronin, B.T. (eds.), 1996. Mud volcanism and fluid venting in the eastern part of the Mediterranean Ridge. Initial results of geological, geophysical and geochemical investigations during the 5th Training-through-Research Cruise of RV Professor Logachev (July-September, 1995). UNESCO Reports in Marine Science, 68, 127 pp.

Kenyon, N.H., and Belderson, R.H., 1973. Bed forms of the Mediterranean undercurrent observed with sidescan sonar. Sedimentary Geology, 9, 77-99.

Kenyon, N.H., Ivanov, M. K., Akhmetzanov, A., and Akhmanov, G. G. (eds), 2001. Interdisciplinary Approaches to Geoscience on the North East Atlantic Margin and Mid-Atlantic Ridge. IOC Technical Series, 60, UNESCO, 134 pp.

Kenyon, N.H., Ivanov, M.K., and Akhmetzhanov, A.M. (eds.), 1998. Cold water carbonate mounds and sediment transport on the Northeast Atlantic Margin. IOC Technical Series, 52, UNESCO, 178 pp.

Kenyon, N.H., Ivanov, M.K., Akhmetzhanov, A.M., and Akhmanov, G.G., (eds), 2000, Multidisciplinary study of geological processes on the Northeast Atlantic and Western Mediterranean margins. IOC Technical Series, 56, UNESCO, Paris, 119 pp.

Kurt, H., Demirbag, E., and Kuscu, I., 2000, Active submarine tectonism and formation of the Gulf of Saros; Northeast Aegean Sea; inferred from multi-channel seismic reflection data: Marine Geology, 65, 13-26.

Lastras, G., Canals, M., and Urgeles, R., 2000. BIG'95: a recent debris flow in the Ebro continental slope, North-western Mediterranean. Geology and Petroleum Geology of Mediterranean Basins Conference, October 2000, Malta.

Limonov, A.F., Woodside, J.M., and Ivanov, M.K. (eds.), 1994. Mud volcanism in the Mediterranean and Black Seas and Shallow Structure of the Eratosthenes Seamount. Initial results of the geological and geophysical investigations during the Third UNESCO-ESF "Training-through-Research" Cruise of RV Gelendzhik (June-July 1993). UNESCO Reports in Marine Science, 64, 173 pp.

Limonov, A.F., Woodside, J.M., and Ivanov, M.K. (eds.), 1992. Geological and geophysical investigations in the Mediterranean and Black Seas. Initial results of the "Training through Research" Cruise of RV Gelendzhik in the Eastern Mediterranean and the Black Sea (June-July 1991). UNESCO Reports in Marine Science, 56, 208 pp.

Lowrie, A., Hamiter, R., Moffett, S., Somoza, L., Maestro, A, and Lerche, I. 1999: Potential pressure compartments sub-salt in the Gulf of Mexico and beneath massive debris flows in the Gulf of Cadiz. GCSSEPM Foundation 19th Annual Research Conference Advanced Reservoir Characterization, 271-280

Maillard, A., Mauffret, A., Watts, A.B., Torné, M., Pascal, G., Buhl, P., and Pinet, B., 1992. Tertiary sedimentary history and structure of the Valencia trough (western Mediterranean). In: E. Banda and P. Santanach (eds.), Geology and Geophysics of the Valencia Trough, Western Mediterranean. Tectonophysics, 203, 57-75.

Maldonado, A., Somoza, L., and Pallarés, L. 1999: The Betic orogen and the Iberian-African boundary in the Gulf of Cadiz: geological evolution (Central North Atlantic). Marine Geology, 155, 9-43.

Malinverno, A., Ryan, W.B.F., Auffret, G., and Pautot, G., 1988. Sonar images of the path of recent failure events on the continental margin off Nice, France. Geological Society of America Special Paper, 229, 59-75.

Martínez del Olmo, W., Garcia-Mallo, J., Leret, G., Serrano, A., and Suárez, J., 1984. Modelo tectosedimentario del Bajo Guadalquivir. I Congreso Español de Geología I, 199-213.

McHugh, C.M.G., and Ryan, W.B.F., 2000. Sedimentary features associated with channel overbank flow: example from the Monterey Fan. Marine Geology, 163, 199-215.

Mienert, J., Posewang, J., and Baumann, M., 1998. Gas hydrates along the northeastern Atlantic margin: possible hydrate-bound margin instabilities and possible release of methane. In: Henriet, J.-P., and Mienert, J. (eds) Gas Hydrates: Relevance to World Margin Stability and Climate Change. Geological Society, London, Special Publications, 137, 275-291.

Migeon, S., Savoye, B., Zanella, E., Mulder, T., Faugeres, J.C., and Weber, O., 2001. Detailed seismic-reflection and sedimentary study of turbidite sediment waves on the Var Sedimentary Ridge (SE France): significance for sediment transport and deposition and for the mechanisms of sediment-wave construction. Marine and Petroleum Geology, 18, 179-208.

Milanovskiy, E.E., 1991. Geology of USSR, Volume 3. Moscow, MSU, 272 pp. (In Russian)

Nakajima, T., Satoh, M., and Okamura, Y., 1998. Channel-levee complexes, terminal deep-sea fan and sediment wave fields associated with the Toyama Deep-Sea Channel system in the Japan Sea. Marine Geology, 147, 25-41.

Nelson, C.H., Baraza, J., Maldonado, A., Rodero, J., Escutia, C., and Barber, J.H. (Jr), 1999. Influence of the Atlantic inflow and Mediterranean outflow currents on Late Quaternary sedimentary facies of the Gulf of Cadiz continental margin. Marine Geology, 155, 99-129.

Parsons, T., Toda, S., Stein, R.S., Barka, A., Dieterich, J.H., 2000. Heightened odds of large earthquakes near Istanbul; an interaction-based probability calculation. Science, 288, 661-665.

Piper, D.J.W., and Perissoratis, C., 1991. Late Quaternary sedimentation on the North Aegean Continental Margin. AAPG Bulletin, 75, 46-61.

Reilinger, R.E., Mcclusky, S.C., Oral, M.B., King, R.W., Toksoz, M.N., Barka, A.A., Kinik, I., Lenk, O., and Sanli, I., 1997, Global Positioning System measurements of present-day crustal movements in the Arabia-Africa-Eurasia plate collision zone. Journal of Geophysical Research, 102, 9983-9999.

Riaza, C., and Martinez del Olmo, W., 1996, Depositional model of the Guadalquivir-Gulf of Cadiz Tertiary basin, In: Friend, P.F., and Dabrio, C.J., (eds). Tertiary basin of Spain: the stratigraphic record of crustal kinematics, Cambridge University Press, 330-338.

Rothwell, R.G., Reeder, M.S:, Anastasakis, G., Stow, D.A.V., Thomson, J., and Kähler, G., 2000. Low-stand emplacement of megaturbidites in the Western and Eastern Mediterranean Sea. Sedimentary Geology, 135, 75-88.

Rothwell, R.G., Thomson, J., and Kähler, G., 1998. Low sea-level emplacement of a very large Late Pleistocene "megaturbidite" in the western Mediterranean Sea. Nature, 392, 377-380.

Shnikov, E.F., 1986. Mud Volcanoes of Kerch-Taman Region: Atlas. Kiev, Naukova Dumka, 200 pp. (in Russian)

Soler, R., Martínez del Olmo, W., Megías, A.G., and Abeguer, J.A., 1983. Rasgos básicos del Neógeno del Mediterraneo Español. Mediterranea, Serie de Estudios Geologicos, 1, 71-82.

Somoza, L., Maestro, A., and Lowrie, A., 1999. Allochtonous Blocks as Hydrocarbon Traps in the Gulf of Cadiz. Offshore Technology Conference OTC 10889, 571-577.

Somoza,L, Hernández-Molina, F.J., Vazquez, J.T., García-García, A., and Díaz del Río,V., 2000. El nivel de "BSR" en el talud superior del Golfo de Cadiz: implicaciones tecto-sedimentarias y paleoceanograficas. V Congreso Geologico de España, July, 2000, Alicante, Spain.

Taymaz, T., Jackson, J., and McKenzie, D., 1991, Active tectonics of the north and central Aegean Sea: Geophysical Journal International, 106, 433-490.

Torrelli, L., Sartori, R., and Zitellini, N. (1997). The giant chaotic body in the Atlantic Ocean off Gibraltar: new results from a deep seismic reflection survey. Marine and Petroleum Geology, 14, 2, 125-138.

Tugolesov, D.A., Gorshkov, A.S., Meisner, L.B., Soloviev, V.V., Chachalev E.M. 1985. Tectonics of Mesozoic - Cenozoic deposits of the Black Sea basin. Moscow, Nedra, 215 pp. (In Russian).

Wilson, R.C.L., Hiscott, R.N., Willis, M.G., and Gradstein, F.M., 1989. The Lusitanian Basin of west-central Portugal: Mesozoic and Tertiary tectonic, stratigraphic, and subsidence history. In: Tankard, A.J and Balkwill, H.R (eds), Extensional tectonics and stratigraphy of the North Atlantic margins. American Association of Petroleum Geologists/Canadian Geological Foundation. AAPG Memoir, 46, 341-361.

Woodside, J.M., Ivanov, M.K., and Limonov, A.F. (eds.), 1997. Neotectonics and Fluid Flow through Seafloor Sediments in the Eastern Mediterranean and Black Seas. Preliminary results of geological and geophysical investigations during the ANAXIPROBE/TTR-6 cruise of RV Gelendzhik, July-August 1996. Vols. 1, 2. IOC Technical Series, 48, UNESCO, 226 pp.

ANNEX I. CORE LOGS

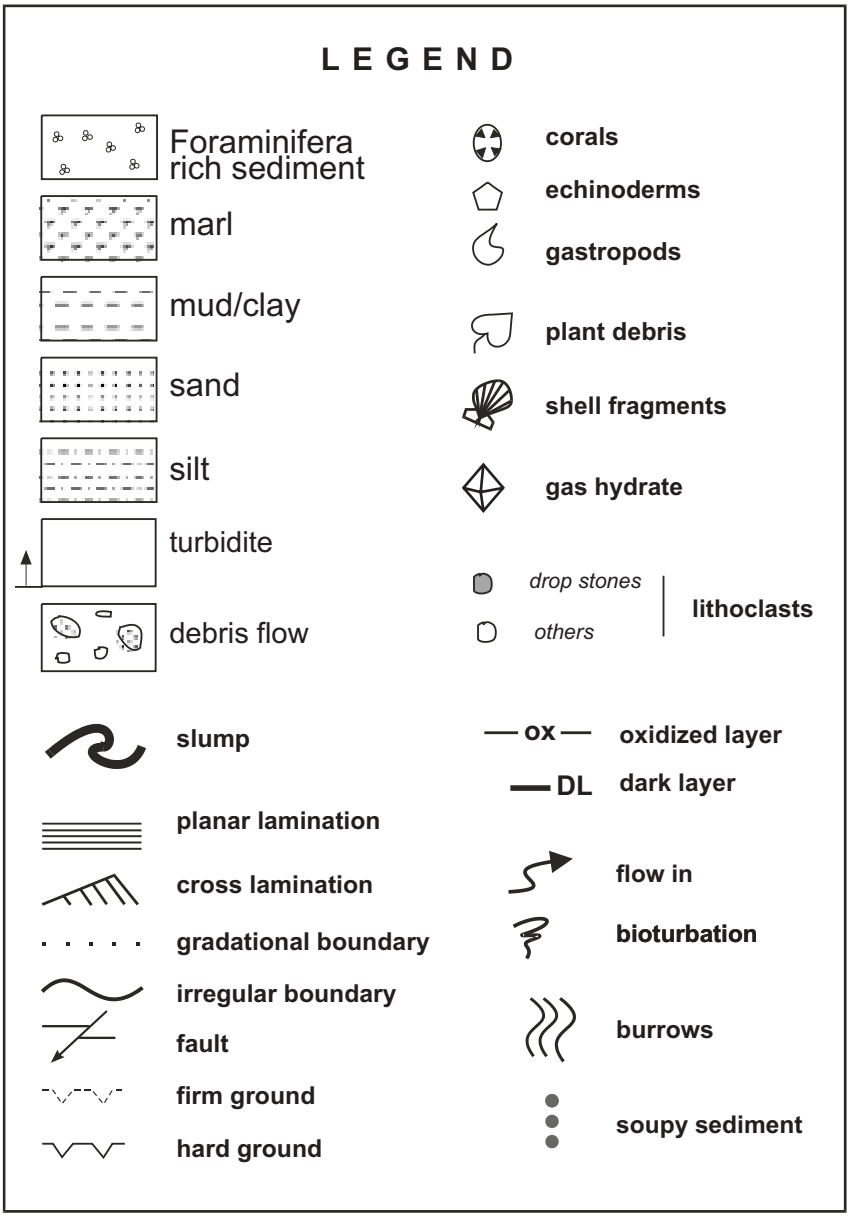

ANNEX I. CORE LOGS (LEG 1, the Black Sea)

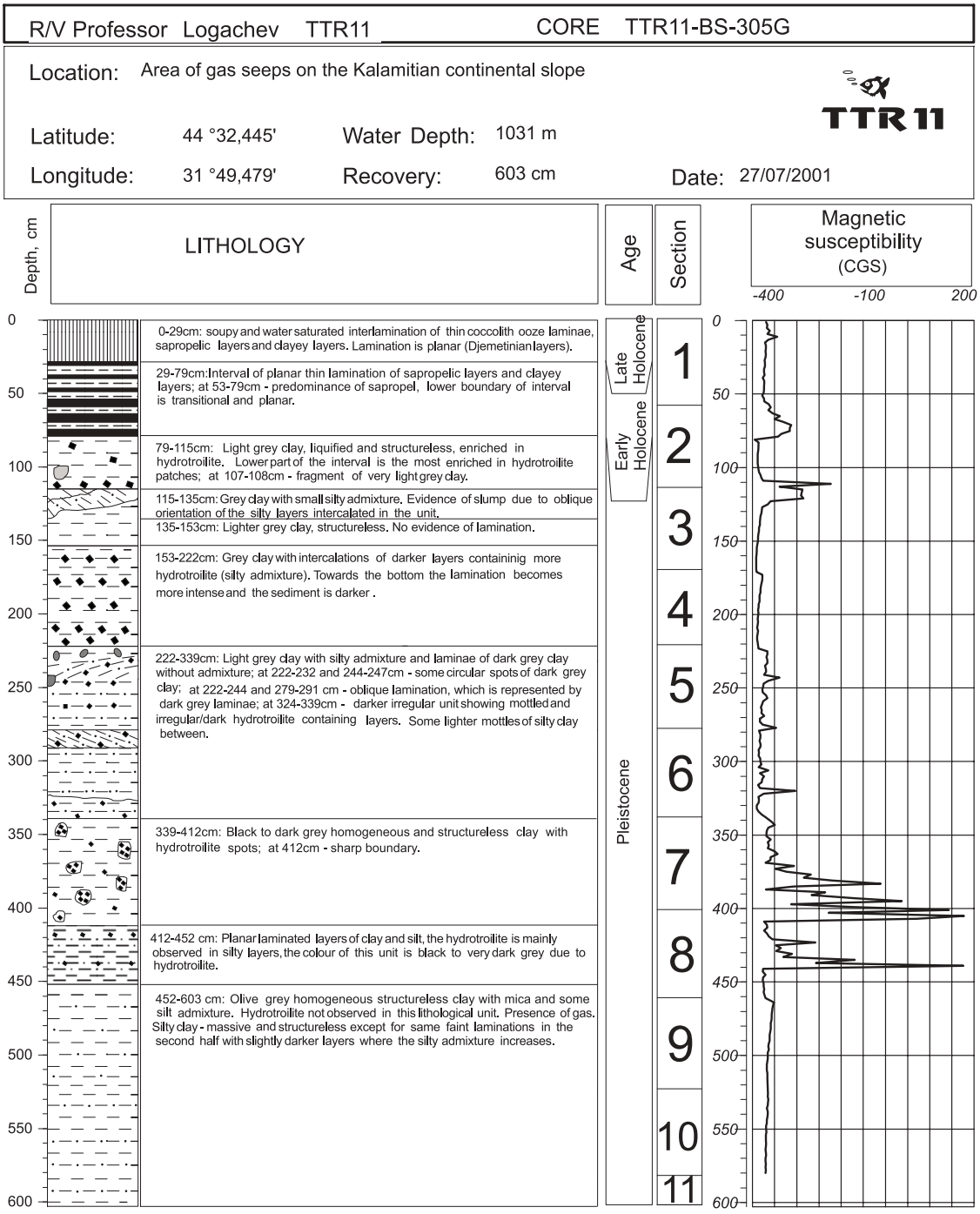

Core log TTR11-BS-305G

ANNEX I. CORE LOGS (LEG 1, the Black Sea)

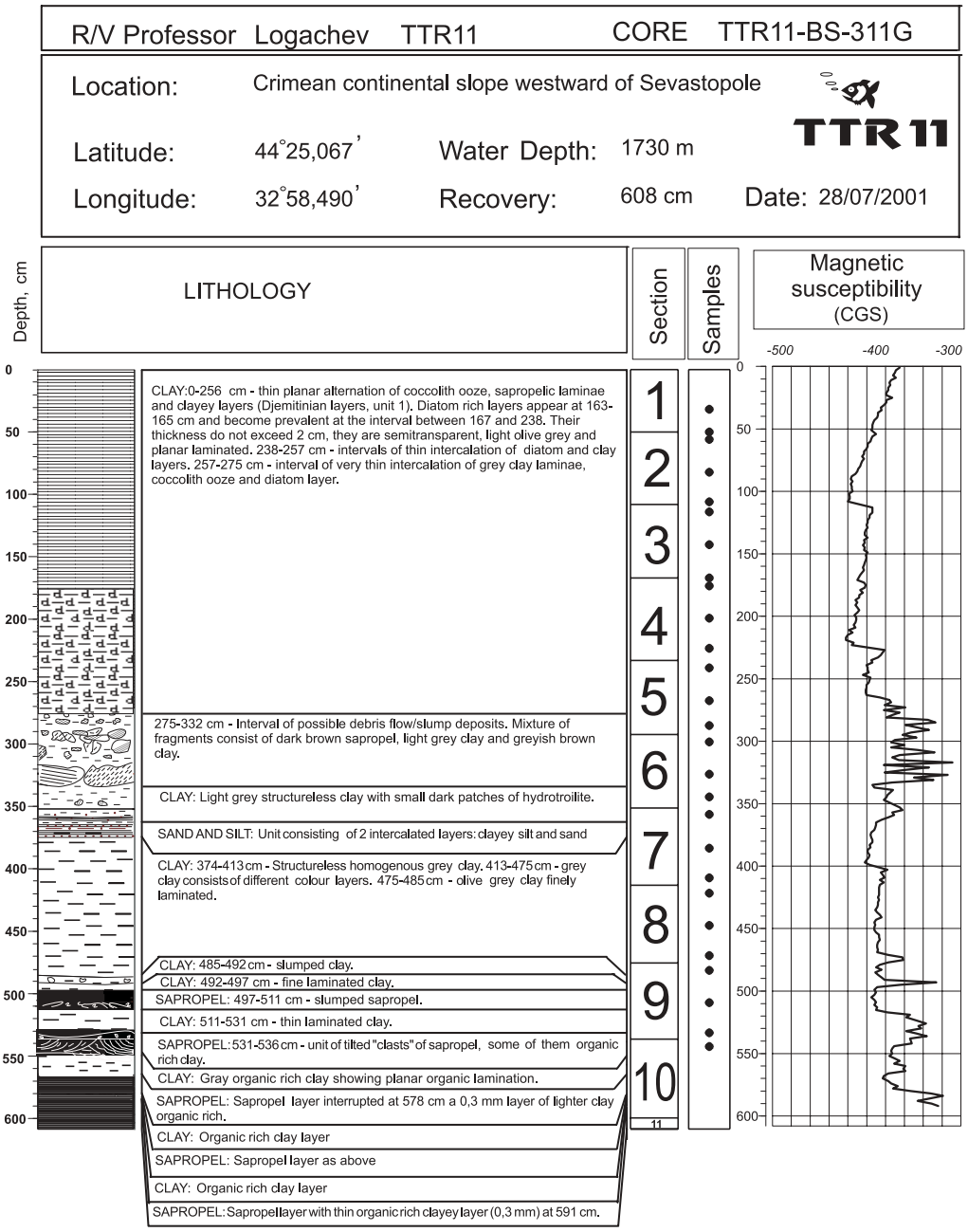

Core log TTR11-BS-311G

ANNEX I. CORE LOGS (LEG 1, the Black Sea)

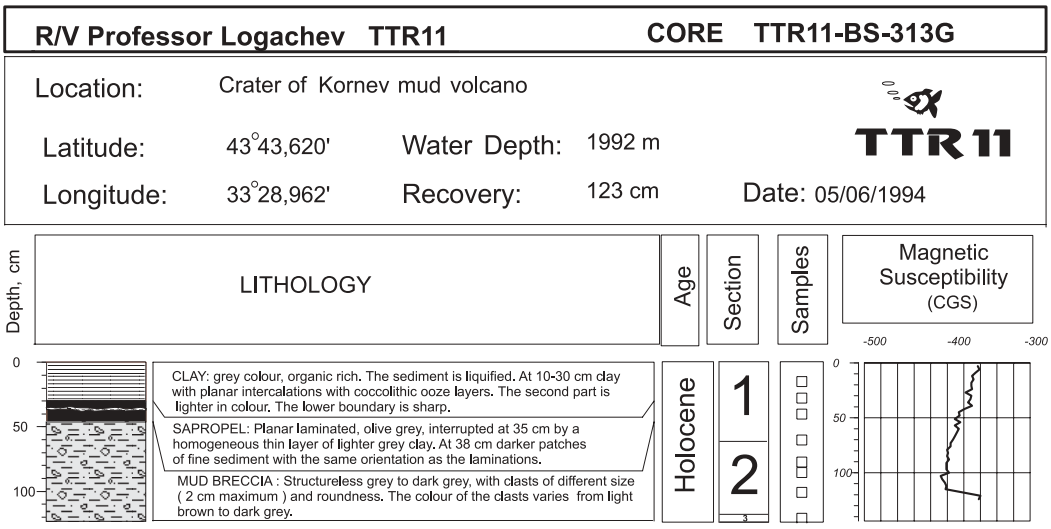

Core log TTR11-BS-313G

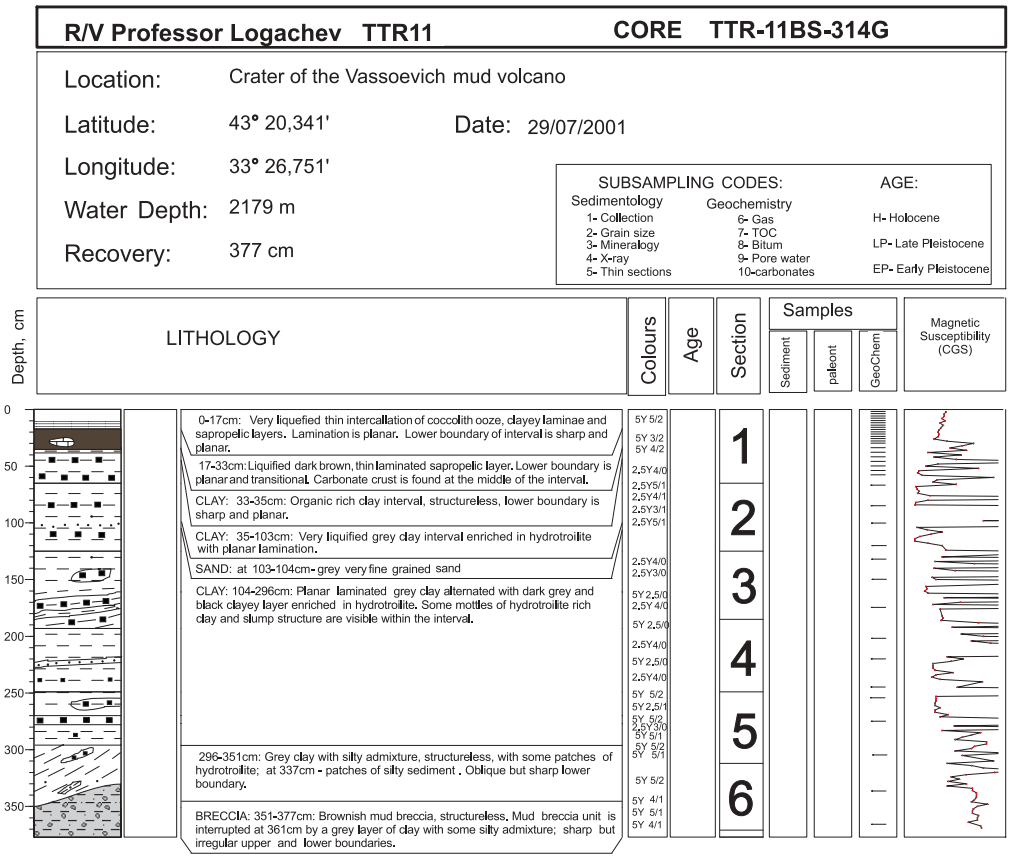

Core log TTR11-BS-314G

ANNEX I. CORE LOGS (LEG 1, the Black Sea)

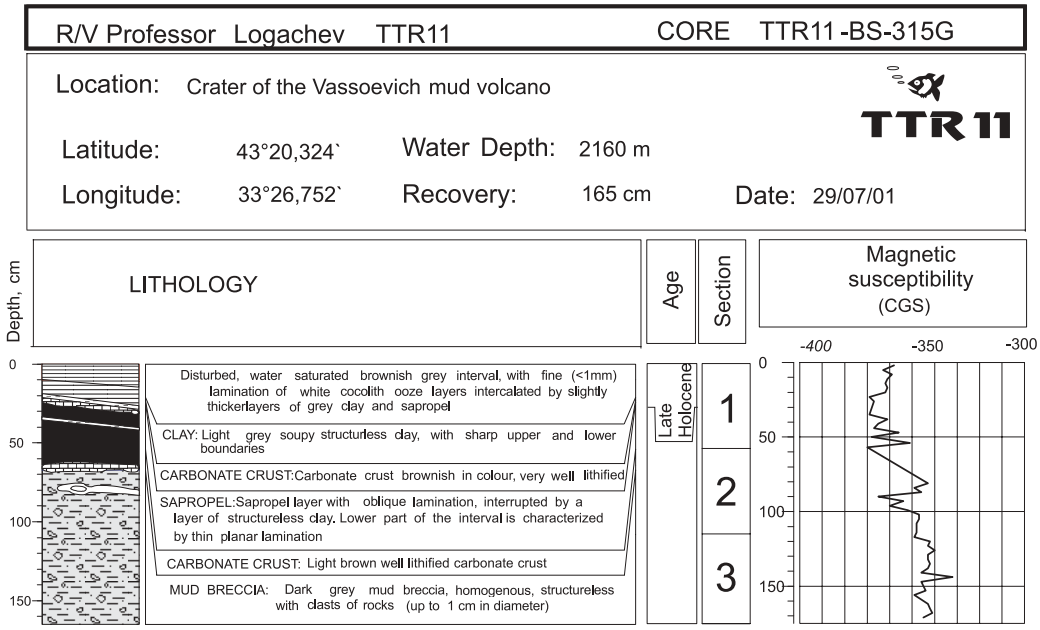

Core log TTR11-BS-315G

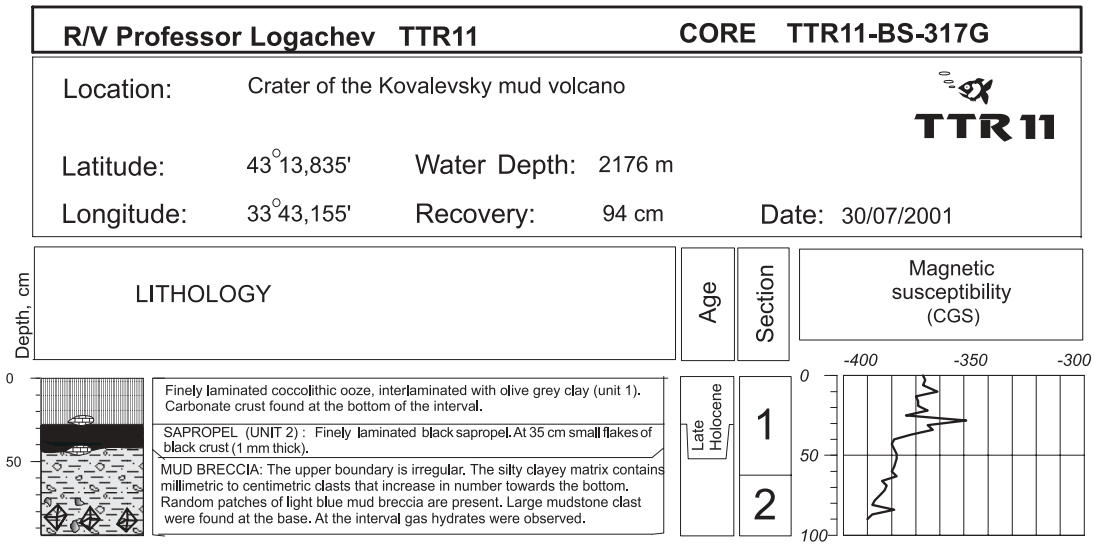

Core log TTR11-BS-317G

ANNEX I. CORE LOGS (LEG 1, the Black Sea)

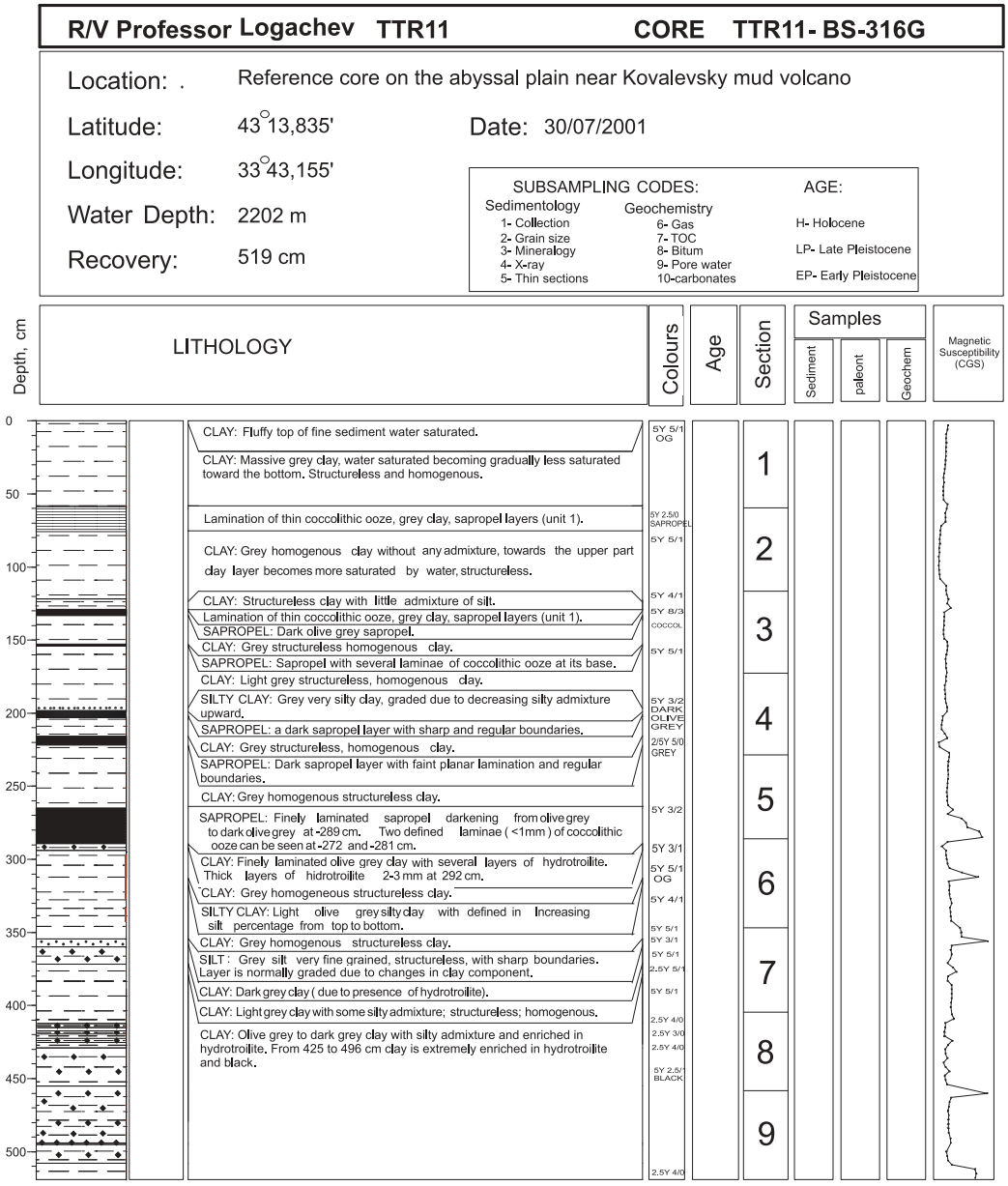

Core log TTR11-BS-316G

ANNEX I. CORE LOGS (LEG 1, the Black Sea)

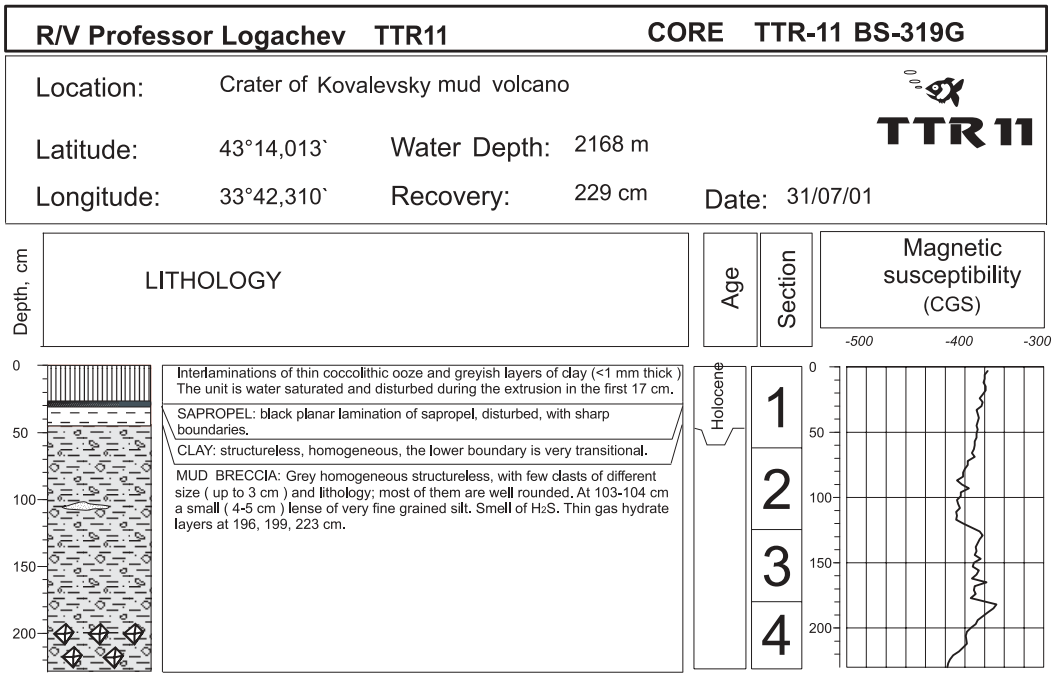

Core log TTR11-BS-319G

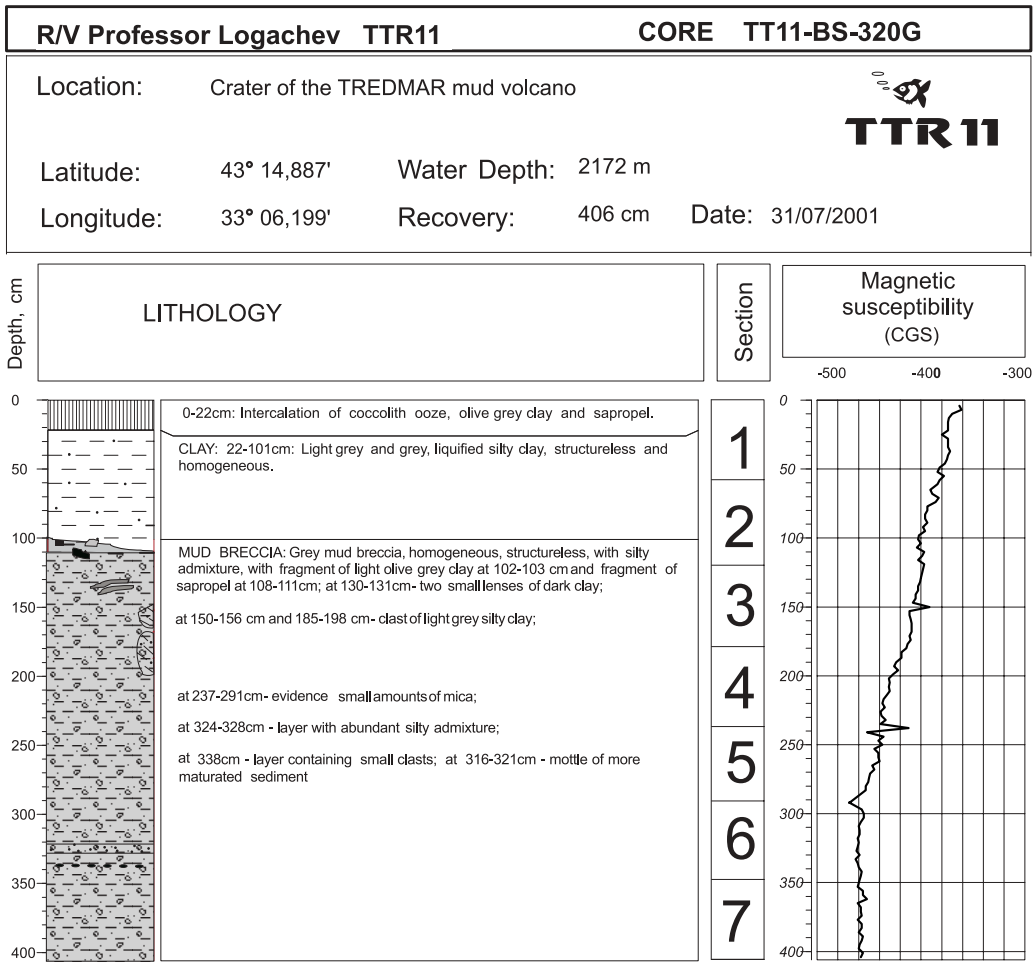

Core log TTR11-BS-320G

ANNEX I. CORE LOGS (LEG 1, the Black Sea)

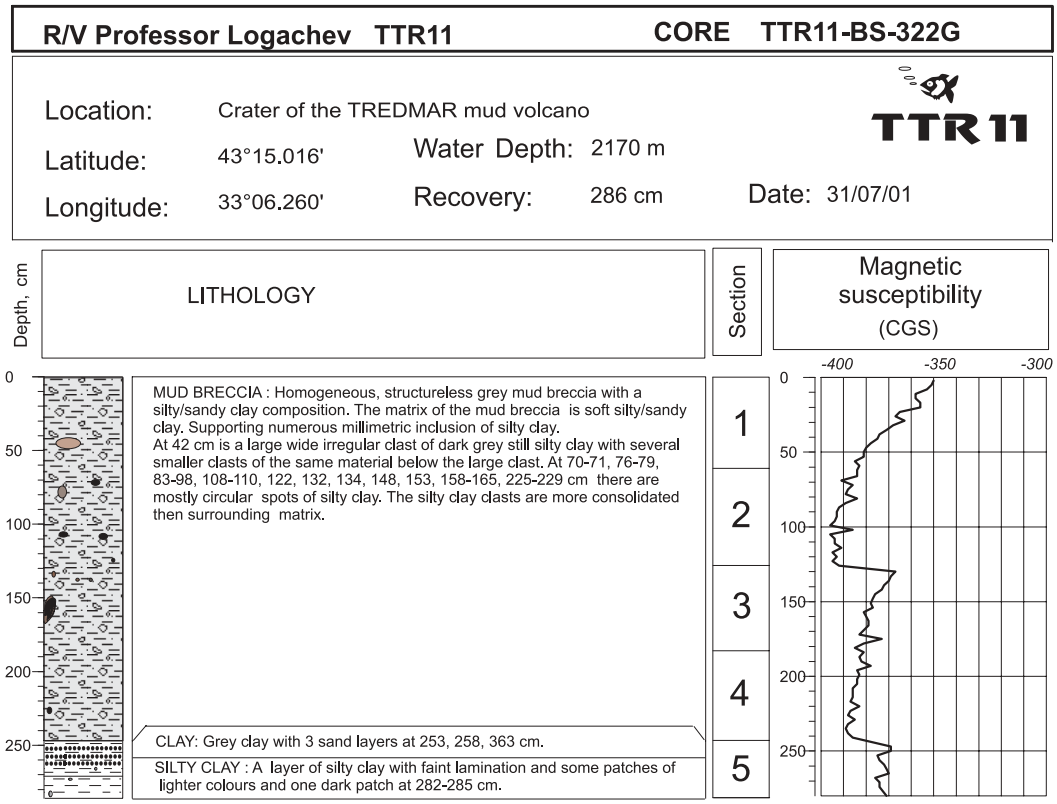

Core log TTR11-BS-322G

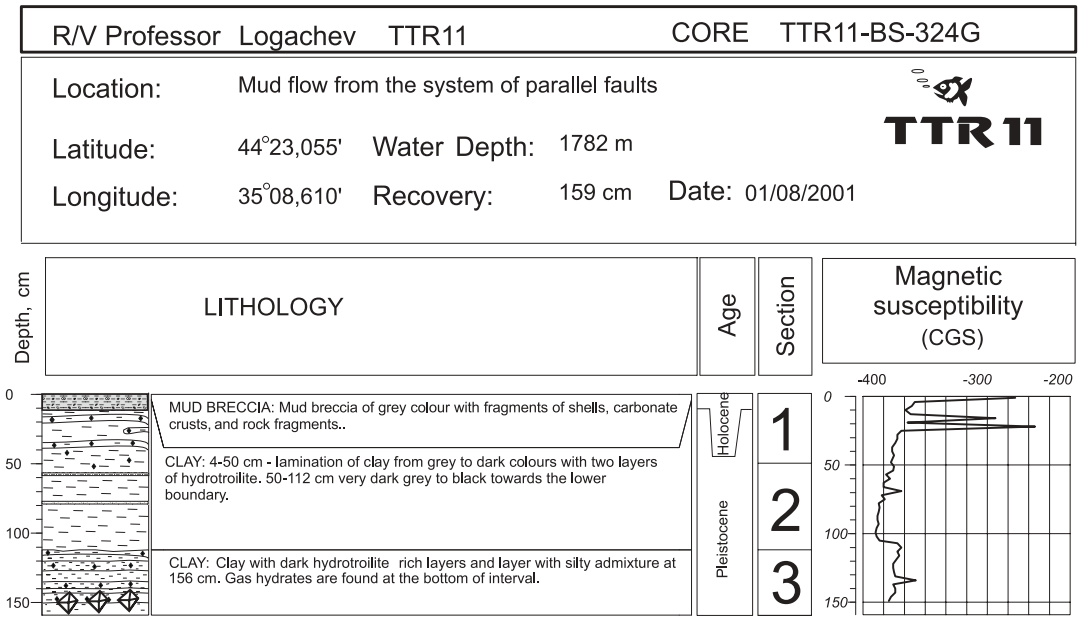

Core log TTR11-BS-324G

ANNEX I. CORE LOGS (LEG 1, the Black Sea)

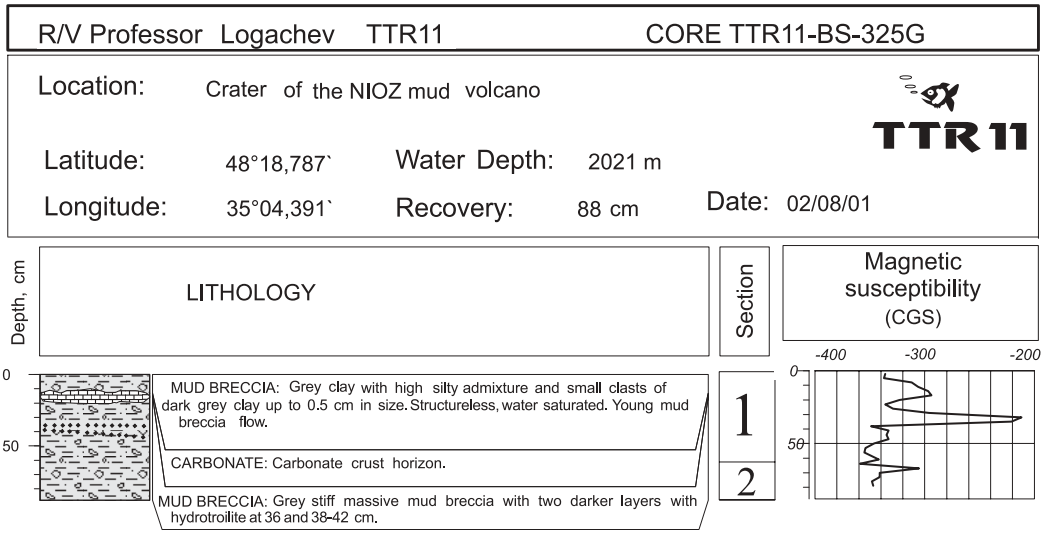

Core log TTR11-BS-325G

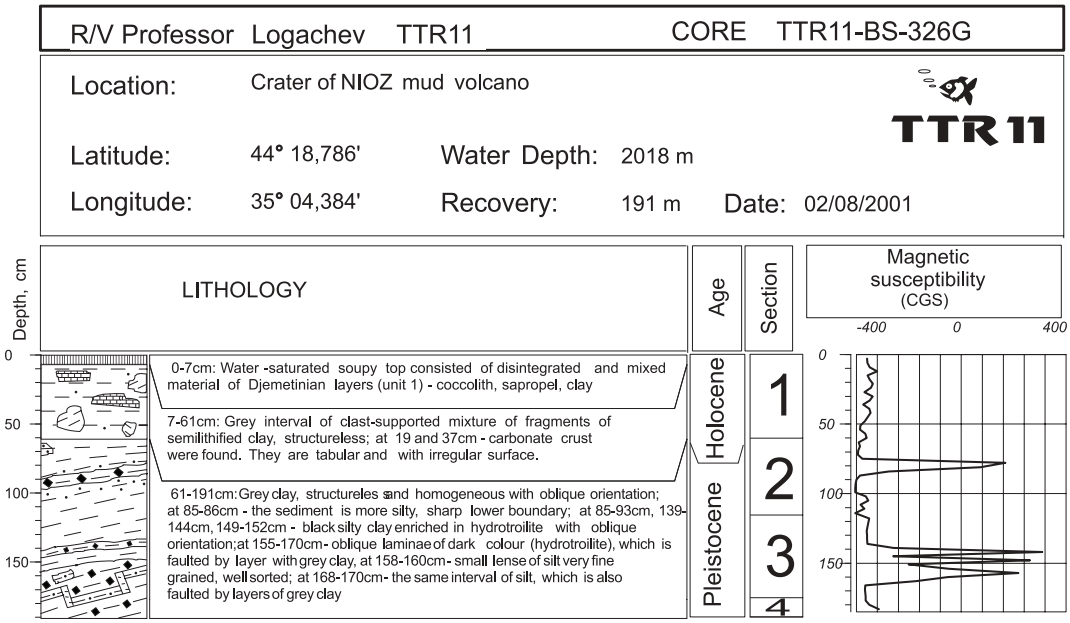

Core log TTR11-BS-326G

ANNEX I. CORE LOGS (LEG 1, the Black Sea)

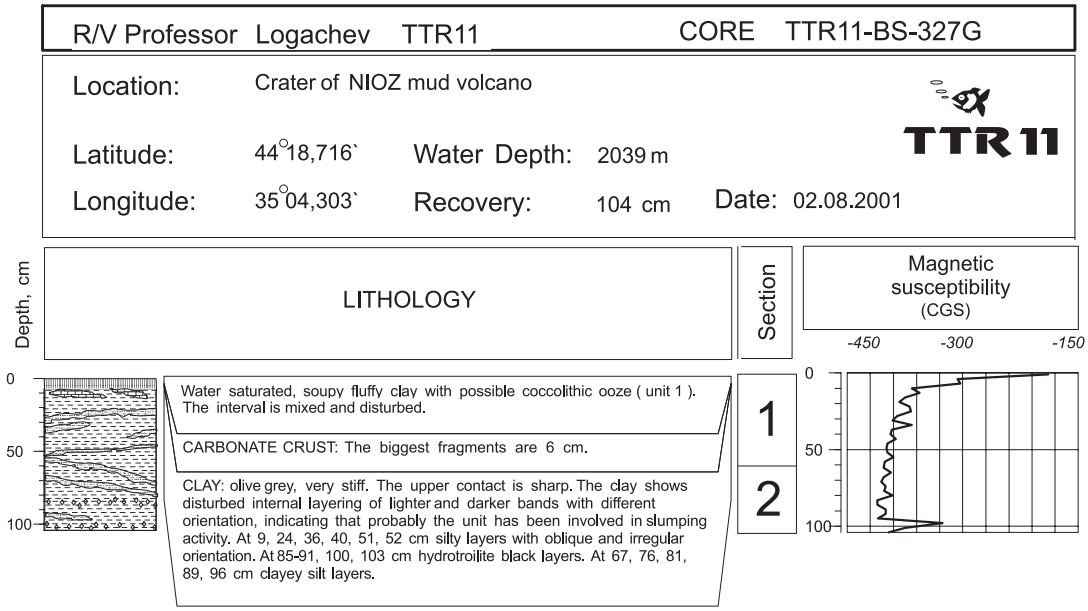

Core log TTR11-BS-327G

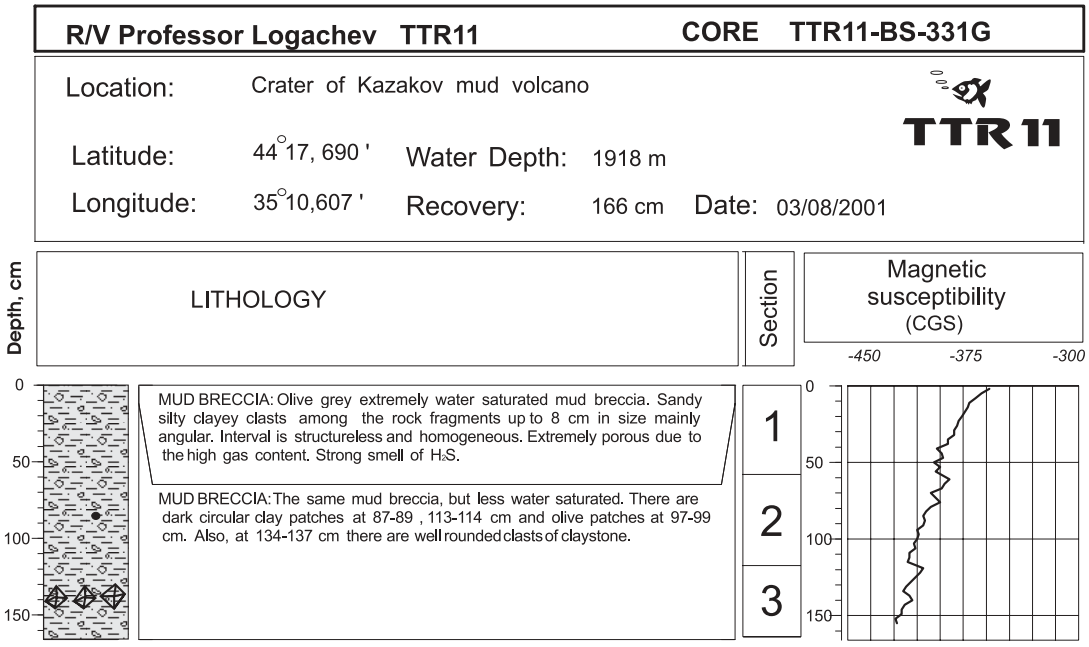

Core log TTR11-BS-331G

ANNEX I. CORE LOGS (LEG 1, the Black Sea)

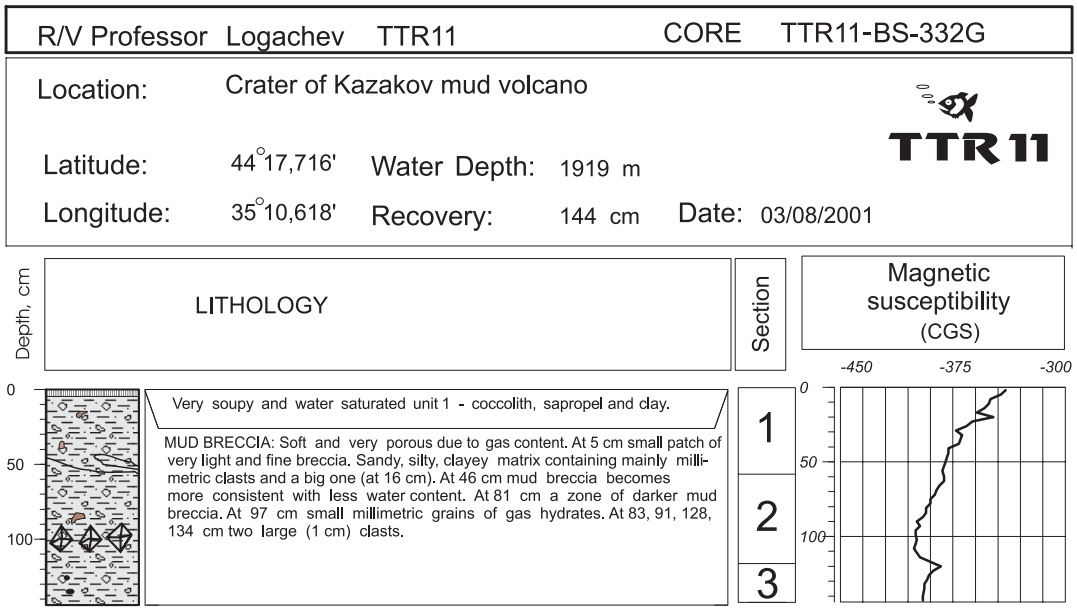

Core log TTR11-BS-332G

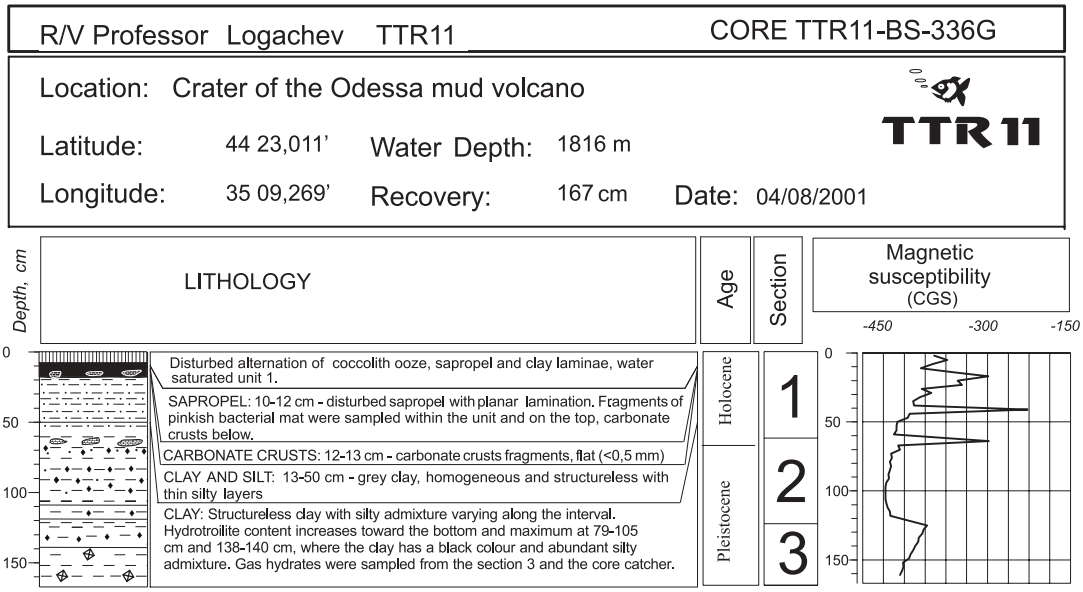

Core log TTR11-BS-336G

ANNEX I. CORE LOGS (LEG 1, the Black Sea)

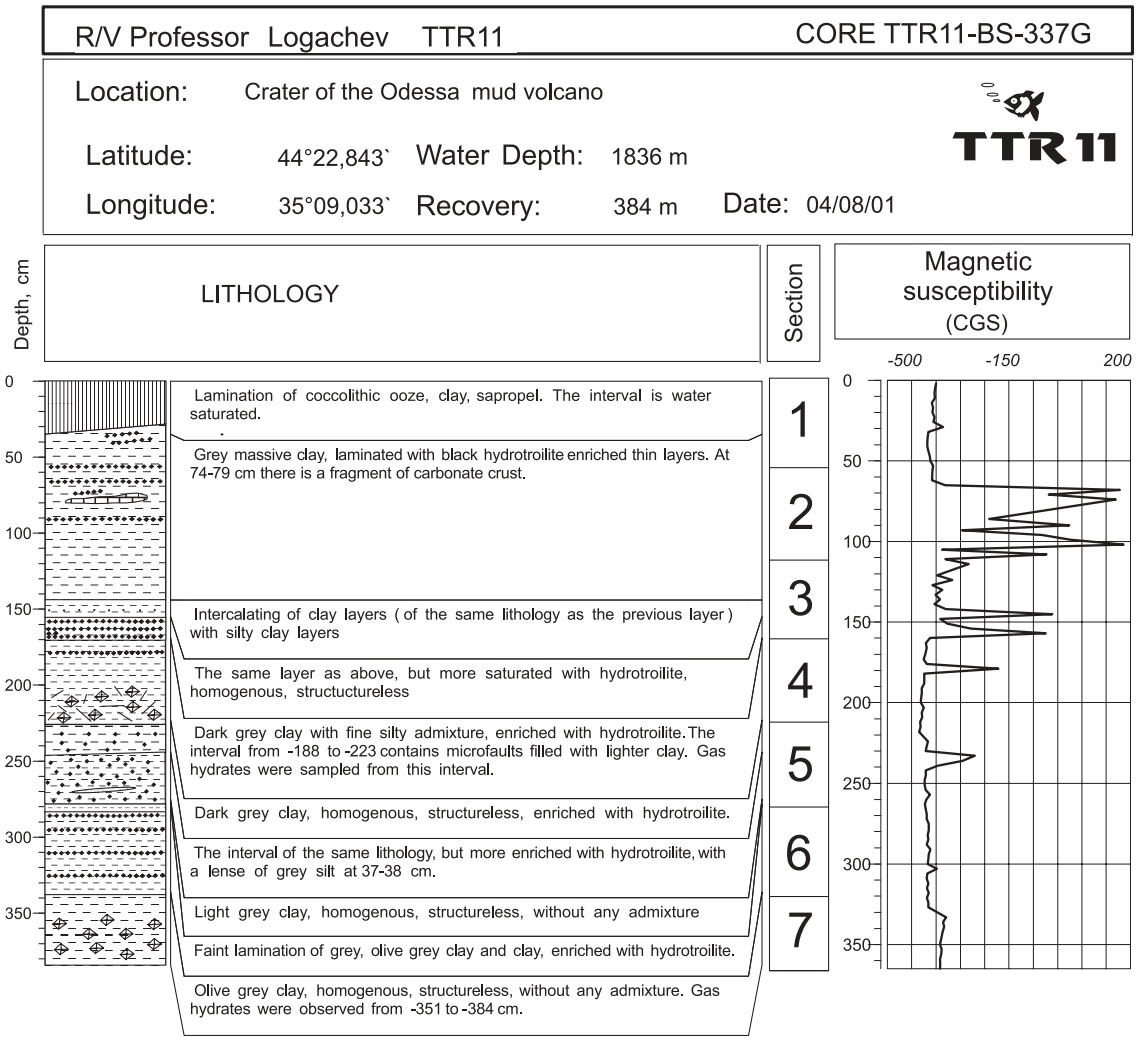

Core log TTR11-BS-337G

ANNEX I. CORE LOGS (LEG 1, the Black Sea)

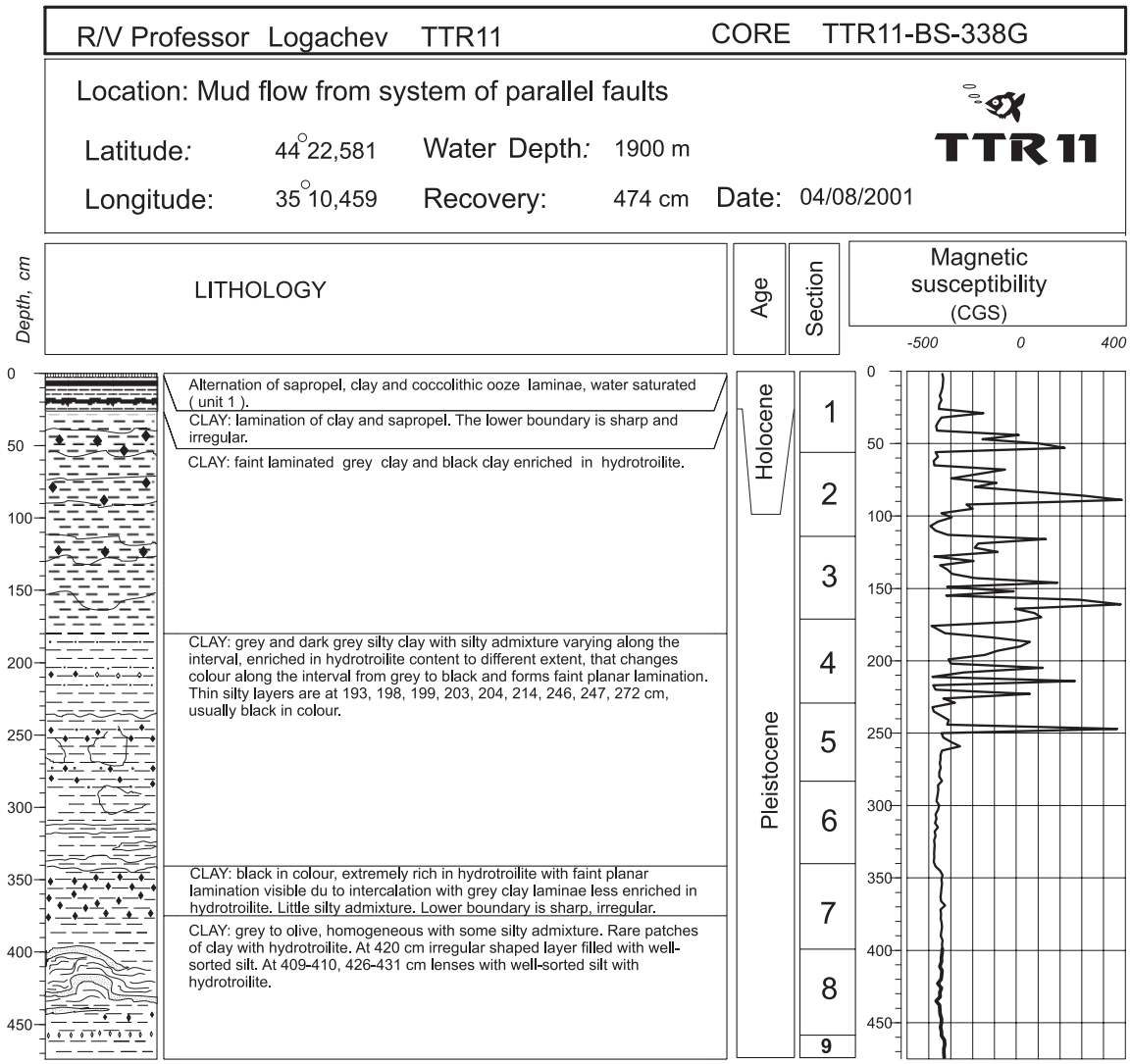

Core log TTR11-BS-338G

ANNEX I. CORE LOGS (LEG 1, the Black Sea)

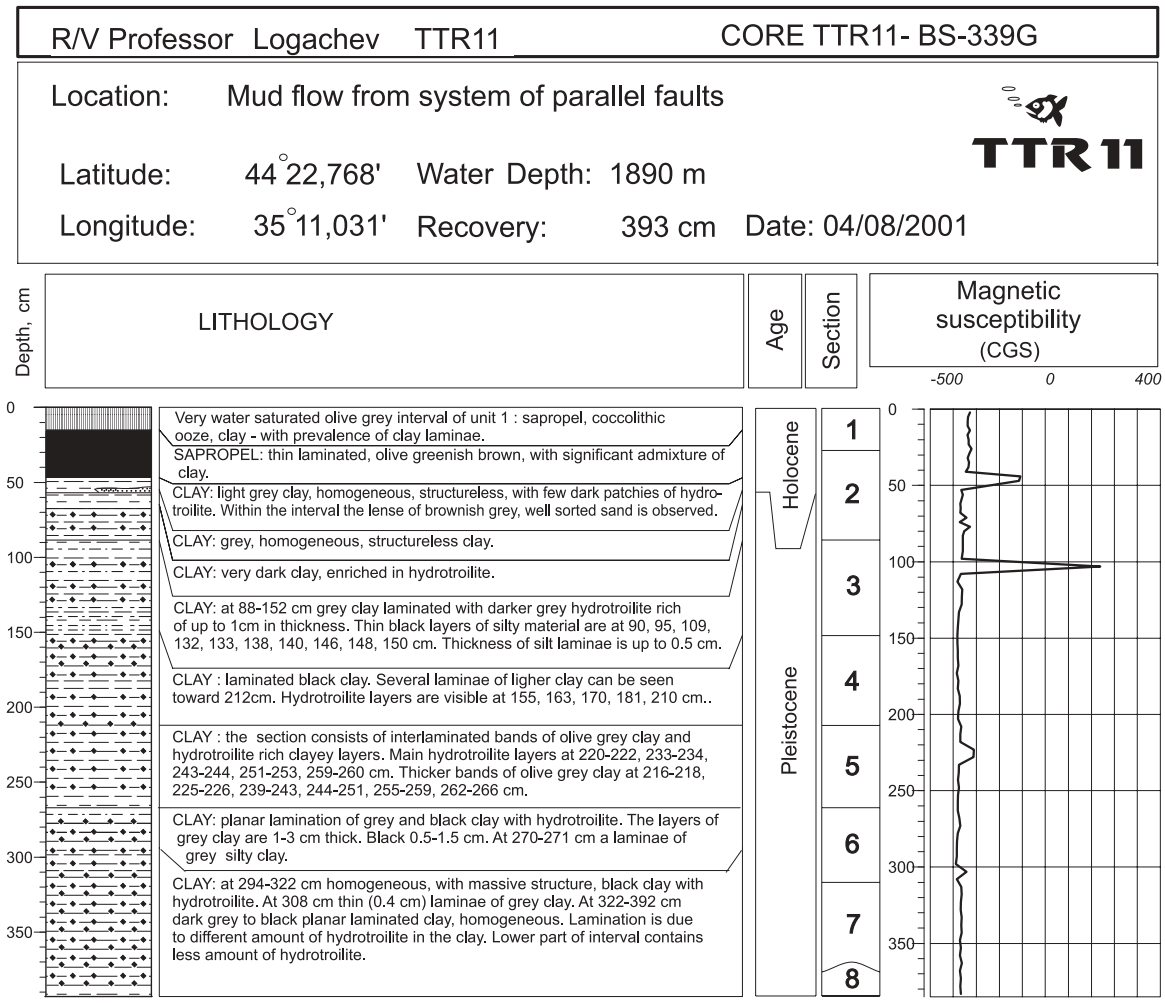

Core log TTR11-BS-339G

ANNEX I. CORE LOGS (LEG 2, the Mediterranean Sea)

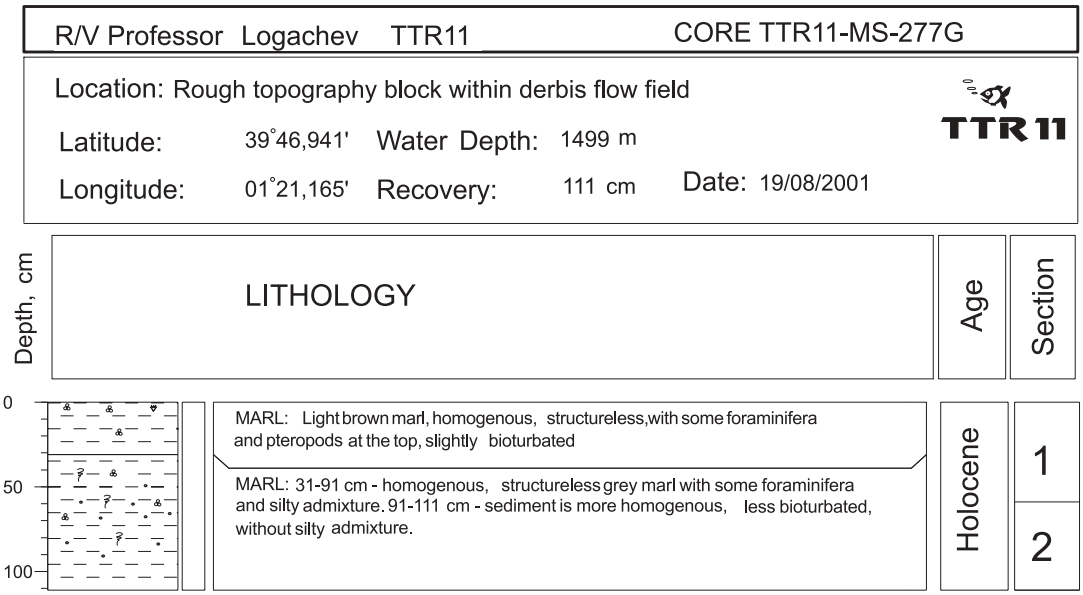

Core log TTR11-MS-277G

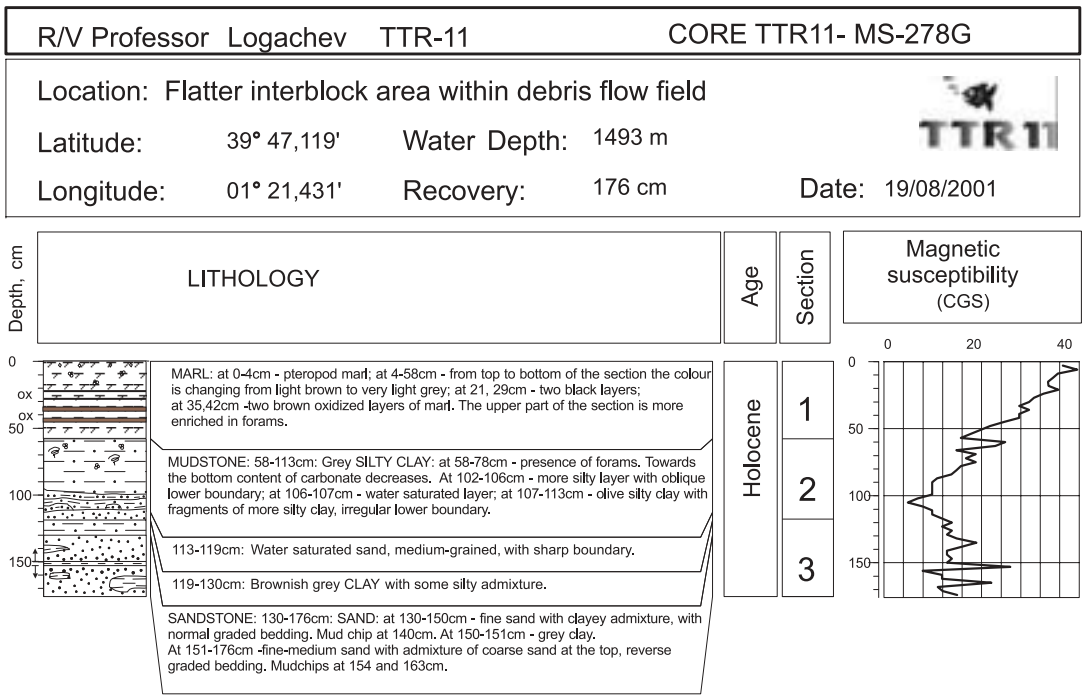

Core log TTR11-MS-278G

ANNEX I. CORE LOGS (LEG 3, the Gulf of Cadiz)

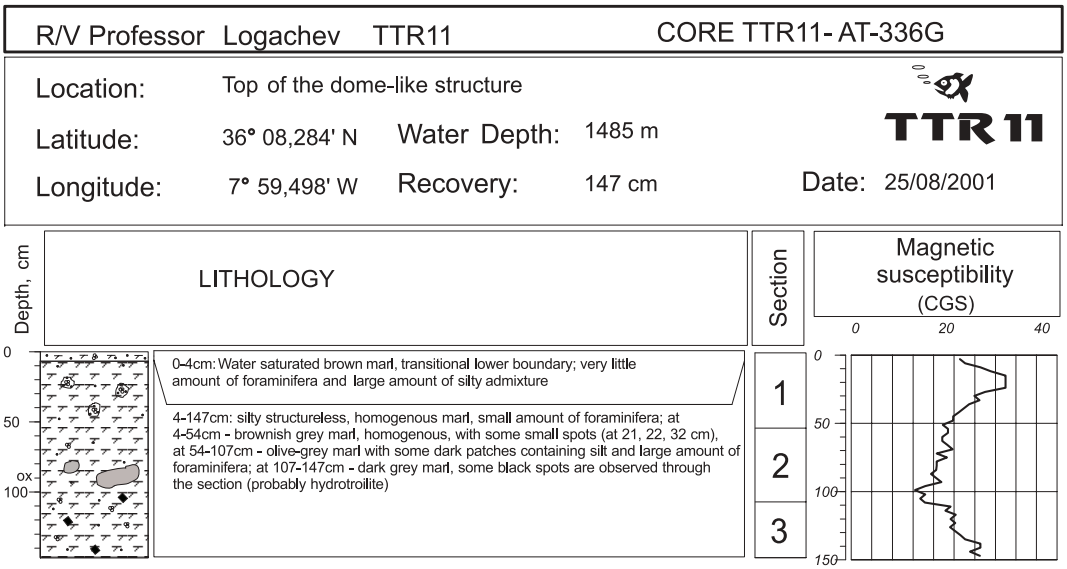

Core log TTR11-AT-336G

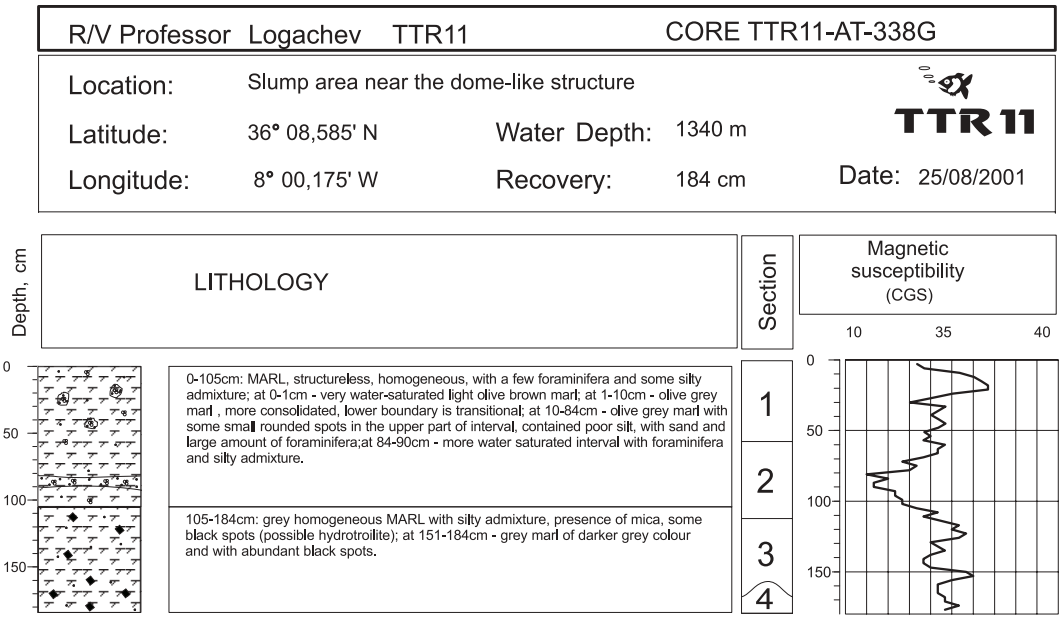

Core log TTR11-AT-338G

ANNEX I. CORE LOGS (LEG 3, the Gulf of Cadiz)

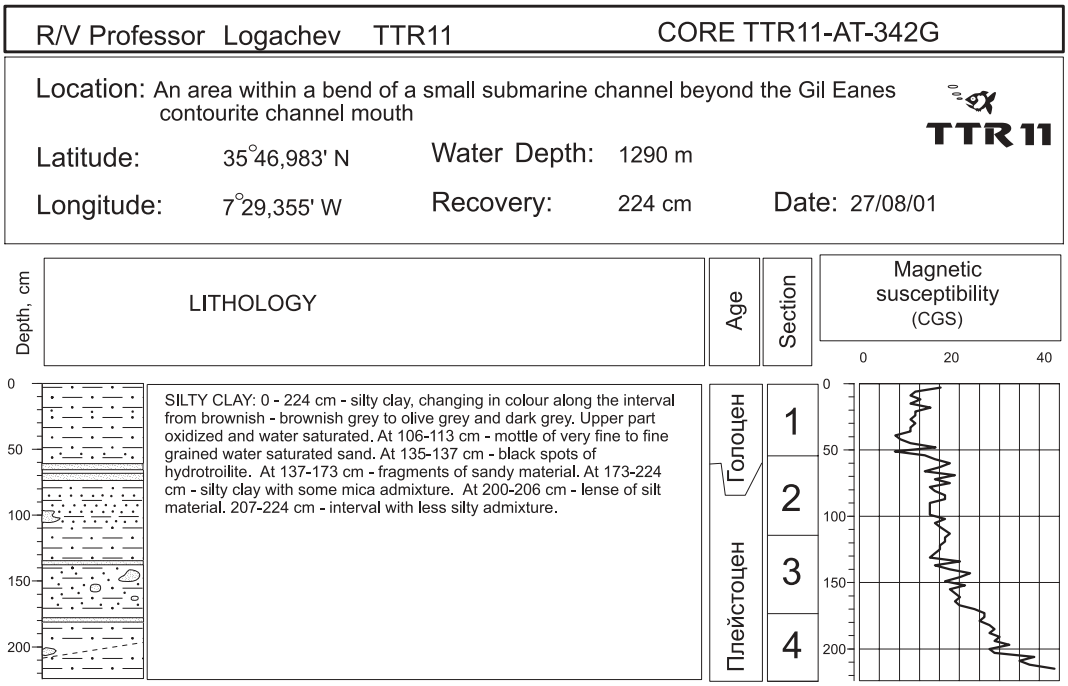

Core log TTR11-AT-342G

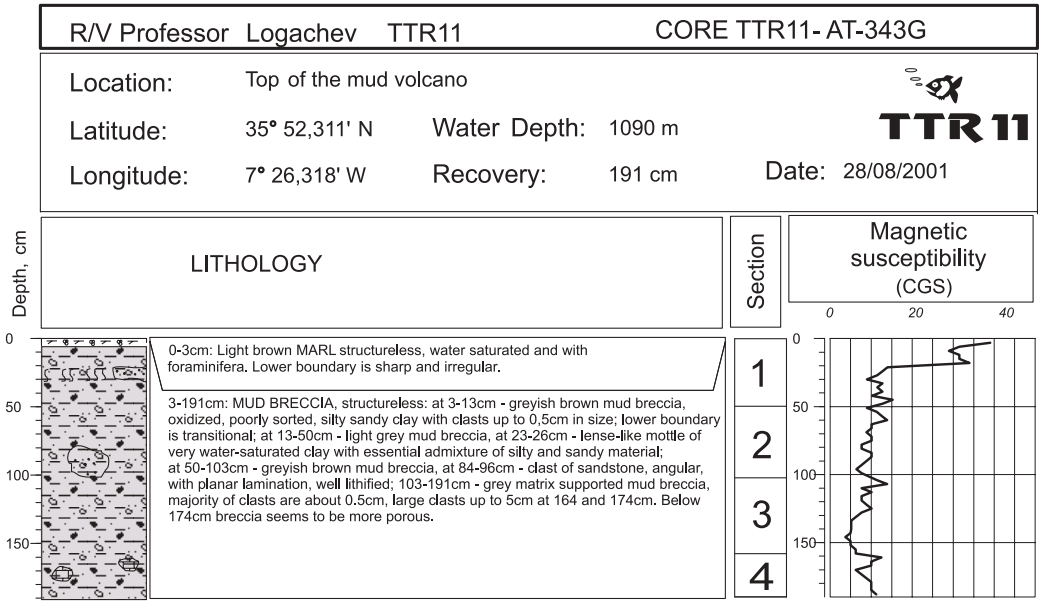

Core log TTR11-AT-343G

ANNEX I. CORE LOGS (LEG 3, the Gulf of Cadiz)

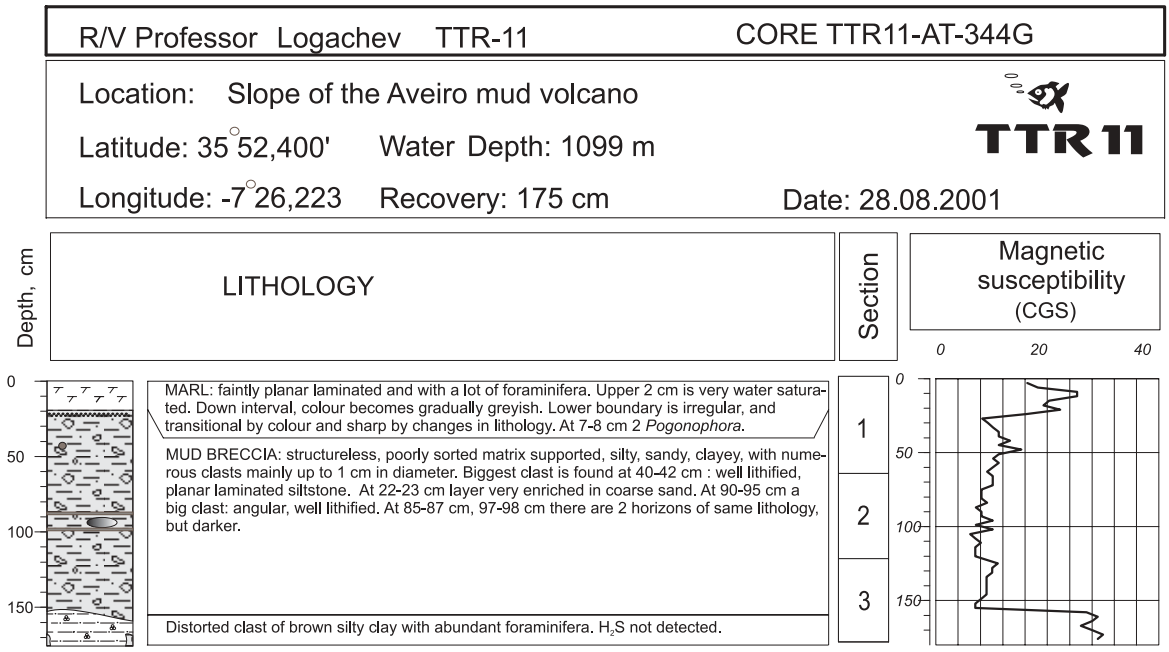

Core log TTR11-AT-344G

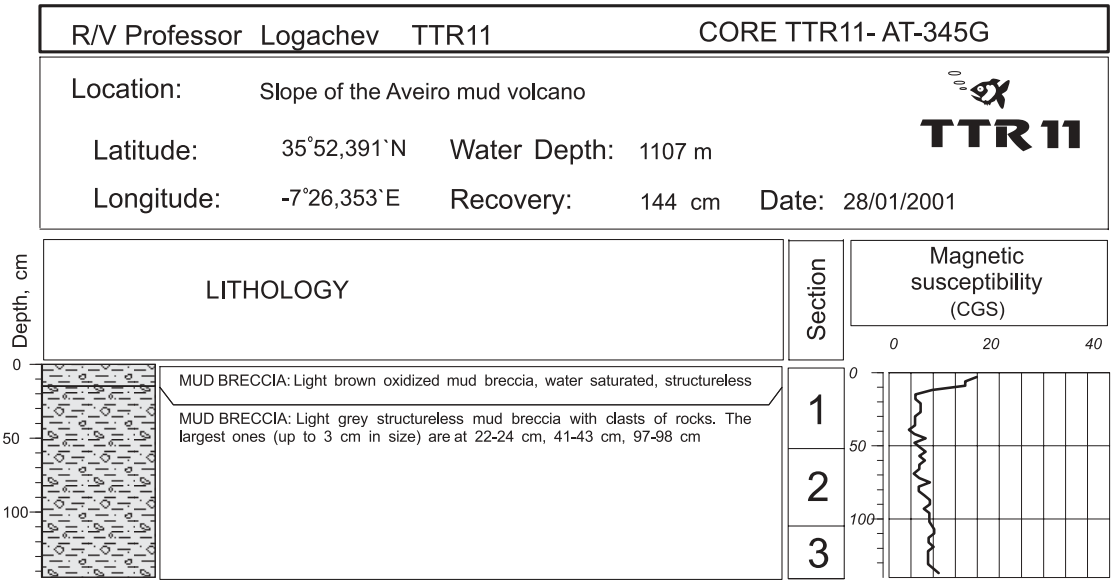

Core log TTR11-AT-345G

ANNEX I. CORE LOGS (LEG 3, the Gulf of Cadiz)

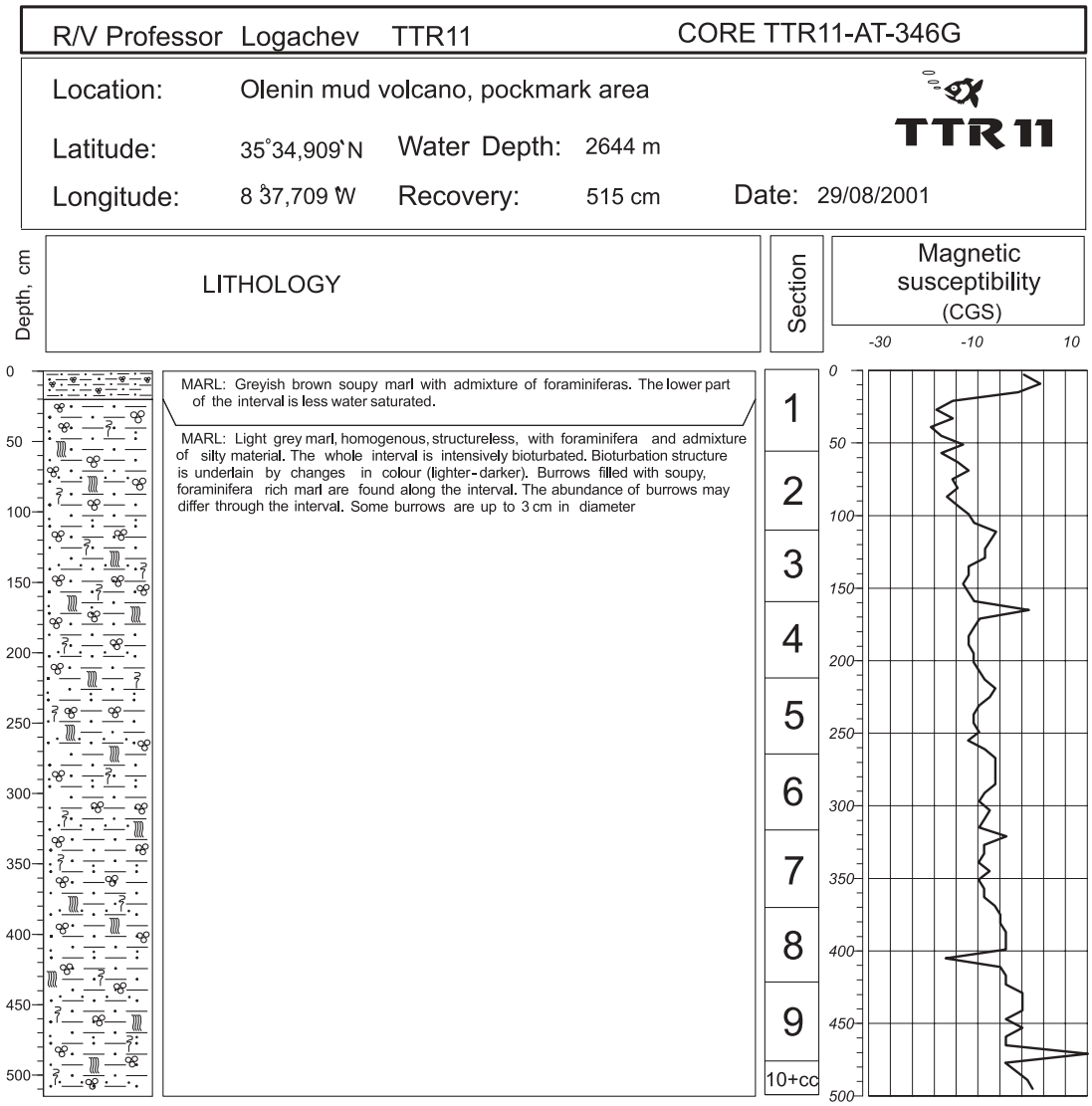

Core log TTR11-AT-346G

ANNEX I. CORE LOGS (LEG 3, the Gulf of Cadiz)

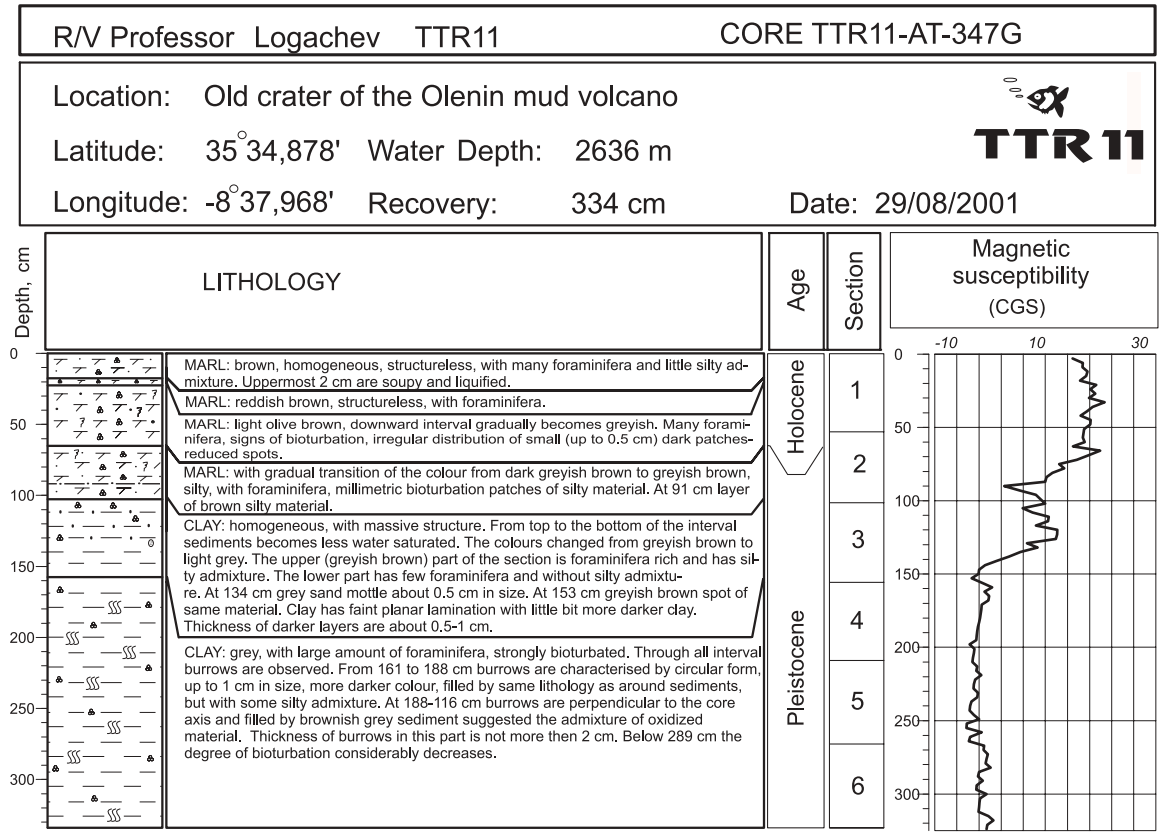

Core log TTR11-AT-347G

ANNEX I. CORE LOGS (LEG 3, the Gulf of Cadiz)

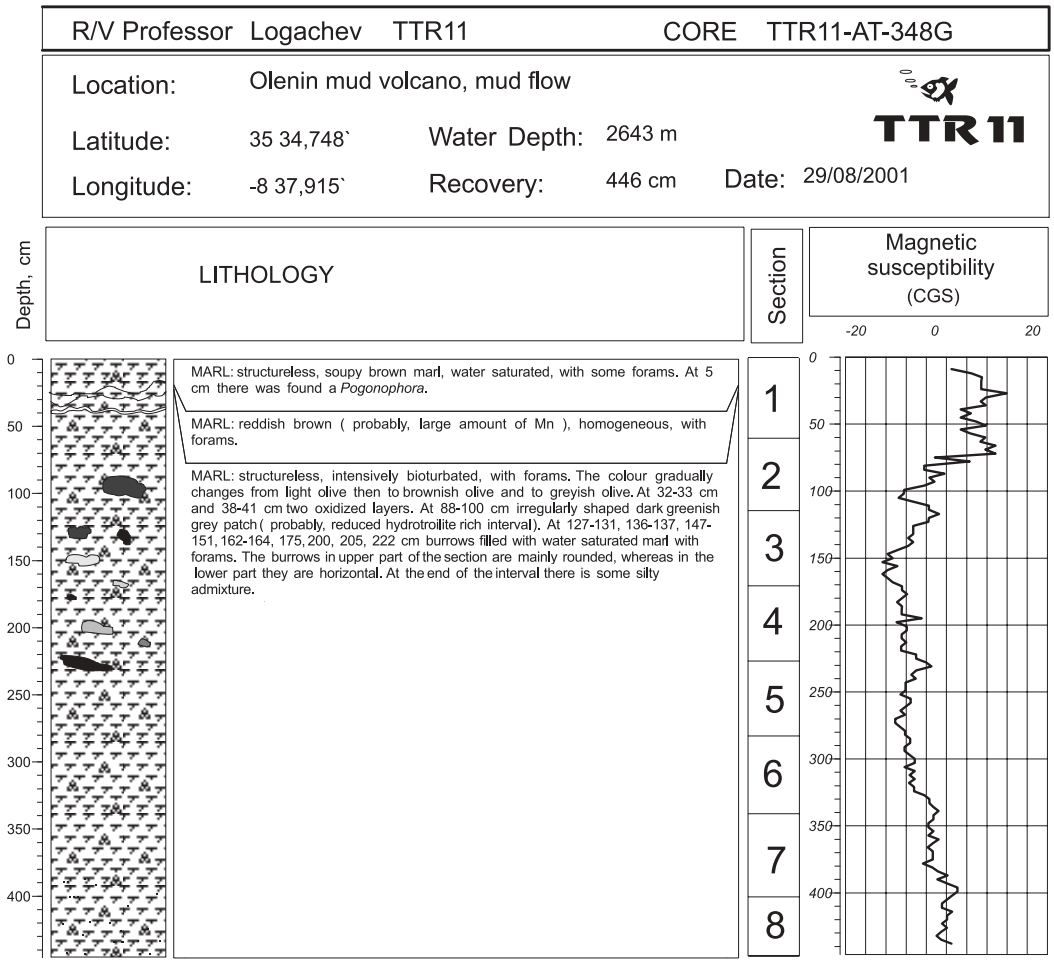

Core log TTR11-AT-348G

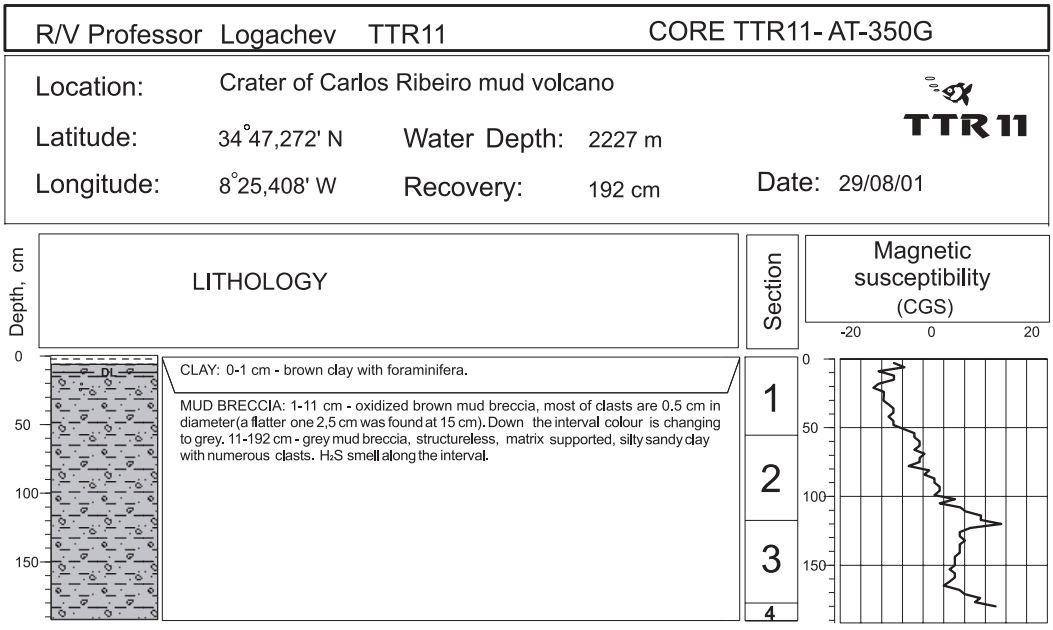

Core log TTR11-AT-350G

ANNEX II. LIST OF TTR-RELATED REPORTS (In order of date)

Limonov, A.F., Woodside, J.M. and Ivanov, M.K. (eds.)., 1992. Geological and geophysical investigations in the Mediterranean and Black Seas. Initial results of the "Training through Research" Cruise of RV Gelendzhik in the Eastern Mediterranean and the Black Sea (June-July 1991). UNESCO Reports in Marine Science, 56, 208 pp.

Limonov, A.F., Woodside, J.M. and Ivanov, M.K. (eds.), 1993. Geological and geophysical investigations of the deep-sea fans of the Western Mediterranean Sea. Preliminary report of the 2nd cruise of the RV Gelendzhik in the Western Mediterranean Sea, June-July, 1992. UNESCO Reports in Marine Science, 62. 148 pp.

"Training-Through-Research" Opportunities Through the UNESCO/TREDMAR Programme. Report of the first post-cruise meeting of TREDMAR students. Moscow State University, 22-30 January, 1993. MARINF, 91, UNESCO, 1993.

Limonov, A.F., Woodside, J.M. and Ivanov, M.K. (eds.), 1994. Mud volcanism in the Mediterranean and Black Seas and Shallow Structure of the Eratosthenes Seamount. Initial results of the geological and geophysical investigations during the Third UNESCO-ESF "Training-through-Research" Cruise of RV Gelendzhik (June-July 1993). UNESCO Reports in Marine Science, 64, 173 pp.

Recent Marine Geological Research in the Mediterranean and Black Seas through the UNESCO/TREDMAR programme and its "Floating University" project, Free University, Amsterdam, 31 January-4 February 1994. Abstracts. MARINF, 94,UNESCO, 1994.

Limonov, A.F., Kenyon, N.H., Ivanov, M.K. and Woodside J.M. (eds.), 1995. Deep sea depositional systems of the Western Mediterranean and mud volcanism on the Mediterranean Ridge. Initial results of geological and geophysical investigations during the Fourth UNESCO-ESF 'Training through Research" Cruise of RV Gelendzhik (June-July 1994). UNESCO Reports in Marine Science, 67, 171 pp.

Deep-sea depositional systems and mud volcanism in the Mediterranean and Black Seas. 3rd post-cruise meeting, Cardiff, 30 January - 3 February 1995. Abstracts. MARINF, 99, UNESCO, 1995.

Ivanov, M.K., Limonov, A.F. and Cronin, B.T. (eds.), 1996. Mud volcanism and fluid venting in the eastern part of the Mediterranean Ridge. Initial results of geological, geophysical and geochemical investigations during the 5th Training-through-Research Cruise of RV Professor Logachev (July-September 1995). UNESCO Reports in Marine Science, 68, 127pp.

Sedimentary basins of the Mediterranean and Black Seas. 4th Post-Cruise Meeting, Training-through-research Programme. Moscow and Zvenigorod, Russia, 29 January-3 February. Abstracts. MARINF,100, UNESCO, 1996.

Woodside, J.M., Ivanov, M.K. and Limonov, A.F. (eds.), 1997. Neotectonics and Fluid Flow through Seafloor Sediments in the Eastern Mediterranean and Black Seas. Preliminary results of geological and geophysical investigations during the ANAXIPROBE/TTR-6 cruise of RV Gelendzhik, July-August 1996. Vols. 1, 2. IOC Technical Series, 48, UNESCO, 226 pp.

Gas and Fluids in Marine Sediments: Gas Hydrates, Mud Volcanoes, Tectonics, Sedimentology and Geochemistry in Mediterranean and Black Seas. Fifth Post-cruise Meeting of the Training-through-research Programme and International Congress, Amsterdam, The Netherlands, 27-29 January 1997. IOC Workshop Reports,129, UNESCO, 1997.

Geosphere-biosphere coupling: Carbonate Mud Mounds and Cold Water Reefs. International Conference and Sixth Post-Cruise Meeting of the Training-through-Research Programme, Gent, Belgium, 7-11 February 1998. IOC Workshop Reports, 143, UNESCO, 1998.

Kenyon, N.H., Ivanov, M.K. and Akhmetzhanov, A.M. (eds.), 1998. Cold water carbonate mounds and sediment transport on the Northeast Atlantic Margin. IOC Technical Series, 52, UNESCO, 178 pp.

Kenyon, N.H., Ivanov, M.K. and Akhmetzhanov, A.M. (eds.), 1999. Geological Processes on the Northeast Atlantic Margin. IOC Technical Series, 54, UNESCO, 141 pp.

Geological Processes on European Continental Margins. International Conference and Eighth Post-cruise Meeting of the Training-Through-

Research Programme, University of Granada, Spain, 31 January - 3 February 2000. IOC Workshop Reports, 168, UNESCO, 2000.

Kenyon, N.H., Ivanov, M.K., Akhmetzhanov, A.M. and Akhmanov, G.G., (eds), 2000, Multidisciplinary study of geological processes on the Northeast Atlantic and Western Mediterranean margins. IOC Technical Series, 56, UNESCO, Paris, 119 pp.

Geological processes on deep-sea European margins. International Conference and Ninth Post-Cruise Meeting of the Training-through-Research Programme. Moscow/Mozhenka, Russia, 28 January - 3 February 2001. IOC Workshop Reports, 175. UNESCO, 2001, 76 pp.

Kenyon, N.H., Ivanov, M. K., Akhmetzanov, A. and Akhmanov, G. G. (eds), 2001. Interdisciplinary Approaches to Geoscience on the North East Atlantic Margin and Mid-Atlantic Ridge. IOC Technical Series, 60, UNESCO, 134 pp.

Geosphere/Biosphere/Hydrosphere Coupling Processes, Fluid Escape Structures and Tectonics at Continental Margins and Ocean Ridges. International Conference and Tenth Post-Cruise Meeting of the Training-through-Research Programme. Aveiro, Portugal, 30 January - 2 February 2002. IOC Workshop Reports, 183. UNESCO, 2002, 50 pp.